Energetics of Interaction between Biomolecules

by Deborah McPhail

a thesis submitted in partial fulfilment for the degree of Ph.D. in the Faculty of Science of the University of Glasgow.

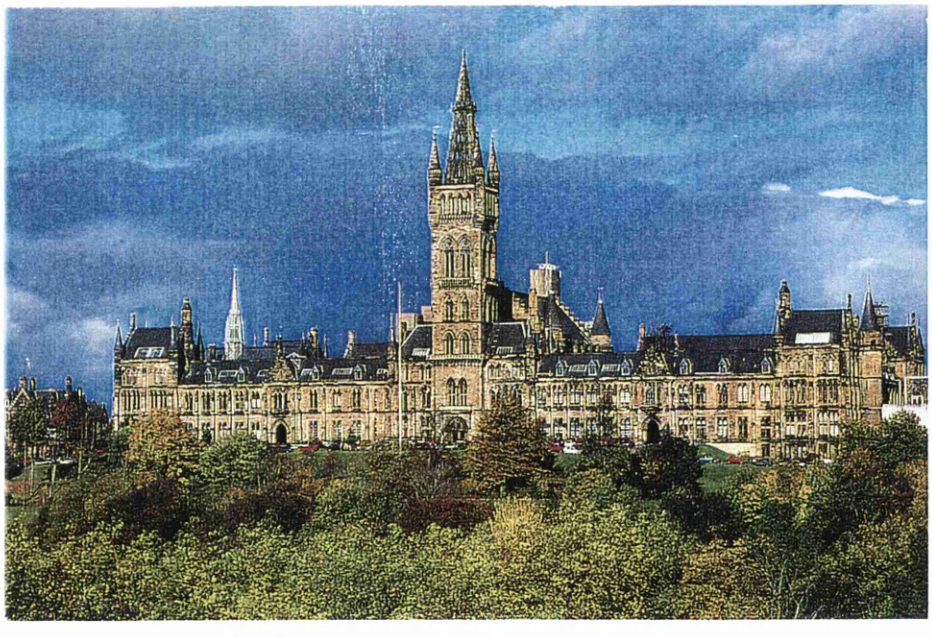

University of Glasgow

ProQuest LLC.
789 East Eisenhower Parkway
P.O. Box 1346
Ann Arbor, MI 48106 – 1346

ACKNOWLEDGEMENTS

I would like to thank my supervisor Alan Cooper for his enthusiasm and encouragement throughout the course of this work and for his meticulous attention to detail. I also wish to thank Andy Freer for all his help with the crystallographic work and also Tino Krell, who deserves a special mention for carrying out the electrospray mass spectrometry experiments on my behalf.

I am also grateful to the other members of the biophysical laboratory- Michelle Lovatt, Stephen Robertson, Steve Ford, Lindsay McDermott, Abdul Wadood and Margaret Nutley for her technical assistance.

Finally, I must thank my family for their continued support and encouragement over the years and especially Grant for keeping me sane.

Deborah McPhail

ABSTRACT

Thermodynamic aspects of the molecular recognition between the antibiotics vancomycin and ristocetin in the absence and presence of bacterial cell wall analogue peptides over a range of conditions has been investigated. Microcalorimetry has been used to study the recognition processes directly by measuring the association/dimerisation constants and enthalpy changes.

Vancomycin has been shown to combine with various peptides, such as N-acetyl-D-Ala, N-acetyl-D-Ala-D-Ala, N-fumaryl-D-Ala and N_{α},N_{ε}-diacetyl-Lys-D-Ala-D-Ala, but most strongly with N_{α},N_{ε}-diacetyl-Lys-D-Ala-D-Ala, the amino acid sequence most closely resembling its natural substrate. Dimerisation of antibiotic in the presence of this ligand was significantly increased from dimerisation in the absence of ligand. This enhancement of vancomycin dimerisation in the presence of ligand is in contrast to ristocetin. Ristocetin dimerisation in the absence and presence of the cell wall analogues, N-acetyl-D-Ala and N_{α},N_{ε}-diacetyl-Lys-D-Ala-D-Ala was similarly studied, but in this case, dimerisation was weakest in the presence of N_{α},N_{ε}-diacetyl-Lys-D-Ala-D-Ala.

Kinetics were used in an attempt to study the vancomycin dimerisation process in the presence of the strongly binding N_{α},N_{ε}-diacetyl-Lys-D-Ala-D-Ala in more detail and a scheme is proposed for the direct dissociation of such dimers in solution.

The precipitation of vancomycin/N-acetyl-D-Ala-D-Ala solutions at the concentrations required for calorimetric dilution measurements allowed successful crystallisation of the complex, which permitted the use of X-ray crystallography to investigate the structure of the complex. However, this remains unresolved due to an uncharacteristically large unit cell for a small molecule, the high symmetry space group and the lack of a suitable model for molecular replacement techniques.

CONTENTS

Chapter 1:
Introduction

1.1 Molecular recognition

The fundamental basis for molecular recognition is the interaction of two or more complementary units facilitated by a variety of intra/intermolecular forces. Molecular recognition is of central importance in biological systems as it is responsible for such vital processes as DNA replication, antibody binding to antigen, enzymatic activity and hormonal regulation, to name but a few. Molecular recognition is so finely tuned that molecules are able to differentiate between targets that differ in as little as one functional group, with such specificity ensuring interaction with the correct receptor. Of primary importance is the responsibility molecular recognition has for ensuring proteins assume the correct conformation for their desired function. Without such recognition, the many functional proteins required by biological systems would incorrectly fold and therefore be unable to initiate the necessary response. Molecular recognition in the structural determination of proteins requires a balance between the various intramolecular non-covalent interactions e.g. electrostatic interactions, hydrogen bonding, van der Waals forces and hydrophobic bonding. Electrostatic interactions can occur between positively and negatively charged amino acid side chain groups. For example, if an amino group of a lysine side chain is located close to a carboxyl group of a glutamic acid residue, since at neutral pH one group will be positively charged and the other negatively charged, there will be an electrostatic force between them. Such interactions are sometimes called salt bridges, which can be broken if the protein is taken to a pH value high or low enough that either partner loses its charge. This loss of salt bridges is a partial explanation for the acid or base denaturation of proteins. The mutual repulsion between the numerous similarly charged groups that are present in acidic or basic solutions contributes further to the instability of the folded structure under these conditions. Many of the amino acid side chains within a protein carry groups which are good hydrogen bond donors or

acceptors allowing the formation of internal hydrogen bonds which contribute to the overall stability of the protein structure. Also, the weak interactions between uncharged molecular groups can also make significant contributions to protein stability. As space filling models of proteins indicate, the interior is tightly packed, allowing maximum contact between side chain atoms. The other factor which makes a contribution to the stability of proteins is the hydrophobic effect. If a protein contains a large number of amino acid residues with hydrophobic side chains, when the polypeptide chain is in the unfolded form, these side chains will be exposed to the surrounding water which will form ordered structures around them. But when the chain folds into its tertiary structure, these hydrophobic side chains become buried within the protein molecule and the water molecules are released to join the surrounding solvent, increasing the randomness of the system and therefore its entropy. However, the entropy of the molecule itself is reduced upon folding since it assumes a more stable conformation. Although these forces are weaker than covalent bonds, they have a major advantage in that they can be readily broken and reformed under physiological conditions. This is a requirement in all biological systems for adaptation to a changing environment. For example, the importance of molecular recognition in protein conformation can be demonstrated by experiments in which the native structure of a protein is destroyed by changing the environmental conditions such as temperature or pH, which will in turn disrupt the intramolecular forces responsible for structure stability. The protein is now denatured and assumes the conformation approaching a random coil with freedom of rotation about bonds in both the polypeptide backbone and side chains. In such cases, all protein function has been lost. However, denaturation is not an irreversible process and if the protein is restored to original conditions it may spontaneously refold into its original structure, restoring the intramolecular forces which are responsible for maintaining the three dimensional structure of the protein and therefore regaining its function. Molecular recognition between groups within the protein is resumed on returning to physiological conditions, illustrating the importance of weak, non-covalent forces in biological systems (Mathews & van Holde,[b] 1990).

A greater understanding of the ways in which molecules carry out their recognition process is of paramount importance, especially in drug design development, where a specific inhibitor can be synthesised based on knowledge of the molecular structure of the target to which the inhibitor will bind. Drug targets can be divided into three main categories, as shown in Figure 1.1 (Saunders, 1993).

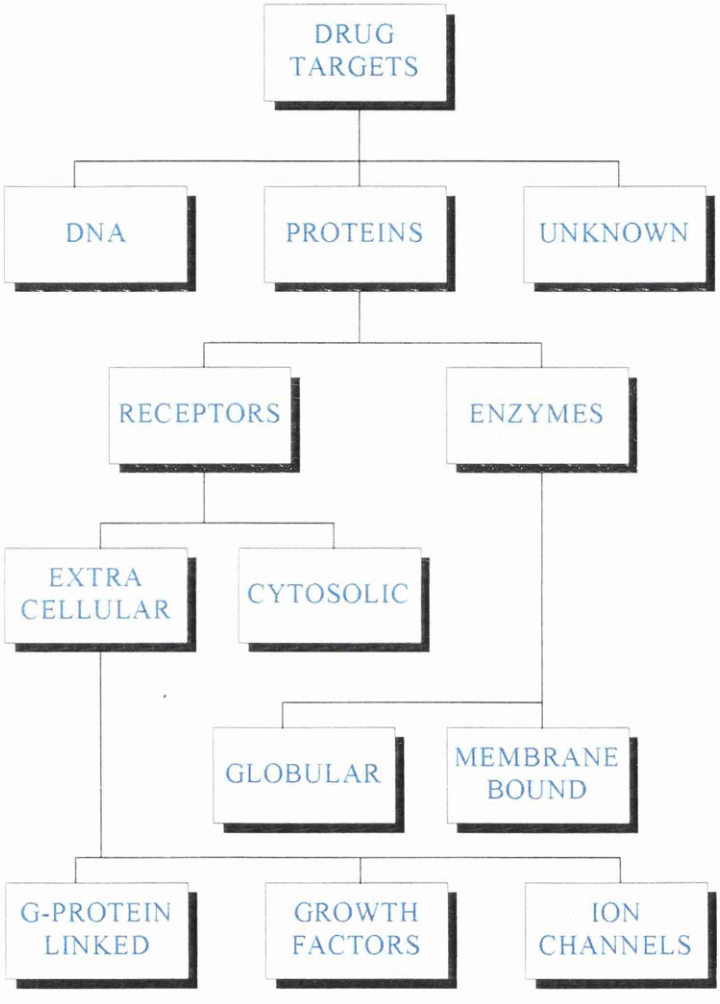

Figure 1.1 Categories of drug targets.

For the synthesis of drugs whose target is an enzyme, it is necessary to know the three-dimensional structure of the enzyme and its mechanism of action. This involves a

combination of techniques, from X-ray crystallography and organic chemistry to site-directed mutagenesis and molecular modelling (Mathews & van Holde,[e] 1990). X-ray crystallography is a complex method by which the electron density within a protein structure can be determined. It is based on the phenomenon of diffraction, whereby a source of X-rays is directed at a crystal which interacts with the electrons on each atom within the structure and causes them to be scattered. The X-rays emitted from these scattered electrons interfere with one another, either destructively or constructively. If constructively, the diffracted beams are recorded as a diffraction pattern on a detector. From this, the location of each atom in the structure can begin to be determined. This method gives a three-dimensional representation of the structure of interest and is useful for providing an overview of the entire molecule so that the way in which binding to the target takes place is clear. Hydrogen bonding may be assigned to the structure from distance measurements, but contributions from other intermolecular forces remain unresolved. Techniques such as microcalorimetry provide information about these forces, although only an overall estimation can be made and not their relative contributions. Microcalorimetry allows the determination of association constants and enthalpy changes, which in turn can provide information on the standard Gibbs free energy and entropy changes. In addition to microcalorimetry, spectroscopic techniques allow a direct estimation of association constants based on absorbance changes upon ligand binding.

1.2 Recent applications of microcalorimetry

In recent times there has been a gradual increase in the use of both differential scanning and isothermal titration microcalorimetry to study biochemical reactions. Both techniques have gained popularity due to their wide range of applicability and the variety of information they can provide, from the energetics and thermal stability of the process to cooperativity.

Differential scanning microcalorimetry has been used to study many biological systems, such as the conformational stability of proteins (Cooper & McAuley-Hecht, 1993 : Burova *et al.*, 1995). A few examples of such an application follows.

Studying the thermal unfolding of the small protein, ubiquitin, in water and methanol mixtures led to important information on the contribution the hydrophobic effect makes to the overall stabilisation of the folded protein (Cooper & McAuley-Hecht, 1993). Differential scanning microcalorimetry experiments showed that ubiquitin is stable in the absence of methanol, yet shows a cooperative thermal unfolding transition at high temperatures. Such an endothermic transition exhibited an increase in specific heat capacity of the unfolded compared with the folded protein. This phenomenon is consistent with the exposure of hydrophobic groups to aqueous solvent upon unfolding and is thought of as a characteristic of hydrophobic stabilisation of folded proteins (Kauzmann, 1959). When the same experiment was carried out in a water and methanol mixture, although the stability of the protein was reduced, it still underwent an endothermic thermal unfolding transition at high temperature, but in this case there was no change in the specific heat capacity. It is thought that this is because folding in mixed solvents lacks the thermodynamic characteristic of the hydrophobic interaction. Clearly this effect is a driving force in the conformational stability of proteins in water, with the contribution made by hydrogen bonding playing a lesser role. Since all polar groups on the protein have a high affinity for water, hydrogen bonds will be formed both intramolecularly between the appropriate groups and intermolecularly with solvent molecules, so even though hydrogen bonding is a neccessity in conformational stability, it does not play a major thermodynamic part. But, replacing some of the water molecules with less polar molecules may shift the balance between these two important contributions. Since hydrogen bonds would be unable to form satisfactorily with non-polar solvent, they will play a greater role in the intramolecular stability of the protein. Although differential scanning calorimetry can provide information on the overall thermodynamic contributions to protein stability, it cannot quantify the individual contributions from various sources.

The folding and conformational stability of adrenodoxin has been studied using differential scanning microcalorimetry (Burova *et al.*, 1995). Adrenodoxin is an iron-sulfur containing protein which participates in the synthesis of steroid hormones by mediating the electron transport from the NADPH-dependant adrenodoxin reductase to mitochondrial cytochromes P450 (Estabrook *et al.*, 1973 : Usanov *et al.*, 1990 : Lambeth, 1990). This study showed that the iron-sulfur cluster makes a major contribution to the conformational stability of the protein, since carrying out thermal denaturation on adrenodoxin alone disrupted the disulphide bridges between the iron ions resulting in an irreversible transition. However, carrying out the same experiment in a buffer system that contains sodium sulphide and mercaptoethanol causes no destruction of the iron-sulphur complex and produces a certain degree of refolding. Such experimental conditions provide a means of studying folding and stability of iron-sulfur proteins in general.

Isothermal titration microcalorimetry has been used to study a diverse range of biomolecular associations between macromolecule and ligand. Such studies have included investigations into adverse side effects from therapeutic treatments (Jakoby *et al.*, 1995) and the recognition process between antibodies and antigens (Leder *et al.*, 1995) to understanding the mechanism of action of protein toxins against bacteria (Evans *et al.*, 1996). A small selection from such a large field will be discussed here in an attempt to illustrate the wide range of applications of such a sensitive method for the direct determination of thermodynamic parameters.

Titration microcalorimetry has been used to study the interaction of tolbutamide, a member of the family of sulfonylureas used to treat type II diabetes mellitus, with human serum albumin (Jakoby *et al.*, 1995). Human serum albumin is the primary serum transport system for a range of metabolites and pharmaceutical agents and tolbutamide can bind to this in the circulation. It has been demonstrated by various workers (Sellers & Koch-Weser, 1971 : Wesseling & Mols-Thurkow, 1975 : Monks *et al.*, 1978 : Anton, 1973) that acidic drugs which bind to human serum albumin can competitively displace

one another from albumin binding sites and in the case of tolbutamide, this displacement can cause hypoglycemia in diabetes sufferers. Knowledge of tolbutamide's albumin binding properties and binding site locations may help predict which other drugs taken in conjunction with tolbutamide have the potential to displace tolbutamide from albumin and increase the risk of hypoglycemia. By using titration microcalorimetry, tolbutamide was found to bind to three sites with equal or comparable affinity and this stoichiometry was independently confirmed by NMR experiments. Titrations of tolbutamide with albumin complexed with each of the drugs, salicylate, clofibric acid and an aspirin analogue TIB, all three of which are known to bind to albumin in the subdomain IIA and IIIA binding cavity, caused stoichiometric reductions in the number of tolbutamide binding sites with increases in mole ratio of competing agent to albumin, accompanied by little or no change in the tolbutamide dissociation constant or molar binding enthalpy, suggesting that all three drugs decreased tolbutamide binding by occupying sites on albumin to which tolbutamide binds. The localisation of tolbutamide binding sites on albumin provide a way in which predictions can be made about which drugs have the potential to displace tolbutamide and increase the risk of a hypoglycemic effect.

Isothermal titration microcalorimetry has been used to study the binding of cytidine 2′-monophosphate (2′CMP) to the active site of ribonuclease A (RNase) (Wiseman *et al.*, 1989). It was suggested that at high concentrations of RNase, the binding process could be complicated by aggregation or dimerisation of RNase into a form which binds 2′CMP less strongly than monomeric RNase, indicated by a decrease in association constant at high concentrations.

This technique has also been used to study the recognition process between immunological agents such as antibodies and antigens (Leder *et al.*, 1995). It is well known that cross-reaction of antibodies with dissimilar, yet related, antigens exists and this seems to suggest that conformational adaptation has a role to play in the recognition process. Cross-reactivity of monoclonal antibodies against peptides that are closely sequence-related but adopt very different conformations in solution has been investigated

in this study using titration microcalorimetry with the monoclonal antibodies 29AB and 13AD, both raised against the 29-residue peptide LZ, which forms a stable coiled coil and the random coil analogue LZ(7P14P) which contains proline substitutions at positions 7 and 14. Titration microcalorimetry of the binding of the monoclonal antibodies 29AB and 13AD to cognate and noncognate peptide antigen showed that the cross-reaction between these antibodies and LZ(7P14P) exhibited a large unfavourable entropy. This was compensated by a more favourable enthalpy and resulted in only a small difference between association constants for LZ and LZ(7P14P). The monoclonal antibody 42PF, raised against the random coil LZ(7P14P), was shown to cross-react with LZ. This cross-reaction was entropically favoured and enthalpically disfavoured. It is thought that the antibody can select and preferentially bind a particular conformer of the peptide, since a stable coiled coil to a random coil is a reversible process, that is complementary to the antibody binding site and that is already present in the solution before binding takes place, rather than following an induced-fit mechanism in which conformational adjustment takes place within the antigen-antibody complex.

A direct measurement of the association between the protein toxin, colicin N to the membrane receptors, OmpF, OmpC and PhoE was carried out using the Omega microcalorimeter (Evans *et al.*, 1996). Colicin N kills sensitive *E. coli* by binding to the trimeric outer membrane protein, OmpF. This was thought to be the unique membrane receptor for colicin N, but this study has shown that OmpC and PhoE can also act as receptors. Isothermal titration microcalorimetry was used to study the binding of the 42 kDa toxin to each of the 120 kDa porin trimers. Thermodynamic data obtained from these titrations showed that colicin N could bind to all three receptors with similar affinities and stoichiometry, but with significant differences in enthalpic and entropic contributions of the standard Gibbs free energies of binding. The binding of colicin N to PhoE and OmpC is entropy driven, with positive entropy contributions, suggesting that binding is accompanied by reorganisation of protein/lipid/solvent structure, giving rise to a more disordered overall structure. In contrast, binding of colicin N to OmpF exhibits a significant negative entropy. This suggests a structural rearrangement of the OmpF-

colicin N complex, producing a more rigid and stable lower entropy system. These changes in protein dynamics may suggest why OmpF is the preferred receptor *in vitro*.

1.3 The vancomycin family of antibiotics

The vancomycin family of antibiotics represent an effective method of control against bacterial infections caused by gram-positive coccal microorganisms (Gerhard *et al.*, 1993) such as staphylococci and streptococci and is effectively the last line in defence against the virulent methicillin-resistant *Staphylococcus aureus* (MRSA), the so-called 'superbug'. MRSA is responsible for many pneumonia and post-surgical infections and is typically resistant to penicillin and ampicillin and other antibiotics such as erythromycin, tetracycline and sulphonomides (Neu, 1992). Therefore, the vancomycin group of antibiotics are of great clinical importance in providing a method of control against such an otherwise resistant bacteria. The first member of the group to be discovered was vancomycin, which was isolated from a strain of *Streptomyces orientalis* in 1956, where it was produced as a secondary metabolite (McCormick *et al.*, 1956). Secondary metabolites are naturally produced substances which do not play an obvious role in the internal economy of the organism that produces them (Maplestone *et al.*, 1992), yet seem to be important for the survival of the producing organism, either by improving its ability to proliferate in a particular area under suitable conditions or providing protection from competition or predation (Vining, 1992). Other members of the group, such as ristocetin, eremomycin, teicoplanin and balhimycin, were obtained from various species of actinomycetes isolated from soil samples (Barna & Williams, 1984). However, our discussion will be restricted to the antibiotics vancomycin and ristocetin.

The vancomycin group of antibiotics exert their bactericidal effect by complexing with D-Alanine-D-Alanine precursor units on the surface of gram-positive bacterial cell walls, thereby preventing their incorporation into the major structural polymer of the cell wall,

peptidoglycan (Barna & Williams, 1984), by impeding the action of the transglycosylases and transpeptidases (Billot-Klein *et al.*,[a] 1994). Peptidoglycan is very important to bacterial cells as it allows them to resist hypotonic shock and lysis (Wright & Walsh, 1992). Once disrupted, death of the cell by lysis can occur when the osmotic pressure varies. In addition, vancomycin is known to affect the permeability of cytoplasmic membranes and may impair the synthesis of RNA (Jordan & Inniss, 1959). Since the bacterial cell must continue to synthesise peptidoglycan in order to grow and divide, inhibition of a step in this process provides a specific way to control the proliferation of bacterial pathogens.

Gram-negative bacteria also have a layer of the cross-linked polysaccharide-peptide complex, known as peptidoglycan, although this is relatively thin and is protected against the vancomycin group antibiotics by an outer membrane of lipopolysaccharide-phospholipid-protein structure. In gram-positive bacteria the peptidoglycan layer is much thicker and much more permeable than the outer layer of the gram-negative species (Mathews & van Holde,[c] 1990), therefore more susceptible to attack from this group of antibiotics. The difference between the cell walls of gram-positive and gram-negative bacteria is illustrated in Figure 1.2 (Mathews & van Holde,[c] 1990).

Peptidoglycan is biosynthesised in three main stages. Firstly, synthesis of N-acetylmuramylpentapeptide, secondly, formation of the polysaccharide chain by polymerisation of N-acetylglucosamine and N-acetylmuramylpentapeptide and thirdly, cross-linking of the individual peptidoglycan strands. The first step begins with the synthesis of UDP-N-acetylmuramic acid from UDP-N-acetylglucosamine. Then the peptide is built up, one residue at a time. The sequence of additions is as follows:

1. L-Alanine
2. D-Glutamate
3. L-Lysine
4. D-Alanyl-D-Alanine

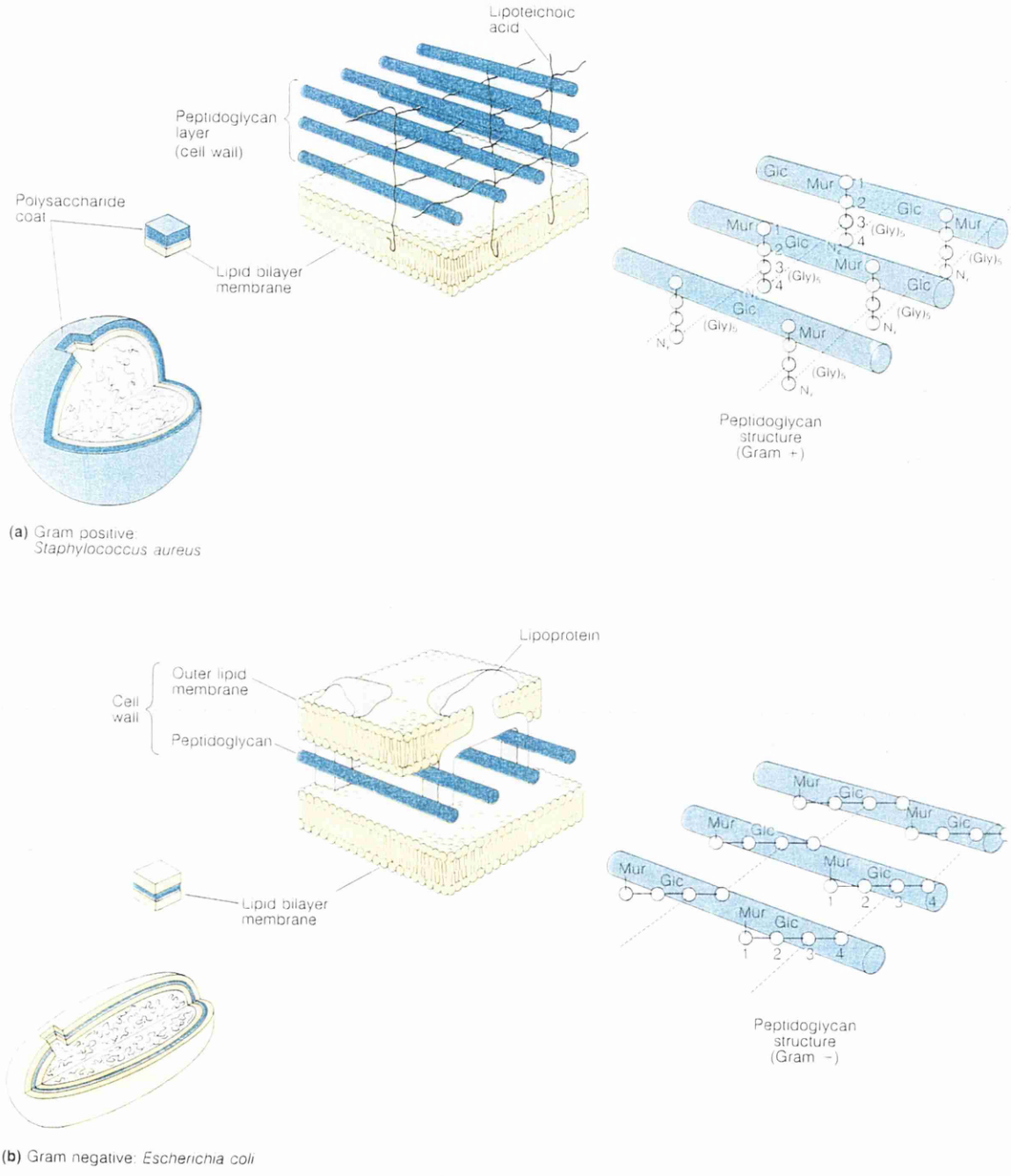

Figure 1.2 Schematic drawings of bacterial cell walls. **(a)** A representative gram-positive bacterium, *Staphylococcus aureus*. **(b)** A representative gram-negative bacterium, *Escherichia coli*. Cylinders represent polysaccharide chains and strings of circles represent peptide chains; dotted lines show links between them. Note the much greater thickness of the peptidoglycan layer in gram-positive bacteria.

The next stage is polymerisation of N-acetylglucosamine and N-acetylmuramylpentapeptide to give a linear peptidoglycan chain. The disaccharide units which make up this chain are joined through 1,4-β glycosidic bonds. This involves a lipid carrier, undecaprenol phosphate. The N-acetylmuramylpentapeptide moeity from UDP-N-acetylmuramylpentapeptide is transferred to the phosphate. This compound then accepts N-acetylglucosamine from UDP-N-acetylglucosamine, followed by the sequential addition of five glycyl residues, from glycyl tRNA.

It is thought that the function of the phospholipid carrier is to transport the peptidosaccharide unit through the membrane, since addition of these precursors to the growing peptidoglycan chain occurs outside the cell. Finally, the cross-linking occurs between adjacent chains, also outside the cell. This involves a transpeptidation reaction, with the enzyme involved forming an acyl-intermediate via the penultimate D-Alanine of the pentapeptide chain, displacing the terminal D-Alanine group that was present before cross-linking occurred (Mathews & van Holde,[d] 1990). This process is illustrated in Figure 1.3 with vancomycin's site of action shown (Greenwood, 1989).

All members of the vancomycin group of antibiotics have similar chemical structures (Barna & Williams, 1984), with variations arising mainly from the number, type and position of sugar components attached to the peptide backbone (Gerhard *et al.* 1993). They are all based on a peptide backbone, with side chains modified through covalent cross-linkage. It is this cross-linkage that imposes conformational restriction on various parts of the molecule. Further modifications include methylation of amines, chlorination of aromatic rings and glycosylation of hydroxyl groups (Waltho & Williams, 1991). All members of the group contain seven aromatic rings, except the first discovered member, vancomycin, which has only five (Barna & Williams, 1984), the structure of which is shown in Figure 1.4 (Waltho & Williams, 1991).

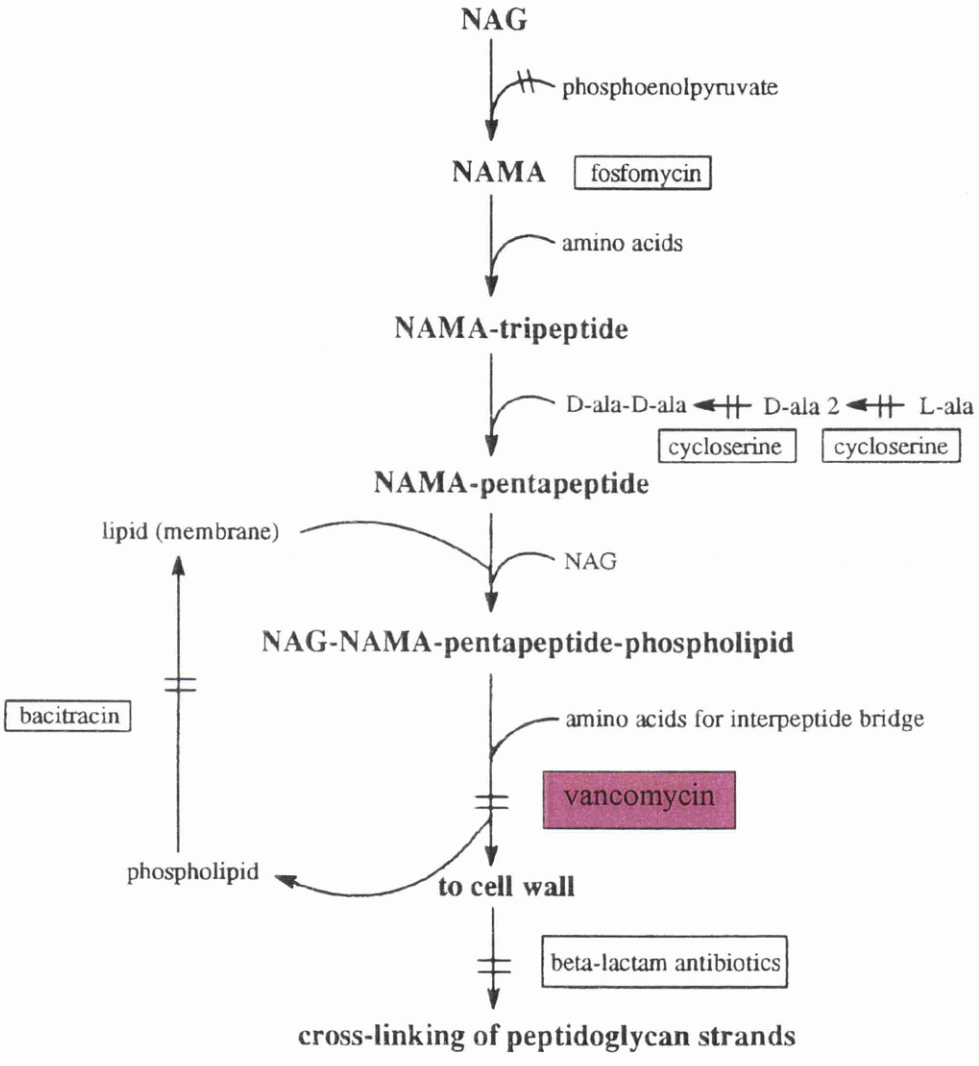

Figure 1.3 Biosynthesis of the bacterial cell wall, showing site of action of vancomycin.

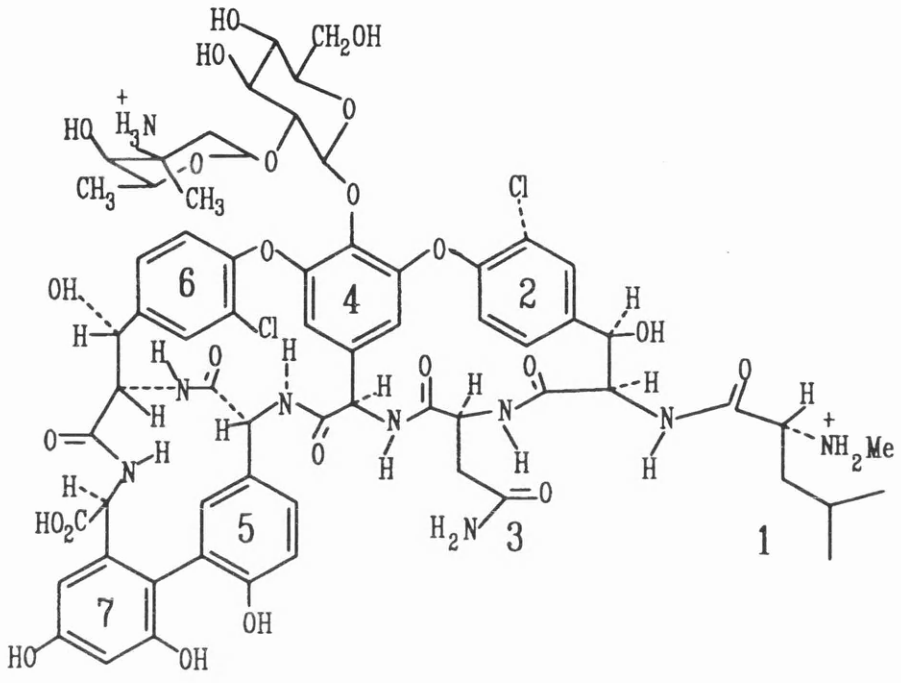

Figure 1.4 The covalent structure of the antibiotic vancomycin and the numbering scheme for the constituent amino residues.

Structural determination of these antibiotics has involved many years of study, although isolation occurred in the early 1950's, it is only recently that the antibiotic structure has become well defined. Techniques used have included NMR (Waltho & Williams, 1989), UV spectroscopy (Nieto & Perkins,[a,b] 1971) and in the case of vancomycin, X-ray crystallography. Early attempts to determine the crystal structure of vancomycin involved the degradation product, CDP-I (Sheldrick *et al.*, 1978) obtained from hydrolysis of the side chain amide linkage of the asparagine residue on vancomycin to form a free carboxylic acid, shown in Figure 1.5 (Antipas *et al.*, 1994). CDP-I exists as two rotamers, CDP-I major (CDP-IM) and CDP-I minor (CDP-Im), the difference between the two being that the orientation of the chlorine on ring 2 differs by 180° (Antipas *et al.*, 1994).

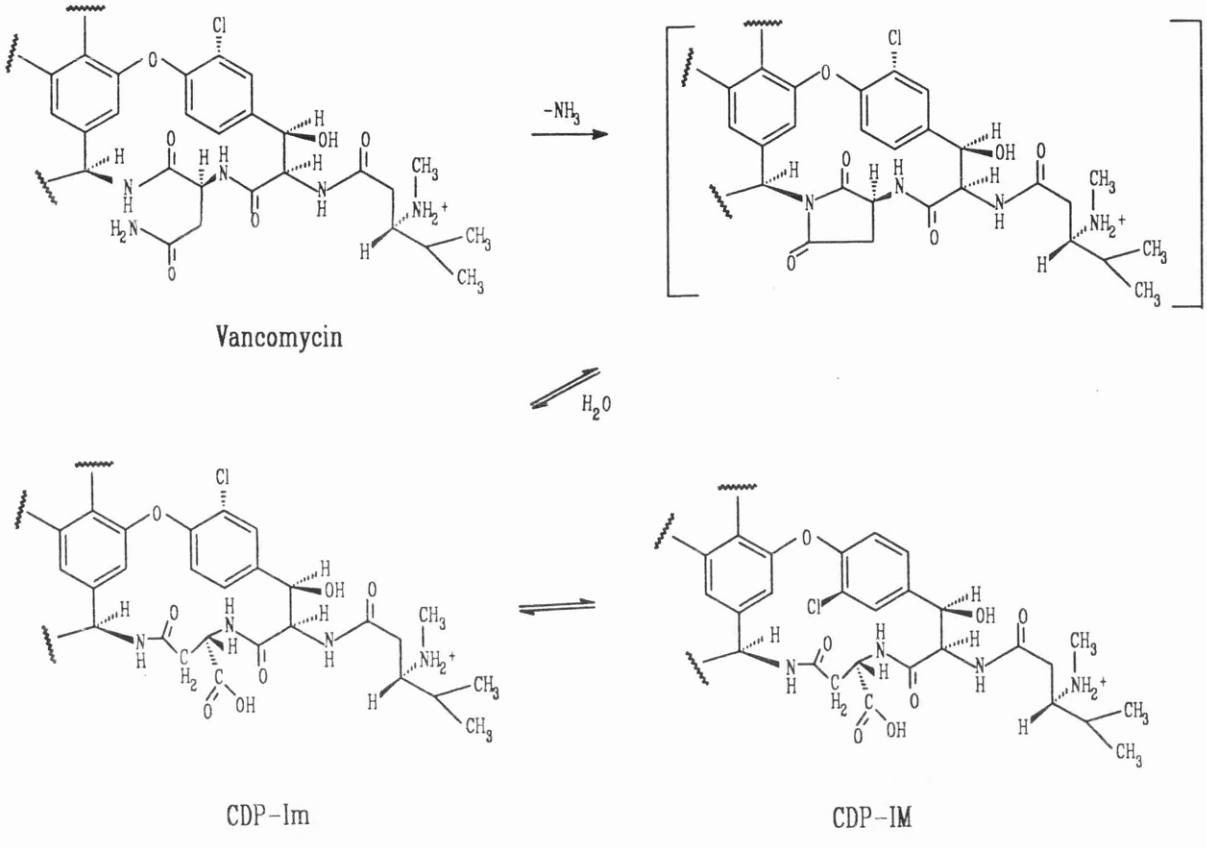

Figure 1.5 Deamidation scheme for vancomycin.

The first reported crystal structure of a naturally occurring member of the vancomycin family which was not the subject of degradation and ring rearrangement was that of ureido-balhimycin, which is obtained as a minor product in the extraction of balhimycin. This is structurally similar to vancomycin since removal of the sugar residues from both vancomycin and balhimycin results in the same compound (Sheldrick *et al.*, 1995). Only recently has it been possible to determine the crystal structure of vancomycin directly (Schafer *et al.*, 1996). NMR studies have involved ristocetin A and the results obtained have also been applied to vancomycin, since both exhibit structural similarities. Both vancomycin and ristocetin are known to contain novel amino sugars. Vancomycin contains the sugar vancosamine, linked via a glucose molecule attached to residue 4. Ristocetin A has ristosamine and the sugar mannose along with a tetrasaccharide

containing arabinose, mannose, glucose and rhamnose attached to residue 4 (Searle *et al.*, 1994).

Vancomycin has been shown to combine with various short peptides, with the strongest binding occurring when the ligand side chain terminates in the amino acid sequence L-Lys-D-Ala-D-Ala (Nieto & Perkins,[a] 1971) i.e. most closely resembling that which is incorporated into bacterial peptidoglycan in the form of N-acetylmuramylpentapeptide. This peptide therefore acts as a substitute for the antibiotic's natural substrate. Pioneering studies on vancomycin showed that residues beyond residue three on the peptide hardly interacted with vancomycin and therefore appeared not to be as important to the binding process (Nieto & Perkins,[a] 1971). Optimum complex formation between vancomycin and ligand was also shown by these researchers to require an L-amino acid, rather than a D-amino acid, in the third position on the peptide and that the end carboxyl group on the peptide must be free.

Binding of vancomycin to ligand occurs via hydrogen bonding between the carbonyl groups of one component and the amino groups of the other component. Three amino groups at the N-terminal end of the antibiotic form hydrogen bonds with the carboxylate ion on the C-terminus of the peptide. Other hydrogen bonds are formed between the carbonyl group on residue 4 and the amino group of the C-terminal alanine on the peptide and between the amino group on residue 7 and the N-acetyl carbonyl group on the peptide (Waltho & Williams, 1991). A conformational change occurs on binding, with the formation of a carboxylate binding pocket into which the peptide fits, through flexibility of the peptide portion of the antibiotic, namely the side chains of residues 1 and 3 i.e. N-methyl-D-Leucine and L-Asparagine, respectively. The hydrophobic leucine side chain forms one side of the binding pocket and asparagine the other (Williamson *et al.*, 1984). Within the binding pocket, the close proximity of the amino groups in the antibiotic to the carboxylate group on the peptide, seems to suggest that some electrostatic stabilisation will occur (Cristofaro *et al.*, 1995). Electrostatic interactions between the peptide carboxylate and the amino groups of the antibiotic are shielded from

solvation by the hydrophobic side chain of residue 1 and to a lesser extent by that of residue 3 (Waltho & Williams, 1989). These electrostatic interactions are known to be strengthened in a less polar environment (Cristofaro *et al.*, 1995) since ions of opposite charge can attract each other more strongly in a medium of lower dielectric constant than in aqueous solution.

The structure of ristocetin is less flexible than vancomycin due to an increase in the number of aromatic rings which impose conformational restrictions on the antibiotic. The side chain that is N-methyl-D-Leucine in vancomycin is replaced by an aromatic side chain in ristocetin, which in turn, is linked to another aromatic ring, further restricting its mobility (Williamson *et al.*, 1984). A diagrammatic representation of the structure of ristocetin is shown in Figure 1.6 (Waltho & Williams, 1991) with a 'ball and stick' model (kindly supplied by D. H. Williams) of the aglycone portion of the antibiotic complexed with peptide in Figure 1.7.

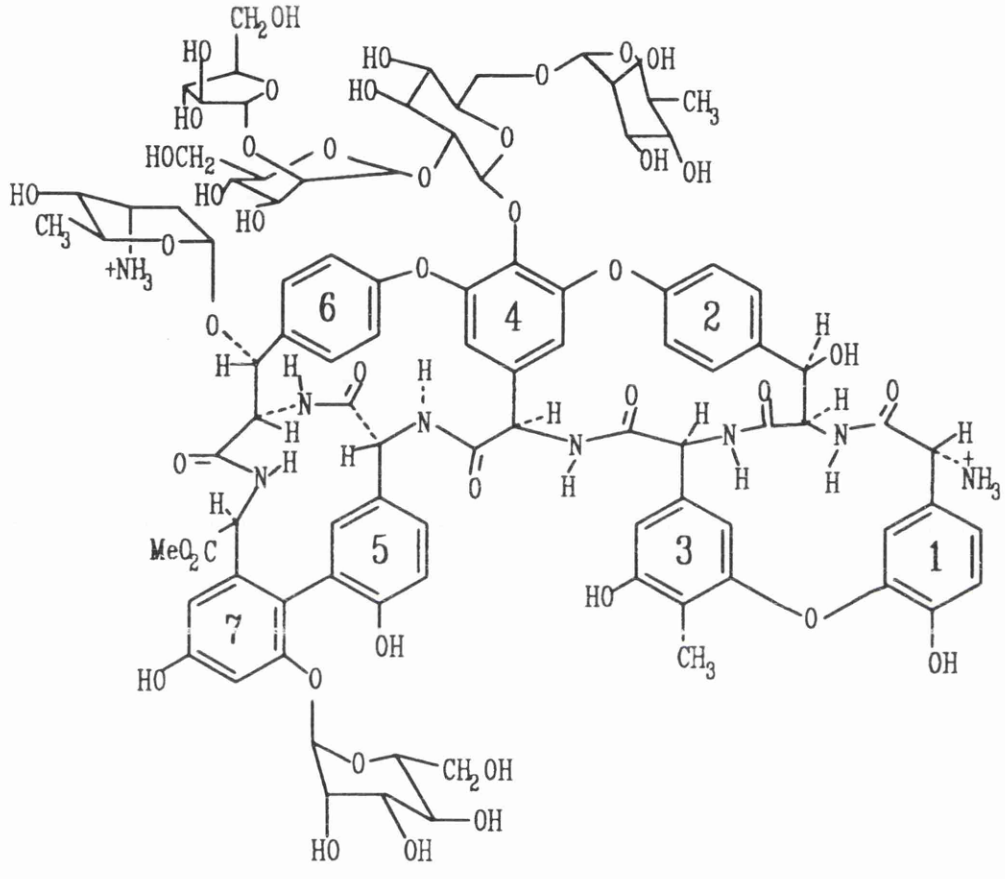

Figure 1.6 The covalent structure of the antibiotic ristocetin and the numbering scheme for the constituent amino residues.

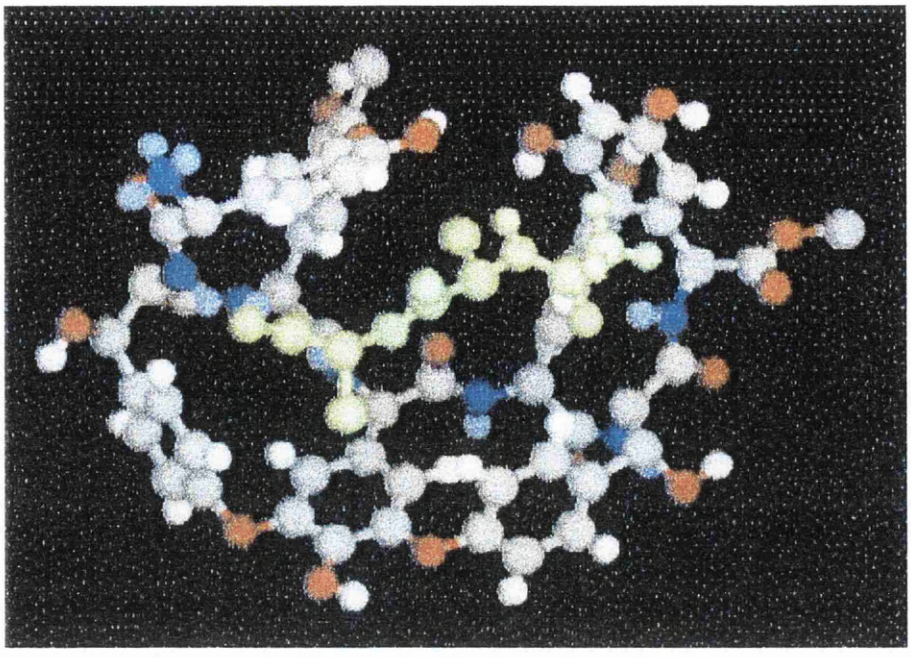

antibiotic colour convention:

grey=carbon, red=oxygen, white=hydrogen, blue=nitrogen, light blue=hydrogens attached to nitrogens

Figure 1.7 Aglycone portion of ristocetin complexed with the cell wall peptide, N-acetyl-D-Ala-D-Ala (non-hydrogens shown in green).

Ristocetin's binding site is similar to that of vancomycin and contains three amino groups situated close together that are able to form hydrogen bonds with a carboxylate ion on the peptide and two other amino groups for further hydrogen bonding. Such an arrangement is shown in Figure 1.8 (Williams & Maplestone, 1992). The ligand to antibiotic hydrogen bonding interactions have optimal geometries within the binding site with carbonyl to amino group distances in the range 1.79-1.85Å, which represents good van der Waals complementarity between cell wall peptide and binding pocket (Groves *et al.*, 1995), see Table 1.1. The antibiotic has hydrophobic regions corresponding to hydrophobic regions on the peptide (Williamson *et al.*, 1984). The hydrophobic regions on the peptide are the methyl groups on the alanine residues which fit into methyl shaped cavities in the antibiotic. As with vancomycin, a conformational change occurs on binding. Ring 4 folds over the carboxylate ion, forming part of the hydrophobic binding

pocket, with rings 2, 3 and the C-terminal alanine methyl group forming the other part (Williamson *et al.*, 1984).

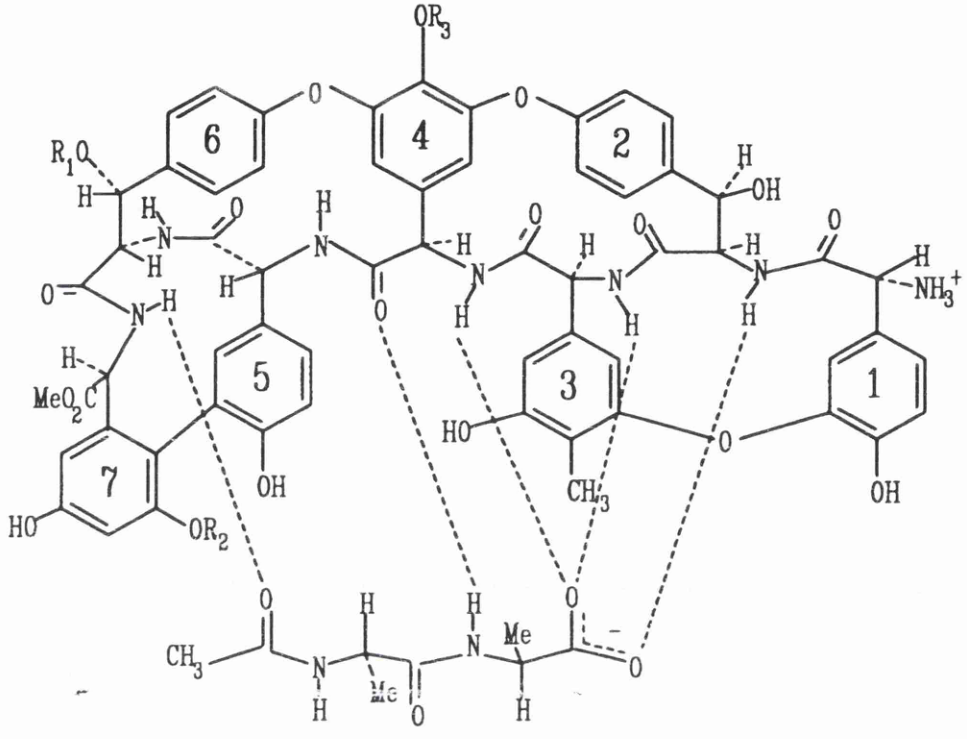

Figure 1.8 Schematic representation of the complex formed between ristocetin and a bacterial cell wall peptide model, N-acetyl-D-Ala-D-Ala. The broken lines indicate the positions of intermolecular hydrogen bonds.

1.3.1 Dimerisation of the antibiotics

Both vancomycin and ristocetin A are thought to aggregate in aqueous solution. This self-association was observed in NMR experiments of ristocetin A and peptide complexes. Such studies showed that certain resonances of ristocetin A and the ristocetin A-tripeptide complex in water are present as two forms in slow exchange (Waltho & Williams, 1989), thought to be monomer and dimer. From this chemical shift evidence and NOEs, it became clear that intermolecular processes were involved in

dimer stabilisation. The NOE data were indicative of the formation of a dimer through the combination of the back faces of the two antibiotic monomers via hydrogen bonds (Waltho & Williams, 1989), leaving the binding sites accessible to peptide. This arrangement is in agreement with that proposed by Sheldrick *et al.*, 1995 from the crystal structure of a balhimycin derivative. All members of the vancomycin group of antibiotics are thought to dimerise, with the exception of teicoplanin which shows no measurable dimerisation, but rather forms non-specific aggregates in aqueous solution (Westwell *et al.*, 1995). The structure of the dimer is shown in Figure 1.9 (Searle *et al.*, 1994). The hydrogen bonding interactions between the peptide backbones of the antibiotic monomers occur in a symmetrical head-to-tail orientation, with the six hydrogen bonds involved (four between the peptide backbone and two between the ristosamine sugars) having carbonyl to amino group distances between 1.8 and 2.3Å (Groves *et al.*, 1995). Other contributions to dimerisation include electrostatic interactions, arising from σ-π interactions, where the C-H bond of one aromatic ring is inserted into the π electron cloud of a second aromatic ring (Groves *et al.*, 1994).

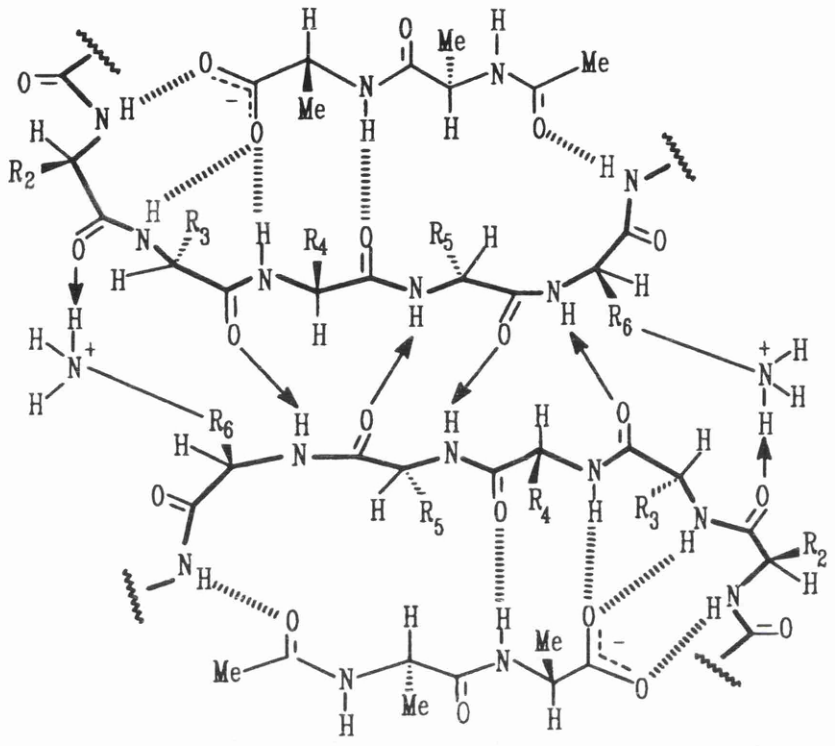

Figure 1.9 Structure of the dimer complex of N-acetyl-D-Ala-D-Ala. Bold lines represent the peptide backbone of the antibiotic. Dashed lines represent hydrogen bonds between ligand and antibiotic, while arrows correspond to hydrogen bonds between the two halves of the dimer.

In addition to the sugar residues on the antibiotics increasing the aqueous solubility of the antibiotics, they are known to make contributions towards both binding selectivity and dimerisation (Gerhard *et al.*, 1993). When vancosamine on vancomycin is selectively removed, the association constant between antibiotic and peptide is significantly reduced (Waltho & Williams, 1991), indicating that it plays a role in the binding process. On complexation with peptide ligand, NOE data show that the methyl group at the 6-position on vancosamine is close to a proton on aromatic ring 2 and also to the methyl group of the C-terminal alanine residue of the peptide ligand. It is this position of vancosamine in the antibiotic-peptide complex that suggests it is an extension of the hydrophobic binding pocket to accomodate the methyl group of the C-terminal

alanine residue by the methyl group on vancosamine that is the major interaction stabilising the complex (Waltho & Williams, 1991). The sugar residues present in both vancomycin and ristocetin A also appear to play a role in the dimerisation process. The interactions between the tetrasaccharides in ristocetin A are shown in Figure 1.10 (Searle *et al.*, 1994). In the case of ristocetin A, the removal of the tetrasaccharide from residue 4 results in a significant decrease in dimerisation constant, suggesting that it is involved in the stabilisation of the dimer, possibly through interaction between disaccharides in the dimer or between disaccharide and peptide portion of the dimer (Gerhard *et al.*, 1993). The tetrasaccharides are arranged in a parallel, head-to-head alignment due to a 180° rotation, producing an overall dimer asymmetry (Groves *et al.*, 1995). Chlorine substituents on the antibiotics also appear to be important in the dimerisation process. Molecular modelling of another vancomycin group antibiotic, eremomycin, showed that there is a region bordered by the ring 6 amino sugar and the aromatic ring 6 of one half of the dimer and the aromatic ring 4, the disaccharide portion and the peptide backbone of the other half of the dimer, into which the ring 2 chlorine substituent of the latter molecule can fit (Gerhard *et al.*, 1993), with this arrangement being thought to stabilise the dimer.

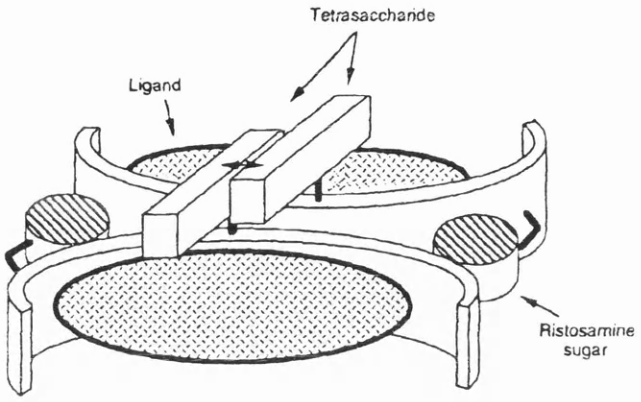

Figure 1.10 Schematic representation of the antibiotic dimer-ligand complex, illustrating the interplay between the various interactions at the ligand-antibiotic interface and dimer interface.

Microcalorimetric binding studies using vancomycin and the dipeptide N-acetyl-D-Ala-D-Ala, and related peptide analogues showed that apparent association constants and enthalpy changes had some dependence on antibiotic concentration. When the concentration of antibiotic was increased, thermal titration curves showed anomalous behaviour, inconsistent with simple 1:1 complex formation, suggesting possible antibiotic aggregation at high concentrations. Only ligand binding studies using much lower antibiotic concentrations gave straightforward 1:1 binding isotherms (Cooper & McAuley-Hecht, 1993), illustrating that the ligand binding properties of the antibiotic dimer are different from those of the monomer. The presence of ligand gives an increase in dimerisation constant of vancomycin e.g. vancomycin alone has a K_{dim} of $700M^{-1}$ but in the presence of acetyl-D-Ala, this is increased to $1300M^{-1}$. This shows that dimerisation is not simply a function of the interactions made at the dimer interface, but also depends on changes in interactions removed from this area e.g. at the binding site (Williams *et al.*, 1994). Therefore, if ligand encourages dimer formation, it follows that dimerisation enhances ligand binding (Mackay *et al.*, 1994). The cooperativity that exists between vancomycin dimerisation and ligand binding can be demonstrated by considering the following ligand induced dimerisation model:

$A + A \rightleftharpoons A_2$				$K_D = [A_2]/[A]^2$	ΔH_D
$A + X \rightleftharpoons AX$				$K_1 = [AX]/[A][X]$	ΔH_1
$A_2 + X \rightleftharpoons A_2X$				$K_2 = [A_2X]/[A_2][X]$	ΔH_2
$A_2X + X \rightleftharpoons A_2X_2$				$K_3 = [A_2X_2]/[A_2X][X]$	ΔH_3
$AX + AX \rightleftharpoons A_2X_2$				$K_D' = [A_2X_2]/[AX]^2$	$\Delta H_D'$

This assumes two identical, non-interacting binding sites on the antibiotic dimer. If $K_2 > K_1$, indicating that a dimer binds ligand more strongly than its corresponding monomer, it seems reasonable to assume that ligand binding will induce dimerisation (Cooper & McAuley-Hecht, 1993). A possible reason put forward for this cooperativity is that the amide dipoles of the antibiotic are ordered more strongly by ligand than solvent, therefore hydrogen bonding at the dimer interface will be strengthened enthalpically but with a compensating cost in entropy due to an increase in the order of the complex (Williams *et al.*, 1994).

Although vancomycin exhibits ligand induced dimerisation, another member of the same group of antibiotics, ristocetin A, exhibits ligand induced dissociation i.e. the presence of cell wall peptides encourages dissociation of the dimer. Therefore, there is anti-cooperativity between ristocetin A dimerisation and ligand binding. It was found that ristocetin A had a dimerisation constant of $500M^{-1}$ in the absence of ligand, with this being reduced to $350M^{-1}$ upon introduction of the natural substrate -L-Lys-D-Ala-D-Ala (Searle *et al.*, 1994). Similar results were found using isothermal microcalorimetry (Cooper & McAuley-Hecht, 1993). It is thought that if the amino group of the sugar attached to residue 6 of ristocetin A forms a salt bridge to the carboxylate anion of the cell wall analogue peptide (Mackay *et al.*, 1994), this arrangement would encourage cooperativity (Searle *et al.*, 1994). Since the ristosamine sugar of ristocetin A is thought to take part in hydrogen bonding at the dimer interface, if a change in orientation

of this sugar residue occurred on ligand binding, this would interfere with the dimerisation process (Searle *et al.*, 1994), possibly resulting in anti-cooperativity between dimerisation and ligand binding. Removal of the tetrasaccharide and mannose substituents of ristocetin A to give ristocetin ψ reduces the dimerisation constant in the absence of ligand by a factor of approximately 10 (Williams *et al.*, 1993). Although dimerisation of ristocetin A is discouraged in the presence of cell wall analogue peptides, dimerisation of ristocetin ψ is enhanced cooperatively in the presence of such ligands, suggesting that although the tetrasaccharide promotes dimerisation of ristocetin A, it interferes anti-cooperatively with dimerisation in the presence of cell wall analogue peptides (Searle *et al.*, 1994). Therefore, the tetrasaccharide appears to be important in the apparent change from cooperativity of ristocetin ψ to anti-cooperativity of ristocetin A. It is also thought that the parallel alignment of the tetrasaccharides in ristocetin A leads to different sugars 'capping' the two ligand binding sites in the dimer and therefore produces significant differences in binding interactions with cell wall peptides occupying the two different sites on the dimer (Groves *et al.*, 1995). In other words, the dimer form of ristocetin A appears to have sites with different affinities for ligand due to a difference in orientation of the tetrasaccharides, possibly contributing to the anti-cooperativity characteristic.

It is thought that dimer formation may play an important functional role *in vivo* during interactions at the cell wall surface. If D-Ala-D-Ala precursor units are concentrated locally on the bacterial cell wall, a dimer would be more efficient at exerting its bactericidal action by being targeted more effectively (Waltho & Williams, 1989). The binding of one half of the dimer to the cell wall makes the second binding event essentially intramolecular, shown in Figure 1.11 (Beauregard *et al.*, 1995), which is more favourable since there would not be such a loss of entropy as if it were intermolecular. Similarly teicoplanin, although not exhibiting dimerisation possibly due to modification of sugars attached to residue 4, anchors itself to the bacterial cell membrane via a fatty acid sidechain on the residue 4 saccharide, also making binding to cell wall peptides an intramolecular process, also shown in Figure 1.11. Therefore promoting

antibacterial action in such a way as to compensate for the lack of dimerisation (Beauregard *et al.*, 1995). The relationship between dimerisation and ligand binding represents a simple model for biological signalling, whereby the formation of a dimer induces some change in the antibiotic, which in turn affects the binding affinity for cell wall analogues (Mackay *et al.*, 1994) and therefore its function.

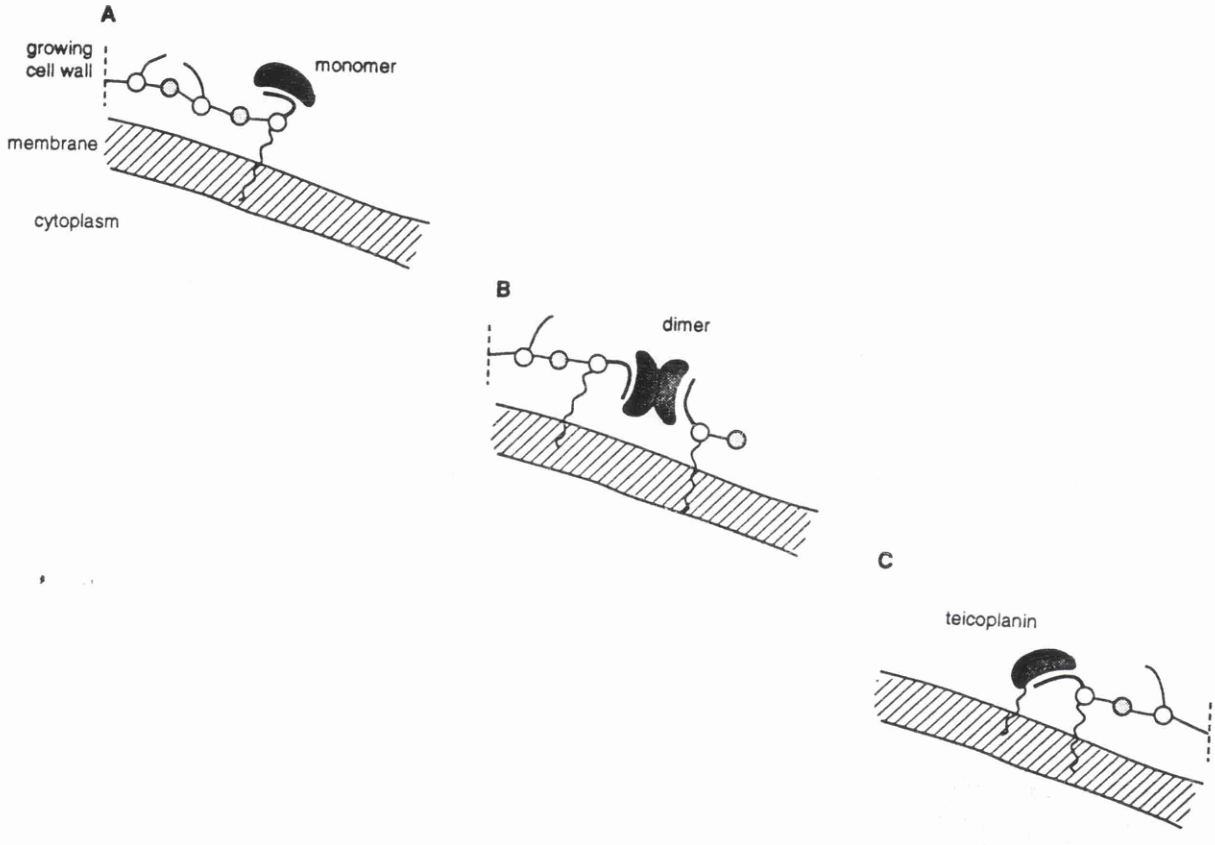

Figure 1.11 Intramolecular binding of dimeric antibiotics and teicoplanin to cell wall subunits illustrating enhancement through the chelate effect. The growing cell wall is attached to a C_{55} lipid, which anchors it to the cytoplasmic membrane while elongation by transglycosylation occurs. Cell wall repeat units are composed of N-acetylmuramate-N-acetylglucosamine disaccharide which carries a pentapeptide terminating in -peptidyl-D-Ala-D-Ala (bold line). (**A**) The binding of two monomeric glycopeptide antibiotics requires two bimolecular steps. (**B**) In contrast, the binding of a glycopeptide dimer is enhanced because the second binding event is essentially intramolecular. (**C**) Teicoplanin, anchored to the membrane through the undecanoyl substituent, binds to the cell wall in an analogous intramolecular manner.

It is important to understand the ways in which these antibiotics achieve dimerisation to allow the synthesis of modified structures which can be more effective as antibiotics due to an increased tendency to dimerise.

1.3.2 Antibiotic resistance

Vancomycin was introduced about 40 years ago to treat penicillin-resistant staphylococci, but due to its high levels of toxicity and the introduction of methicillin, vancomycin soon became an alternate agent, assuming the role of second-line therapy (Fekety, 1995). With the increase in methicillin resistance in *Staphylococcus aureus* and penicillin resistance in enterococci, vancomycin was reintroduced as a therapeutic agent in an attempt to control this increase in antibiotic resistance. The extensive use of vancomycin to treat infections caused by gram-positive bacteria, has now led to the appearance of vancomycin resistance in enterococci. Until the mid 1980s, there was little evidence of the emergence of vancomycin resistance in gram-positive bacteria (Woodford & Johnson, 1994), but now it is known that such resistance has arisen, the mechanism by which this occurs has begun to be investigated.

Bacteria can resist antibiotics in a variety of ways, such as chromosomal mutation or induced expression of a latent chromosomal gene or by exchange of genetic material through transformation, transduction, conjugation by plasmids or transposition (Neu, 1992). There are three glycopeptide resistance phenotypes in enterococci i.e. VanA, VanB and VanC, with all three phenotypes arising from a common resistance mechanism. The VanA type is transferable and exhibits high level resistance to vancomycin and cross-resistance to teicoplanin. The VanB type is non-transferrable and is resistant to low vancomycin concentrations and sensitive to teicoplanin. Both VanA and VanB are inducible, whereas VanC is constitutive i.e. non-inducible and shows low level resistance to vancomycin and sensitivity to teicoplanin (Woodford & Johnson, 1994). Since the target for vancomycin is the -D-Ala-D-Ala terminus in peptidoglycan

strains and is produced by the enzyme D-Ala-D-Ala ligase, the *vanA*, *vanB and vanC* genes produce ligases with altered substrate specificities and result in the production of altered peptidoglycan side chains that are not 'recognised' by vancomycin, therefore conferring resistance (Woodford & Johnson, 1994).

Enterococci of the VanA phenotype produce precursors with side chains terminating in D-Ala-D-Lactate which are then incorporated into the peptidoglycan. It is thought that a modification of the peptidoglycan biosynthetic pathway of this sort could be tolerated without compromising the overall structure of the peptidoglycan (Rasmussen & Strominger, 1978 : Allen *et al.*, 1992). The *vanA* gene product is a D-Ala-D-Ala ligase of altered substrate specificity (Bugg *et al.*,[a,b] 1991) and forms this D-Ala-D-Lactate peptide, but another two genes *vanH* and *vanX* are also responsible for the expression of resistance. The *vanH* gene product is an α keto acid dehydrogenase which catalyses the formation of D-Ala-D-Lactate (Billot-Klein *et al.*,[b] 1994) from pyruvate, but the function of the *vanX* gene product has not been determined.

In the VanA *Enterococcus faecium* strain, the *vanA*, *vanH* and *vanX* genes are present on a transposable element. This transposon also carries two genes (*vanS* and *vanR*) that regulate the expression of glycopeptide resistance and two genes (*vanY* and *vanZ*) which are not essential for resistance expression (Woodford & Johnson, 1994). If conjugative transposition occurs, it is possible that resistance could spread to other species (Neu, 1992). Although the mechanism of glycopeptide resistance has been determined in more detail for enterococci of the VanA resistance phenotype, the *vanB* and *vanC* genes are also known to encode alternative D-Ala-D-Ala ligases (Woodford & Johnson, 1994).

At present, vancomycin is used to treat the staphylococcal infection, MRSA (methicillin-resistant *Staphylococcus aureus*). MRSA is a virulent microorganism killing around 20 people in the UK each year. Health authorities believe it can be found in half of the UK's hospitals due to its prevalence in a high number of cases of post-surgical infections. MRSA resistance to other antibiotics is well known, therefore its susceptibility to

vancomycin makes this antibiotic the last line in defence against such infections. Since vancomycin resistance has emerged in enterococcal species, if this resistance can be transferred from vancomycin to MRSA, conventional antibiotics will be unable to respond, therefore increasing the need for novel antibiotics to which resistance has not yet developed. Rather than relying entirely on the soil for bacteria and fungi to produce antibiotics, our search for appropriate antibacterial compounds could be widened to include bacteria from the marine environment. It is well documented that there are bacteria that produce inhibitory substances in the marine environment, even if they are not specifically antibiotic producers (Austin, 1989). Therefore, it may be possible to clinically produce a compound derived from marine bacteria to inhibit MRSA, keeping us one step ahead of this bacteria's increasing resistance.

1.4 Non-covalent interactions

The interplay of the many weak non-covalent interactions involved in molecular recognition creates a complex model, the individual factors of which are now becoming more clearly understood. Even though these forces are relatively weak, they are still large enough to ensure that the correct molecules interact with each other. Such interactions are important in biological systems due to their ability to be broken and reformed under physiological conditions. If forces were too strong, the rapid change in interactions that usually occur would be perturbed, therefore having a detrimental effect on the living system. The energy of the strongest weak bond is only about ten times greater than the average energy of kinetic motion at 25°C ($2.5 kJmol^{-1}$). Since there is a significant spread in the energies of kinetic motion, there will be a large number of molecules with sufficient kinetic energy to break even the strongest weak bond at physiological temperatures (Watson *et al.*, 1987). Non-covalent interactions are fundamentally electrostatic in origin and the types involved in biological systems are as follows:

1.4.1 Hydrogen bonding

An important interaction in biological systems is the hydrogen bond. It is formed for example, between a covalently bonded hydrogen atom on a donor group (-OH or $\diagup$N-H$\diagdown$) with a pair of non-bonding electrons on an acceptor group (O=C $\diagdown$ or N $\diagup\!\!\diagup$ or S $\diagdown$). The strength of the donor depends upon its electronegativity i.e. how much negative charge has been withdrawn from the hydrogen atom. In biological systems, the only atoms that have appropriate electronegativities to act as donors are oxygen and nitrogen. Hydrogen bonds are both non-covalent and covalent in character. They are non-covalent in the respect that there is a major electrostatic contribution arising from the partial positive charge on the hydrogen of the donor group being attracted by the negative charge concentrated on the unpaired electrons of the acceptor group. The covalent character of the bond is indicated by the fact they are directional in nature (more so than van der Waals forces although less so than covalent bonds). By directional we mean that in a hydrogen bonding arrangement there is for example, one O-H covalent bond and one H...O hydrogen bond. If the O-H...O are all co-linear then the hydrogen bond will be strongest, but if the geometry of the surrounding framework means that a 'line' drawn along the covalent bond doesn't go through the other O atom then the bond will be weaker. The energy of the hydrogen bond *in vacuo* (10-30kJmol^{-1}) is considerably higher than that of most other non-covalent interactions (Watson *et al.*, 1987) and therefore is the strongest non-covalent interaction.

1.4.2 Hydrophobic effect

The hydrophobic effect is the name given to the process by which non-polar substances minimise their contacts with water and can be illustrated by considering the introduction of a hydrophobic molecule into the aqueous phase. A non-polar group can neither accept or donate hydrogen bonds so that water molecules at the surface of the cavity occupied by the non-polar group cannot hydrogen bond to other molecules in the usual way. In order to recover this loss in hydrogen bonding energy, the water molecules orientate

themselves to form as many hydrogen bonds as possible in a network which encloses the cavity containing the non-polar group (Voet & Voet,[b] 1990). This has two thermodynamic effects. One being the reduction in entropy due to ordering of the water molecules resulting in a more ordered structure than in bulk solvent and the other is due to the reduction in enthalpy caused by the increase in the number of water-water hydrogen bonds, since bond formation is exothermic and this causes the system to go to a lower enthalpy. The entropy is further decreased as the non-polar molecule itself loses much of its original rotational and translational entropy (Aronow & Witten, 1960 : Howarth, 1975). This ordering of water molecules to form hydrogen bonded 'cage-like' structures is in contrast to the hydration shells formed around polar substances. In order to minimise these effects, non-polar molecules reduce their hydrophobic surface area in contact with solvent, by forming the classical oil drop from which solvent is excluded. The hydrophobic effect therefore results not from the attractive forces between the non-polar molecules but rather results from the mutual repulsion of solute and solvent molecules which is driven by solvent entropy requirements. It is this effect which energetically drives polypeptide chains within the aqueous environment of the cell to assume configurations that effectively isolate their non-polar side groups within the interior of the protein molecule into which water molecules cannot penetrate (Watson *et al.*, 1987). The hydrophobic effect can also be approached in another way. On complexation with another molecule or upon protein folding, these hydrophobic regions become buried within the molecule, forcing the ordered water molecules out to join the surrounding bulk solvent. This increases the randomness of the system and therefore its entropy (Mathews & van Holde,[b] 1990). This is accompanied by an increase in enthalpy due to the reduction in water-water hydrogen bonds. The hydrophobic effect only stabilises proteins near ambient temperatures. On an increase in temperature, the loss of entropy brought about by the ordering of water molecules around hydrophobic residues in the unfolded protein is diminished, which contributes to instability of the folded protein (Perutz, 1992). This effect is frequently referred to as hydrophobic bonding, although it is not hydrophobic bonds which are formed between non-polar groups in an

aqueous solution, but rather an absence of bonds. The bonds which form between such groups are due to van der Waals attractive forces (Watson *et al.*, 1987).

1.4.3 Electrostatic interactions

Such interactions occur between charged groups, since charged entities exert forces on one another. The energy required to separate two charged particles (q_1 and q_2) from a distance r, to an infinite distance is given by Coulombs Law:

$$U = \frac{kq_1q_2}{\varepsilon r^2} \qquad (1.1)$$

where U = energy of interaction

k = a constant (9.0×10^{9} JmC^{-2})

ε = dielectric constant for the medium

The presence of a dielectric medium between charges has the effect of reducing the interaction energy between them. Dielectric effects arise from the electric field between charges polarizing the material involved. However, once these charges are placed in a dielectric medium, which can be thought of as being made up of a large number of microscopic dipoles, the electric field caused by these dipoles will oppose the original electric field, causing a reduction in the electric field potential and therefore in the interaction energy between the charges. The dipoles of the material will orientate themselves along the field lines in such a way so that its positive end points towards the negative charge and vice versa. The microscopic dipoles of the medium have two sources, electric polarizability and orientational polarizability. The first occurs when an atom is placed in an electric field and the electron cloud around the nucleus is displaced, inducing a dipole. This dipole then contributes to the dielectric constant of the medium. The second arises if the molecules of the material have an intrinsic dipole moment which is free to rotate. If this is the case, the dipoles will always tend to align themselves to

oppose the external field. The larger the dipole moment, the greater the induced field and therefore the greater the dielectric constant.

Water has a very high dipole moment due to the electronegativity of the oxygen and since the hydrogen to oxygen bond is short, with a dielectric constant of 78.5, whereas organic solvents such as methanol and benzene have much lower values i.e. 32.6 and 2.3, respectively. Therefore, in non-polar solvents, ions of opposite charge attract each other more strongly than they would in aqueous solution (Voet & Voet,[a] 1990).

Electrostatic interactions between molecules are modified in the presence of small ions, such as those from salts in the same solution. These small ions will collect around a macromolecule of opposite charge forming a counter-ion atmosphere which screens it from another molecule. The larger the concentration of small ions present, the more effective this screening will be. The quantitative expression of this effect is called the Debye-Huckel theory and is expressed in terms of an effective radius (Debye radius) r_D, of the counter-ion atmosphere, as follows:

$$r_D = \frac{K}{I^{1/2}} \qquad (1.2)$$

where K = constant depending on dielectric constant of medium
I = ionic strength

The Debye radius strongly depends on ionic strength i.e. the higher the ionic strength the shorter the Debye radius, therefore the greater the ionic screening effect. The effect of ionic screening on the interaction between charges in the presence of salt can be approximated by the following expression:

$$U_I = U.e^{-r/rD} \qquad (1.3)$$

where U_I = interaction energy in the presence of salt

U = interaction energy in the absence of salt

r = distance between charges

r_D = Debye radius

Ionic strength is defined as:

$$I = \frac{1}{2} \sum_i M_i Z_i^2 \qquad (1.4)$$

where M_i = molarity

Z_i = stoichiometric charge

For a 1:1 electrolyte like NaCl, $Z_{Na+} = +1$, $Z_{Cl-} = -1$ and since $M_{Na+} = M_{Cl-} = M_{NaCl}$, the ionic strength is equal to the molarity. This, however is untrue for divalent and trivalent ions since these make a greater individual contribution to the ion atmosphere surrounding the charged macromolecule than do monovalent ones, since the square of the ion charge is included in calculating the ionic strength. Ionic strength of the medium has a major influence on the screening process. At low ionic strengths, the counter-ion atmosphere is diffuse and highly expanded, making screening ineffective. However, at high ionic strengths, the counter-ion atmosphere shrinks and becomes concentrated around the macromolecule, making screening more effective (Mathews & van Holde,[a] 1990).

1.4.4 van der Waals forces

van der Waals bonding is the name given to weak forces that exist between all atoms and are responsible for numerous interactions of varying strengths between non-bonded neighbouring atoms. The energy of this bond varies between 4.2 and 8.4 $kJmol^{-1}$, only slightly greater than the kinetic energy of heat motion (Watson *et al.*, 1987). They are essentially electrostatic in origin and make a major contribution to hydrogen bonding.

van der Waals forces are most effective when there is close packing between the molecules. There are essentially two types, dipole-dipole and dispersion (or London) forces. Dipole-dipole forces occur only when the molecules concerned are polar i.e. have permanent dipole moments. These dipole moments arise ($\mu = qR$) when electric charges +q and -q are separated by a distance R. Dipole-dipole forces are brought about when there is a favourable electrostatic interaction between neighbouring opposite partial charges. Two molecules which have no net charge or permanent dipole moment can also attract each other if they are close enough, since the electronic charge in a molecule is never static but fluctuates. If two molecules approach each other very closely, they will synchronise their respective fluctuating charges to generate an attractive force. These forces are known as dispersion forces and are significant only at short range (Mathews & van Holde,[a] 1990). Therefore, two neighbouring molecules interact through their instantaneous, rather than permanent dipoles (Atkins *et al.*, 1988). Individually, these dispersion forces are extremely weak, however when the great number of interatomic contacts in a protein are considered these forces make a major contribution to determining their conformations (Voet & Voet,[b] 1990). When molecules or atoms become so close together that their outer electron clouds overlap, there is a mutual repulsion between them, which increases as the distance between their centres decreases. If we combine this repulsive energy with the attractive energy from one of the forces mentioned above, the energy of a pair of molecules will vary with distance of separation as shown in Figure 1.12 (Mathews & van Holde,[a] 1990) such that the most stable distance between the centres of two molecules represents a balance between both attractive and repulsive forces. The repulsive potential is so high at short distances that it effectively acts as a barrier, preventing further approach of the molecules. This distance represents the van der Waals radius. In biochemistry it is useful to apply the concept of the van der Waals radius not only to single atoms but also to groups of atoms. Table 1.1 shows the effective radius of some atoms and groups of atoms for closest molecular packing. Each individual interaction contributes only a small amount to the overall negative enthalpy of interaction, but the sum of them can have powerful stabilising effects (Mathews & van Holde,[a] 1990). Since van der Waals forces are always

present, whether a molecule has a permanent dipole or not, we are unable to distinguish this force from other non-covalent interactions which may be involved. Therefore, measurements taken for other interactions will more likely than not also contain a contribution from van der Waals forces.

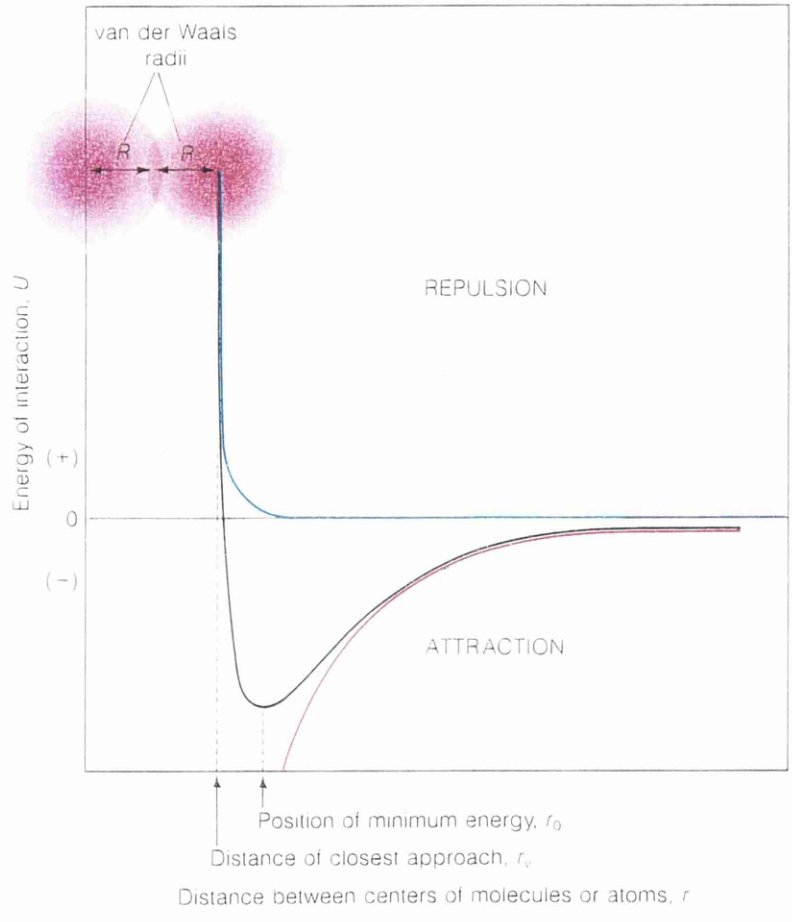

Figure 1.12 Non-covalent interaction energy between two approaching atoms or molecules. The energy (U) required to separate the particles when they are a distance *r* apart is graphed versus *r* (solid black line). This energy is the sum of two curves; the red line represents the attractive force, the blue line the repulsive force. The latter changes so rapidly with *r* that it acts effectively as a barrier, defining the distance of closest approach (r_V) and the van der Waals radii (R). The position of minimum energy (r_0) is usually very close to r_V.

Atoms/Groups	Radius (nm) (1Å = 0.1nm)
H	0.12
O	0.14
N	0.15
C	0.17
S	0.18
P	0.19
-OH	0.14
$-NH_2$	0.15
$-CH_2-$	0.20
$-CH_3$	0.20

Table 1.1 van der Waals radii of some atoms and groups of atoms (Mathews & van Holde,[a] 1990).

1.5 Basic thermodynamics

The thermodynamic parameters important in antibiotic dimerisation and ligand binding are the standard enthalpy change ($\Delta H°$), the standard entropy change ($\Delta S°$), the standard Gibbs free energy ($\Delta G°$) and the molar heat capacity change (ΔC_p). The ° sign denotes standard molar values.

We can define the standard enthalpy change ($\Delta H°$) at constant pressure by the following equation:

$$\Delta H° = \Delta U° + P\Delta V \qquad (1.5)$$

where U is the internal energy of the system tied up in the form of molecular motions and forces

ΔU° is the change in internal energy of the system

P is the pressure

ΔV is the change in volume

Every substance has an internal energy and this takes the form of the sum of the kinetic and potential contributions to the energy of all atoms, ions and molecules within the system. It is the grand total energy of the system. It is impossible to measure internal energy itself since it includes the energies of all the electrons and all the components of the atomic nuclei. But there is no difficulty associated with the measurement of changes in internal energy, since all we need to do is monitor the energy supplied or lost as heat or work. When energy is transferred into the system by heating or doing work on it, the increased energy is stored in the increased kinetic and potential energies of the molecules. Likewise when energy is lost, it is given up by the molecules as they lose kinetic or potential energy. The internal energy change can be expressed as:

$$\Delta U^\circ = q + w \qquad (1.6)$$

which takes into account the two ways in which the energy of a system can be changed.

where q is the energy supplied to the system as heat

w is the energy supplied to the system as work

A positive value of q or w means that energy is supplied to the system and a negative value signifies that energy has been lost from the system. The distinction between heat and work can be thought of in terms of differences in atomic motion produced in the surroundings. Heat is the transfer of energy that achieves or utilises disorderly motion in the surroundings, whereas work is the transfer of energy that achieves or utilises uniform motion in the surroundings. Equation 1.6 shows that work and heat are equivalent ways

of changing the internal energy of the system. It does not matter if we supply energy as heat or work or a combination of both, the change in internal energy will be the same. Heat supplied to the system can be withdrawn as work and vice versa. The internal energy of a system can be thought of as a bank, which can accept and make deposits in either of two currencies, heat or work. An important characteristic of the internal energy of a system is that it is a state function i.e. a physical property that depends only on the current state of the system and is independent of the path by which that state function was reached (Atkins,[a] 1996). Measurement of the changes in internal energy of an open system are difficult since it involves two variables, heat and work. However, by carrying out the reaction in a closed container which cannot change its volume (therefore no work can be done on the surroundings by expansion), the change in internal energy can be simplified to:

$$\Delta U^\circ = q \text{ (at constant volume)} \qquad (1.7)$$

Therefore, to measure a change in internal energy we need only measure the heat absorbed or liberated from a system which cannot change its volume.

When a quantity of energy, q, is used to heat a system open to the atmosphere, the change in U is less than q because the system does work by pushing back the atmosphere as it expands. If the constant external pressure is P and the system increases volume by ΔV, the work the system does as it expands is $P\Delta V$ and the internal energy changes by q less this quantity of work, as follows:

$$\Delta U^\circ = q - P\Delta V \qquad (1.8)$$

Since we define the enthalpy change at constant pressure as:

$$\Delta H^\circ = \Delta U^\circ + P\Delta V \qquad \text{(from equation 1.5)}$$

then

$$\Delta H^\circ = q - P\Delta V + P\Delta V \qquad (1.9)$$

therefore the energy transferred by heating causes an exactly equal change in enthalpy since

$$\Delta H^\circ = q \text{ (at constant pressure)} \qquad (1.10)$$

The enthalpy change is simply a modification of the internal energy of a system by taking into account the work of expansion when a system is heated at constant pressure. Enthalpy is equal to the heat evolved or absorbed by the system (at constant pressure) during the process. Exothermic reactions liberate heat and are denoted by negative ΔH° values, whereas endothermic reactions which require heat are denoted by positive values. These relations are consistent with the choice of the name 'enthalpy', which is derived from the Greek words meaning 'heat inside'. Enthalpy changes can be determined directly from microcalorimetry or calculated from equilibrium constants (K) over a temperature range, using the van't Hoff expression:

$$\frac{\delta \ln K}{\delta\left(\frac{1}{T}\right)} = -\frac{\Delta H^o}{R} \qquad (1.11)$$

The temperature dependence of the equilibrium constant for any process represents an effective method for estimating the enthalpy change. A plot of experimental data of lnK against 1/T gives a line with a slope equal to the van't Hoff enthalpy divided by R. In simple cases this slope is linear, but generally the temperature dependence of ΔH (due to ΔC_p, see chapter 5) results in a curved van't Hoff plot which is more complex to analyse (Cooper, 1996). From the derivation of this equation it is shown that the equilibrium constant of an exothermic reaction decreases with increasing temperature and vice versa for an endothermic reaction. These observations are consistent with Le Chateliers principle. A reduction in temperature favours an exothermic reaction, for the heat

released tends to oppose the lowering of temperature. An increase in temperature favours an endothermic reaction, for the heat absorbed tends to oppose the increase of temperature (Atkins,[b] 1996).

The standard entropy change ($\Delta S°$) at the molecular level can be expressed as:

$$\Delta S° = R\ln(w_{free}/w_{bound}) \qquad (1.12)$$

where R is the gas constant ($8.314 Jmol^{-1}K^{-1}$)

w_{free}/w_{bound} represents the ratio of the number of ways in which the system may exist in either the free or bound states

If w_{free} is greater than w_{bound}, then $\Delta S°$ will be positive due to an increase in entropy and vice versa. For changes taking place in an isolated system, entropy always increases or stays the same ($\Delta S \geq 0$) until it has reached equilibrium, where it stops increasing ($\Delta S=0$). So that, left to themselves, the molecules within the system will become as disordered as possible giving rise to an increase in entropy.

A simple definition for the change in entropy is:

$$\Delta S = \frac{q}{T} \qquad (1.13)$$

where q is the energy transferred reversibly as heat

T is the temperature at which transfer takes place

Heat rather than work appears in this equation because to transfer energy as heat we make use of the disorderly motion of molecules whereas work involves the orderly motion (as described previously). Therefore, we are measuring the degree of disorder which is proportional to the energy transfer that takes place by making use of disorderly

motion rather than orderly. The temperature term takes into account the disorder that is already present. If energy is transferred as heat to an already hot object, then the consequence of this additional energy will be less significant than if the object were cool (Atkins,[b] 1996). Therefore it is important to make the distinction.

In order to decide whether a reaction is spontaneous i.e. has a natural tendency to occur, or not, it is essential to consider the entropy of both the system and the surroundings. For example, a reaction may appear to be spontaneous by considering the system only, but there may be a more than compensating decrease in the entropy of the surroundings so that the overall entropy change is negative. The standard reaction entropy for the surroundings is:

$$\Delta S^\circ_{(\text{surroundings})} = -\frac{\Delta H^o}{T} \tag{1.14}$$

The total standard reaction entropy is the sum of the changes that take place in the system and in the surroundings:

$$\Delta S^\circ_{(\text{total})} = \Delta S^\circ_{(\text{surroundings})} + \Delta S^\circ_{(\text{system})}$$

$$= -\frac{\Delta H^o}{T} + \Delta S^\circ_{(\text{system})} \tag{1.15}$$

multiplying by -T

$$-T\,\Delta S^\circ_{(\text{total})} = \Delta H^\circ - T\Delta S^\circ_{(\text{system})}$$

which gives the equation

$$\Delta G^\circ = \Delta H^\circ - T\Delta S^\circ \tag{1.16}$$

We can see from equation 1.15 that at constant temperature and pressure the change in standard Gibbs free energy of a system is proportional to the overall change in entropy of the system plus its surroundings. The standard Gibbs free energy has both enthalpic and entropic components as demonstrated in the previous equation. The phenomenon of entropy-enthalpy compensation occurs when enthalpy and entropy changes brought about by experimental conditions tend to move in such a way that they tend to cancel each other out in the free energy term, resulting in changes in Gibbs free energy which are significantly less (see later). The Gibbs free energy is the balance at constant pressure and temperature between the tendencies of a system to maximise its entropy and to minimise its enthalpy (Smith, 1990). The condition for a reaction being spontaneous changes from $\Delta S>0$ in terms of the total entropy to $\Delta G<0$ in terms of the Gibbs energy.

Once a reaction has reached equilibrium, the standard Gibbs free energy can be related to the equilibrium constant (K) by the following equation:

$$\Delta G^{\circ} - RT\ln K \qquad (1.17)$$

where R is the gas constant
T is temperature (K)

When heat energy is added to a system at constant volume, not only does the internal energy rise, but also the temperature of the system. This suggests a relationship between the internal energy of a system and its change in temperature. For small temperature increases, the rise in temperature is proportional to the amount of heat supplied, which can be expressed as:

$$dT = \frac{q}{C_p} \qquad (1.18)$$

where dT is the increase in temperature

q is the heat supplied

C_p is the heat capacity

Since the increase in temperature is inversely proportional to the heat capacity, a system with a large heat capacity undergoes only a small increase in temperature for a given input of heat. The heat capacity of a substance depends on the size of the sample and can be reported as the specific heat capacity (the heat capacity divided by the mass of the sample i.e. $JK^{-1}g^{-1}$) or as we have in our studies, as the molar heat capacity (the heat capacity divided by the amount of substance i.e. $JK^{-1}mol^{-1}$) (Atkins,[a] 1996). The accepted definition of specific heat capacity is the amount of heat which a gram of a given substance has to exchange with its surroundings under certain conditions in order to change its temperature by one degree (Hemminger & Hohne, 1984). The change in heat capacity (ΔC_p) can provide information for example on the hydrophobic interactions between antibiotic and ligand and between antibiotic monomers in the aggregated form, since temperature dependence effects have been shown to be consistent with solvation changes associated with the burial of non-polar surfaces during macromolecular associations (Weber, 1993 : Weber, 1995 : Spolar & Record, 1994). A negative ΔC_p value suggests an increase in hydrophobic interactions and a positive value suggests a decrease in these interactions. The total enthalpy of a system in a particular state at a particular temperature can be calculated from heat capacity data, as follows:

$$H = \int C_p.dT \quad + \quad H_0 \qquad (1.19)$$

where H_0 is the ground state energy (at 0K)

The magnitude of the heat capacity data is related to entropy and the number of ways there are of distributing the added heat energy to the system. This can be illustrated in the following example, if a system has only a few ways of distributing added heat energy, then little energy would be required to raise the temperature and ΔC_p would be relatively

low. Conversely, if a system had numerous ways of distributing the heat energy, more heat would be required to raise the temperature and ΔC_p would be high. This can be expressed in the definition of a small entropy change at constant pressure, as follows:

$$dS = \frac{dH}{T} = \left(\frac{Cp}{T}\right).dT \qquad (1.20)$$

and the total entropy of the system is given by the following integrated heat capacity expression:

$$S = \int \left(\frac{Cp}{T}\right).dT \qquad (1.21)$$

These equations relate both enthalpy and entropy to the heat capacity of the system (Cooper, 1996). Calorimetry is a powerful technique which can determine these parameters from direct measurement.

These quantities are absolute values, but since we are usually interested in changes in enthalpy and entropy from one state to another, these can be re-written as:

$$\Delta H = H_B - H_A = \int \Delta C_p.dT + \Delta H(0) \qquad (1.22)$$

$$\Delta S = S_B - S_A = \int \left(\frac{\Delta Cp}{T}\right).dT \qquad (1.23)$$

where ΔC_p is the heat capacity difference between states A + B at a given temperature

$\Delta H(0)$ is the ground state enthalpy difference between A + B

These can be related to a standard reference temperature T_{ref}, giving:

$$\Delta H(T) = \Delta H(T_{ref}) + \int \Delta C_p.dT \tag{1.24}$$

$$\Delta S(T) = \Delta S(T_{ref}) + \int \left(\frac{\Delta Cp}{T}\right).dT \tag{1.25}$$

Indicating that both ΔH and ΔS are temperature dependent. These can be integrated to give approximate expressions for the temperature dependence of ΔH and ΔS with respect to some reference temperature (T_{ref}).

$$\Delta H(T) = \Delta H(T_{ref}) + \Delta C_p.(T-T_{ref}) \tag{1.26}$$

$$\Delta S(T) = \Delta S(T_{ref}) + \Delta C_p.\ln\left(\frac{T}{T_{ref}}\right) \tag{1.27}$$

For small changes in temperature with respect to absolute T_{ref}, $\delta T = T - T_{ref}$, these become:

$$\Delta H(T) = \Delta H(T_{ref}) + \Delta C_p.\delta T \tag{1.28}$$

$$\Delta S(T) = \Delta S(T_{ref}) + \Delta C_p.\ln\left(1 + \frac{\delta T}{T_{ref}}\right) \approx \Delta S(T_{ref}) + \Delta C_p.\frac{\delta T}{T_{ref}} \tag{1.29}$$

using the approximation $\ln(1 + x) \approx x$, for $x \ll 1$. Consequently, to the extent that this approximation is valid:

$$\Delta G(T) = \Delta H - T.\Delta S \approx \Delta H(T_{ref}) - T.\Delta S(T_{ref}) - \Delta C_p.\delta T^2/T_{ref} = \Delta G(T_{ref}) \tag{1.30}$$

to first order in δT. Moreover, over a limited temperature range for which this approximation is valid:

$$\Delta H(T) \approx \Delta H(T_{ref}) + T_{ref}.(\Delta S - \Delta S(T_{ref})) \quad (1.31)$$

so that a plot of ΔH versus ΔS would appear linear with slope T_{ref}. Although much could be made of the significance of such a linear correlation and the nature of T_{ref} as some sort of 'characteristic temperature', it is simply a mathematical consequence arising from experimental data covering a limited temperature range. The T_{ref} arising from such a correlation would simply be that temperature for which the approximation (δT small) is most appropriate, i.e. somewhere in the experimental observable range (McPhail & Cooper, 1997). This phenomenon of entropy-enthalpy compensation occurs when $\Delta C_p \neq$ zero, the origin of which could be solvation changes during macromolecular associations. Not only can entropy-enthalpy compensation arise from the temperature dependence of enthalpy and entropy, but also from pH and ionic strength.

1.6 Aims of thesis

The main aim of this work is to provide a greater understanding of the interactions involved in the recognition between members of the vancomycin group of antibiotics and their target cell wall peptides using microcalorimetry and how their efficiency in promoting such interactions can be altered by dimerisation. In addition, X-ray crystallography has been used in an attempt to resolve the way in which vancomycin dimers in the presence of ligand are formed. However, this proved not to be as trivial a problem as first thought, although with further work it is possible that a structure can be determined, since the growth conditions of suitable crystals have been well defined.

It is thought that the ability of these antibiotics to dimerise may represent an important functional role, therefore it is of central importance to understand their basis of action, not only from an academic point of view, but also as a means of designing potential

variants with a propensity to dimerise, in order to produce an antibiotic therapy capable of keeping us one step ahead of the increasing incidence of antibiotic resistance.

This work is essentially an extension of that carried out by K. E. McAuley-Hecht (1993), in which the molecular recognition of the vancomycin group of antibiotics was studied using microcalorimetry over a temperature and concentration range. This study suggested that the ligand binding affinities of these antibiotics were affected by concentration, therefore further work was required to investigate this phenomenon more fully.

Chapter 2:
Microcalorimetry

2.1 Introduction to microcalorimetry

Calorimetry is a technique which can be used to study the energy transactions within a sample during a biological process. Such a technique allows the direct determination of thermodynamic parameters, such as enthalpy changes, rather than relying on indirect methods involving the measurement of equilibrium constants at various temperatures and application of the van't Hoff equation. Since it measures heat directly, it is the only technique which allows simultaneous determination of all thermodynamic parameters in a single experiment, therefore providing greater accuracy. The range of applicability of calorimetry is wide and has extended down to absolute zero and to temperatures in excess of 1000°C (Skinner, 1969), depending upon the construction of the apparatus. Early calorimeters were known to be slow to equilibrate and use, but over the years much faster calorimeters have been developed and the sensitivity of such instruments has increased to 0.1μW, hence why sometimes referred to as microcalorimeters (Koenigbauer, 1994). It is this increased sensitivity which is of importance in biological applications, since we are usually measuring changes in weak non-covalent forces and generally want to use a small amount of sample. The recent development of sensitive instruments allows the measurement of heat effects from reactions involving as little as nanomole amounts of reactants (Spokane & Gill, 1981 : Donner *et al.*, 1982 : McKinnon *et al.*, 1984 : Ramsay *et al.*, 1986 : Myers *et al.*, 1987 : Schon & Freire, 1989 : Wiseman *et al.*, 1989). The types of biological studies carried out using microcalorimetry have included such diverse topics as the measurement of enzyme activities (Monk & Wadso, 1969), thermodynamics of proton binding to proteins, such as chymotrypsin, lysozyme and ribonuclease (Shiao & Sturtevant, 1970) and the study of conformational changes such as the acid denaturation of lysozyme by guanidine hydrochloride (Atha & Ackers,

1971). More recently, however, it has been used to investigate a range of processes from peptide and antibiotic interactions to protein folding (Cooper & McAuley-Hecht, 1993). There are different types of microcalorimeters that can be used to provide thermodynamic information on various processes. Basically, they can be thought of as belonging to two groups, adiabatic or conduction. The adiabatic (from the Greek for 'not passing through') system is thermally insulated from its surroundings so that any heat produced from within the microcalorimeter remains contained. In this case, the temperature change of the microcalorimeter brought about by the process under investigation is measured. In a purely adiabatic system, the rise in temperature associated with a reaction is equal to the heat input divided by the heat capacity of the system (Skinner, 1969). Therefore, the heat associated with the process can be calculated if the temperature rise is measured and the apparent heat capacity of the system is known (Langerman & Biltonen, 1979). In contrast, the conduction microcalorimeter, sometimes known as heat leak, heat flow or heat flux microcalorimeter (Wadso, 1992), is thermally connected to its surrounding heat sink, so that any heat produced in the microcalorimeter is transferred from it. Here, the rate of heat flow from the microcalorimeter to the heat sink is measured. In a heat conduction microcalorimeter, heat evolved in the reaction vessel is conducted through a thermopile before it is absorbed by the surrounding heat sink, which is usually a metal block (Skinner, 1969). In modern instruments, the thermopile usually consists of semi-conducting thermocouple plates, with the heat flow driven by the temperature difference between the reaction vessel and the heat sink. In practice, a certain fraction (usually about 25%) of the heat evolved in the reaction vessel will not pass the thermopile on its way to the heat sink, but will pass through other components such as leads and stirrer shafts etc. However, in a well designed instrument this fraction is constant and is incorporated in the calibration constant and therefore does not lead to any systematic error (Wadso, 1992). Between both these extremes lies the isothermal microcalorimeter, where the microcalorimeter is insulated from its surroundings and the surrounding heat sink is maintained at a constant temperature. Heat produced within the microcalorimeter results in an associated increase in temperature of the microcalorimeter, followed by a

gradual return to the temperature of the surroundings. The microcalorimeter temperature before and after the process is measured as a function of time. The maintenance of a constant temperature environment is essential to the proper calculation of heat transfer between microcalorimeter and surrounding jacket (Skinner, 1969) and is facilitated by a feedback system which ensures the cells and jacket remain at the same temperature. A more detailed overview of the different forms a microcalorimeter can take is discussed in this chapter.

The LKB microcalorimeter (now Thermometric) is based on the heat leak principle, with sample and reference cells contained within a temperature controlled heat sink. The basic layout of a typical isothermal microcalorimeter which uses the heat leak principle is shown in Figure 2.1 (Cooper & Johnson,[a] 1994).

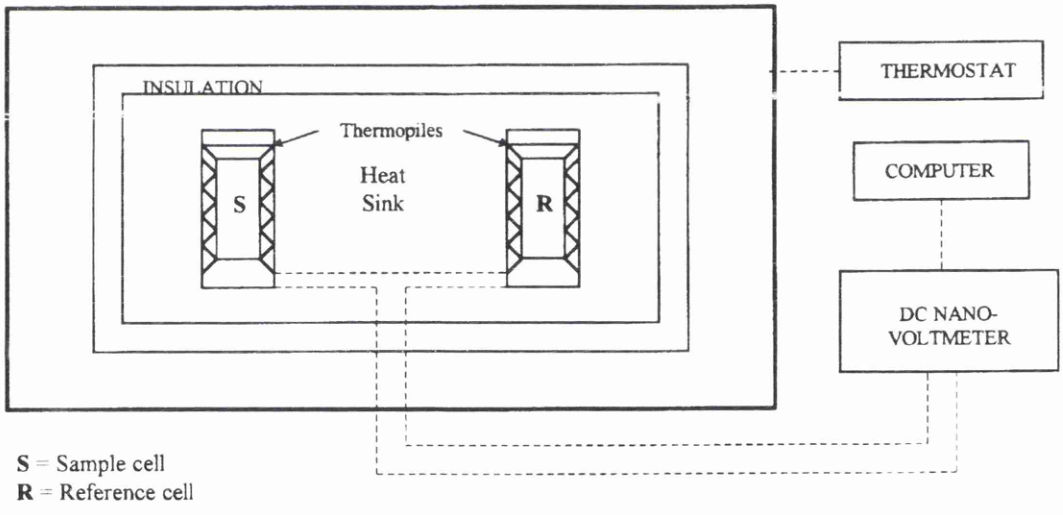

Figure 2.1 Basic layout of a microcalorimeter which uses the heat leak principle. Sample and reference thermopiles are connected back-to-back in series to give differential measurements.

When a reaction occurs in the sample cell, heat flows between the cells and the heat sink. Solid-state thermopiles are connected between each cell and the heat sink, so that the heat produced in the sample cell passes through them and generates a voltage (V) which

is proportional to the temperature difference (ΔT) between the cells and the sink, which in turn is proportional to the rate of heat flow (dQ/dt), as follows:

$$\frac{dQ}{dt} = k_1 \Delta T \qquad \text{and} \qquad V = k_2 \Delta T \tag{2.1}$$

Therefore

$$\frac{dQ}{dt} = kV$$

where k is the calibration constant of the microcalorimeter. The heat of reaction is obtained by integration of equation 2.1, as follows:

$$Q = k \int V.dt \tag{2.2}$$

This type of microcalorimeter is slow to equilibriate, yet has the advantage of being reliable and simple to use. It also has the capability to be adapted for special purposes, into for example a batch or flow system, which are currently used to study biological processes.

The batch microcalorimeter, a schematic view of the cell configuration of which is shown overleaf in Figure 2.2 (Cooper & Johnson,[a] 1994), involves the equilibration of two reactant solutions on either side of a split compartment sample cell, for example, antibiotic solution in one compartment and ligand in the other, with the reference cell containing only buffer.

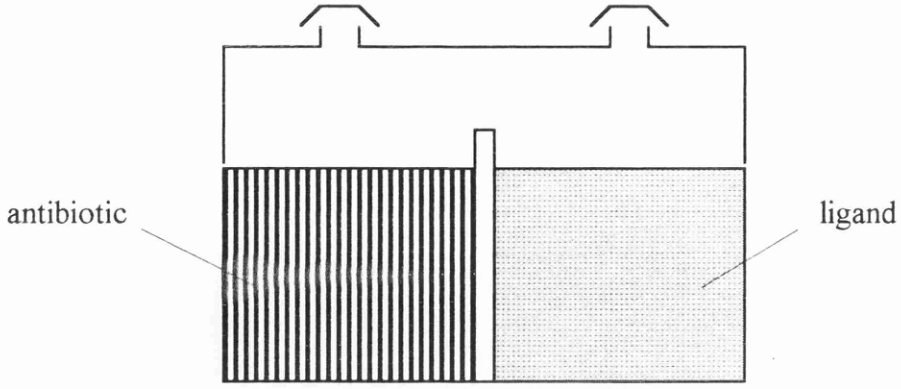

Figure 2.2 Schematic view of the cell configuration of a batch system, used for different experiments in isothermal microcalorimetry.

Typical cell volumes are between 1 and 10mls. Mixing is then obtained by the rotation of the sample cell and the heat effect produced is measured. In this microcalorimeter, it is not necessary to carry out individual controls if the heat of dilution is small, instead only one dilution in the reference cell is required, with its associated heat effect cancelling out the similar heat effect occurring upon mixing in the sample cell (Biltonen & Langerman, 1979). The disadvantages of this type of microcalorimeter are that the contents of the microcalorimetric vessel are not easily accessible and that manipulations can be difficult to perform (Lamprecht, 1980). In addition, since loading of the solutions into the reaction vessels requires that the heat sink and air bath be exposed to the environment, there is a disturbance of the existing equilibrium between the components (Biltonen & Langerman, 1979). Microcalorimeters used for studies of chemical or biological processes can be performed batch wise as described above or flow vessels can be used in continuous flow or stopped flow experiments. A flow through system, the cell configuration of which is shown in Figure 2.3 (Cooper & Johnson,[a] 1994), permits a gas or liquid to enter the cell, interact with the sample and exit the chamber for further analysis downstream.

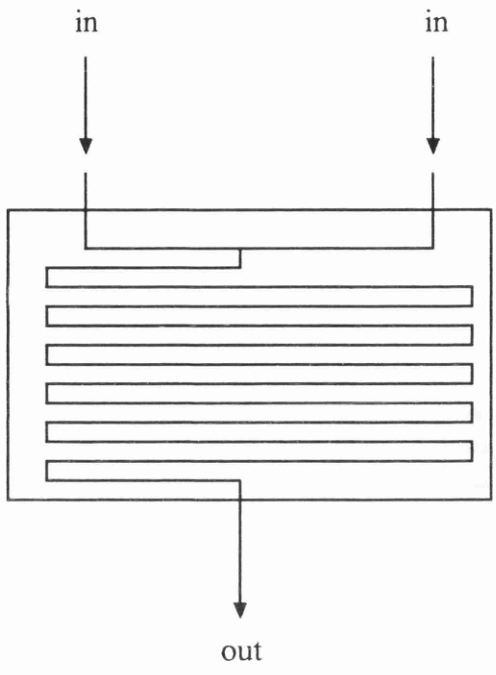

Figure 2.3 Schematic view of the cell configuration of a flow system, used for different experiments in isothermal microcalorimetry.

In this type of microcalorimeter, the reactants are pumped, either using peristaltic or precision syringe pumps (Cooper & Johnson,[a] 1994), separately through a heat exchanger into a microcalorimetric cell, where they mix and a steady-state heat effect is observed, after which the reactants pass out of the microcalorimeter. The heat exchanger means that equilibration times prior to the experiment can be neglected. This technique requires much more sample material and is less sensitive than the batch system, however problems associated with the maintenance of thermal equilibrium in the batch microcalorimeter can be overcome by this system when applied to microbiology for example, since all manipulations are carried out in external fermentors so that there is no disruption of the thermal equilibrium of the microcalorimetric cell (Lamprecht, 1980). Flow techniques can be used for enzyme assays and the determination of the apparent rate of enzyme-catalysed reactions (Langerman & Biltonen, 1979). In both the batch and flow arrangements, vessels composed of glass or inert metals, for example, gold or platinum, are fitted with electrical calibration heaters (Cooper & Johnson,[a] 1994).

The Microcal Omega ultrasensitive isothermal titration microcalorimeter, an external view of which is shown in Figure 2.4, is a more recent development which uses a feedback system for the determination of reaction heats (Cooper & Johnson,[a] 1994).

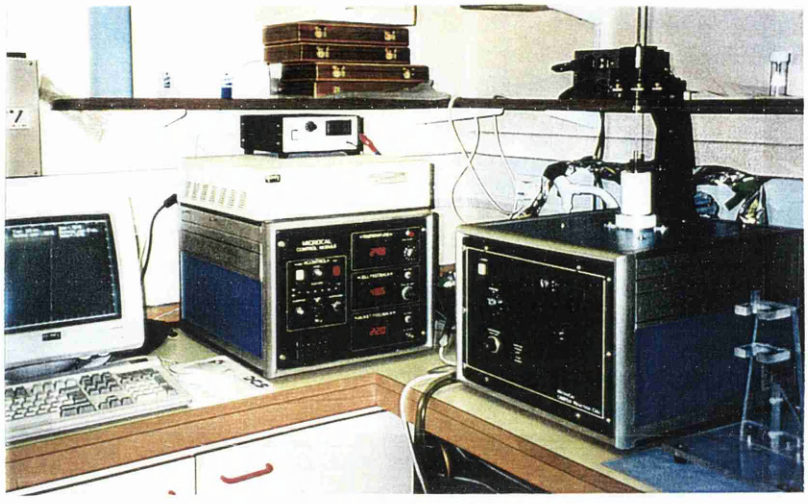

Figure 2.4 The Microcal Omega ultrasensitive isothermal titration microcalorimeter.

It consists of two matched sample and reference cells mounted in an adiabatic jacket, which prevents an interchange of heat with the surroundings and a unique sample cell delivery system, shown in Figure 2.5 (Wiseman *et al.*, 1989). The jacket must be evacuated at low temperature to prevent condensation within the instrument which would interfere with the data collected. The sample and reference cells are constructed from Hastelloy C and have a volume of approximately 1.4mls. The reference cell is usually filled and periodically replaced with purified water containing sodium azide to prevent microbial growth. Both cells have long narrow access tubes through which sample can either be introduced or removed using long needled syringes. Each cell has two heaters distributed over the outer flat surface with a special thermoelectric device containing oriented crystals of bismuth telluride, sandwiched between the two inner surfaces to measure the temperature difference between the two cells. A junction wire thermopile is connected between the adiabatic jacket and the outer circumference of the two cells to monitor the temperature difference between the cells and the jacket and

through a feedback system control the heater currents to ensure that the cells and jacket remain at the same temperature. During an experiment, a small constant power of less than a milliwatt is distributed in the heater of the reference cell, which activates the cell feedback system to drive the difference in temperature between the two cells back to zero (Wiseman *et al.*, 1989). When experiments are carried out at a lower than ambient temperature, a circulating refrigerating bath is used to cool the jacket (Bundle & Sigurskjold, 1994). The difference in electrical energy required to maintain the sample and reference cell at the same temperature is used as a measure of the energetics occurring in the sample (Cooper & Johnson,[a] 1994). The rotating injection syringe inserted into the sample cell serves to deliver the required aliquot of injectant, mix the reactants and evenly distribute heats produced by each injection. Injection syringes (25-250μl) are made from precision-bored glass with long stainless steel needles which have a stirring paddle attached to the end. The syringe is mounted in a low friction bearing assembly which contains an attached timing wheel. This assembly can then be easily inserted into the Teflon loading barrel of the sample cell and the timing wheel coupled to a stirring wheel. This will allow the syringe to be rotated at a constant speed, usually 400 r.p.m. The syringe plunger is mechanically coupled to a precise digital stepping motor which serves to deliver the required aliquots of injectant from the syringe, the amount of which is determined in the injection schedule e.g. number of injections, volume per injection and time between injections. Once the injection schedule has been created with the accompanying interactive software, the experiment can be left to run with no further operative involvement (Wiseman *et al.*, 1989). The main advantages of this over earlier instruments is that equilibration times are significantly reduced with an entire titration experiment now taking only about an hour to complete rather than a full day and less sample material is required than with batch techniques (Wadso, 1983). Results obtained are analysed using the accompanying software package, Origin. The treatment of data obtained from such single-injection ITC experiments involves carrying out controls to take into account the heats of dilution and mixing within the overall heat of the experiment of interest. However, dual-injection instruments have been developed which allow differential measurements of reference and sample responses and therefore

more accurate determinations of the overall heat of reaction. Since this instrument can compensate for heats of dilution and mixing this eliminates the need for separate experiments. This method is more precise as it fails to introduce any additional error arising from the consideration of separate measurements (Freire *et al.*, 1990).

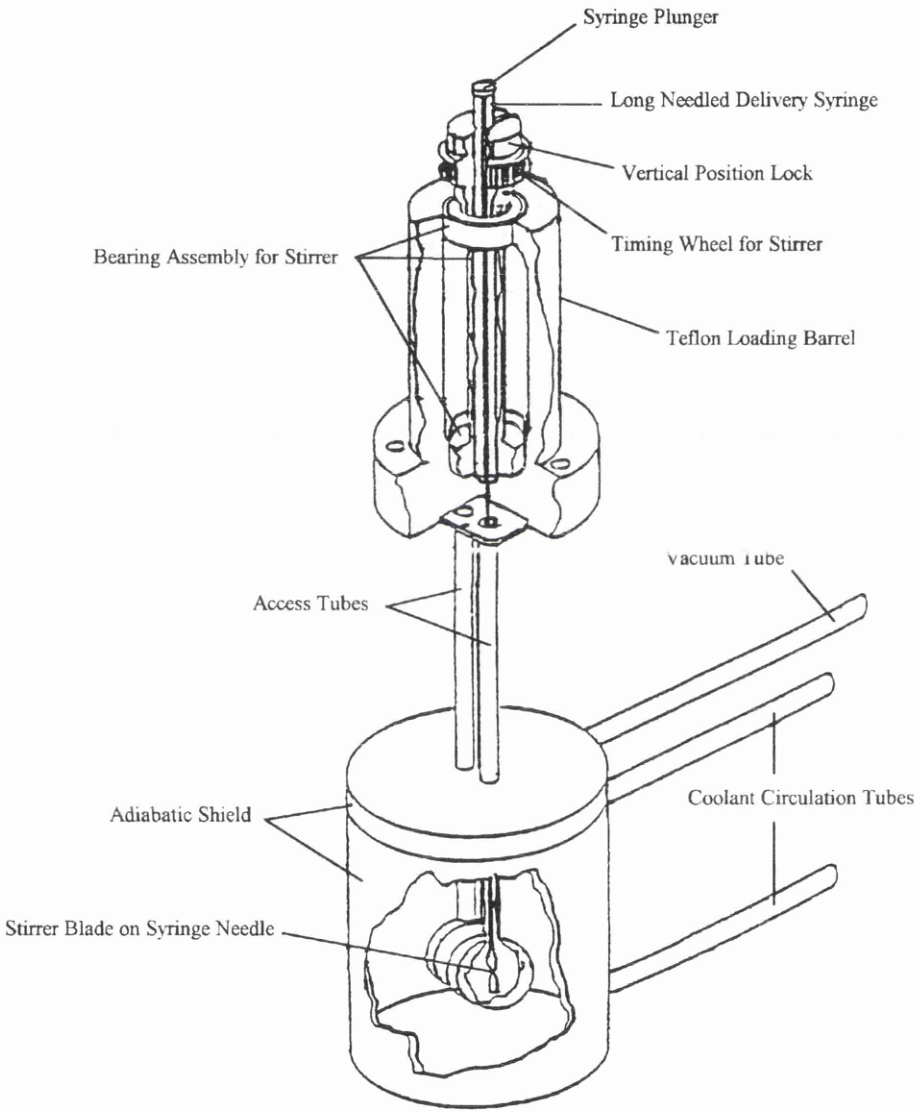

Figure 2.5 Drawing of the microcalorimeter cells, adiabatic shield and injection/stirrer assembly

Isothermal titration microcalorimetry is routinely used in the study of non-covalent interactions involved in processes which occur at essentially constant temperature, but is non-specific and cannot differentiate between individual forces e.g. hydrogen bonding, van der Waals forces, hydrophobic and electrostatic interactions which play a role in the process, but rather gives an estimate of the total interactions involved. In the binding of ligand for example, there are several important sources of thermodynamic change that give rise to the overall enthalpy and entropy. These include the change in solvation of the ligand and the macromolecule, the interaction between the ligand and the binding site through hydrogen bonds, van der Waals forces and electrostatic interactions, the release and absorption of protons by the macromolecule, ligands and buffer, a conformational change in ligand or macromolecule required for or induced by the association reaction and changes in the state of aggregation of either reactant (Eftink & Biltonen, 1980). Isothermal titration microcalorimetry (ITC) can generally be thought of as a non-destructive technique, since samples can be recovered and recycled after use. However, denaturation of proteins, for example, can occur after long periods of stirring and equilibration in the calorimeter (Cooper & Johnson,[a] 1994). This method is routinely used in binding studies since nearly all such associations are accompanied by a change in enthalpy and will therefore produce a calorimetric signal (Bundle & Sigurskjold, 1994), however, we have also been able to use it in dimerisation studies where dissociation from the dimer form produces a signal. A heat pulse is produced by each syringe injection, a typical profile of which is shown in Figure 2.6. When these are corrected for baseline and integrated over time, give the total heat exchange during the event (Cooper & Johnson,[a] 1994). For the binding of vancomycin to ligand, three control experiments are carried out under identical conditions to take into account the heats of dilution, mixing and stirring of the reactants and are subtracted from the experiment of interest, whereas only one control is required in dimerisation studies to take into account the heat of stirring. Binding interactions in biological systems can be measured conveniently and with high accuracy if the receptor protein is available in approximately 0.1-1.0μmol quantities and the binding constant is in the range 10^4-$10^8 M^{-1}$. However, weak binding can also be

studied if it is possible to increase the ligand concentration sufficiently (Bundle & Sigurskjold, 1994) for the association to produce a thermal profile.

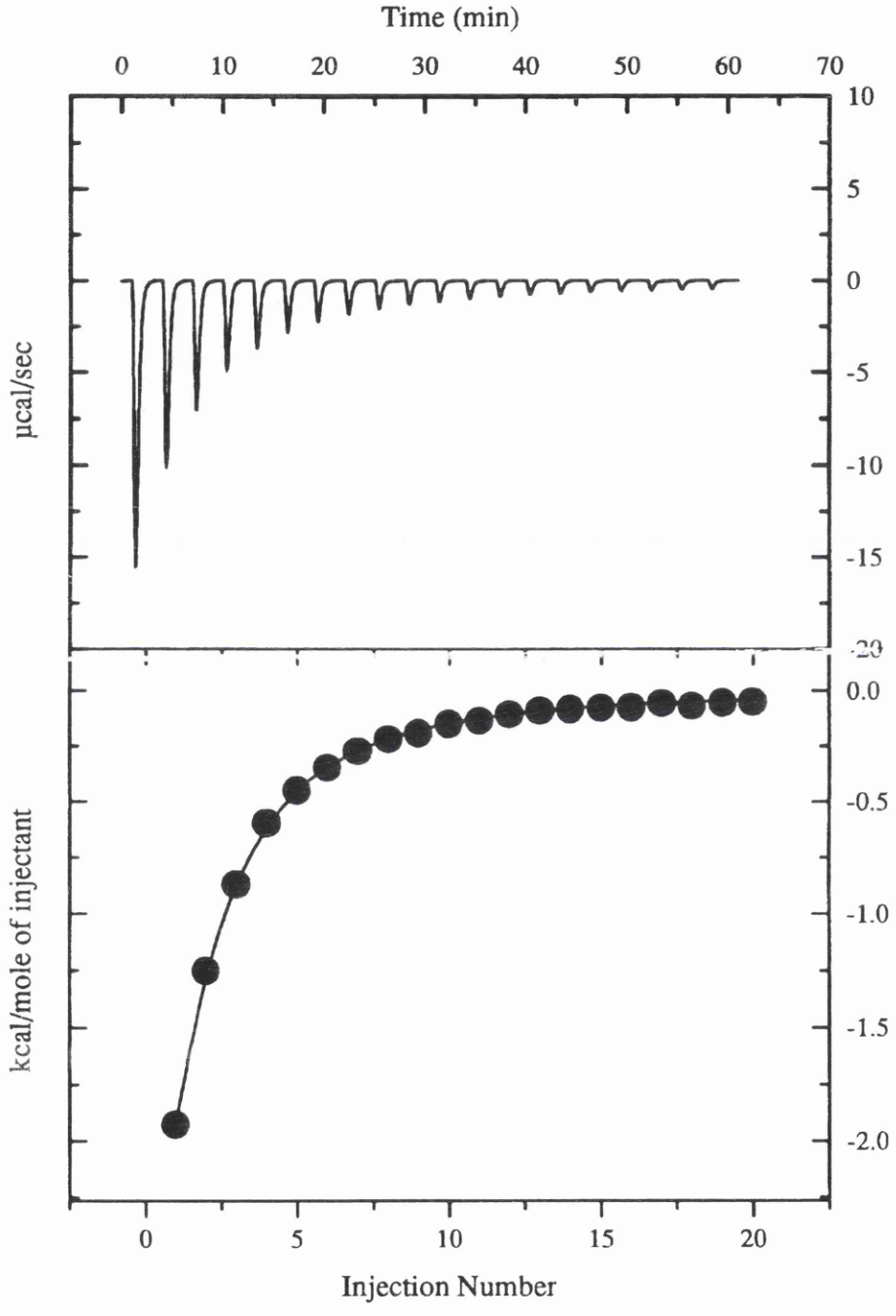

Figure 2.6 A typical ITC profile produced by the binding of vancomycin to N-fumaryl-D-Ala.

Microcalorimeters have also been developed to study processes which are initiated by a change in temperature. This method is called differential scanning microcalorimetry (DSC). The differential scanning microcalorimeter routinely used for biomolecular samples in solution is the Microcal MC-2, an external view of which is shown in Figure 2.7, with a schematic view of the microcalorimetric unit of a typical differential scanning microcalorimeter in Figure 2.8 (Cooper & Johnson,[b] 1994).

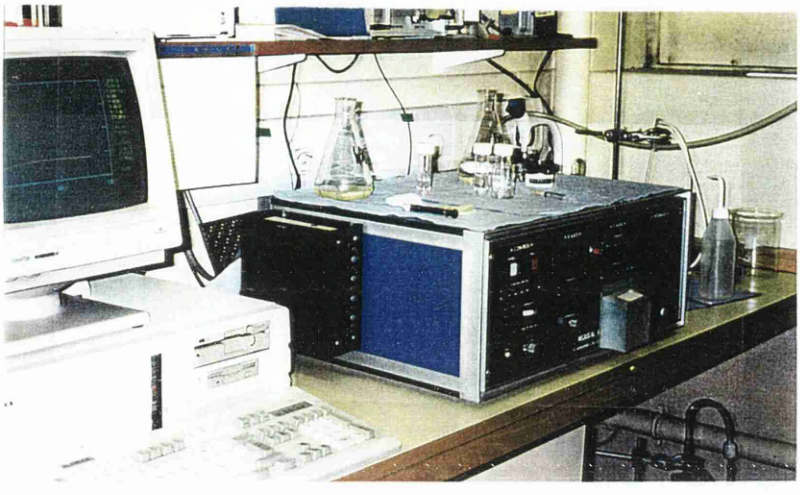

Figure 2.7 The Microcal MC-2 differential scanning microcalorimeter.

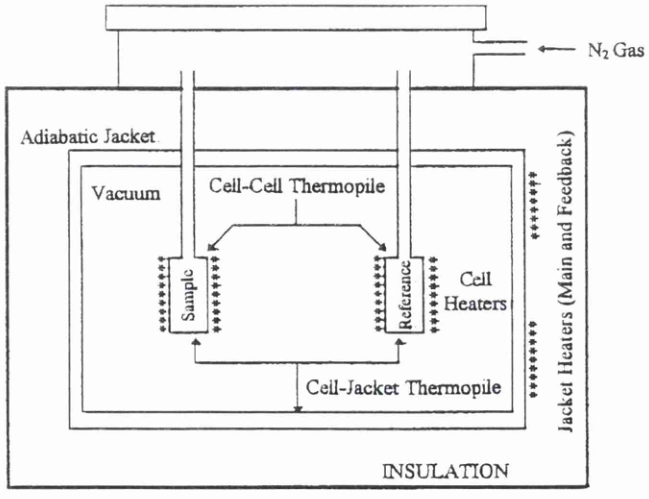

Figure 2.8 Schematic view of the microcalorimetric unit of a typical differential scanning microcalorimeter.

This model is based on successful earlier designs by Privalov (Privalov, 1980 : Privalov & Potekhin, 1986) and consists of two matched, pillbox shaped cells, the sample and reference, suspended by their filling capillaries in an adiabatic chamber, which is composed of aluminium. Both cells are constructed of an inert metal e.g. Tantallum, and are equal in loading volume, between 1 and 2mls. The cells are fixed in place, which not only makes cleaning and loading easier, but also reduces the risk of damage by the operator. A nitrogen gas pressure head is used to inhibit bubble formation within the cells, which would affect equilibration and baselines. The differential method of measuring is based on the difference in heat capacity of the sample against a standard. Evaluation of the heat capacity difference at each point in a temperature range, requires the sample and reference cells to be heated simultaneously under the same conditions. This evaluation has two steps, the first being the determination of the instrumental baseline. This involves filling both sample and reference cells with the same solution, usually buffer, allowing equilibration and then carrying out a scan. Secondly, the buffer in the sample cell is replaced by the sample of interest and a comparison of the two scans allows the difference in heat capacity of the two cells to be determined (Privalov, 1980). During operation of the apparatus, the temperature of the adiabatic jacket is raised by applying constant power to the main jacket heaters. The jacket can be cooled by a circulating refrigerated waterbath. Feedback control systems monitor temperature differences between the cells and the jacket and supply power to the cell heaters so that the cell temperatures are as similar as possible to that of the jacket. The difference in power supplied to the sample and reference cells is recorded as a function of temperature and is related to the heat capacity difference between them. Standard samples of pure hydrocarbons of known melting temperatures are used for temperature calibration and heat capacity calibration is carried out by using the differential heat capacity data of standards i.e. dilute sodium chloride and urea solutions (Cooper & Johnson,[b] 1994). This model of microcalorimeter has a computer interface with advanced software for the collection and analysis of data

DSC is based on the principle that if the temperature of a system is raised by the introduction of heat, it will adjust its equilibrium position and the temperature dependence of this shift can be directly related to the heat capacity of the system (Langerman & Biltonen, 1979). A DSC experiment produces a transition with an associated specific heat, the integral of which over temperature, gives the specific microcalorimetric enthalpy of the process (Sturtevant, 1987). A typical profile is shown in Figure 2.9 (Cooper & Johnson,[b] 1994).

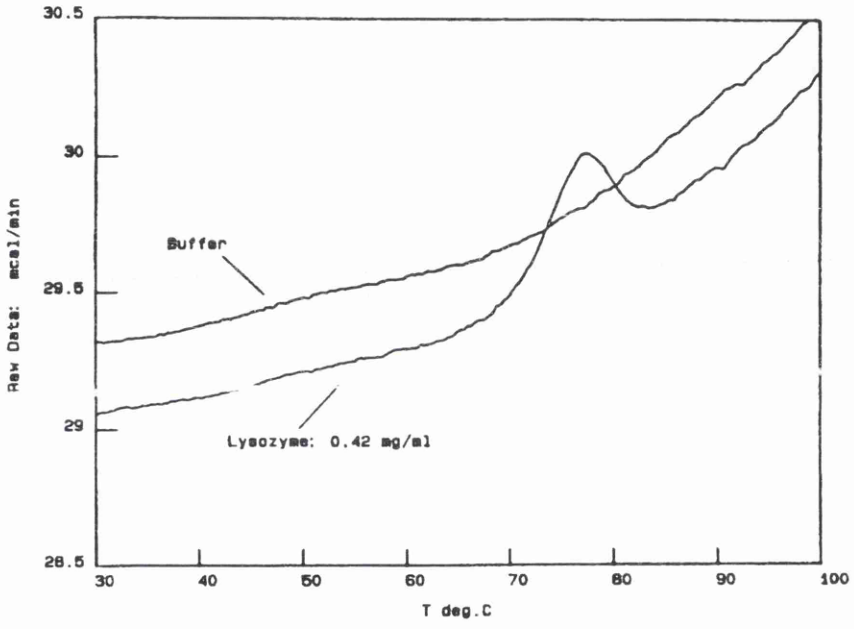

Figure 2.9 Typical DSC raw data for thermal denaturation of hen egg-white lysozyme.

Such an experiment can not only give information on the energetics, thermal stability and cooperativity of the process (Cooper & Johnson,[b] 1994), but ideally resolve all the structural transitions that a system undergoes as it is perturbed by a systematic temperature variation (Krishnan & Brandts, 1978). For example, bovine serum albumin is folded into three distinct structural units, which can unfold nearly independently (Decker & Foster, 1966 : Zurawski *et al.*, 1975) giving rise to multiple transitions, which are detected by the microcalorimeter, giving some insight into the structural properties of

the protein. Similar transitions can be identified with nucleic acids. Multiple transitions are produced from tRNA melting, indicating six structural domains, each capable of semi-independent melting (Privalov *et al.*, 1975). DSC has been routinely used to study protein unfolding and denaturation, unwinding of base-paired nucleic acids (Krishnan & Brandts, 1978) and the study of DNA-ligand interactions, such as the binding of antitumour drugs to DNA (Marky *et al.*, 1983). Effective use of DSC has also been made in studying more complex systems, such as the human erythrocyte membrane (Jackson & Brandts, 1970). Over the years, DSC has proved to be a useful tool for studying the conformational or phase transitions of highly cooperative structures, however it cannot be used to study small molecules, transitions of which will not be detected by the microcalorimeter unless they form aggregates showing intermolecular cooperation (Sturtevant, 1987).

Each type of microcalorimeter mentioned above has its own area of specific application. The titration microcalorimeter is primarily used to measure heats of formation of complexes in solution and from this provide information on the enthalpy and equilibrium constant of the process under investigation from a single set of measurements, which in turn leads to entropy and free energy changes. The batch and flow systems provide similar information for liquids and gases, but are less frequently used due to the long equilibration times involved and more than one loading of the system is required to produce a complete titration curve. In addition to providing information on enthalpy changes like the above mentioned examples, the differential scanning microcalorimeter can also give some insight into thermal stability, structure and cooperativity of the process. Clearly, the choice of microcalorimeter depends not only on the sample form and process to be studied but also on the information required.

2.2 Calculation of thermodynamic parameters from experimental data

When studying an association reaction, such as the binding of ligand to antibiotic, the observed heat effect is the sum of the heats produced from this binding event (Q_r) the heats of dilution of the components of the solutions (Q_{dil}) and the heat associated with the physical process of mixing (Q_{mix}). Q_{mix} may also include the viscous heat associated with flowing solutions (Biltonen & Langerman, 1979).

$$Q_{obs} = Q_r + Q_{dil} + Q_{mix} \tag{2.3}$$

It is important that these accompanying heats are determined individually in the form of control experiments and taken into account in the final estimation of the enthalpy of binding. The individual experiments that should be carried out are detailed in Table 2.1.

	Syringe	**Sample Cell**
Q_{obs}	Ligand	Antibiotic
Q_1	Buffer	Antibiotic
Q_2	Ligand	Buffer
Q_3	Buffer	Buffer

Table 2.1 Titration experiments carried out to take into account the contribution made to the observed enthalpy of association by heats of dilution and mixing of components.

The overall heat of binding of all injections is therefore equal to

$$Q_r = Q_{obs} - Q_1 - Q_2 + Q_3 \tag{2.4}$$

Q_3 is added on because it has already been subtracted in Q_1 and Q_2. The heats of dilution are usually negligible, however in some cases they can make a significant contribution to

the overall enthalpy, therefore it is important that these heats are determined experimentally and considered in the final estimation.

If an antibiotic solution is titrated to saturation i.e. all binding sites are occupied by ligand, then the enthalpy change is equal to the total reaction heat divided by the antibiotic concentration ($[A]_t$):

$$\Delta H^\circ = \frac{Q_r}{[A]_t} \tag{2.5}$$

In addition to the determination of the enthalpy of the reaction, association constants can also be calculated, using heat transfer as a measure of the extent of a reaction:

$$Q_r = \frac{[AL]\,\Delta H^\circ}{[A]_t} \tag{2.6}$$

where $[A]_t$ is the total concentration of antibiotic and [AL] is the concentration of the complex. Equation 2.6 can be expressed in terms of the association constant and the free ligand concentration ([L]) for simple 1:1 binding, as follows:

$$Q = \frac{K_a[L]\,\Delta H^\circ}{1 + K_a[L]} \tag{2.7}$$

By rearranging this gives:

$$\frac{1}{Q} = \frac{1}{\Delta H^\circ} + \frac{1}{K_a\,[L]\,\Delta H^\circ} \tag{2.8}$$

By constructing a double reciprocal plot of 1/Q against 1/[L], enthalpy changes and association constants can be determined. ΔH° is obtained from the intercept on the y-

axis and K_a from the gradient of the line. This is a simple method used to analyse experimental data, but has two major disadvantages. Firstly, such a plot is biased and places more weight on less accurate points and secondly, the free ligand concentration at equilibrium must be known. This is approximately equal to the total ligand concentration only when binding is weak. Instead, another method for analysing experimental data is employed, which uses the relationship for the observed heat as a function of total antibiotic and ligand concentration:

$$Q = -\Delta H^{\circ}(N[A]_t + [L]_t + 1/K_a) \{1 - (1-4N[A]_t[L]_t/(N[A]_t + [L]_t + 1/K_a)^2)^{1/2}\}/2[A]_t$$

where N is the number of independent binding sites (2.9)

For a system with multiple sets of independent binding sites, the observed heat effect as a result of ligand binding is given by:

$$Q = \sum_{i=1}^{j} \frac{N_i \Delta H_i [L] K_i}{1 + K_i [L]} \qquad (2.10)$$

where j is the number of sets of distinct binding sites, K_i, ΔH_i and N_i are the apparent association constant, enthalpy change and number for each set of sites, respectively (Freire *et al.*, 1990).

Titration curves can also be analysed using a two sets of sites model, if both binding sites are separate and distinct from each other. If there are more than two sets of sites, fitting is more difficult since there will be three variable parameters for each set of sites.

Further complications arise when the binding sites are not distinct from each other, but are interactive, where the binding of ligand to one site may either increase or decrease the binding affinity for ligand in the other site, making data analysis much more complex.

2.3 Data analysis

As previously shown, microcalorimetric data from binding experiments can be analysed to give various thermodynamic parameters, such as enthalpy change (ΔH), association constant (K_a) and the number of binding sites per mole of macromolecule (N). Using the Omega titration microcalorimeter, the raw data produced is a record of the cell feedback signal as a function of time. Using the accompanying software package Origin, the first step in analysing the raw data is to integrate the area below each of the peaks, both for the association of interest and the controls. The heats of dilution of these controls are subtracted from the corresponding antibiotic-ligand association heats to give corrected heat values. The heats are then plotted against injection number and a theoretical fit made to the data using a least-squares approach, to give values of ΔH, K_a and N. Calculation of the number of binding sites is influenced by the concentration of sample in the syringe. If this is unknown or has not been determined accurately e.g. by UV spectroscopy, then for simple 1:1 binding, $N \neq 1$. In situations where binding is weak, it may be necessary to fix one of the parameters e.g. N=1, so that a better fit to the experimental data can be made.

The analysis of data from dimerisation experiments is similarly carried out using the accompanying software to integrate peaks and correct for controls. The calculation of enthalpy change (ΔH) and dimerisation constant (K_{dim}) from this data, however, is carried out by specifically-written software using a dimer dissociation model.

The models used in both the analysis of binding and dimerisation experimental data are given in the following sections.

2.3.1 Model for one set of sites

For 1:1 binding, the binding constant is related to the ligand concentration, [L], and the fraction of sites occupied by ligand, θ, by the equation:

$$K = \frac{\theta}{(1-\theta)[L]} \tag{2.11}$$

and

$$[L]_t = [L] + N\theta[A]_t \tag{2.12}$$

where $[L]_t$ and $[A]_t$ are the bulk ligand and bulk antibiotic concentrations. Combining equations 2.11 and 2.12 gives the quadratic equation:

$$\theta^2 - \theta \left[1 + \frac{[L]_t}{N[A]_t} + \frac{1}{NK[A]_t} \right] + \frac{[L]_t}{N[A]_t} = 0 \tag{2.13}$$

The total heat content of the solution, Q, is equal to:

$$Q = N\theta[A]_t \Delta H V_0 \tag{2.14}$$

where ΔH is the enthalpy of binding and V_0 is the active cell volume. Solving equation 2.13 for θ and substituting into equation 2.14 gives:

$$Q = \frac{N[A]_t \Delta H V_0}{2} \left[1 + \frac{[L]_t}{N[A]_t} + \frac{1}{NK[A]_t} - \sqrt{\left[1 + \frac{[L]_t}{N[A]_t} + \frac{1}{NK[A]_t} \right]^2 - \frac{4[L]_t}{N[A]_t}} \right] \tag{2.15}$$

This equation can be solved for Q_i given values of N, K and ΔH at the end of the ith injection. The calorimeter measures differences in heat between injections i.e. between the ith and (i-1)th injections, approximating to

$$\Delta Q_i = Q_i - Q_{(i-1)} \tag{2.16}$$

A small correction factor is employed in this model to take into account the volume of liquid which is displaced from the constant volume calorimeter sample cell upon subsequent injections, by measuring the difference between the original volume in the sample cell and that after the final injection.

Accompanying software allows initial guesses of the fitting parameters N, K and ΔH to be made automatically and substituted into equation 2.15 to obtain values of ΔQ_i for each injection. These calculated values of ΔQ_i are then compared with experimental values and new values of the fitting parameters are found using statistical methods until there is an optimum fit between experimental and calculated ΔQ_i values (ITC Tutorial Guide, 1993).

2.3.2 Model for dimer dissociation

The heats of dilution data for a simple monomer-dimer system are analysed as follows, assuming that only monomer or dimer states of macromolecule, P, are possible assuming a monomer-dimer equilibrium:

$$P + P \rightleftharpoons P_2 \quad ; \quad \Delta H_{dim} \quad ; \quad K_{dim} = [P_2]/[P]^2 \tag{2.17}$$

the equilibrium concentration of monomers is given by:

$$[P] = \{(1 + 8.K_{dim}.C)^{1/2} - 1\}/4.K_{dim} \quad (2.18)$$

where C is the total concentration of P, expressed as a monomer:

$$C = [P] + 2[P_2] \quad (2.19)$$

In a titration dilution experiment we measure the heat change (δq) when a small volume (δV) of concentrated solution (concentration C_0) is injected into the calorimeter cell (volume V_0) containing initially buffer but, for later injections, more dilute solution. The heat arises from dimers present in the higher concentration solution that dissociate upon entering the lower concentration environment.

For the ith injection of a series the observed heat is given by:

$$\delta q_i = \Delta H_{dim} \{V_0([P_2]_i - [P_2]_{i-1}) - \delta V([P_2]_0 - [P_2]_{i-1}) \quad (2.20)$$

where $[P_2]_0$, $[P_2]_{ith}$ and $[P_2]_{i-1}$ are the dimer concentrations in the original (syringe) solution and in the calorimeter cell after the ith and (i-1)th injections with total concentrations C_0, C_i and C_{i-1}, respectively. The last term in this expression is a small correction factor to allow for the quantity of solution displaced from the constant volume microcalorimeter cell during each δV addition.

Equations 2.17 to 2.19 are used in standard non-linear regression (least squares) analysis to fit experimental dilution data and obtain estimates of K_{dim} and ΔH_{dim}. Similar, although more algebraically complex expressions may be derived for dissociation processes involving higher oligomers or other mechanisms. Such mechanisms frequently give sigmoidal dilution thermal profiles, in contrast to the hyperbolic shapes shown in our series of experiments and this might give empirical indications that the process under investigation is more complex than simple dimers can model (McPhail & Cooper, 1997).

2.4 Associated heat effects

In addition to the heats associated for example, with ligand binding, are accompanying heats of dilution and mixing, as discussed previously. These heats will be incorporated into the overall heat of binding and will obscure the true interpretation of experimental data, unless appropriate controls are carried out and taken into account in the final calculations. Less obvious sources of heat are also possible due to contamination of the sample, changes in the state of aggregation of the binding species or from conformational changes of the macromolecule on binding. Interpretation of such data can therefore provide additional information to the thermodynamics of ligand binding. It is also important to avoid unwanted protonation reactions from differences in buffer composition, therefore all solutions should be prepared in identical buffers. Often processes will be accompanied by a release of protons which normally would be taken up by the buffer present (Wadso, 1983), producing heat effects. Calorimetry measures the total of all heat effects in any reaction occurring in the sample and will include any heat due to the uptake or release of protons by the buffer in addition to the heat of the reaction of interest (Cooper & Converse, 1976). If experiments are carried out in buffers with different enthalpies of protonation, the observed enthalpies of binding will vary (Sturtevant, 1962). The parameters obtained can then be used to calculate the number of moles of protons being released to the buffer. The observed enthalpy (ΔH_{obs}) will equal the enthalpy of the association reaction plus an additional heat contribution from the association of the protons and buffer molecules:

$$\Delta H_{obs} = \Delta H_0 + \Delta n \, \Delta H_b \qquad (2.21)$$

where ΔH_0 is the enthalpy change in the absence of buffer effects and ΔH_b is the heat of protonation of the buffer. By plotting ΔH_{obs} against ΔH_b a straight line should be produced with a slope equal to Δn and an intercept equal to ΔH_0.

Chapter 3:
X-ray Crystallography

3.1 Crystallisation

The word 'crystal' comes from the Greek 'krustallos' meaning 'clear ice' and it is from this meaning that crystals are thought of as symbols of purity and perfection (Giege & Ducruix, 1992). In basic terms, crystals are composed of regular three-dimensional arrays of atoms, molecules or ions, the basic building blocks of which are the asymmetric units which are arranged according to their well-defined symmetries (forming space groups) into unit cells which are repeated in three-dimensions throughout the entire crystal. The interaction, or diffraction, of X-rays of the appropriate wavelength (~1Å) with such a regular lattice is the basis for determining the three-dimensional structure by crystallography. The detailed information obtained from such X-ray crystallographic studies can, for instance, give insights into the possible mechanisms of enzymatic activity which can then allow us to correlate structure with function.

The first prerequisite for solving the three-dimensional structure of a biological macromolecule in this way is the production of well-ordered crystals. There are important differences between the crystallisation of small organic/inorganic molecules and biological macromolecules, although in terms of crystal morphology, both show the same diversity. If we first consider crystal size, both small molecules and macromolecules form crystals which are small, with volumes rarely greater than $10mm^3$. Macromolecular crystals tend to have poor mechanical properties and high solvent content (50-80%) (Matthews, 1968 : McPherson, 1982) and therefore are extremely fragile and sensitive to external conditions. This fragility is due to both the weak intermolecular forces between macromolecules within the crystal lattices and the high solvent content. Therefore, more gentle techniques are required for crystallisation of macromolecules. It is important that macromolecular crystals are kept in a mother liquor

environment to prevent dehydration, which may lead to destruction of the crystal lattice. Mother liquor is the name given to the solution containing all crystallisation chemicals. The high solvent content within such crystals is an important feature as it allows the formation of solvent channels, through which small molecules may diffuse. This property is used to the best advantage in the preparation of heavy-atom derivatives which are needed to solve the structures of such large molecules (see section 3.2.2). Macromolecules also tend to have large unit cells (up to 1000Å for virus crystals). Although crystals are taken as symbols of purity, the morphology of a crystal does not correlate with crystal quality. In other words, just by looking at a crystal it is impossible to tell if it is suitable for structural analysis. The only way in which this can be determined is if the crystal provides high resolution diffraction data (Giege & Ducruix, 1992).

In the early days of crystallography, the main interest of many scientists was in the development of X-ray methods to determine the crystal structures of small molecules, rather than in improving crystallisation techniques for macromolecules. However, it is the production of suitable crystals which diffract to high resolution and have prolonged stability in the X-ray beam which is of central importance to structure determination and in protein work it is only recently that this has been realised. The first major breakthrough occurred during the 1960s upon the development of crystallisation micromethods (Giege & Ducruix, 1992). This pioneering work was the result of structural studies on a macromolecule which was reluctant to crystallise and was only available in limited amounts (McPherson, 1982). Further improvements came with the discovery that the addition of specific compounds to crystallisation solvents could influence the crystallisation process (Kim & Rich, 1968 : Dock *et al.*, 1984 : Michel, 1982 : Arnoux *et al.*, 1989).

The crystallisation of macromolecules is influenced by a much larger number of variable parameters, as shown in Table 3.1 (Giege & Ducruix, 1992), than the corresponding crystallisation of small molecules, with their optimum stability in aqueous solution

restricted to a narrower pH and temperature range than small molecules. The stability of biological macromolecules in solution relies on a subtle balance between those interactions responsible for their conformation and solvent-solute interactions. Such interactions can be modified by the intrinsic physico-chemical parameters in Table 3.1. For example, an increase in temperature increases the disorder of the solvent molecules and allows macromolecular conformations of a higher free energy to form. A change in pH affects both solute and solvent charges which may also influence structural conformation. In addition, the presence of organic solvents can produce a modification of the dielectric constant and therefore change the various intramolecular interactions (Ries-Kautt & Ducruix, 1992). The main difference between crystal growth of these molecules is their conformational flexibility and chemical versatility, therefore making them more sensitive to external conditions (Giege & Ducruix, 1992). For optimum crystal growth from such molecules it is important to carefully control all biological and physical parameters, so that the growth of suitable crystals can be reproduced.

Intrinsic physico-chemical parameters:

- Supersaturation (concentration of macromolecules and precipitants)
- Temperature, pH (fluctuations of these parameters)
- Time (rates of equilibration and of growth)
- Ionic strength and purity of chemicals (nature of precipitant, buffer, additives)
- Diffusion and convection (gels, microgravity)
- Volume and geometry of samples and set-ups (surface of crystallization chambers)
- Solid particles, wall and interface effects (homogeneous versus heterogeneous nucleation)
- Density and viscosity effects (differences between crystal and mother liquor)
- Pressure, electric, and magnetic fields
- Vibrations and sound (acoustic waves)
- Sequence of events (experimentalist versus robot)

Biochemical and biophysical parameters:

- Sensitivity of conformations to physical parameters (temperature, pH, ionic strength, solvents)
- Binding of ligands (substrates, cofactors, metal ions, other ions) & specific additives (reducing agents, non-ionic detergents, polyamines....)
- Related with properties of macromolecules (oxidation, hydrophilicity versus hydrophobicity, polyelectrolyte nature of nucleic acids ....)
- Ageing of samples (denaturations or degradations)

Biological parameters:

- Rarity of most biological macromolecules
- Biological sources and physiological state of organisms or cells (thermophiles versus halophiles or mesophiles, growing versus stationary phase....
- Bacterial contaminants

Purity of macromolecules:

- Macromolecular contaminants (odd macromolecules or small molecules)
- Sequence (micro) heterogeneities (fragmentation by proteases or nucleases-fragmented macromolecules may better crystallise, partial or heterogeneous post-translational modifications, . . .)
- Conformational (micro) heterogeneities (flexible domains, oligomer, and conformer equilibria, aggregations, denaturations ....)
- Batch effects (two batches are not identical!)

Table 3.1 Parameters affecting the crystallisation (and/or solubility) of macromolecules.

Purification of macromolecules plays a central role in crystallisation. The development of crystals of suitable size for use in X-ray crystallography requires good quality monocrystals with a high degree of order. Purity however, is not always required, since crystals of macromolecules can often be obtained from mixtures, although crystals

obtained in this way are mostly small or grow in polycrystalline masses, are not well shaped and are often of bad diffraction quality and therefore unsuitable for diffraction studies. As well as protein impurity, lack of homogeneity (see later in this section) of the sample is thought to be the main cause of unsuccessful crystallisations, e.g. denatured material often precipitates first and introduces heterogenous nuclei along with microcrystalline precipitation of the macromolecule (Zeppezauer, 1971). The major methods used in purification processes are listed in Table 3.2 (Lorber & Giege, 1992). Isolation procedures for proteins usually involve a fractionation step, whereby either a precipitant is added or physical changes are introduced by altering the temperature or pH conditions of the solution in order to reduce solubility or denature unwanted macromolecules.

Cell culture
- Fermentors, culture plates, thermostated cabinets
- High capacity centrifuges or filtration devices for cell recovery

Cell disruption
- Mechanical disruption devices (grinders, glass bead mills, French press)
- Chemical or biochemical treatments (e.g. permeation of cells by enzymes, phenol treatment for recovery of small RNAs)
- Others (e.g. sonication, freezing/thawing)

Centrifugation
- Centrifuges (low speed to eliminate cell debris or recover precipitates and high speed to fractionate sub-cellular components)

Dialysis and ultrafiltration
- Dialysis tubings, hollow fibers or membranes (various porosities and sizes)
- Concentrators (various capacities from 50µl to several litres, high flow rate membranes with low macromolecule-binding and various cut-offs)

Chromatography (use preferentially metal-free systems)
- Low pressure chromatography or HPLC columns and matrices
- Other equipment including pumps, programmer, on-line absorbance detector, fraction collector, recorder

Preparative electrophoresis or isoelectric focusing
- Electrophoresis apparatus for large rod or slab gels
- Preparative liquid IEF apparatus (column or horizontal rotating cell)
- Power supplies

Detection, characterization, and quantitation
- Spectrophotometer, fluorimeter
- pH meter, conductimeter, refractometer (for monitoring solutions and chromatographic elutions)
- Liquid scintillation counter (for radioactivity detection)
- Analytical electrophoresis and IEF equipment.

Table 3.2 Methods and equipment used for the purification of biological macromolecules.

The addition of ammonium sulphate to a protein solution is frequently used as a purification technique (Jakoby, 1971). The ammonium sulphate is used to 'salt-out' the protein. This effect utilises a change in solubility of proteins. In solutions with a high

salt concentration, much of the water which would normally solvate the protein molecules is bound up in the hydration shells of the numerous salt ions, therefore making it less available to the protein and decreasing its solubility. By varying the concentration of ammonium sulphate, proteins with different solubilities can be extracted from a protein mixture. This procedure can be used to remove minor impurities from a protein solution prior to crystallisation.

Not only is the solubility of a protein determined by the amount in solution, but also by the characteristics of the solvent. Changes in the solvent structure brought about by the presence of buffer, salts and other additives can also affect the solubility of biological macromolecules. This can occur either directly through the interaction of these additives with the different functional groups of the macromolecule resulting in a modification of the overall structural conformation or indirectly through modification of the structure and properties of the solvent e.g. a change in pH will result in a change in the net charge of the macromolecule (e.g. a protein) which in turn may affect intermolecular interactions which are responsible for maintenance of the tertiary structure (Ries-Kautt & Ducruix, 1992). Once minor impurities have been removed, higher resolution separations may be employed, usually involving a series of chromatographic techniques, such as Fast Protein Liquid Chromatography (FPLC). Such methods may be based upon for example, separation of the contaminants from the macromolecule by charge, size or hydrophobicity, depending on the nature of the chromatography column used. Normally, molecular sieve and gel filtration chromatography is used to improve the homogeneity of the protein. Techniques such as electrospray mass spectrometry (see section 3.4) can be used to check the purity of the sample (this was carried out on the vancomycin complex), although it does not form the basis of a purification method. In many cases carrying out a final FPLC stage on the protein prior to crystallisation is beneficial. This may be due to the removal of minor contaminants, such as ageing or degradation products which can accumulate during storage, or of small molecules such as peptides, amino acids, carbohydrates or nucleotides. If contaminants are not removed prior to the crystallisation they may compete for sites on growing crystals, producing lattice faults

which can lead to internal disorder, irregular faces and secondary nucleation, poor diffraction or even early cessation of growth.

In addition to purification of the protein itself, crystallisation agents must also be pure. Common precipitants such as ammonium sulphate and polyethylene glycol (PEG) can have major contaminants associated with them when obtained from commercial batches. For example, ammonium sulphate can be contaminated with calcium ions, magnesium ions, and lead sulphate, whereas PEG can be with chlorine ions, nitrate ions, phosphate ions and sulphate ions (Lorber & Giege, 1992). Therefore, repurification is strongly recommended before use.

Not only must macromolecules be free from contaminants, but they must also be conformationally pure (Giege *et al.*, 1986). It is possible that denatured macromolecules such as proteins, or macromolecules with small structural changes can affect crystal growth more than contamination from other unrelated molecules. Heterogeneity in pure macromolecules (often called microheterogeneity) is a widespread phenomenon, causes of which are shown in Table 3.3 (McPherson,[a] 1985). The most common causes are uncontrolled fragmentation and post-synthetic modifications. Fragmentation can be caused by proteases (enzymes which catalyse the splitting of proteins into smaller peptide fractions and amino acids) or nucleases (enzymes which split the DNA chain). The presence of small quantities of proteases or nucleases can be a problem, since these can alter the structure of the macromolecule during storage or during the crystallisation process (Giege & Ducruix, 1992). A variety of commercial protease and nuclease inhibitors are available which can be added to the sample solution prior to crystallisation. Post-synthetic modifications can also influence crystallisation. Some modifications are reversible (e.g. phosphorylation) whereas others are not (e.g. glycosylation or methylation). Modifications to amino acid residues can produce conformational changes within the protein. Impurities and microheterogeneities are two important factors which can influence the crystallisation process. Therefore, before any crystallisation trials are carried out. care must be taken to maintain a high level of purity to ensure reproducibility

of results (Lorber & Giege, 1992). Processes such as lyophilisation or heat denaturation must be avoided, since these can introduce conformational heterogeneity, therefore preventing the growth of large crystals (Zeppezauer, 1971)

- Presence, absence or variation in a bound prosthetic group, coenzyme or metal ion
- Variation in the length or composition of the carbohydrate moeity on a glycoprotein
- Proteolytic modification of the protein during the course of isolation
- Oxidation of sulfhydryl groups during isolation
- Reaction with heavy metal ions during isolation or storage
- Presence, absence or variation in posttranslational side chain modifications such as methylation, amidination or phosphorylation
- Microheterogeneity in the amino or carboxyl terminus or modification of termini
- Variation in the aggregation or oligomer state of the protein association/dissociation
- Conformational instability due to the dynamic nature of the molecule
- Microheterogeneity due to the contribution of multiple but nonidentical genes to the coding of the protein
- Partial denaturation of sample
- Different animals or preparations of enzyme sources

Table 3.3 Factors contributing to heterogeneity.

In principle, the crystallisation of a macromolecule is little different from that of a small molecule. The growth of crystals from any sample requires the gradual creation of a supersaturated solution of the biological molecule, by modifying the properties of the solvent through equilibration with precipitating agents or by altering some physical property, such as temperature or pH, from which it can then enter into a crystalline or amorphous phase upon returning to equilibrium. An amorphous precipitate can be produced from highly concentrated solution where supersaturation has been reached too rapidly (McPherson,[a] 1985). A supersaturated solution contains more than the equilibrium amount of solute and this state is reached when the chemical potential of the solute in solution is greater than that of the crystal. The chemical potential is defined as the change in Gibbs free energy with respect to the change in amount of the component with pressure, temperature etc. Supersaturation can be achieved by varying any of the parameters which influence the chemical potential, such as temperature, pressure or protein concentration (Mikol & Giege, 1992).

Crystallisation involves three important steps, nucleation, growth and cessation of growth. The nucleation phase involves the initial formation of aggregates. Nucleation is homogenous if it occurs in bulk solvent or heterogenous if it occurs on solid particles such as dust or on the glass walls of experimental equipment. In order for a new phase (i.e. from liquid to solid) to be created, an energy barrier called the activation energy of germination must be overcome. This energy barrier decreases with supersaturation and increases with the interfacial crystal/solution free energy. Therefore, high supersaturation can reduce the energy threshold and encourage nucleation. Likewise, the presence of foreign particles within the solvent can increase the frequency of nucleation due to the reduction in the free interfacial energy. This allows a lower supersaturation to be used when working with heterogenous rather than homogenous nucleation. The conditions required for nucleation are not necessarily the same for optimal growth of crystals, since crystals do not grow in all supersaturated solutions. The crystallisation process can be represented by the diagram in Figure 3.1 (Mikol & Giege, 1992).

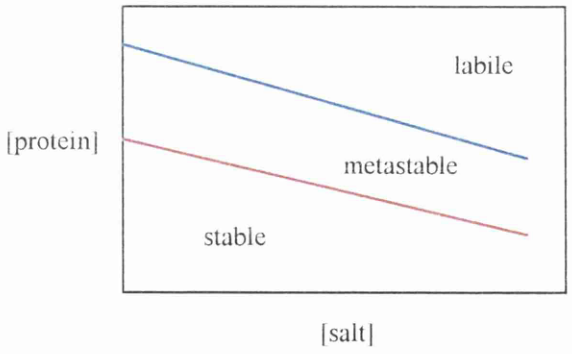

Figure 3.1 The diagram is divided into three sections. The stable (undersaturated) region where crystallisation is not possible; the metastable (supersaturated) region where nuclei cannot be formed, but crystals can grow and the labile (supersaturated) region where spontaneous crystallisation can occur. The red line represents the solubility curve and the blue line the supersolubility curve.

Ideally, supersaturation conditions which induce the formation of a single nucleus within the labile region should be chosen. This will, in turn, result in a decrease of the overall supersaturation since the excess solute will crystallise out of solution and accordingly, as growth occurs, the system will be pushed into the metastable region where regular crystal growth can proceed (Mikol & Giege, 1992). This may be partially achieved by seeding the solution with small, crushed microcrystals, which provides nucleation sites for further crystal growth and frequently leads to the production of large crystals (Davies & Segal, 1971). The rate of nucleation can be increased by a high solubility since there will be an increase in the number of free molecules in solution which will be more likely to associate with each other (Mikol & Giege, 1992). The supersaturation stage from which crystals can be recovered is achieved by allowing the slow evaporation of solvent from the sample or by altering some of the various parameters shown in Table 3.1, to allow the macromolecules sufficient time to order themselves in a crystalline lattice. The theory behind crystal growth can be thought of in two stages. Firstly, the mass transfer from the bulk of the solution to the crystal/solution interface and secondly, the attachment of the molecule on the crystal, with the first stage being influenced by diffusion and convection due to density-driven gradients. In the case of a perfect crystal, growth occurs two-dimensionally. A molecule hitting the surface of a crystal has little chance of being retained since only a small number of complementary bonds can be formed. However, once these adsorbed molecules form a two-dimensional nucleus on the surface of the crystal which exceeds a critical size, growth can proceed, with this nucleus now being able to incorporate molecules which may collide with the crystal surface (Mikol & Giege, 1992). The overall shape a crystal takes is determined by the relative growth rate of the faces. This can depend on both internal factors (structure bonds) and external factors (supersaturation, impurities etc.) (Mikol & Giege, 1992). In some cases, supersaturation requires the use of salt as a precipitant of which ammonium sulphate is the most commonly used (it is reported as the precipitant in 45% of the crystallisation conditions tabulated by Gilliland, 1988) due to its high solubility in water and its strong salting-out properties (Green, 1931 : Green, 1932). In addition, it does not tend to induce protein denaturation (Von Hippel & Schleich, 1969 : Timasheff &

Arakawa, 1985). In general, salt precipitated crystals possess good mechanical strength (Zeppezauer, 1971). The purpose of a precipitant is to exclude macromolecules from the bulk solvent, therefore aiding supersaturation.

Precipitants fall into three main classes; salts, organic solvents and the PEGs. Organic solvents bind water molecules and prevent them from interacting with macromolecule, therefore reducing the capacity of the system to fully solvate the solute (McPherson,[a] 1985) and are used in cases where crystals grown from salt solutions are unsatisfactory (Zeppezauer, 1971). However, many proteins can be denatured by organic solvents, therefore the choice of appropriate organic solvent is important and limited in number (Lee & Lee, 1981). PEG works by disrupting the natural structure of water and replacing it with a more complex network which has both water and polyethylene glycol as its constituents. This restructuring of solvent results in the macromolecules being excluded from solvent and therefore promotes phase separation (McPherson,[b] 1985). This was shown in the work of Lee & Lee, 1981, whereby experiments were carried out to study the preferential solvent interactions between proteins and PEG. This work showed that when proteins were introduced into a PEG solvent, the PEG was excluded from the protein domains. The precise mechanism by which PEG promotes crystallisation is still not fully understood, although it is thought that it is the unfavourable electrostatic interactions which arise from the introduction of proteins into a PEG solvent and the resulting instability which aids phase separation. Proteins with a small net charge do not appear to cause as much instability to the system as those with a higher net charge, therefore PEG is thought to be more effective as a crystallising agent for a highly charged protein, since phase separation will be encouraged. Phase separation is brought about by the system as it tries to reach a state of stability. In addition, the more hydrophilic the protein, the greater the instability induced in the solvent system, therefore PEG is thought to be better at promoting crystallisation of a highly hydrophilic protein than a more hydrophobic one (Lee & Lee, 1981). Nucleation and growth can be affected by both the shape and volume of sample drops, increasing the need for a well defined geometry of crystallisation chambers. Once growth has begun, it

is important that constant conditions are maintained in order to sustain the continued, ordered addition of single molecules, or ordered aggregates to the surface of the developing crystal (McPherson,[a] 1985).

After the growth phase, comes the cessation phase. Although the precise mechanism affecting cessation of growth is not fully understood, many hypotheses have been proposed, from the depletion of macromolecules from the crystallisation media and growth defects to ageing of the molecules (Giege & Ducruix, 1992). Another possibility is that during crystal growth, errors due to either chemical impurities or structural defects are incorporated until they accumulate to such an extent that further aggregation becomes unfavourable (Feher & Kam, 1985). In fact, anything in the solution which does not include either solute or solvent is thought of as an impurity e.g. crystallising agents or buffer salts. Such impurities can affect the crystal form if they can interact specifically with the macromolecule producing a new compound which will then be crystallised and therefore lead to errors associated with the overall crystal structure determination (Mikol & Giege, 1992). Many of the factors which appear to influence the crystallisation of macromolecules are still poorly understood and it is only after many trials in which the various parameters have been sequentially altered that the correct conditions for crystallisation can be determined. It is impossible to adhere to a rigid set of rules as to what the conditions or constituents of the mother liquor should be without prior trials. Care must be taken not to choose conditions that may denature or damage the macromolecule in any way (McPherson,[a] 1985).

There are many methods commonly used to crystallise biological molecules, the main aim of which is to bring the biological sample to a supersaturated state. The most popular of these methods is vapour diffusion and is discussed in section 3.1.1. As shown in Table 3.1, there are many variable parameters which can influence crystallisation of macromolecules. In addition, the method of crystallisation chosen can also affect both nucleation and growth stages. Therefore, it is advisable to use a series of different techniques until the optimum conditions for the growth of suitable crystals are reached.

Whichever crystallisation method is used, high concentrations of biomolecules are required. To achieve such high concentrations, dialysis may be needed to concentrate the biological macromolecule. After dialysis, the concentration of macromolecule is most commonly determined by measuring the absorbance of a small aliquot of sample which has been diluted with buffer to produce an absorbance of less than 1.0 (above 1.0 readings are generally less reliable) at either 280nm for proteins or 260nm for nucleic acids on a spectrophotometer. If the sample contains additives which absorb within the same range as the macromolecule, then subtraction of the reference cell absorbance from that of the sample should be carried out.

3.1.1 Vapour diffusion

Vapour diffusion techniques are the most widely used in crystallisation, especially for the growth of crystals from small molecules. It is ideal for gradually approaching the conditions of crystallisation. The principle behind this technique is that a small volume of biological macromolecule in solution with buffer, crystallising agent and additives is equilibriated against a much larger volume of solution containing crystallising agent at a higher concentration than in the droplet. The process of equilibration proceeds by the diffusion of water or organic solvent (if present) until the vapour pressure in the droplet equals the one of the reservoir. Supersaturation of the macromolecules is achieved by the evaporation of water. All solids and liquids give off vapours which consist of atoms or molecules of the substances that have evaporated from the condensed forms and these atoms or molecules exert a vapour pressure. If equilibration occurs by water exchange from the drop to the reservoir, it will lead to a change in the volume of the sample drop and therefore the concentration of all components of the drop will change. For a species with a vapour pressure higher than water, the exchange will occur from reservoir to drop. The same principle applies for hanging drops, sitting drops and sandwich drops, schematic representations of which are given in Figure 3.2 (Ducruix & Giege, 1992). Generally this method is used to ensure that all constituents in the drop are concentrated.

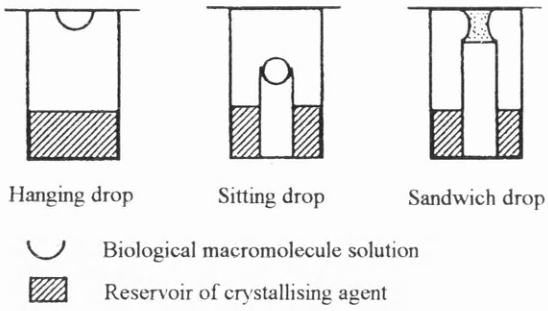

Figure 3.2 Schematic representation of hanging drop, sitting drop and sandwich drop.

Vapour diffusion techniques provide an easy way to vary the physical parameters during the crystallisation process. Supersaturation can be altered by varying the temperature or pH conditions (McPherson,[a] 1985). If ammonium sulphate is used as the crystallising agent, pH changes occur due to ammonia transfer following ammonium/ammonia equilibrium and the pH of the sample droplet can be influenced by that of the surrounding reservoir of solvent. In aqueous solutions, ammonium ions dissociate into ammonia and hydrogen ions according to the equilibrium $NH_4^+ \rightleftharpoons NH_3 + H^+$ and the NH_3 leaves the aqueous solution and enters the vapour phase. If the concentrations of the ammonia in the sample drop are different from those in the reservoir due to differences either in pH or in total ammonium species concentration, they will tend toward an equilibrium by ammonia exchange between the drop and the reservoir so that both $[NH_3]$ and pH are the same. This can be illustrated by considering the following cases. If a sample drop has an initial pH 9.0, and the reservoir a pH 8.0, $[NH_3]$ is higher in the drop than the reservoir. Therefore, NH_3 diffuses from the drop to the reservoir, resulting in an acidification of the drop until both drop and reservoir equal the same pH and $[NH_3]$. Conversely, if the reservoir has a higher pH than the drop, NH_3 will diffuse from the reservoir to the drop and alkalinize the drop until both $[NH_3]$ and pH are the same (Mikol *et al.*, 1989). Therefore by varying the pH of the reservoir, the pH of the sample droplet can be adjusted. This represents a simple way to alter the crystallisation conditions. If the solubility of a macromolecule is pH dependent, any variations in pH

brought about by the diffusion of NH_3 between the drop and the reservoir represents one way to reduce supersaturation so that after nucleation, conditions can be changed to promote optimal crystal growth. In addition, by varying the volume of the droplet it is possible to influence the kinetics of crystallisation and therefore the crystal size. The geometry of the drop proved to be an important consideration for nucleation using the vapour diffusion technique when crystallising a subunit of ribosomes from *Bacillus stearothermophilus* (Yonath *et al.*, 1982). Other factors which affect the equilibration rate are dilution of the drop and temperature (Mikol & Giege, 1992).

One way of quantifying the influence of the various crystallisation parameters (which can be altered to produce high quality, monocrystals of suitable size) on the solubility of biological macromolecules is to produce solubility diagrams. The two-dimensional solubility diagram illustrated in Figure 3.3 (Ries-Kautt & Ducruix, 1992) shows the relationship between protein solubility and one other parameter e.g. crystallising agent concentration (all other parameters must be constant). The diagram in Figure 3.3 is composed of four distinct zones. The area under the solubility curve is the *undersaturation* zone, which is produced when less than the equilibrium amount of protein is dissolved and in this region crystals will never grow. The solubility curve represents the equilibrium between the saturated protein and the crystallised protein and divides the undersaturated from the supersaturated zones. Above the solubility curve is the *metastable* zone in which a supersaturated solution will not nucleate but will sustain growth of crystals. The next zone is the *nucleation* zone, in which the excess of biological macromolecule separates as a crystal form, initiating the formation of new crystals. Lastly, the *precipitation* zone is where supersaturation is reached too quickly and the excess protein separates from the solution immediately in an amorphous state. The solubility curve can be determined experimentally either by the crystallisation of a supersaturated solution or by dissolution of crystals in an undersaturated solution. It is important for both methods that only one parameter is varied and biological macromolecule is checked for stability (Ries-Kautt & Ducruix, 1992).

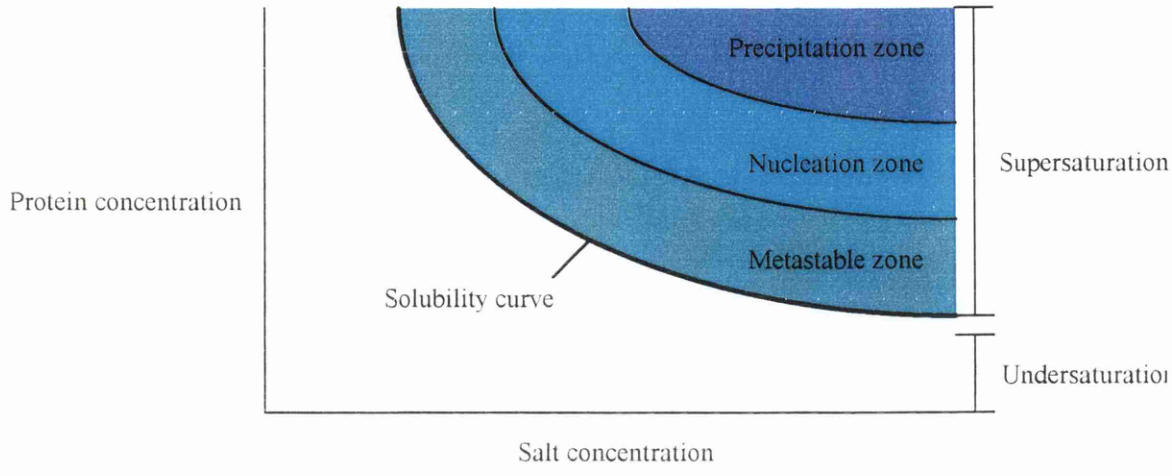

Figure 3.3 Two-dimensional solubility diagram showing the change in protein concentration with crystallising agent concentration.

3.2 X-ray diffraction

Once crystals of a suitable size have been obtained by the methods described previously, the next stage is to check whether they will produce a good diffraction pattern from which the structure of the macromolecule can be determined. There is nothing more frustrating than carrying out the various crystallisation steps to produce large crystals and then discovering either that they do not diffract or that they rapidly decay in the X-ray beam. This section will give an overview of the techniques involved to produce an X-ray diffraction pattern and solve the structure.

Before any discussion of X-ray analysis, it is important to understand the composition of the crystal. Basically, the crystal can be thought of in terms of a regular, repeating array of atoms or molecules in three-dimensions. Such an object can be described with the aid of a lattice, which is simply a geometric construction defined by three axes (a, b and c) and three angles (α, β and γ) between them. The basic building block of the crystal can then be described by these dimensions and the angles between them and is called the unit cell and along each axis a point will repeat at a distance known as the unit cell repeat.

Although the unit cell and the lattice produced by its repetition have a characteristic symmetry, the arrangement of molecules within the unit cell itself may also have symmetry, giving rise to what is known as the asymmetric unit. It is this symmetry which gives rise to the space group. This allows the crystallographer only to need to locate the atoms within the asymmetric unit rather than in the entire unit cell, since the atoms here will be repeated throughout the unit cell according to their symmetry (Sawyer & Turner, 1992).

3.2.1 Data collection

Now that we understand the basic anatomy of the crystal we can begin to discuss how X-rays are used to produce a diffraction pattern. X-rays are used because in order to observe the individual atoms within the macromolecular structure, it is necessary to use a radiation of a similar wavelength to the interatomic distances (1.5Å) and X-rays lie within this region in the electromagnetic spectrum (Sawyer & Turner, 1992). X-rays are emitted when electrons jump from a higher energy level to a lower one and are produced in the laboratory by accelerating a beam of electrons into a metal anode. The electrons decelerate as they plunge into the metal producing collisions with electrons of other atoms. Such a collision expels an electron and an electron of higher energy drops into the vacancy produced, emitting the excess energy as an X-ray photon (Atkins,[c] 1996). The metal determines the wavelength of emitted radiation. Generally, copper is the metal of choice and the characteristic wavelength of radiation produced is 1.542Å (Sawyer & Turner, 1992). The high voltages involved in this process cause the metal plate to rapidly heat up and therefore there has to be a cooling procedure to prevent the plate from melting. This can be achieved by rotating anode X-ray generators, whereby the metal plate is revolved so that different parts are heated up each time (Branden & Tooze, 1991). Synchrotron radiation can also be used. A synchrotron is a large-scale particle accelerator, which when electrons are used is capable of providing a high intensity X-ray source. The orbit of particles in this device is produced by magnetic fields that increase, with time, proportional to the increased momentum of the particles.

while the radius during acceleration remains constant. Synchrotron radiation can have a wide spectrum of wavelengths from radio waves to X-rays, therefore has many applications.

In diffraction experiments a narrow and parallel beam of X-rays from the source is directed at a mounted crystal to produce diffracted beams which are then recorded on an electronic detector. Most of the X-rays, however, travel straight through the crystal. These undiffracted beams are prevented from also hitting the detector by being collected in the beam stop. This is a small cup of 1mm diameter which is filled with lead and sits between the crystal and the detector (usually as close as possible to the crystal to avoid air scatter and background reflection) and is carefully aligned with the collimater through which the primary beam of X-rays travels, the crystal and the centre of the detector. A schematic view of a typical diffraction experiment is given in Figure 3.4 (Branden & Tooze, 1991).

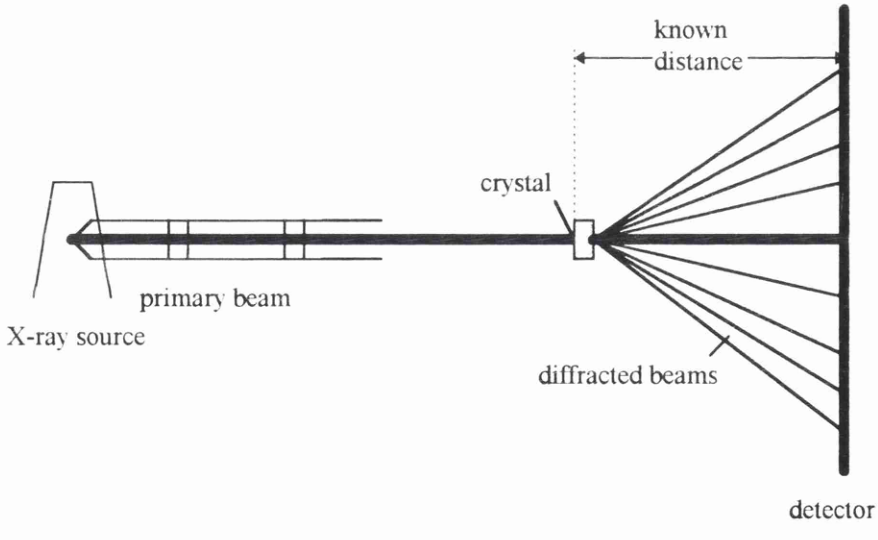

Figure 3.4 A narrow beam of X-rays is taken out from the X-ray source. When the primary beam hits the crystal, most of it passes straight through, but some is diffracted by the crystal. These diffracted beams, which leave the crystal in many different directions, are recorded on a detector.

The primary beam of X-rays can cause damage to the crystal by producing free radicals of the protein or solvent molecules which can then go on to damage other molecules in the crystal. The heat generated by passing X-rays through a crystal can be so intense that in time it can burn directly through the crystal, therefore the crystal is cooled to increase its life span. The primary beam of X-rays must strike the crystal from a variety of directions to produce all possible diffraction spots, therefore it is rotated in the X-ray beam (Branden & Tooze, 1991).

As mentioned previously, when X-rays strike a crystal, most of the X-rays travel straight through. But some interact with the electrons within the atoms causing them to oscillate. These oscillating electrons act as another source of X-rays and emit their radiation in all directions. This phenomenon is known as scattering. When these electrons are arranged within atoms in a regular three-dimensional form as in a crystal, these emitted X-rays can interfere with each other producing either destructive interference, where they effectively cancel each other out or constructive interference, where they enhance each other. It is diffracted beams of this latter effect which produce intense diffraction spots which can be recorded by the detector (Branden & Tooze, 1991). A typical diffraction pattern is shown in Figure 3.5 (Voet & Voet,[b] 1990).

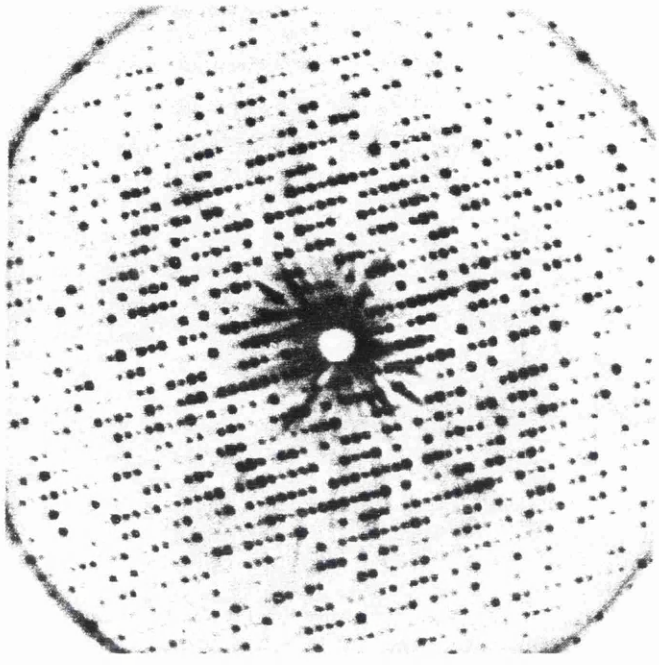

Figure 3.5 An X-ray diffraction photograph of a single crystal of sperm whale myoglobin. The intensity of each diffraction maximum (the darkness of each spot) is a function of the crystal's electron density.

It is important to realise that each atom in the crystal contributes to every reflection and that the intensity of the reflected X-ray beam depends upon the atomic arrangement within the unit cell (Sawyer & Turner, 1992). Since it is the electrons which diffract the X-rays, if the atom has a large number of electrons within its atomic arrangement there will be a greater number of scattered electrons and therefore a greater chance of constructive interference. It is this principle which is used in isomorphous replacement. This involves artificially introducing heavy atom derivatives which have a large number of electrons into the crystal structure to enhance the intensity of the reflected X-ray beam.

Further explanation of how X-rays are scattered by crystals is given by Bragg's law. This shows how the diffraction of X-rays by a crystal can be regarded as the reflection of the primary beam by sets of parallel planes through the unit cells of a crystal, hence why the term reflection is frequently used to indicate an intense spot arising from constructive

interference. This law predicts that since X-rays which are reflected from adjacent planes within the unit cell travel different distances, diffraction only occurs when the difference in distance is equal to an integral number of wavelengths. When the pathlength difference is equal to one wavelength, the reflected waves are in phase and interfere constructively. The relationship between the spacing of the planes, d, the wavelength, λ and the angle at which the emergent ray is observed relative to the direction of the planes is given by:

$$n.\lambda=2d.\sin\theta \qquad (3.1)$$

A schematic representation of this relationship is given in Figure 3.6 (Sawyer & Turner, 1992). The order of diffraction, n, which is the number of wavelengths difference between the scattering from adjacent planes influences the angle of scattering. The higher the order or the greater the number of wavelengths difference between rays reflected from adjacent planes, the larger the angle of scattering. The direction of a diffracted X-ray beam depends upon the orientation of the crystal lattice and the intensity of the X-ray beam on the atomic arrangement of the unit cell (Sawyer & Turner, 1992), the more electrons in the outer electron shell, the greater the intensity. The primary use of Bragg's law is in the determination of the spacing between the layers of atoms. Once the angle θ, corresponding to a reflection, has been determined from the position of the diffracted spot on the detector and the order of diffraction has also been calculated from the positioning of this diffracted spot and the wavelength which is determined from the source is known, d can then be calculated (Atkins,[c] 1996).

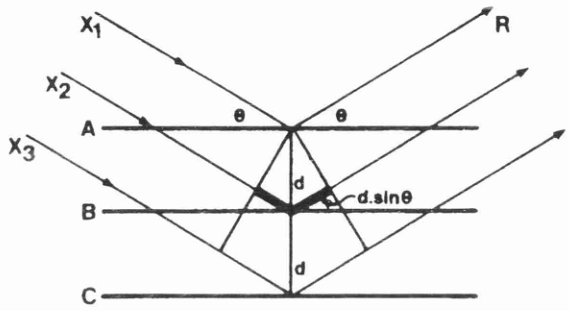

Figure 3.6 X-rays (X_1, X_2, X_3) reflected from lattice planes A, B, C. To observe a scattered beam of X-rays in direction R, the thickened path must equal a whole number of wavelengths.

3.2.2 Data processing

Once a diffraction pattern containing many reflections has been produced, these reflections must be indexed to provide information on the unit cell dimensions of the crystal. If we consider a three-dimensional array of points, we can distinguish the sets of planes on which the points lie by the distances along the axes at which the planes intersect them. This way of labelling the planes using Miller indices is commonly used in crystallography. Miller indices take the reciprocal of the co-ordinates and remove any inconvenient fractions (Atkins,[c] 1996). The letters *h*, *k* and *l* are then used to refer to these indices (Sawyer & Turner, 1992). It is not necessary to index every reflection within the crystal, just those within the unique part of the cell i.e. the asymmetric unit. By applying the space group symmetry it is possible to index all further reflections, although in practice crystallographers only work with the molecule within the asymmetric unit.

Now is the time to introduce the concept of the reciprocal lattice. Lattice points within a crystal in real space can be related to points in diffraction space or reciprocal space.

These points make up another lattice, known as the reciprocal lattice, whose axes and angles are derived from those of the crystal. Crystallographers therefore, tend to discuss the X-ray diffraction pattern in terms of the reciprocal lattice. The concept of reciprocal space may be developed by introducing the related concept of the Ewald sphere, shown in Figure 3.7 (Sawyer & Turner, 1992), in order to help understand the diffraction of X-rays from a crystal.

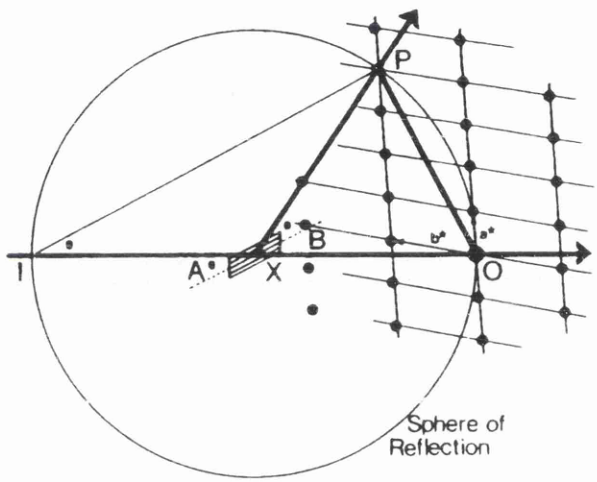

Figure 3.7 The Ewald construction. For clarity, this is shown as a planar diagram but IXO is the diameter of a sphere of radius $1/\lambda$.

As the crystal is rotated in the X-ray beam, the reciprocal lattice also moves about a fixed origin. Figure 3.7 shows a beam of X-rays passing through the crystal, X, to the origin, O, and being diffracted to P. With the crystal, X, as centre, a sphere is drawn of radius $1/\lambda$, and the origin, O, of the reciprocal lattice is taken as the point where the X-ray beam leaves the sphere after passing through the crystal. As the crystal is rotated about the *z*-axis, the reciprocal lattice rotates until the point P lies on the surface of the sphere. The reciprocal lattice point P represents the Bragg reflection from a set of planes indexed as *hkl*. Reflections only occur when the reciprocal lattice points lie on the sphere of reflection, therefore explaining why the crystal must be rotated in the X-ray

beam to produce all possible reflections. The Ewald sphere provides a way of relating the orientation of the crystal to the diffraction pattern. The higher the symmetry of the crystal, the less data needs to be collected. A diffraction pattern also has a centre of symmetry since reflections in opposite directions along the same crystal plane must have the same intensity (Sawyer & Turner, 1992). The lattice type and symmetry elements within a crystal can lead to a phenomenon known as systematic absences. This effect is best illustrated by considering Figure 3.6. If the X-ray beam X_3 is one wavelength behind that of X_1, it follows that X_2 must be half a wavelength behind, since the lattice planes are equal distances apart. Therefore, X_2 will cancel out the positive contributions made by X_3 and X_1, leading to absences of reflections. In other words, lattice planes midway between planes separated by the unit cell repeat can lead to a systematic absence of reflections (Sawyer & Turner, 1992).

One of the major crystallographic problems in solving protein structures is determining the phase of each reflection. The waves of X-ray radiation of the primary beam are in-phase i.e. the amplitude, intensity and wavelength are all the same. However, upon diffraction by the crystal, the waves become out-of-phase. Therefore, it is unknown which phase the diffracted X-rays are in when they hit the detector. The information, therefore, needs to be recombined in the correct phase relationship to determine the position of the atoms which give rise to the reflected beams. Figure 3.8 (Branden & Tooze, 1991) shows two diffracted beams which are out-of-phase.

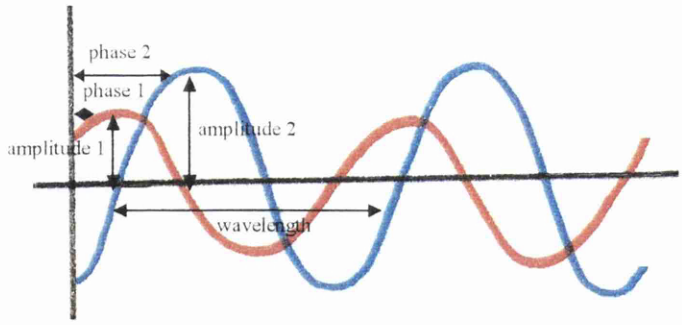

Figure 3.8 Two diffracted beams, each of which is defined by three properties: amplitude, which is a measure of the strength of the beam and which is proportional to the intensity of the recorded spot; phase, which is related to its interference with other beams and wavelength, which is set by the X-ray source.

A phase must be calculated for each reflection to be included in the calculation of an electron density map. The more reflections phased, the clearer the map and better the resulting protein model will be. In reporting a structural model, the resolution of data is usually included. This refers to the minimum plane spacing included in the calculation e.g. for a 2.5Å, all reflections with plane spacings greater than or equal to 2.5Å will be included. The higher the resolution, the greater the amount of X-ray data which must be collected (Sawyer & Turner, 1992).

For large molecules such as proteins, the phase problem can be solved by isomorphous replacement. As mentioned previously, this method involves the introduction of heavy atoms as new X-ray scatterers into the unit cell of the crystal. Problems arise if there are a large number of molecules within the asymmetric unit, since the heavy atoms may become liganded to each molecule, giving an extremely difficult Patterson to interpret. In such cases, molecular replacement (see section 3.3) may be applicable if a similar structure already exists, as was the situation with vancomycin. It is important that upon the preparation of a heavy atom derivative, the protein crystallises in a similar size of unit cell and with the same space group as the native protein. Such pairs of compounds will be isomorphous. This method has been the basis of all new protein structures.

Isomorphous replacement is usually performed by diffusing different heavy metal complexes into the solvent channels of already formed protein crystals. The protein molecules within the crystal may expose functional side chains to these channels which will bind the heavy atoms, allowing the heavy atom positions to be related to the structure of the protein. Since heavy atoms (e.g. Hg) contain significantly more electrons than light atoms of proteins (e.g. H, N, C, O and S) they will scatter X-rays more strongly, therefore all diffracted beams will increase with intensity provided constructive interference occurs (Branden & Tooze, 1991). It is the difference in intensity of the diffracted beams in the presence of heavy atoms which is the basis behind phase determination.

Now that we understand the principle of isomorphous replacement, how do we find phase differences between diffracted spots from intensity changes following heavy atom substitution? The intensity differences are used to deduce the position of the heavy atoms within the unit cell and Fourier transformations are then used to give maps of the vectors between the heavy atoms, producing the so-called Patterson maps. From these maps, the atomic arrangement of the heavy atoms are determined. Once the positions of the heavy atoms have been determined, it is possible to calculate the amplitudes and phases of their contribution to the diffracted beam. This is best explained by considering the relationship between structure factors (an expression used to illustrate the relationship between the combined scattering of X-rays for all atoms in the unit cell compared to that for a single electron) and electron density. The former deals with intensity and phases and the latter deals with the position of the atom and the number of electrons, more precisely the density of electrons and their distribution around the atom. The production of the Patterson map provides the position of the heavy atom which can then be related to the structure factor which will then provide an estimate of the phase of that reflection. Knowledge of these parameters can then be used to provide information on the phase of the contribution from the protein in the absence of heavy metal atoms. From above, we know the phase and amplitude of the contribution to the diffracted beam from the heavy atoms and the amplitude of the protein alone from the intensity of the

beam before heavy atoms were introduced. We also know the amplitude of the protein/heavy atom complex. Therefore, we know one phase and three amplitudes. From this it is possible to calculate if the interference between beams is constructive or destructive, as shown in Figure 3.9 (Branden & Tooze, 1991) and therefore provide an estimate as to the phase of the protein. From such estimates, two different phase angles are possible and the correct one needs to be determined. In order to distinguish between these two possibilities a second heavy metal complex must be used, which will also produce two possible solutions, only one of which will have the same value as the previous attempts and therefore represents the correct solution. Although this appears to be an ideal technique, there are drawbacks. Accuracy can be compromised in such determinations due to errors in the measured amplitude and also frequently intensity differences after isomorphous replacement are too small to measure and trials with other heavy metal atoms need to be carried out (Branden & Tooze, 1991).

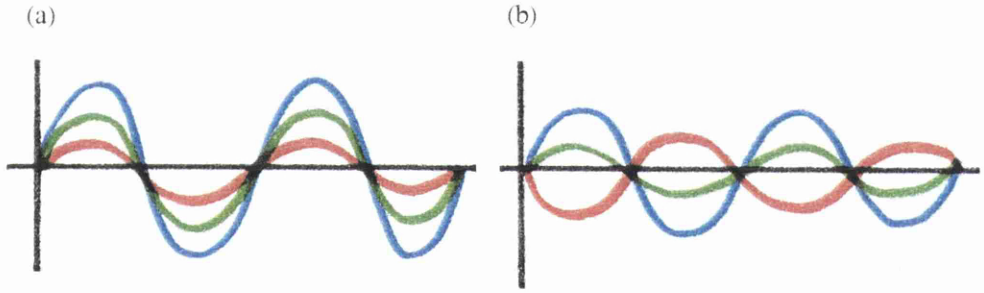

Figure 3.9 The diffracted waves from the protein part and the heavy metals interfere with each other in crystals of a heavy atom derivative. If this interference is constructive as in (a) waves red and green will combine to produce wave blue which has a greater amplitude. The interference will be destructive as in (b) if waves blue and red cancel each other out to a certain degree to produce wave green which has a lower amplitude.

Once the amplitudes and phases have been determined, they can then be used to produce an electron density map of the unit cell. This map, an example of which is given in Figure 3.10 (Ladd & Palmer, 1994), then has to be interpreted in terms of individual amino acid

side chains which may extend into the regions of high electron density. This procedure is difficult, since the map contains errors, mainly due to incorrect phase angle determination or can be hampered by poor resolution of the diffraction data. The lower the value of resolution, the greater the detail which can be observed, therefore it is advantageous to try and get data to as low a resolution value as possible. If this can be achieved, for example at 3Å, it is possible to discriminate between the electron density of individual amino acids, whereas at higher values such as 5Å, it is only possible to obtain the overall shape of the molecule. Intermolecular forces such as hydrogen bonds can be determined from distance measurements from the electron density map, since the distance between the atom attached to the hydrogen in the weakly acidic donor group and the acceptor atom is known to be between 2.7-3.1Å (Voet & Voet,[b] 1990). Other interactions can be estimated from the orientations of particular amino acids. After the electron density of the map has been produced and structural features identified, a model of the structure can be developed. This however, is not as easy as it sounds because we need to decide how the polypeptide chain fits into the regions of electron density. Therefore, it is essentially a trial and error process. Once a possible fit between the polypeptide chain and the electron density has been obtained a model can be produced using computer graphics to provide a possible three-dimensional structure of the protein (Branden & Tooze, 1991).

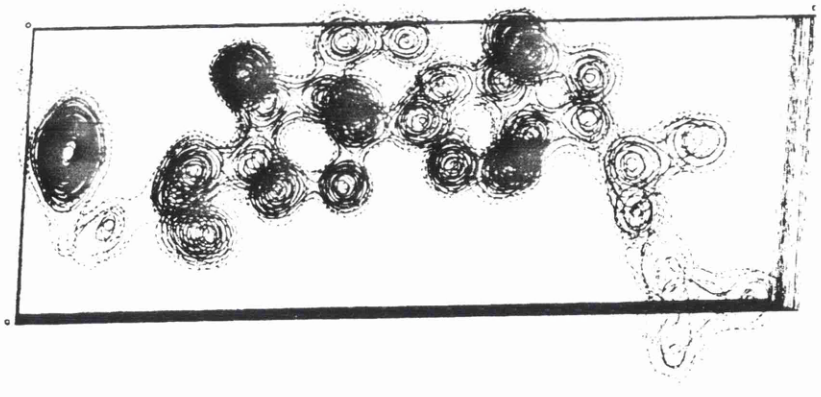

Figure 3.10 A typical three-dimensional electron density contour map, the contours of which connect points of equal electron density.

The initial model obtained from electron density maps will always contain a certain degree of errors, mainly from differences between the experimentally observed amplitudes and those calculated for a crystal containing the model rather than the real molecule. These errors can be reduced by crystallographic refinement of the model, where this difference is expressed as an R factor (residual disagreement). This value ranges from 0.0 for exact agreement to 0.59 for total disagreement, but generally speaking the value is usually between 0.15 and 0.20 for a good protein structure determination. It must be remembered that the model never corresponds exactly to the crystal due to errors, for example from the inaccurate determination of the presence of solvent molecules or slight differences in the orientation of individual residues. The model simply represents an average of molecules which are present in the crystal. The lower the resolution value the greater the likelihood that there will be accurate interpretation of the electron density map. Refined structures at around 2Å usually contain no major errors in the orientation of individual residues, but at a resolution of around 3Å it is possible to make such errors. These errors usually arise from incorrect connections between secondary structures. For example, α helices and β strands within the protein are rigid and well characterised in the electron density map, however, connecting loop regions are more flexible and therefore the corresponding electron density is less well defined. It is therefore easy to incorrectly assign loop regions between these elements of protein secondary structure (Branden & Tooze, 1991).

In recent years, solving the structure of proteins using X-ray crystallography has been made easier by the development of electronic area detectors connected to microcomputers with sophisticated software which automatically collects and processes data. Historically, X-ray film was the method of collecting diffraction data. Now direct read-out electronic systems have replaced the wet chemistry of developing such film. There are principally three types of detectors commonly used by crystallographers, the Image Plate, the Charge Coupled Device (CCD) and the Multiwire Proportional Counter (MWPC), each of which will be dealt with in turn. The principle of operation behind the Image Plate is the photo-stimulated luminescence of $BaFBr:Eu^{++}$ crystals. X-rays ionise

Eu^{++} to Eu^{+++} causing the electrons to be trapped in a metastable level. An electron is released by visible light illumination and returns to Eu^{++}. Flooding with light illumination is used to return the crystals to their original ionisation state, so the film can be re-used. The exposed image plate is then scanned by a laser which then provides a digital read-out of the position and intensity of each reflection. The plate is essentially 'measuring' the change in ionisation of the crystals due to the reflected X-rays hitting the plate at different positions and intensities. The CCD involves a semi-conductor (silicon) detector in which the sensitive area is divided into a large number of elements. Incident radiation is converted into charge and the stored charge is used to build up a 'digital' image. The MWPC (e.g. Siemens-Xentronics) is composed of a sealed chamber filled with Xe gas at 4atm and a two-dimensional grid of wires under a set potential. X-rays entering the chamber (through a mylar window) ionise the Xe gas. This ionisation is detected by a change in potential of the grid wires. Since the wires are connected to an electronic decoder, the position and intensity of the X-ray reflections can be recorded and stored. Such advances now allows data collection times to be reduced from many months to just a few days and compared with film, electronic detectors require less exposure time and can be processed automatically (Kabsch, 1988). Once electron density maps have been interpreted, possible models of the protein structure can be produced using graphics packages specifically designed for this purpose which use semi-automatic methods for the model building based on knowledge of similar solved protein structures from a large crystallographic database, ultimately allowing more rapid solving of the structure than would have been possible several years ago. This reinforces crystallography as a powerful technique for structure determination, although nuclear magnetic resonance (NMR) is increasingly being used to obtain three-dimensional models of small protein molecules. also

3.3 Molecular replacement

Molecular replacement is an important component of X-ray analysis since it allows the unknown structure of a protein/small molecule to be determined from a model of an homologous molecule, the crystal structure of which has already been established. This method is advantageous in that often proteins with unrelated functions exhibit structural similarities, therefore it is possible to relate such apparently different molecules with this technique to help solve an unknown structure. It is a computationally simple technique, but can often be fraught with difficulties, as discussed later and can be carried out by sophisticated software packages, such as AMORE, which require little intervention by the user. If the model shows good complementarity with the molecule of interest, this process can take just minutes to complete. The more different the model is to the unknown structure, the more difficult and laborious the process. Also, the higher the space group symmetry, the harder the task, as was the case with the vancomycin complex (see chapter 6). The purpose of this section is to give a brief overview of the procedures involved in this technique.

The molecular replacement method can be thought of as involving three steps (Harding, 1985), each of which is discussed as follows:

1) Finding a structure model for all or a sufficiently large part of the molecule in the unknown structure.
2) Finding the orientation and position in the cell of the model structure by rotation and translation functions.
3) Calculating phases from the model and an electron density map which allow the remainder of the structure to be found and refined.

As mentioned previously, the basic building block of the crystal is the unit cell within which is located the asymmetric unit which contains a number of molecules related by their symmetry into space groups. Once a model molecule of similar structure to the

molecule of interest is obtained, the function of molecular replacement is to superimpose this model over the unknown structure, by rotation and translation, to produce a fit. This process will always require six variables to be specified, three for the rotation about the origin and three for the translation e.g. the amount of motion in the *x*, *y* and *z* directions (Blow, 1985). A fit is not required for every molecule within the asymmetric unit, since many will be related by symmetry and therefore will effectively cancel each other out. One advantage of this technique is that it is possible to remove parts of the model which are not expected to be present in the molecule of interest, if a more appropriate model cannot be found. One of the main problems in producing a fit, however, is errors. If errors in the initial model are sufficiently large, convergence to the correct solution may be prevented (Leslie, 1985).

3.4 Electrospray mass spectrometry

As mentioned previously, this novel technique can be used to estimate the purity of samples prior to crystallisation. It is based on the separation of charged particles according to their mass-to-charge ratios and has the ability to measure molecular masses with a precision of ±0.01% (Nairn *et al.*, 1995). A typical experimental setup is shown in Figure 3.11 (Mann & Wilm, 1995). A solution of the molecules of interest is passed through a needle which is kept at a high electric potential. At the end of this needle, the solution is dispersed into a mist of small, highly charged droplets containing the sample. From this, desorption of the sample ions from the droplets occurs and the sample is released into the gas phase. Once the ions are in this phase, they then enter the vacuum of a mass spectrometer (Mann & Wilm, 1995). Here, the ions are accelerated in an electric field of high potential and then become deviated in a magnetic field, which varies to give a trajectory of ions, the radius of which depends on the mass-to-charge ratio, so that different ions will hit the detector at different positions. A signal is then generated, the intensity of which is proportional to the number of ions arriving (Frigerio, 1974). The resulting mass spectrum can then be used to determine the molecular mass of the sample constituents, provided that the components differ by at least 0.1% in molecular

mass. This technique represents an effective way to check for the presence of impurities within a sample, since such compounds will clearly show up in the resulting signal.

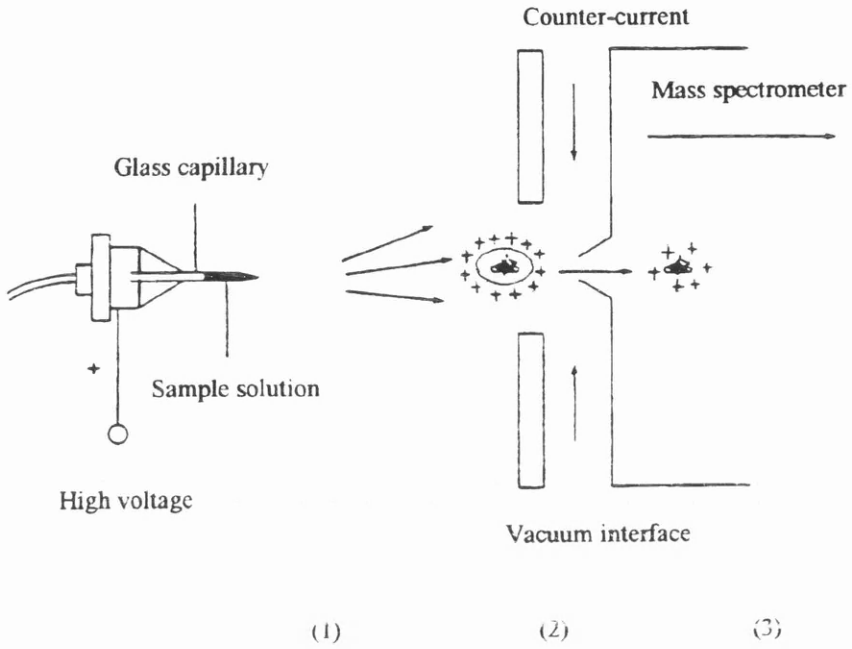

Figure 3.11 The three main steps of electrospray mass spectrometry are (1) Formation of small, highly charged droplets by electrostatic dispersion of a solution under the influence of a high electric field (2) Desorption of protein ions from the droplets into the gas phase (assisted by a counter-current of hot N_2 gas) (3) Mass analysis of the ions in a mass spectrometer.

Chapter 4:
Materials and Methods

4.1 Antibiotics and cell wall analogues

Vancomycin (HCl), ristocetin (sulphate salt), N-acetyl-D-Ala, N-acetyl-D-Ala-D-Ala and N_{α},N_{ε}-diacetyl-Lys-D-Ala-D-Ala were all supplied from Sigma Chemical Co. and were used without further purification. N-fumaryl-D-Ala was kindly provided by Dr D. H. Williams, Cambridge University.

4.2 General chemicals

All other chemicals used were of A.R. grade.

4.3 Preparation of antibiotic samples for microcalorimetry and UV difference spectroscopy

Antibiotic and peptide samples were prepared in various buffers over a pH range. Buffers used were 0.1M citrate at pH 3, 0.1M acetate at pH 5, 20mM citrate at pH 5.1, 0.1M sodium phosphate at pH 7, 0.1M PIPES (piperazine-N,N'-bis(2-ethanesulfonic acid) at pH 7, 0.1M MOPS (3-(N-morpholino)propanesulfonic acid) at pH 7, 0.1M Imidazole at pH 7, 0.1M TRIS (tris(hydroxymethyl)aminomethane) at pH 8 and 0.1M sodium phosphate at pH 11. Molecular weights are as follows: vancomycin = 1485.7; ristocetin = 2063; N-acetyl-D-Ala = 131.1; N-acetyl-D-Ala-D-Ala = 202.2; N_{α},N_{ε}-diacetyl-Lys-D-Ala-D-Ala = 372.4; N-fumaryl-D-Ala = 185. Concentrations of vancomycin ranged from approximately 0.1-0.3mM in microcalorimetric binding experiments and 2.0-3.0mM in dimerisation experiments. Ristocetin concentrations used were approximately 3.0mM. The concentrations of ligand used depended upon their

affinity for antibiotic, for example approximately 50mM N-acetyl-D-Ala, 7.0mM $N_{\alpha},N_{\varepsilon}$-diacetyl-Lys-D-Ala-D-Ala, 3.5mM N-acetyl-D-Ala-D-Ala and 50mM N-fumaryl-D-Ala in binding experiments and 90-100mM N-acetyl-D-Ala, 1.0-5.0mM $N_{\alpha},N_{\varepsilon}$-diacetyl-Lys-D-Ala-D-Ala and 1.5-3.0mM N-acetyl-D-Ala-D-Ala in trial dimerisation experiments. The concentration of vancomycin in kinetics experiments using UV difference spectroscopy ranged between 3.5-5.5mM and $N_{\alpha},N_{\varepsilon}$-diacetyl-Lys-D-Ala-D-Ala between 5.2-6.2mM. The vancomycin and N-acetyl-D-Ala-D-Ala concentrations used for the determination of the association constant using UV difference spectroscopy was 0.02mM and 1.8mM, respectively.

4.4 Estimation of vancomycin concentration by UV absorption

Vancomycin absorbs at around 280nm due to the presence of phenolic groups. From the knowledge of the absorbance at this wavelength and the extinction coefficient, it is possible to calculate the corresponding concentration according to the Beer-Lambert law. The molar extinction coefficient E_{280nm} = 6690$dm^3mol^{-1}cm^{-1}$ at pH 7 (Nieto & Perkins [a,b], 1971) was used for all determinations.

4.5 Procedure using Omega titration microcalorimeter

The reference cell contained degassed, distilled water and acted as a control. The sample cell was filled with either antibiotic, buffer or ligand solution, depending on whether it was binding or dimerisation, respectively, that was of interest. This filling procedure was carried out taking care to avoid air bubbles that may be trapped in the cell. The sample cell can hold approximately 1.4mls of sample. After loading of the sample, the temperature of the cells were set (15-45°C) and allowed to reach thermal equilibrium, this taking just a few minutes. The injection syringe was then filled with either antibiotic or ligand, depending on the process to be studied. The syringe was then mounted in the sample cell and secured in place by a cap fitting. The standard number of revolutions per minute of the syringe was 400.

When the baseline was stable (RMS noise 0.04μJ sec^{-1} or less) an injection schedule was prepared. For binding studies, this typically involved 20×5μl injections of ligand at 3 minute intervals into the cell containing antibiotic and for dimerisation studies, 12×20μl injections of antibiotic and ligand at 3 minute intervals into the sample cell containing buffer or unbound ligand. The experiment was then started, with appropriate controls carried out under identical conditions.

The sample cell was cleaned with excess water and stored in distilled, degassed water containing 0.05% sodium azide, to prevent bacterial contamination. The syringe was rinsed out with ethanol. The experimental data were corrected for heats of dilution of controls. Buffer/buffer dilutions showed small heats, which were negligible compared to the heats associated with binding or dimerisation. The data were analysed using Origin software, the one set of sites model for binding and a simple monomer-dimer model for dimerisation (see chapter 2), to give values of K and ΔH from which ΔG° and ΔS° were calculated.

4.6 Calibration of the Omega titration microcalorimeter

A calibration constant is required to convert the observed signal to a heat quantity. Calibration of the Omega microcalorimeter can be carried out either electrically or chemically. Electrical calibration uses standard heater resistors which heat the sample cell at a chosen rate for a selected period of time. The integral of the heat pulse should correspond to the known applied heat, giving rise to a calibration constant (McAuley-Hecht, 1993). This calibrates thermal sensitivity, however a more accurate determination of the calibration of the entire system, including sample volume is obtained using a series of standard reactions (Cooper & Johnson,[a] 1994). Reactions commonly used include the heat of protonation of tris(hydroxymethyl)aminomethane, the heat of ionisation of water (Grenthe *et al.*, 1970) and the binding of N-acetylglucosamine to hen egg-white lysozyme (Cooper, 1974), although no prior calibration was required in our series of experiments. If either the neutralisation of base or the ionisation of TRIS is used as a

calibration at concentrations low enough to produce the expected heat effects, it should be remembered that absorption of carbon dioxide or impurities in the water can make a significant contribution to the heat effects.

4.7 Determination of association constants using UV difference spectroscopy

This method was used to provide information on the binding affinity of vancomycin for the cell wall analogue peptide, N-acetyl-D-Ala-D-Ala. It involves changes in the spectral properties of the antibiotic when binding to ligand occurs. If the change in absorbance of antibiotic is proportional to the extent of complex formation with ligand then the fractional degree of association (f) is given by:

$$f = \Delta A/\Delta A_{max} = K_a [L] / (1 + K[L]) \qquad (4.1)$$

where ΔA is the change in absorbance, ΔA_{max} is the total change in absorbance between the antibiotic in the fully liganded state and the unliganded state, K_a is the association constant and [L] is the ligand concentration (McAuley-Hecht, 1993). The association constant for the binding of antibiotic to ligand can then be determined from absorbance changes as a function of ligand concentration.

The binding of vancomycin to N-acetyl-D-Ala-D-Ala was studied using UV difference spectroscopy on a Shimadzu UV-160A UV/visible spectrophotometer. This method followed that used by Billot-Klein,[a] (1994) and involved injecting measured aliquots (2-6 µl) of ligand into the sample cell (1cm pathlength quartz cuvette) containing vancomycin, all of which were prepared in 20mM citrate buffer, pH 5.1. The same vancomycin solution was also contained in the reference cell. The sample was left for 15 minutes to equilibriate to room temperature before a spectrum was taken. After a series of absorbance readings were recorded, a binding curve was produced from a plot of

changes in absorbance between 252 and 288nm against ligand concentration. From this binding curve, the association constant was determined.

4.8 Determination of rate constants using UV difference spectroscopy

First order kinetics were applied to the dissociation of vancomycin from the dimer form in the presence of the ligand $N_{\alpha},N_{\varepsilon}$-diacetyl-Lys-D-Ala-D-Ala. A reduction in UV absorbance over time resulted from the dilution of the antibiotic-peptide complex and when analysed in terms of the conventional first order expression:

$$\ln (A-A_{\infty} / A_{o} - A_{\infty}) = -kt \qquad (4.2)$$

where A_o is the initial absorbance, A_∞ is the final absorbance, A is the absorbance at a particular time (t), a graph of which gives a slope with a gradient equal to -k, from which the apparent rate constant for the process can be determined.

The rate of vancomycin dissociation from the dimer form in the presence of $N_{\alpha},N_{\varepsilon}$-diacetyl-Lys-D-Ala-D-Ala was studied using a Shimadzu UV-160A UV/visible spectrophotometer with thermostatted cell holder. This method involved the addition of measured (10-30μl) aliquots of vancomycin and ligand into the sample cell (1cm path length quartz cuvette) containing buffer. The same buffer was placed in the reference cell. Similar rate constants were obtained if ligand was placed in the dilution buffer or not. Since vancomycin dissociation produced a decrease in absorbance, these absorbance changes at 283nm (Perkins, 1969) could be used to give an estimation of the rate constant by first order kinetics.

4.9 Calibration of the glass electrode in deuterium oxide

Since glass electrodes measure ion activities rather than actual concentrations, equal concentrations of H^+ and D^+ will give different pH meter readings. To compensate for

this, an empirical correction of 0.45 was added to the observed meter reading when a glass electrode standardised with a buffer solution in ordinary water was used to measure acidity in heavy water. This correction converts the operational pH to a value on a pD scale (Covington *et al.*, 1968).

4.10 Preparation of antibiotic and ligand samples for use in X-ray crystallography

Vancomycin and N-acetyl-D-Ala-D-Ala solutions were prepared and set up in a 24 well crystallisation tray using the sitting drop method of crystallisation. This involved adding measured aliquots of both antibiotic (17μl) and ligand (11μl) to the sample well and filling the surrounding volume (0.75ml) with the same buffer used to prepare the samples. Equilibrium between the sample drop and the surrounding volume of buffer was slowly reached through vapour diffusion, with supersaturation occurring by loss of water from the sample to the larger reservoir of buffer, therefore forming crystals. This process was both pH and concentration dependant. Two morphologies of crystals were obtained by varying the buffer composition. Small, torpedo shaped crystals formed in 0.1M phosphate buffer at pH 7, but these were too fragile to use for data collection. After many crystallisation trials in which these parameters were varied, the optimum conditions for growth of more rounded, suitable crystals (0.12×0.02mm) from which data could be collected were 5.41mM N-acetyl-D-Ala-D-Ala and 4.63mM vancomycin at pH 7.6 in 0.1M Imidazole maleic buffer. All crystallisations were carried out at room temperature. Crystal growth was slow and took several months.

4.11 Determination of crystal density

The experimental determination of crystal density was based on the method described by Mikol & Giege, (1992). This involved preparing a series of Ficoll solutions (from 30%-60% w/w) by mixing appropriate amounts of Ficoll and water. These solutions were gently stirred and heated to 55°C in a waterbath over a hotplate. The solutions took

about an hour to dissolve, becoming viscous on cooling. The gradient was prepared in a glass test-tube with an inner diameter of 4mm, so that crystals could be easily observed, with fractions layered by decreasing density. After the addition of each layer, the tube was centrifuged for 5min at 1000g. Once all layers were added, the entire gradient was smoothed by a longer centrifugation i.e. 1h at 3000g. The gradient was then calibrated with drops of a mixture of carbon tetrachloride/toluene, the densities of which were determined using a PAAR Digital Densitymeter, DMA 35. These drops act as markers. The tube was centrifuged for 5min at 3000g after the addition of each marker. The crystal was introduced along with a small volume of mother liquor at the top of the gradient, on the tip of a needle. The tube was centrifuged for 55min at 1000g. The tube was then mounted in a clamp stand and the distance of each of the markers from the bottom of the tube was measured using a travelling microscope. Once the distance between the bottom of the tube and the crystal has been determined, it is possible to extrapolate the appropriate density.

4.12 Estimation of the purity of antibiotic and ligand samples using electrospray mass spectrometry

(Performed by Tino Krell)

The individual vancomycin and N-acetyl-D-Ala-D-Ala solutions for use with this technique were prepared by dissolving in distilled water. A solution of the complex was prepared by removing the excess buffer from some microcrystals by sequential washes with distilled water (4 washes given) and grinding them up and dissolving in some distilled water. This solvent is preferred over ionic buffers because such buffers disturb the spraying process and compete with analyte molecules for charges (Mann & Wilm, 1995).

Mass spectrometry was performed on a VG Platform quadrupole mass spectrometer (2-3000a.m.u. range) fitted with a pneumatically assisted electrospray source and controlled

via VG Mass-Lynx software. Carrier solvent (1:1(v:v) acetonitrile/water) infusion was controlled at 10μl/min using a Harvard syringe pump. Capillary voltages were between 2.8 and 3.2kV, extraction cone voltages 20-30V and the focussing cone voltage offset by +10V. The source temperature was set at 65°C, the nebulising gas flow at 10 l/h and the drying gas flow at 250 l/h. Lens stack voltages were adjusted to give maximum ion currents. The M_r range 200-1800 was scanned with a sweep time of 5s. The instrument was calibrated over this range immediately before use with horse heart myoglobin supplied by Sigma Chemical Co. Samples for analysis were diluted with an equal volume of 4% (v:v) formic acid in acetonitrile and 10-20μl aliquots injected directly into the carrier system. This procedure was carried out for vancomycin and N-acetyl-D-Ala-D-Ala alone and for the vancomycin/N-acetyl-D-Ala-D-Ala complex found in the crystals.

4.13 Crystallography data collection

An intact crystal was chosen and mounted in a glass capillary along with some mother liquor to prevent the crystal from drying out. A Siemans-Xentronics area detector on a rotating anode was used to collect data, with copper K_α radiation of wavelength 1.5418Å. A collimated beam of X-rays from the source (0.3mm diameter) was directed onto the crystal to produce diffraction spots. To produce all possible diffraction spots the crystal was rotated in the beam during the experiment and the diffraction data recorded on the area detector. The detector was placed 250mm from the crystal to achieve best spot separation. Each frame of data was collected at a crystal rotation about the ϕ axis of 0.1°, at exposures of 400 seconds per frame. From the first data set, 628 frames were collected, determined by the Laue symmetry of the crystal. The Laue symmetry provides the most basic of crystal information and is used prior to unit cell determination. Since our crystal showed hexagonal symmetry, the reciprocal lattice repeats every 60°. Therefore, since we were collecting data in 0.1° sections, we needed ~600 frames. With the crystal to detector distance at 250mm, it was not possible to record the whole reciprocal lattice on one image. To do this, we took two angular sections of the lattice,

one at -20° and one at -5° to collect both high and low resolution data. Data resolution was to 2.8Å, but was more complete at 3.0Å. A total of 2391 frames were collected from seven data sets.

4.14 Crystallography data processing

Data processing was carried out using the program XDS. This program first collects a number of strong spots which are then indexed to produce the unique cell and orientation matrix. This is produced by measuring the shortest distance between spots and indexing them within the unit cell to produce a series of co-ordinates. This orientation matrix is then used to index all other reflections in the data set. From this, the unit cell dimensions, systematic absences and space group can be determined. With this information all the data frames collected are then scanned to collect all possible reflections. The intensity profile for each reflection is accurately measured and used to produce a list of *hkl* reflections with their associated intensities. The advantage of using XDS to carry out data processing is that it is essentially a 'black box' program needing little intervention from the operator and the printout gives good guidance statistics as to the validity of the results. Errors can arise from weak reflections which would give a poor orientation matrix and from poor spot separation. However, both our data sets were processed without any problems.

Chapter 5:
Microcalorimetry and Spectroscopy
Results and Discussion

5.1 Microcalorimetry

The main aim of these studies was to extend previous work on the vancomycin group of antibiotics (Perkins, 1969 : Nieto & Perkins,[a,b] 1971 : Rodriguez-Tebar *et al.*, 1986 : McAuley-Hecht, 1993 : Cooper & McAuley-Hecht, 1993 : Mackay *et al.*, 1994 : Searle *et al.*, 1994) with a view to obtaining a greater understanding of the interactions involved in molecular recognition. A brief account of these previous studies follows.

Early studies on vancomycin were carried out by Perkins, (1969) using spectroscopic techniques. In this work, the minimum requirement for peptide binding to antibiotic was determined as a D-Ala-D-Ala peptide with the C-terminus free and the N-terminus acetylated. Further studies (Nieto & Perkins,[a] 1971) explored the specificity of the antibiotic binding site by carrying out amino acid substitutions at each position and measuring association constants. Associations between antibiotic and peptide were also shown to depend on pH (Nieto & Perkins,[b] 1971). Such pioneering studies clearly showed that the efficiency of molecular recognition between antibiotic and peptide depends on the size and conformation of the peptide side chain. Much later, microcalorimetry was introduced to study the recognition process between antibiotic and peptide. In one such study, Rodriguez-Tebar *et al.*, (1986) carried out experiments to investigate acetyl-D-Ala and acetyl-D-Ala-D-Ala binding to vancomycin, using the older LKB batch microcalorimeter with titration assembly and an LKB flow microcalorimeter over a narrow temperature range (25-37°C). Such experiments produced various thermodynamic parameters for the associations, but carrying out similar experiments over a much wider temperature range and with the more sensitive Omega microcalorimeter was thought to be more valuable in terms of reducing the

errors associated with the calculation of enthalpy changes and therefore in the determination of other thermodynamic parameters. In addition, it was unclear from this study what concentration of antibiotics were used and therefore if dimerisation effects were a factor. Other microcalorimetric work carried out to study the binding of vancomycin and ristocetin to N-acetyl-D-Ala, N-acetyl-D-Ala-D-Ala and N_{α},N_{ε}-diacetyl-Lys-D-Ala-D-Ala over a concentration and wider temperature range (20-45°C) (McAuley-Hecht, 1993 : Cooper & McAuley-Hecht, 1993) using the Omega microcalorimeter, produced results on the thermodynamics of the interactions involved at the antibiotic binding site and suggested the possibility of antibiotic aggregation affecting the binding affinity for cell wall analogues. NMR has been used to estimate dimerisation constants for vancomycin in the presence and absence of cell wall analogues (Mackay *et al.*, 1994), results from which have suggested cooperativity between vancomycin dimerisation and ligand binding. Similarly, dimerisation constants for ristocetin A aggregation have been estimated from NMR studies (Searle *et al.*, 1994), which suggest that the presence of ligand has a small anti-cooperative effect on ristocetin dimerisation.

Our studies are seen as an extension of this previous work, whereby microcalorimetric titrations were carried out over a wider range of conditions than before, supplementing our knowledge of the molecular recognition process. In addition, more detailed studies were performed on vancomycin and ristocetin dimerisation, providing further information on the thermodynamics of the contrasting properties of otherwise similar members of the same group of antibiotics.

5.1.1 Binding studies using isothermal titration microcalorimetry

The binding of vancomycin to various cell wall analogue peptides has been carried out using a Microcal Omega Ultrasensitive Isothermal Titration Microcalorimeter. Titration of vancomycin solutions with the peptides N-acetyl-D-Ala, N-acetyl-D-Ala-D-Ala and N_{α},N_{ε}-diacetyl-Lys-D-Ala-D-Ala were studied as a function of both temperature (15-45°

C), pH (3-11) and ionic strength. Association with N-fumaryl-D-Ala was carried out at 25°C only, due to lack of material. Further binding experiments with $N_{\alpha},N_{\varepsilon}$-diacetyl-Lys-D-Ala-D-Ala were carried out in acetate and deuterium oxide. Enthalpy changes (Δ H) and association constants (K_a) were determined from the Microcal Origin software package using the one set of sites model and standard Gibbs free energy ($\Delta G°$) and entropy ($\Delta S°$) changes were then calculated with standard deviations shown in brackets. van't Hoff enthalpies were calculated from the gradient of the line from plots of lnK against 1/T. Molar heat capacity changes (ΔC_p) were determined from the gradient of the line obtained from plots of ΔH against T.

The association of cell wall analogue peptides by the injection of small aliquots into the microcalorimeter cell containing antibiotic is an exothermic process consistent with complex formation between antibiotic and ligand. A sequence of injections gives a series of exothermic heat pulses which after integration and correction for control experiments, gives the absolute heat uptake per injection. In such an injection series, successive injections become progressively less exothermic as antibiotic saturation is reached.

All experiments were carried out in sodium phosphate buffer (pH 7, 0.1M) unless stated otherwise.

All deuterium oxide and acetate experiments and those involving changes in pH and ionic strength were carried out at 25°C.

Typical thermal profiles given in the following section show: *Upper panel*; exothermic responses for the injection of ligand into vancomycin solution. *Lower panel*; integrated heat effects (controls removed) with theoretical fits to a 'one set of sites' binding model.

Figures in parentheses are standard deviations of multiple experiments. (-) single determination only.

Data in tables are quoted in the SI unit of Joules, whereas figures generated by Origin are in calories (1 cal = 4.184J).

5.1.1.1 Vancomycin binding studies

5.1.1.1.1 N-acetyl-D-Ala

This short peptide combines only weakly with vancomycin, shown by the small association constants. Steric repulsion for side chains in the L-configuration in residue 1 has been shown from UV difference spectroscopy, but for side chains in the D-configuration in residue 1, a methyl group appears to be the optimum size for complexation with vancomycin (Nieto & Perkins,[a] 1971). Association constants are further reduced by increasing temperature, illustrating that the antibiotic-peptide complex is weakened at elevated temperatures, with enthalpies becoming more exothermic, corresponding to a negative change in molar heat capacity. Results are shown in Table 5.1(a), with a typical binding isotherm in Figure 5.1.

Complex formation between antibiotic and peptide occur over a wide pH range, however at the extremes of pH binding affinity is reduced. Optimum binding appears to occur around neutral pH, shown by the large association constants, whereas above pH 8 associations become too weak to be measured. Binding to this peptide is weak at neutral pH and at basic pH where the complex is less stable and binding affinity is reduced even further, associations become so weak that they are indistinguishable from the heats of

dilution, consequently no binding data was obtained above pH 8. Results are shown in Table 5.1(b).

Temperature (°C)	K_a (M^{-1})	ΔH ($kJmol^{-1}$)	ΔG° ($kJmol^{-1}$)	ΔS° ($JK^{-1}mol^{-1}$)	ΔC_p ($JK^{-1}mol^{-1}$)
15	505 (75)	-31.2 (4.6)	-14.9	-57	
25	295 (30)	-36.6 (2.4)	-14.0	-76	-330 (75)
35	205 (5)	-40.3 (1.1)	-13.6	-86	
45	140 (35)	-41.0 (10.2)	-13.1	-88	

Table 5.1(a) Vancomycin binding to N-acetyl-D-Ala at various temperatures.

pH	K_a (M^{-1})	ΔH ($kJmol^{-1}$)	ΔG° ($kJmol^{-1}$)	ΔS° ($JK^{-1}mol^{-1}$)
3	190 (-)	-19.3 (-)	-13.0	-21
5	320 (50)	-23.1 (6.4)	-14.3	-29
7	295 (30)	-36.6 (2.4)	-14.0	-76
8	215 (40)	-29.2 (1.6)	-13.3	-53

Table 5.1(b) Vancomycin binding to N-acetyl-D-Ala at various pH.

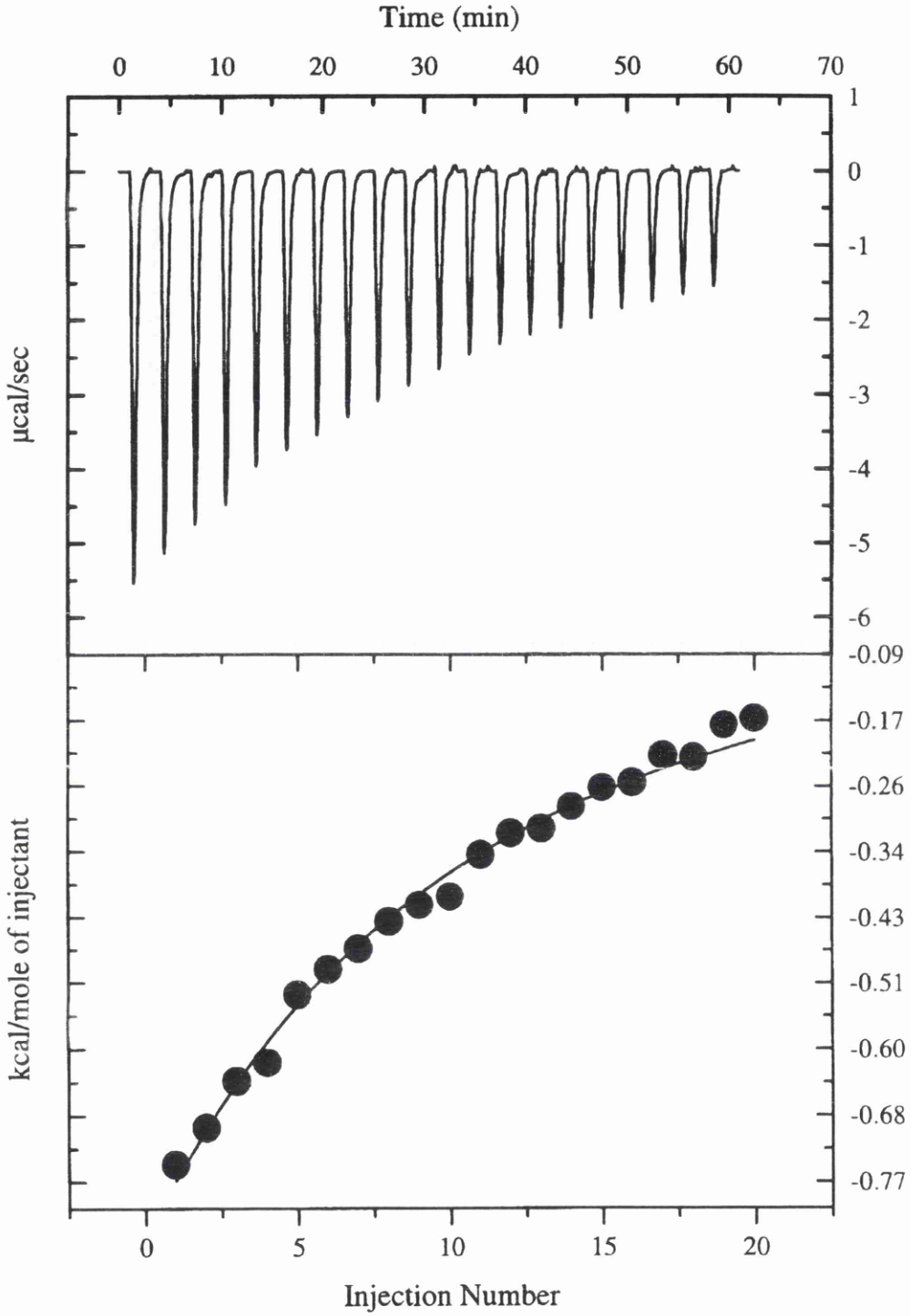

Figure 5.1 Vancomycin (0.28mM) binding to N-acetyl-D-Ala (47.38mM) at pH 7.0, 25°C.

5.1.1.1.2 N-acetyl-D-Ala-D-Ala

This dipeptide associates more strongly with vancomycin than N-acetyl-D-Ala, shown by a significant increase in association constants. The introduction of a second alanine residue clearly enhances antibiotic binding. As for residue 1, a methyl group in the D-configuration side chain of residue 2 appears to be the optimum size for complexation with antibiotic (Nieto & Perkins,[a] 1971). As before, an increase in temperature reduces binding affinity and causes it to become more exothermic, corresponding to a negative change in molar heat capacity. Results are shown in Table 5.2(a), with a typical binding isotherm in Figure 5.2.

Optimum binding of vancomycin to this dipeptide occurs at neutral pH, with measurable associations occurring over the pH range 3-11. Results are shown in Table 5.2(b).

Temperature (°C)	K_a (M^{-1})	ΔH ($kJmol^{-1}$)	$\Delta G°$ ($kJmol^{-1}$)	$\Delta S°$ ($JK^{-1}mol^{-1}$)	ΔC_p ($JK^{-1}mol^{-1}$)
15	26.0×10^3 (7655)	-26.3 (7.0)	-24.3	-7	
25	12.3×10^3 (3695)	-33.4 (8.2)	-23.3	-35	-285 (120)
35	8.5×10^3 (590)	-35.4 (2.9)	-23.2	-40	
45	6.1×10^3 (925)	-35.1 (3.4)	-23.0	-38	

Table 5.2(a) Vancomycin binding to N-acetyl-D-Ala-D-Ala at various temperatures.

pH	K_a (M^{-1})	ΔH ($kJmol^{-1}$)	ΔG° ($kJmol^{-1}$)	ΔS° ($JK^{-1}mol^{-1}$)
3	2.2×10^3 (375)	-40.9 (10.6)	-19.1	-73
5	5.7×10^3 (2100)	-31.1 (9.5)	-21.4	-32
7	12.3×10^3 (3695)	-33.4 (8.2)	-23.3	-35
8	4.9×10^3 (-)	-33.5 (-)	-21.0	-42
11	1.4×10^3 (235)	-30.5 (1.6)	-17.9	-42

Table 5.2(b) Vancomycin binding to N-acetyl-D-Ala-D-Ala at various pH.

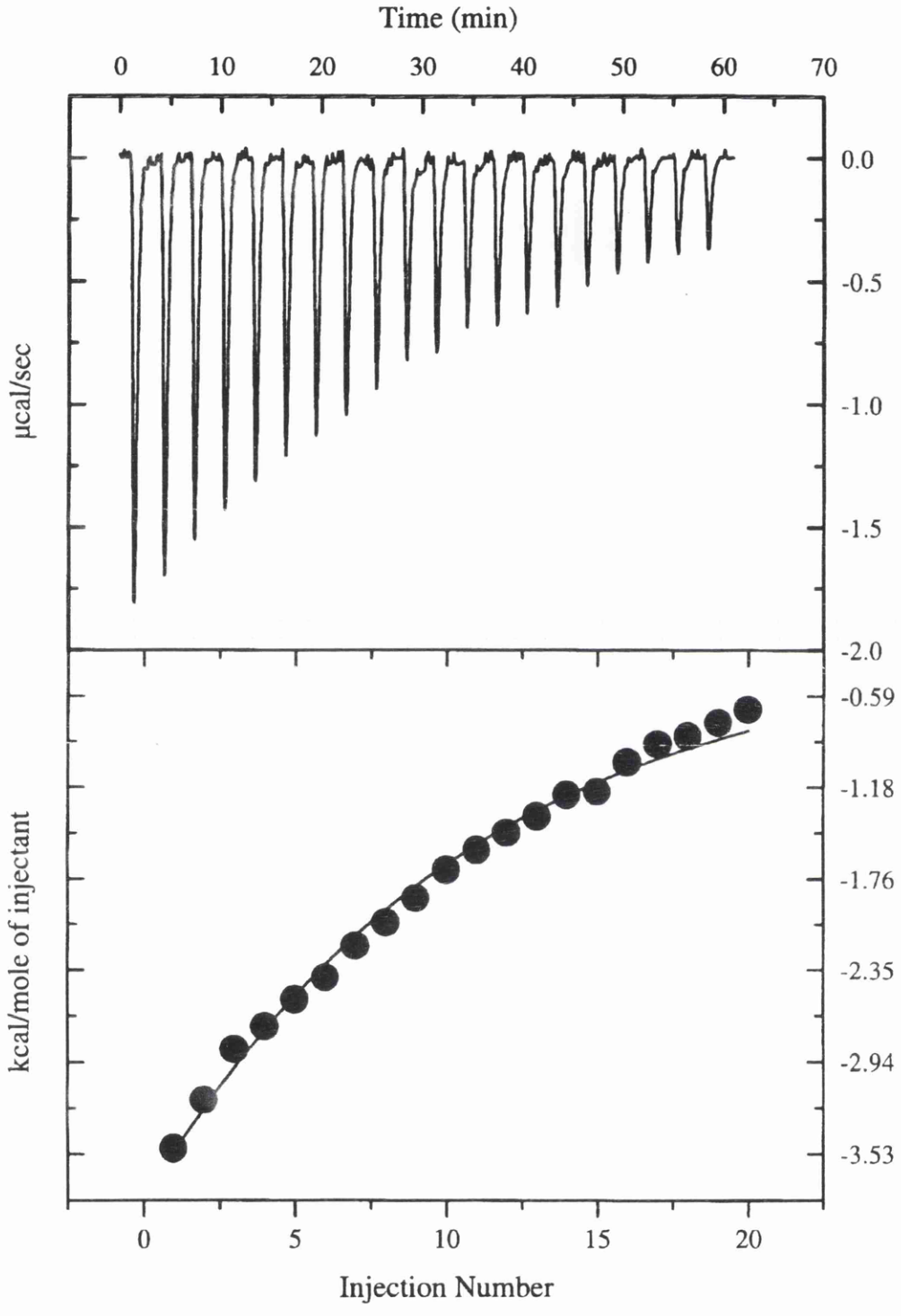

Figure 5.2 Vancomycin (0.07mM) binding to N-acetyl-D-Ala-D-Ala (3.60mM) at pH 7.0, 25°C.

5.1.1.1.3 N-fumaryl-D-Ala

This dipeptide associates more strongly with vancomycin than N-acetyl-D-Ala, but less than N-acetyl-D-Ala-D-Ala, this being consistent with data obtained by Cooper & McAuley-Hecht, 1993. The fumaryl group in this analogue appears to be able to play a role in the binding process, since association constants are increased by a factor of approximately 10 from that associated with binding to N-acetyl-D-Ala. It is possible that the terminal carboxyl on the fumaryl group can hydrogen bond to the amino group at the C-terminus of the antibiotic. Results are shown in Table 5.3, with a typical thermal profile shown in Figure 5.3.

Temperature (°C)	K_a (M^{-1})	ΔH ($kJmol^{-1}$)	ΔG° ($kJmol^{-1}$)	ΔS° ($JK^{-1}mol^{-1}$)
25	2610 (500)	-27.9 (3.5)	-19.5	-28

Table 5.3 Vancomycin binding to N-fumaryl-D-Ala.

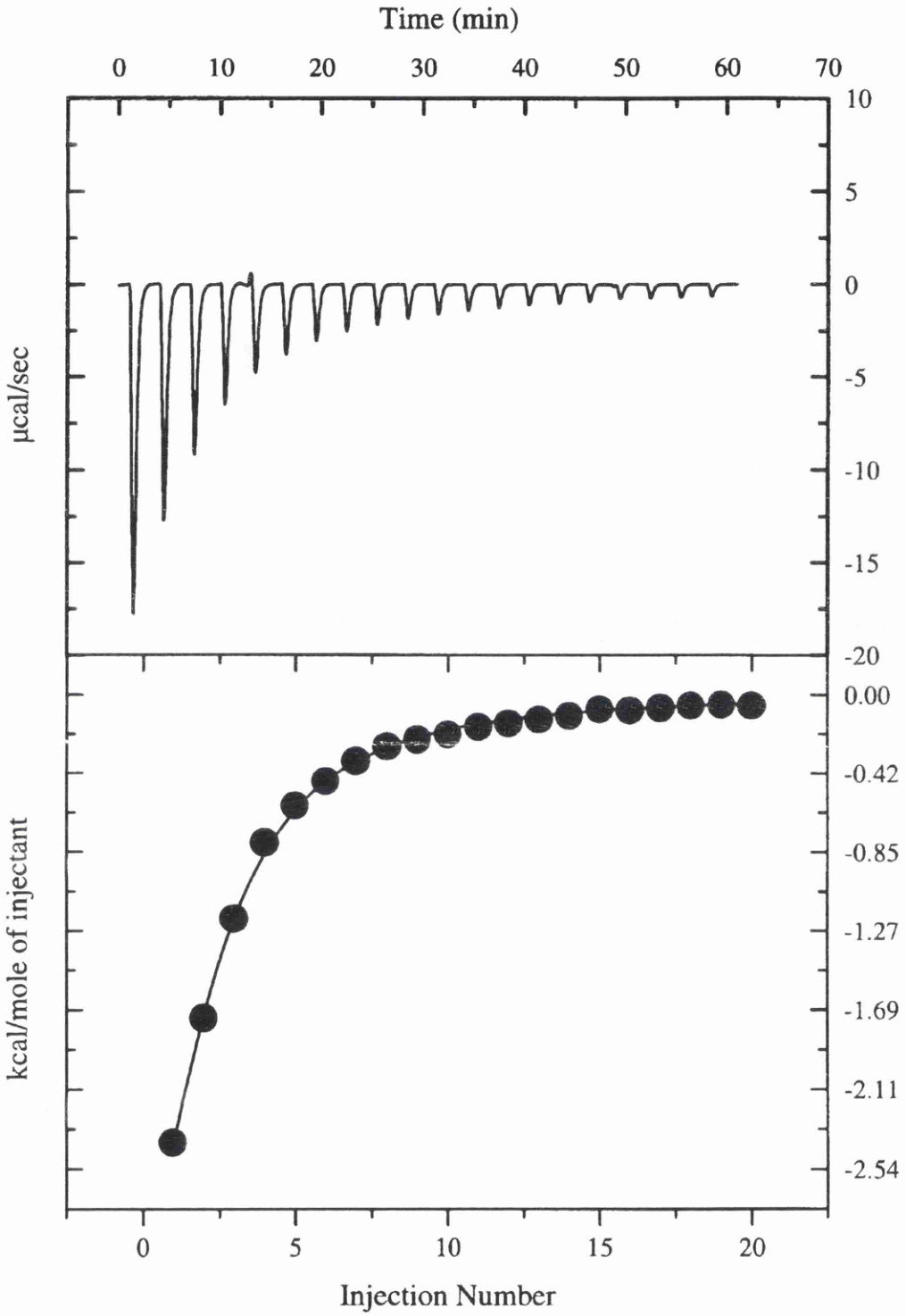

Figure 5.3 Vancomycin (0.29mM) binding to N-fumaryl-D-Ala (47.29mM) at pH 7.0, 25°C.

5.1.1.1.4 N_{α},N_{ε}-diacetyl-Lys-D-Ala-D-Ala

This tripeptide closely resembles the antibiotic's natural substrate, N-acetylmuramylpentapeptide present in bacterial peptidoglycan and binds most strongly to vancomycin, since the side chain of lysine at residue 3 is of the L-configuration coupled with methyl groups on the D-configuration side chains of both residues 1 and 2, with these conditions being the optimum for complex formation (Nieto & Perkins,[a] 1971). This is shown by high association constants and a different binding isotherm profile shown in Figure 5.4, consistent with tight binding. In this case, strong binding affinity appears to arise from a significant increase in enthalpy change. An increase in temperature causes binding to become both weaker and more exothermic. Association with this tripeptide over a temperature range results in a negative change in molar heat capacity. Results are shown in Table 5.4(a).

Antibiotic associations with this peptide occur over a wide pH range, again with optimum binding occurring at neutral pH. Results are shown in Table 5.4(b).

Temperature (°C)	K_a (M^{-1})	ΔH ($kJmol^{-1}$)	ΔG° ($kJmol^{-1}$)	ΔS° ($JK^{-1}mol^{-1}$)	ΔC_p ($JK^{-1}mol^{-1}$)
15	8.2×10^5 (-)	-50.3 (-)	-32.6	-61	
25	4.9×10^5 (1.4×10^5)	-56.9 (3.5)	-32.5	-82	-525 (40)
35	3.6×10^5 (-)	-60.5 (-)	-32.8	-90	
45	1.4×10^5 (-)	-66.6 (-)	-31.3	-111	

Table 5.4(a) Vancomycin binding to N_α,N_ε-diacetyl-Lys-D-Ala-D-Ala at various temperatures.

pH	K_a (M^{-1})	ΔH ($kJmol^{-1}$)	ΔG° ($kJmol^{-1}$)	ΔS° ($JK^{-1}mol^{-1}$)
3	1.3×10^5 (-)	-53.4 (-)	-29.2	-8
5	5.8×10^5 (-)	-41.5 (-)	-32.9	-29
7	4.9×10^5 (1.4×10^5)	-56.9 (3.5)	-32.5	-82
8	3.0×10^5 (-)	-36.2 (-)	-31.3	-17
11	1.5×10^5 (-)	-37.7 (-)	-23.8	-47

Table 5.4(b) Vancomycin binding to N_α,N_ε-diacetyl-Lys-D-Ala-D-Ala at various pH.

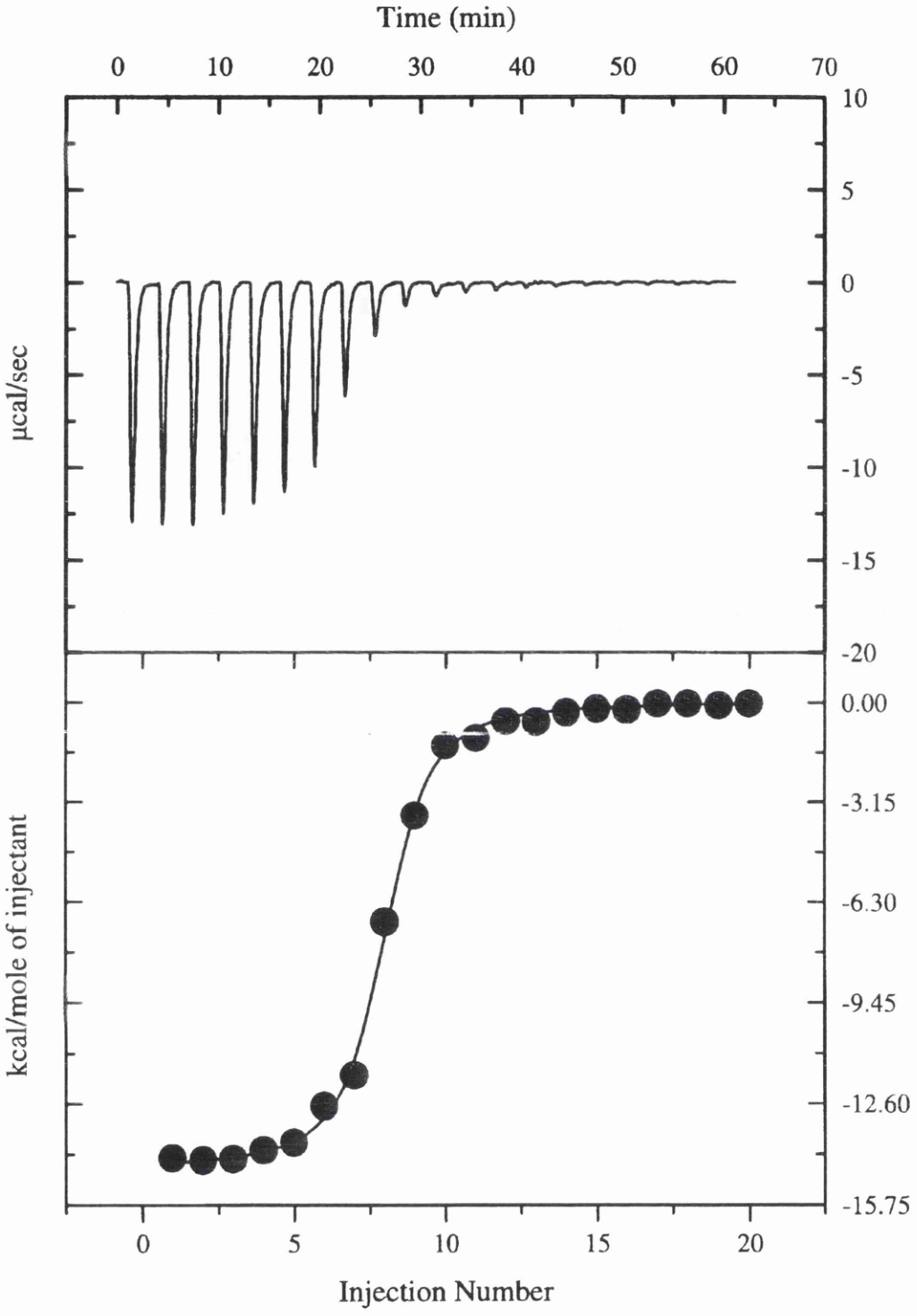

Figure 5.4 Vancomycin (0.28mM) binding to N_{α},N_{ε}-diacetyl-Lys-D-Ala-D-Ala (6.46mM) at pH 7.0, 25°C.

van't Hoff and ΔC_p plots are shown in Figures 5.5-5.8 and 5.9-5.12, respectively. Comparison of microcalorimetric and theoretical van't Hoff plots are shown in Figures 5.13-5.15. van't Hoff enthalpies were calculated using a simple 2-state model and are shown in Table 5.5 with entropy-enthalpy compensation plots in Figures 5.16 and 5.17.

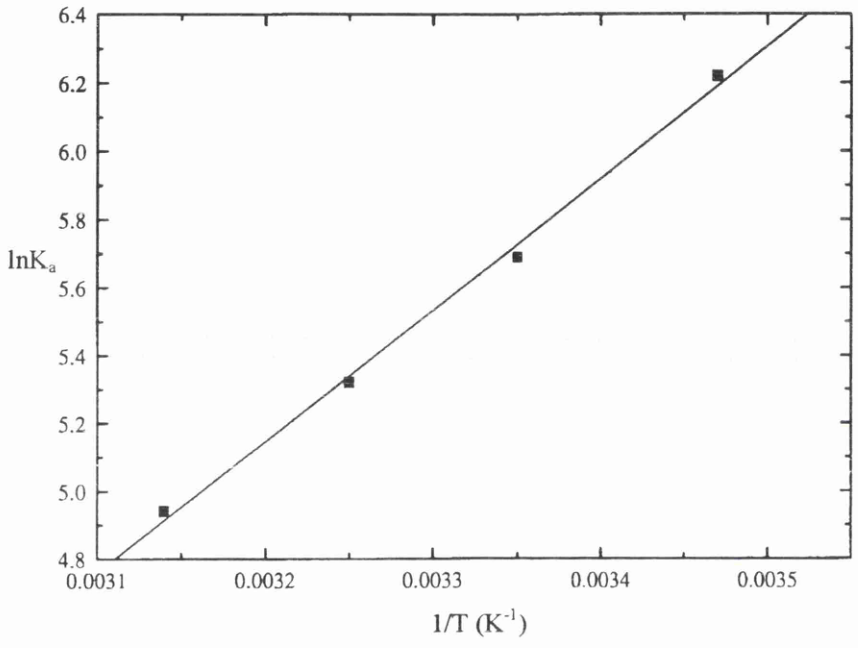

Figure 5.5 van't Hoff plot of vancomycin binding to N-acetyl-D-Ala.

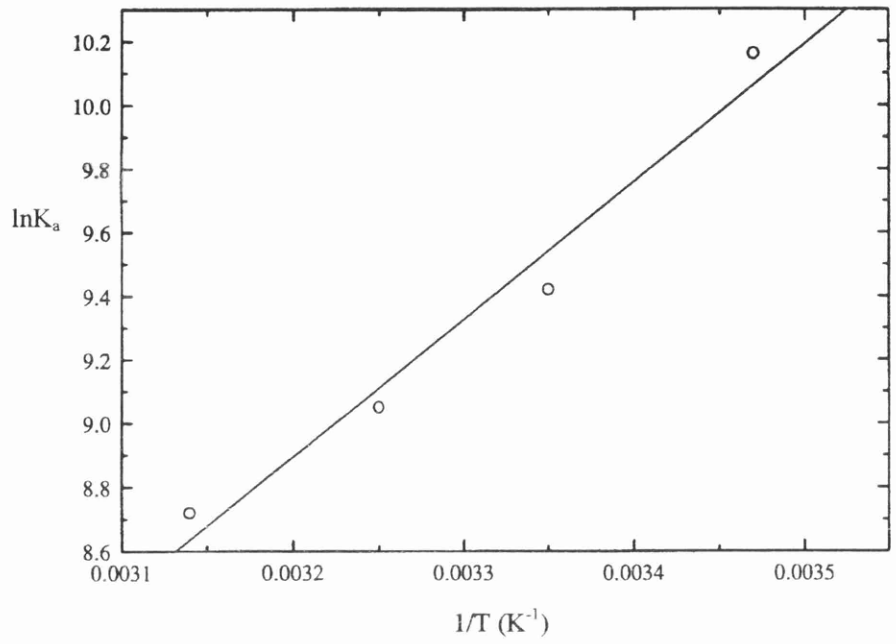

Figure 5.6 van't Hoff plot of vancomycin binding to N-acetyl-D-Ala-D-Ala.

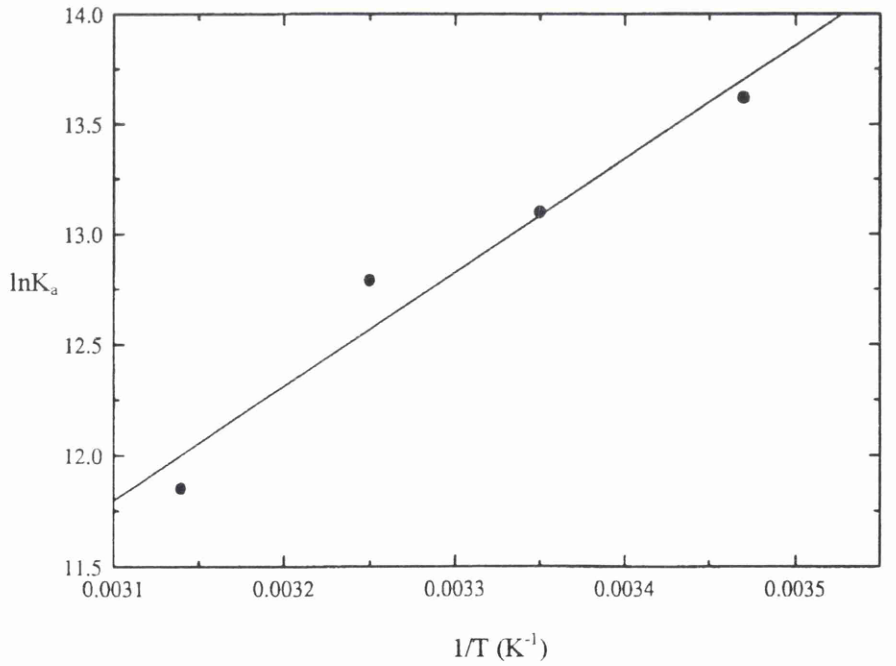

Figure 5.7 van't Hoff plot of vancomycin binding to N_α,N_ε-diacetyl-Lys-D-Ala-D-Ala.

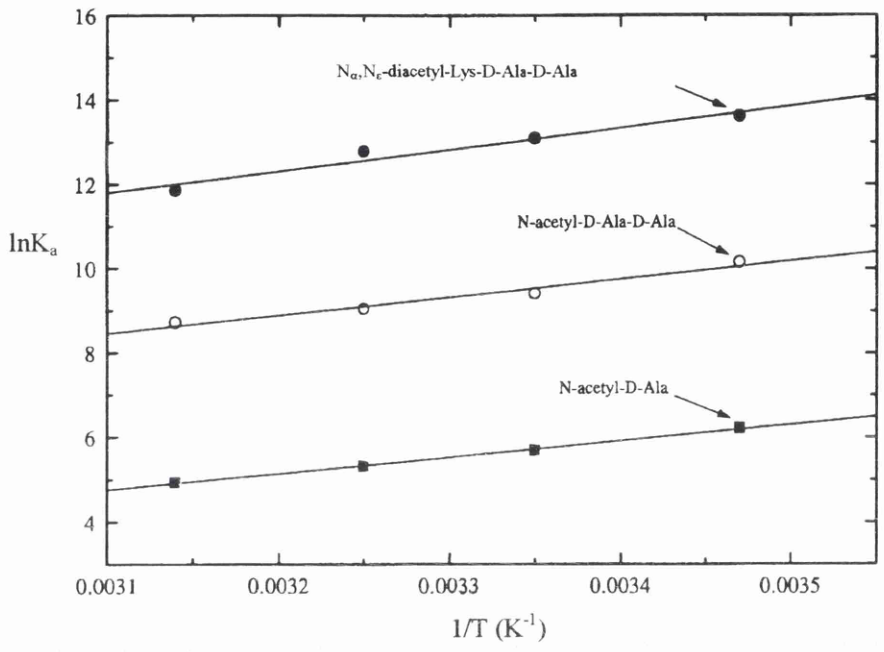

Figure 5.8 Summary of all van't Hoff plots of vancomycin binding.

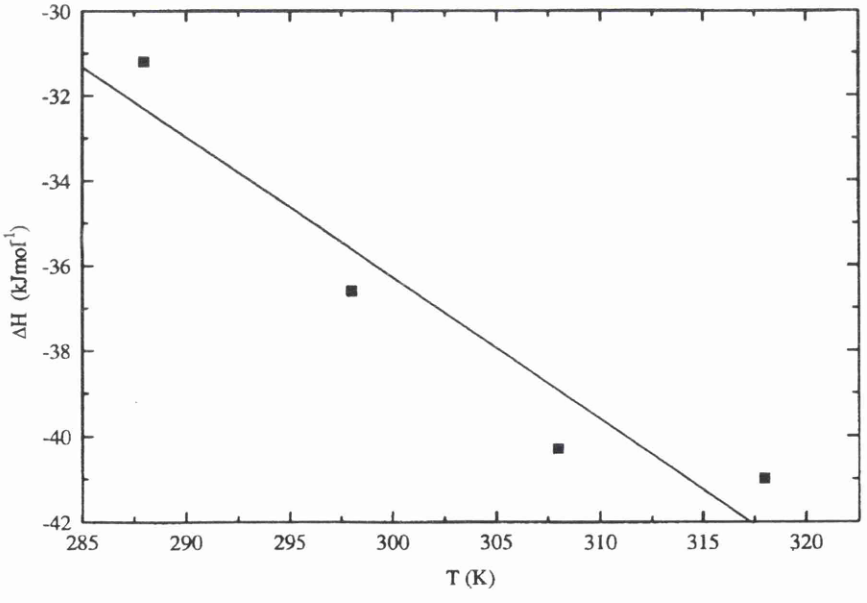

Figure 5.9 ΔC_p plot of vancomycin binding to N-acetyl-D-Ala.

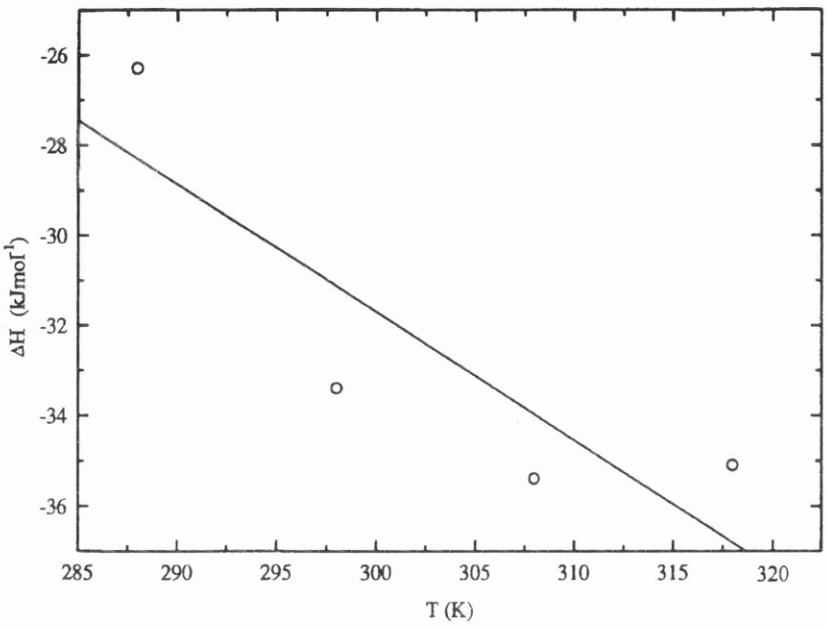

Figure 5.10 ΔC_p plot of vancomycin binding to N-acetyl-D-Ala-D-Ala.

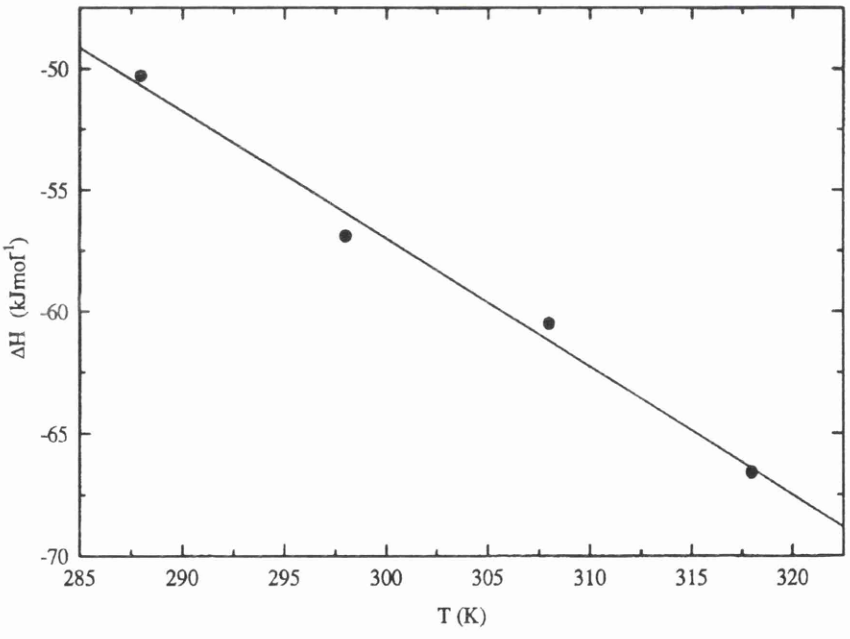

Figure 5.11 ΔC_p plot of vancomycin binding to N_α,N_ε-diacetyl-Lys-D-Ala-D-Ala.

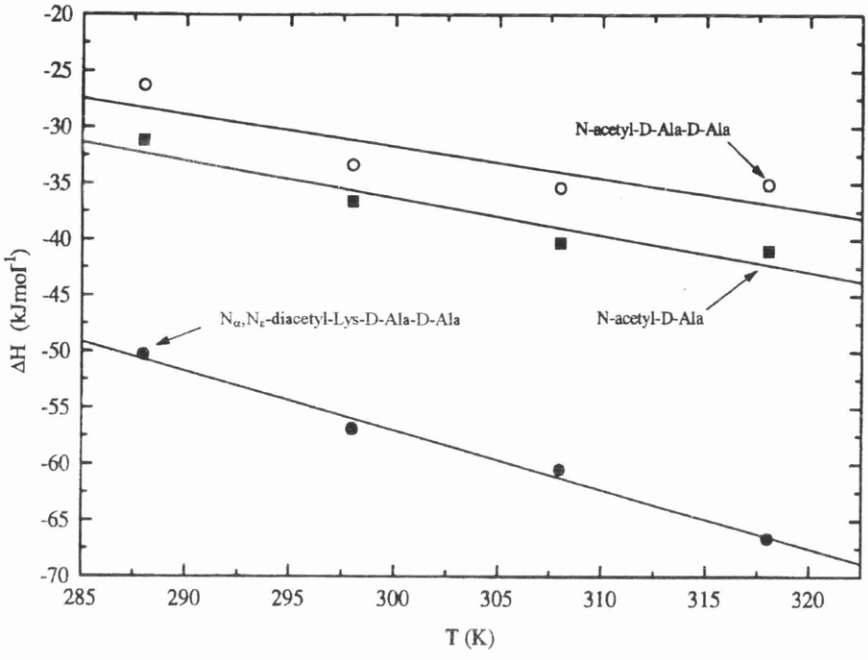

Figure 5.12 Summary of all ΔC_p plots of vancomycin binding.

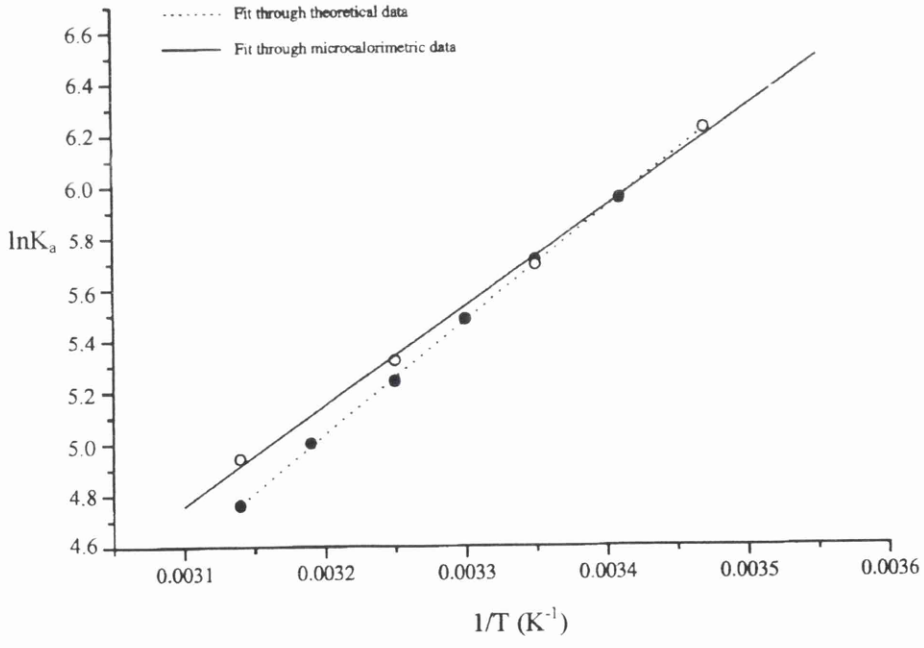

Figure 5.13 Comparison of microcalorimetric and theoretical van't Hoff plots of vancomycin binding to N-acetyl-D-Ala.

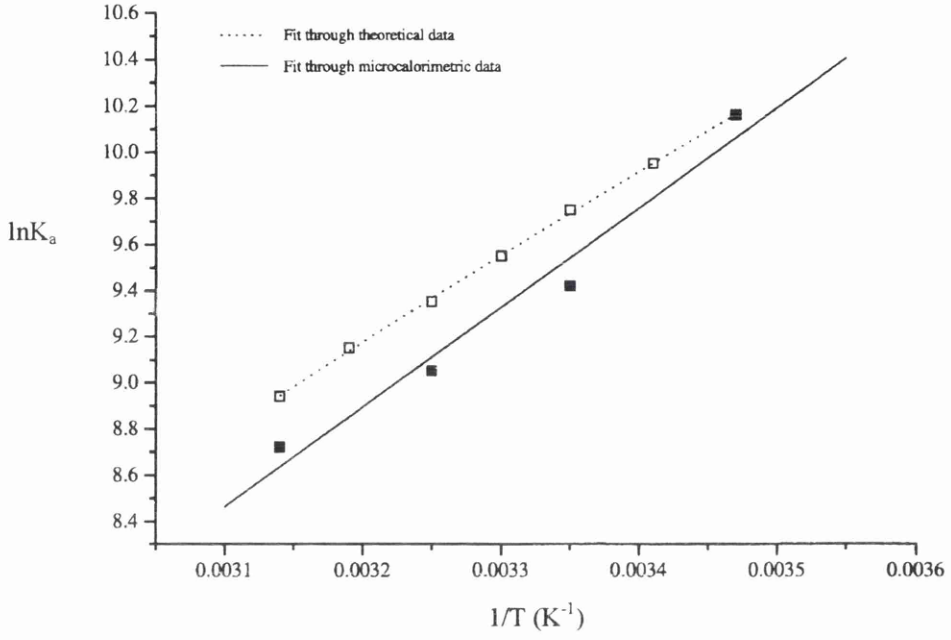

Figure 5.14 Comparison of microcalorimetric and theoretical van't Hoff plots of vancomycin binding to N-acetyl-D-Ala-D-Ala.

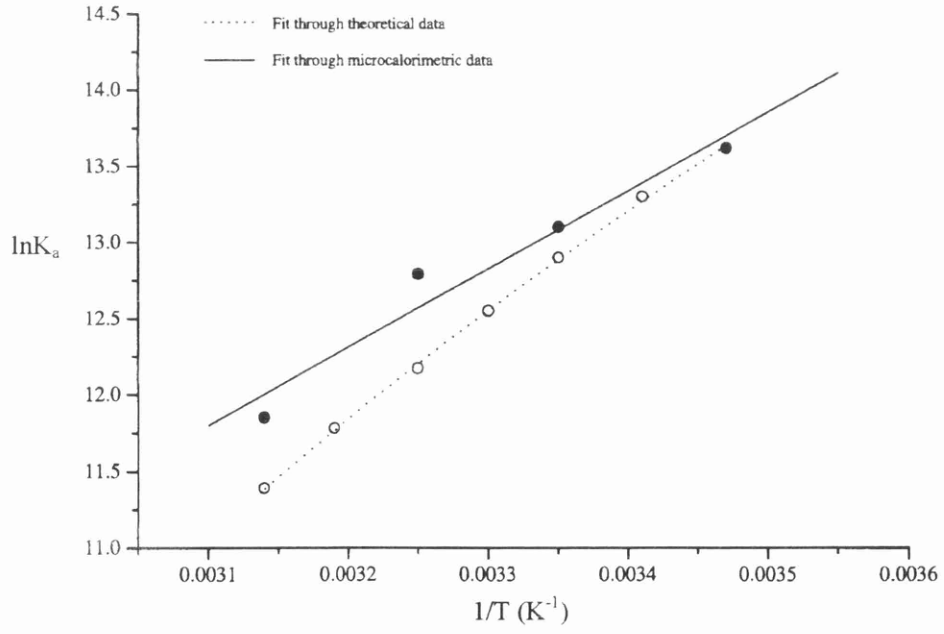

Figure 5.15 Comparison of microcalorimetric and theoretical van't Hoff plots of vancomycin binding to N_α,N_ε-diacetyl-Lys-D-Ala-D-Ala.

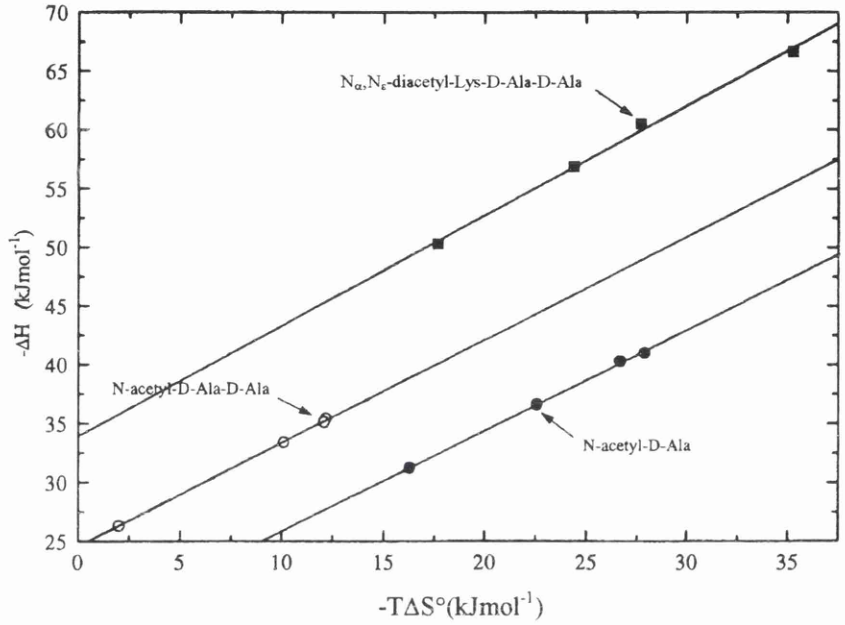

Figure 5.16 Entropy-enthalpy compensation plot of vancomycin binding to cell wall analogue peptides at various temperatures.

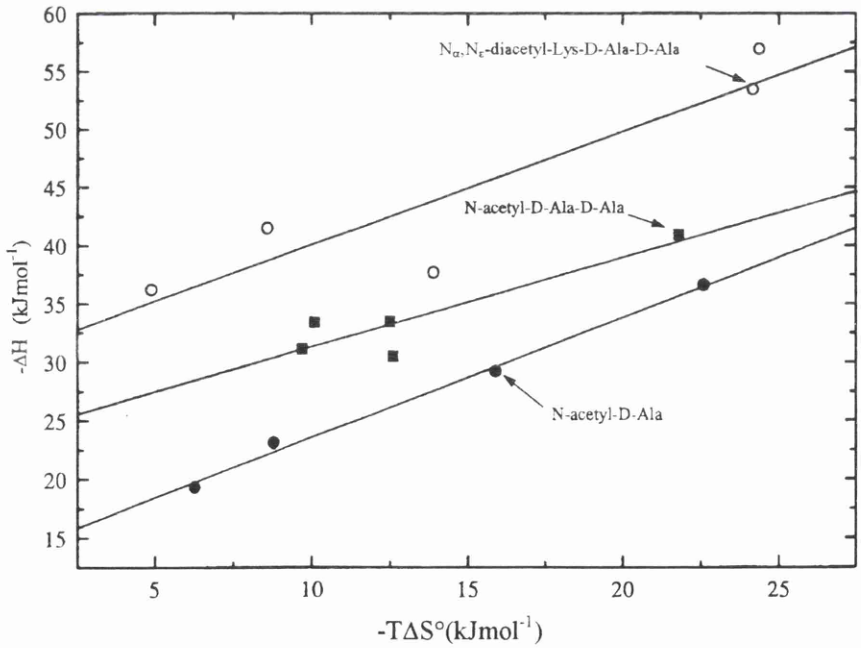

Figure 5.17 Entropy-enthalpy compensation plot of vancomycin binding to cell wall analogue peptides at various pH.

	van't Hoff enthalpy ($kJmol^{-1}$)
N-acetyl-D-Ala	-32.2 (1.4)
N-acetyl-D-Ala-D-Ala	-35.9 (4.5)
N_α,N_ε-diacetyl-Lys-D-Ala-D-Ala	-42.8 (6.8)

Table 5.5 van't Hoff enthalpies of vancomycin binding to cell wall analogue peptides.

5.1.1.1.5 Acetate

Vancomycin binding to N_α,N_ε-diacetyl-Lys-D-Ala-D-Ala in the presence of increasing concentrations of acetate reduces the association constants and apparent enthalpy suggesting competition between the acetate anion which acts as a weak ligand and N_α,N_ε-diacetyl-Lys-D-Ala-D-Ala for the antibiotic binding site (Cooper & McAuley-Hecht, 1993). The binding of ligand to antibiotic would require displacement of this anion, therefore producing a reduction in the apparent association constant. However, salt effects may also play a role in the reduction of thermodynamic parameters, therefore it is important that these effects are explored more fully by repeating the experiment under the same conditions, but in the presence of salts of various ionic strengths. Results are shown in Table 5.6, with typical binding isotherms in Figure 5.18.

	K_a (M^{-1})	ΔH ($kJmol^{-1}$)	$\Delta G°$ ($kJmol^{-1}$)	$\Delta S°$ ($JK^{-1}mol^{-1}$)
no acetate	4.9×10^5 (1.4×10^5)	-56.9 (3.5)	-32.5	-82
0.1M acetate	2.1×10^5 (0.5×10^5)	-45.0 (1.5)	-30.4	-49
0.5M acetate	1.3×10^5 (0.7×10^5)	-39.5 (2.0)	-29.2	-35

Table 5.6 Vancomycin binding to N_α,N_ε-diacetyl-Lys-D-Ala-D-Ala in the absence and presence of various concentrations of acetate.

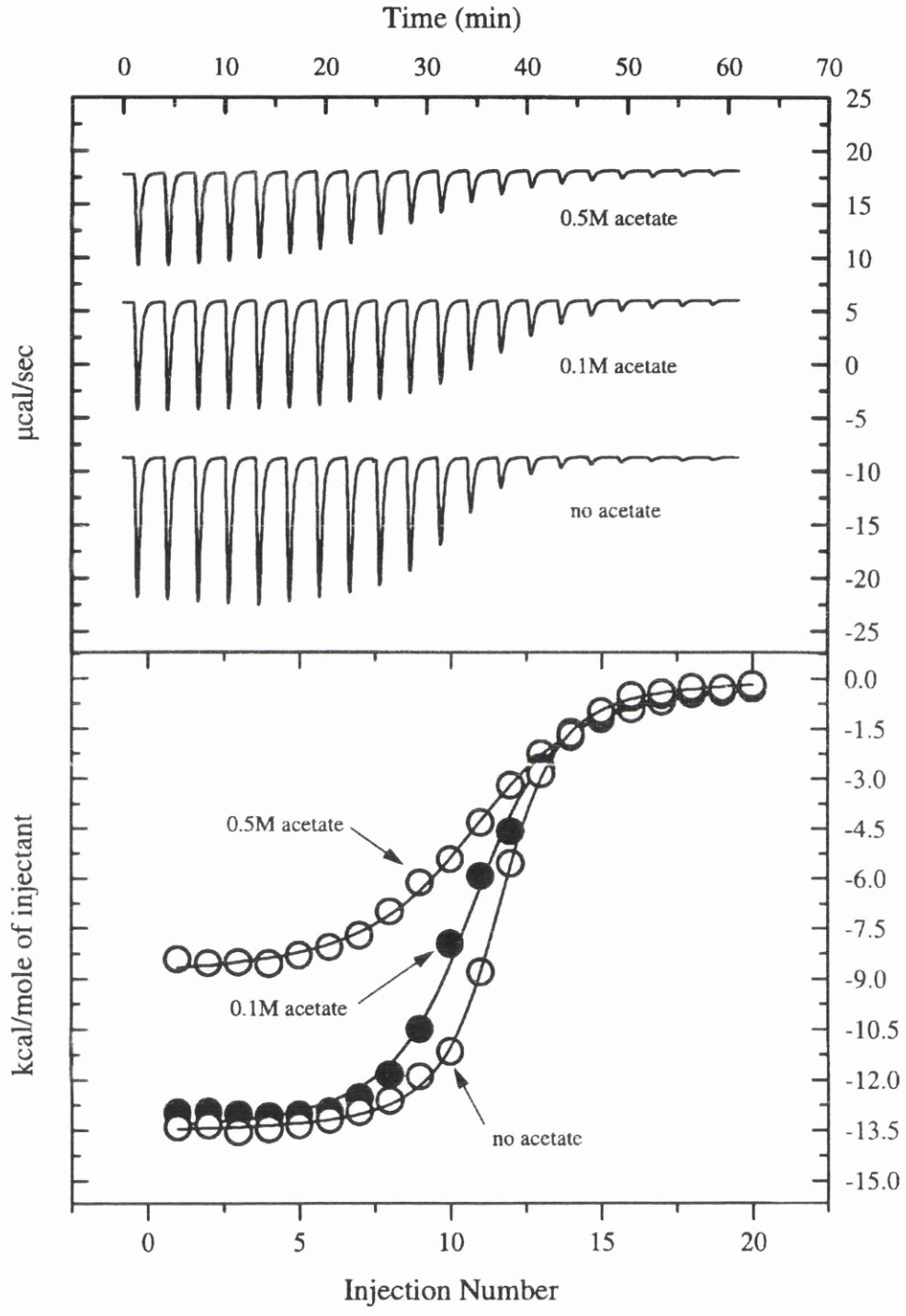

Figure 5.18 Vancomycin (0.34mM, 0.32mM, 0.30mM) binding to $N_{\alpha},N_{\varepsilon}$-diacetyl-Lys-D-Ala-D-Ala (5.80mM, 6.40mM, 5.56mM) in the absence and presence of 0.1M and 0.5M acetate respectively, at pH

5.1.1.1.6 Salt

As shown previously, the presence of acetate appeared to reduce the association constants between vancomycin and $N_{\alpha},N_{\varepsilon}$-diacetyl-Lys-D-Ala-D-Ala. To study this effect further, vancomycin binding to this strongly binding ligand was carried out in the presence of salts with different ionic strengths in MOPS buffer (pH 7, 0.1M) to test the contribution made by electrostatic interactions to the total interactions involved at the antibiotic binding site. High ionic strengths are known to be more efficient at screening out electrostatic interactions, shown by a decrease in association constants, although association between vancomycin and $N_{\alpha},N_{\varepsilon}$-diacetyl-Lys-D-Ala-D-Ala in the presence of $CaCl_2$ shows only a negligible reduction in binding affinity from that in the presence of KCl. These results suggest that a contribution to the total interactions involved at the antibiotic binding site is made by electrostatic interactions and that the acetate presumably has an ionic strength mediated effect on the binding as well as an indirect competitive binding effect. Using MOPS buffer rather than phosphate, due to difficulties in dissolving high concentrations of salt in this buffer (calcium ions reacted to form insoluble phosphates), the enthalpy of vancomycin binding to $N_{\alpha},N_{\varepsilon}$-diacetyl-Lys-D-Ala-D-Ala in the absence of salt was reduced, without a significant change in association constant. Similar results were shown with vancomycin dimerisation in the absence of ligand (see section 5.1.2.1.6). This suggests that buffer ionisation heats may be involved, since microcalorimetry measures the total heats occurring during the process, not just those associated with the reaction of interest. Results are shown in Table 5.7, with typical binding isotherms in Figure 5.19.

	K_a (M^{-1})	ΔH ($kJmol^{-1}$)	$\Delta G°$ ($kJmol^{-1}$)	$\Delta S°$ ($JK^{-1}mol^{-1}$)
no salt	4.2×10^5 (0.5×10^5)	-48.9 (0.1)	-32.1	-56
0.1M KCl	2.5×10^5 (1.1×10^5)	-46.7 (0.3)	-30.8	-53
0.1M $CaCl_2$	2.4×10^5 (0.8×10^5)	-49.0 (2.1)	-30.7	-61

Table 5.7 Vancomycin binding to N_α,N_ε-diacetyl-Lys-D-Ala-D-Ala in the absence and presence of salts of various ionic strengths.

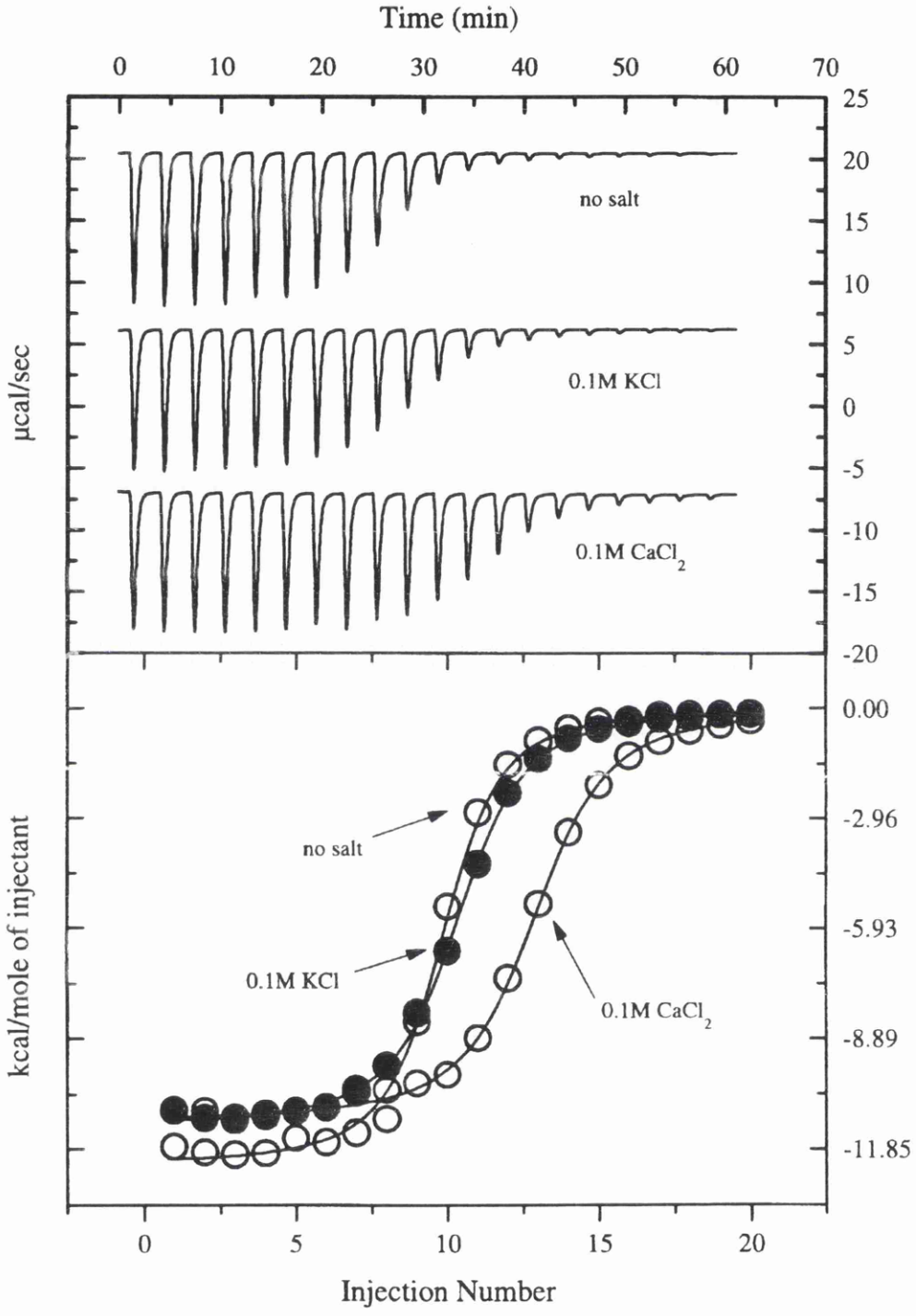

Figure 5.19 Vancomycin (0.28mM, 0.22mM, 0.29mM) binding to N_{α},N_{ε}-diacetyl-Lys-D-Ala-D-Ala (7.09mM, 6.75mM, 5.66mM) in the absence and presence of 0.1M KCl and 0.1M $CaCl_2$ respectively, in 0.1M MOPS buffer at pH 7.0, 25°C.

5.1.1.1.7 Deuterium oxide

There appears to be little difference in vancomycin binding to $N_{\alpha},N_{\varepsilon}$-diacetyl-Lys-D-Ala-D-Ala in either water or deuterium oxide, with association constants being very similar when standard deviations are considered. However, enthalpy changes are slightly more exothermic in deuterium oxide than in water. Solvent isotopic substitution affects binding due to differences in the interaction between solute and solvent. The enhanced enthalpic interaction in deuterium oxide is compensated by a nearly equal decrease in entropy, therefore leading to little or no difference in the free energy of binding in either deuterium oxide or water. In such experiments however, it is difficult to recreate identical conditions since solvent isotopic substitution also affects pK values of ionisable groups. Therefore, the protonation states of ionisable groups will not be identical in light or heavy water (Chervenak & Toone, 1994) (see chapter 4). Results are shown in Table 5.8, with typical thermal profiles in Figure 5.20.

Temperature (°C)	K_a (M^{-1})	ΔH ($kJmol^{-1}$)	ΔG° ($kJmol^{-1}$)	ΔS° ($JK^{-1}mol^{-1}$)
25	7.8×10^5 (4.5×10^5)	-60.4 (3.9)	-33.6	-90

Table 5.8 Vancomycin binding to $N_{\alpha},N_{\varepsilon}$-diacetyl-Lys-D-Ala-D-Ala in deuterium oxide.

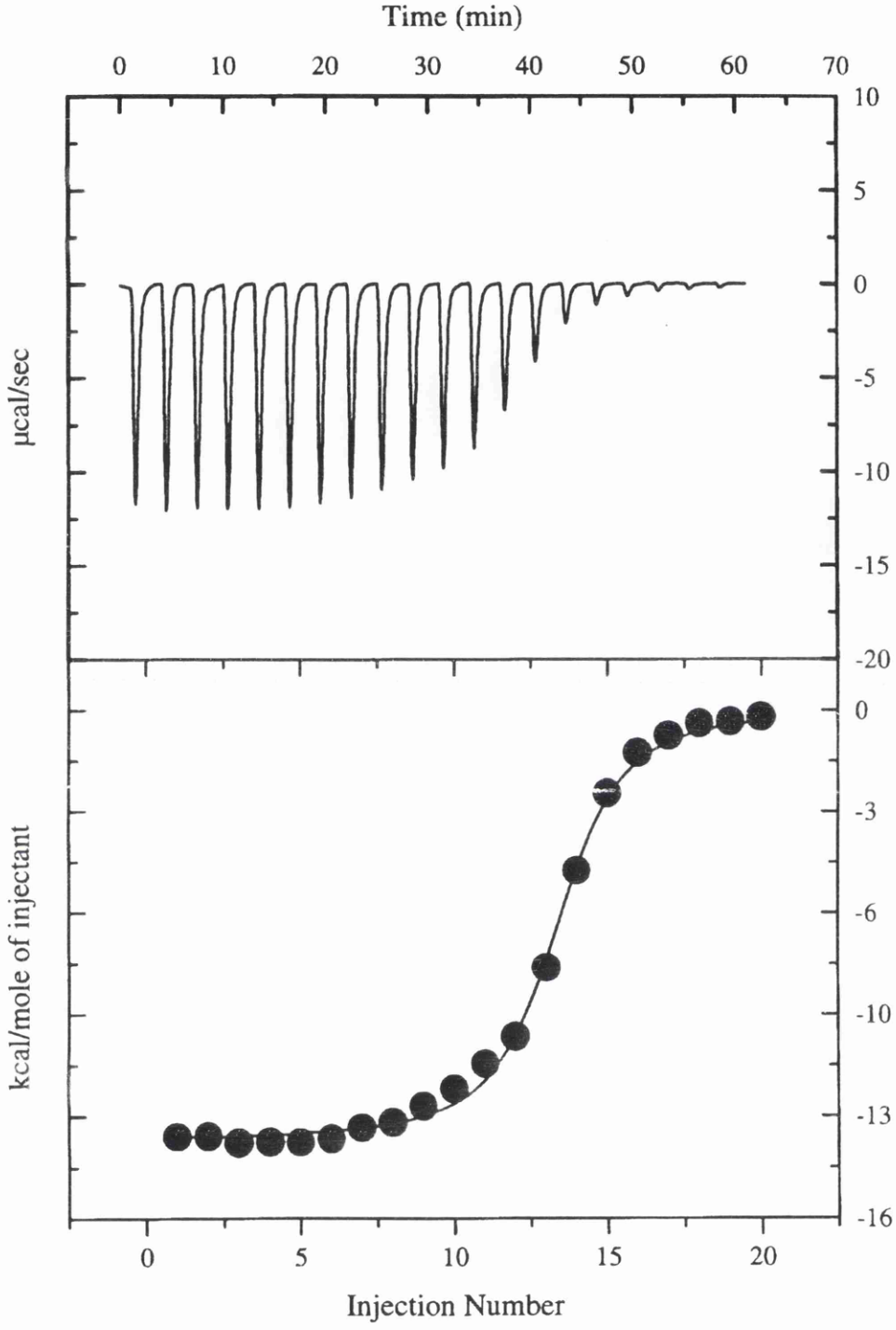

Figure 5.20 Vancomycin (0.31mM) binding to N_{α},N_{ε}-diacetyl-Lys-D-Ala-D-Ala (6.90mM) in deuterium oxide at pD 7.0, 25°C.

5.1.1.1.8 Discussion

The efficiency of molecular recognition between antibiotic and peptide clearly depends on the size and conformation of the peptide side chain, as shown from our results and in the work detailed by Nieto & Perkins,[a] (1971). In simple terms, vancomycin binds the weakest to the peptide N-acetyl-D-Ala, more strongly to N-acetyl-D-Ala-D-Ala and the most strongly to N_{α},N_{ε}-diacetyl-Lys-D-Ala-D-Ala. In order to try and explain this behaviour it is important to understand the structure of the individual complexes involved.

Within the binding site of vancomycin, shown in Figure 5.21 (McAuley-Hecht, 1993), are four amino groups and one carboxyl group which can, in the case of N-acetyl-D-Ala-D-Ala, form three hydrogen bonds with the terminal carboxyl group and one to the amino group and one to the carbonyl group of the peptide. All in all, the antibiotic/peptide complex is stabilised by five hydrogen bonds. In addition to hydrogen bonding, other important non-covalent interactions will be involved at this site, for example, hydrophobic interactions between the methyl groups on the two alanine residues of the peptide and the phenolic rings of the antibiotic, electrostatic interactions between the charged carboxyl group on the peptide and the amino group on the antibiotic, steric repulsion and van der Waals forces. All of which will contribute to some extent to the binding affinity for cell wall analogues. In comparison, vancomycin binding to the smaller peptide N-acetyl-D-Ala will have four of the five hydrogen bonds still in place, but the hydrogen bond to the carbonyl group will be absent, as will the corresponding hydrophobic interaction between the second alanine residue's methyl group and the phenolic group on the antibiotic. Hydrogen bond formation is thought to be accompanied by small enthalpic changes, but by larger entropic changes due to a stabilisation of the complex and therefore a reduction in the randomness of the structure. The hydrophobic effect is entropy driven, therefore in principle both hydrogen bonding and hydrophobic interactions work in tandem, cancelling each other out to some degree. The overall change is illustrated thermodynamically by an increase in the entropy

(~40JK^{-1}mol^{-1}) associated with vancomycin binding to N-acetyl-D-Ala compared with N-acetyl-D-Ala-D-Ala.

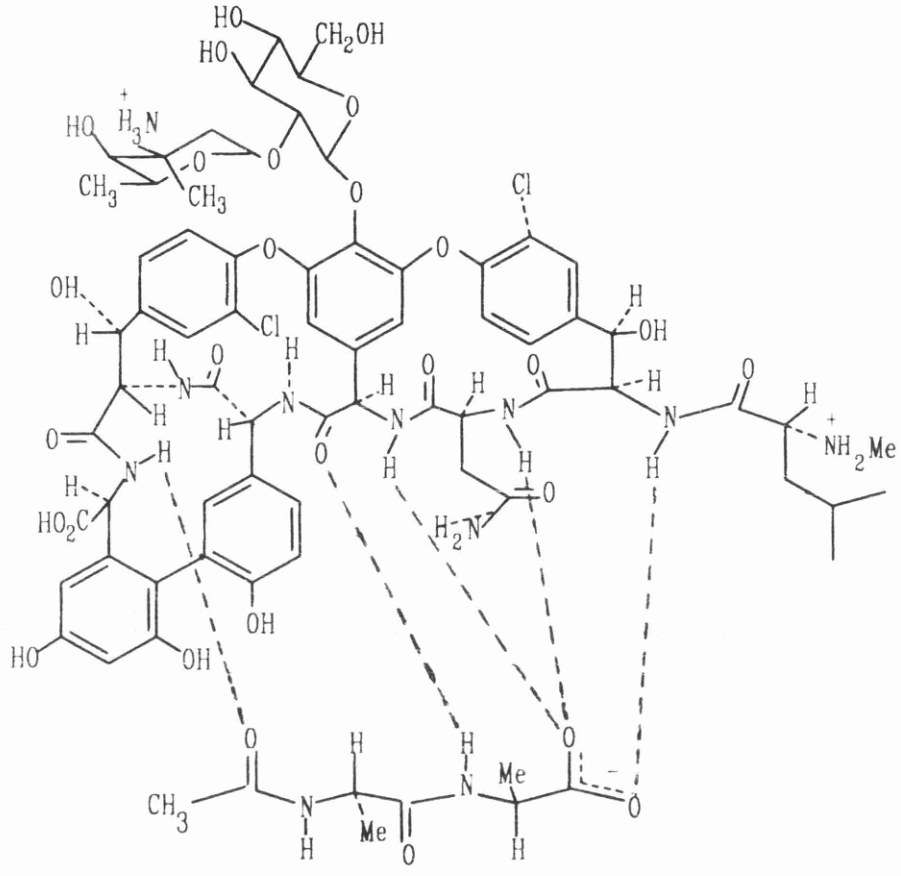

Figure 5.21 Schematic representation of the complex formed between vancomycin and a bacterial cell wall peptide model, N-acetyl-D-Ala-D-Ala. The broken lines indicate the positions of intermolecular hydrogen bonds.

Binding of vancomycin to the tripeptide $N_{\alpha},N_{\varepsilon}$-diacetyl-Lys-D-Ala-D-Ala involves the addition of a lysine residue to the peptide and a further two acetyl groups, the methyl groups of which contribute to the hydrophobic interactions at the binding site, leading to further stabilisation of the overall structure and contributing to an increase in binding affinity. Although an increase in binding affinity to this ligand is attributed to hydrophobic interactions due to the addition of the lysine residue, it was thought that a hydrogen bond might be formed between the hydroxyl group on ring seven and the

acetyl group on the lysine residue in $N_{\alpha},N_{\varepsilon}$-diacetyl-Lys-D-Ala-D-Ala, with such an arrangement providing extra stabilisation for the tripeptide complex. A study of the phenolic groups of ψ-aglycoristocetin (tetrasaccharide and mannose substituents removed from ristocetin A) was carried out using NMR spectroscopy (Rajagopalan *et al.*, 1995) in order to more fully understand phenolic function. From this study, however, there was no evidence for strong hydrogen bonding between phenolic hydroxyl groups of the antibiotic and carbonyl groups of the peptide. Although phenolic groups do not appear to play a direct role in the binding process i.e. via hydrogen bonding, they must have a functional role in order to justify their presence, although what form this role would take is unclear.

For all vancomycin binding to peptide scenarios, the molar heat capacity changes were large and negative, which is thought to be due to a contribution from hydrophobic interactions typical of macromolecular associations in water (Weber, 1993 : Weber, 1995 : Spolar and Record, 1994), though contributions from other interactions cannot be ruled out. It is therefore suggested that the binding process is accompanied by a removal of hydrophobic surface area from solvent, such as transfer of the peptide from water to a more hydrophobic environment within the complex and from the conformational change which takes place on binding resulting in the burial of some hydrophobic side chains of the antibiotic.

Since negative molar heat capacity changes are taken as evidence of significant hydrophobic interaction in the binding process, it can be correlated with changes in exposed non-polar surface area during complexation (Spolar & Record, 1994). Using the empirical procedure of Spolar & Record, (1994) together with the estimated heat capacity changes, it is possible to estimate the burial of non-polar surface areas to be from 250Å for vancomycin binding to N-acetyl-D-Ala and 390Å for binding to $N_{\alpha},N_{\varepsilon}$-diacetyl-Lys-D-Ala-D-Ala. Therefore, vancomycin binding to $N_{\alpha},N_{\varepsilon}$-diacetyl-Lys-D-Ala-D-Ala covers more non-polar surface area than binding to N-acetyl-D-Ala. Such changes in solvation and surface area seem to contribute much to the heat capacity of the

process, resulting in a higher molar heat capacity value associated with vancomycin binding to $N_{\alpha},N_{\varepsilon}$-diacetyl-Lys-D-Ala-D-Ala, which also brings about a large temperature variation in both enthalpy and entropy compared with binding to weaker ligands.

The molar heat capacity values were calculated from the temperature dependence of the enthalpy changes of the process. But these can also be determined from the degree of curvature in the van't Hoff plot. By plotting a graph of lnK against 1/T, we assume that ΔH is constant with respect to T, allowing us to calculate the van't Hoff enthalpy from the slope. A linear relationship is produced in simple cases providing the molar heat capacity is equal to zero. However, in more complex cases the temperature dependence of enthalpy due to the molar heat capacity gives rise to a curved plot. Regression analysis on our plots obtained from microcalorimetric data show linear slopes, but when theoretical values for the association constant were calculated from the temperature dependence of enthalpy and entropy (see equations 1.26 and 1.27) over a wider range of temperatures and a fitting function performed, a curve was produced in all cases consistent with $\Delta C_p \neq$ zero. Polynomial regression on these points were carried out to show the difference between theoretical and microcalorimetric data within experimental error. van't Hoff enthalpies are independent of the calorimetric enthalpy and were calculated from these plots for vancomycin binding to each of the cell wall peptides, showing a slight difference between the calculated van't Hoff enthalpies of association and those observed from microcalorimetry (Naghibi *et al.*, 1995), the greatest difference being in the binding of vancomycin to $N_{\alpha},N_{\varepsilon}$-diacetyl-Lys-D-Ala-D-Ala. This discrepancy is possibly due to regression analysis being carried out on a slope assumed to be linear, although the scatter of points suggests there may be more of a curve to the data. Caution must be exercised in interpreting data in this way, since only four temperature points are considered. To resolve this, titrations should be carried out over a wider range of temperatures at smaller intervals. If the data points follow a curve, rather than carrying out linear regression analysis and determining the enthalpy from the slope, the data should be fitted to a curve and the enthalpy obtained from any point on it. Since the curvature of our data was not so pronounced (R=0.97) this procedure did not seem

necessary. Vancomycin binding to N_{α},N_{ε}-diacetyl-Lys-D-Ala-D-Ala exhibits the largest free energies. This gives an indication of the tightness of binding involved compared with the relatively low free energies associated with weaker binding to N-acetyl-D-Ala.

Efficient molecular recognition between antibiotic and peptide has been shown to depend on pH, as shown by our results and in studies by Nieto & Perkins,[b] (1971). From studies of acid-base titrations of vancomycin, it was concluded that vancomycin contained carboxyl, amino and phenolic groups (Higgins *et al.*, 1958). Nieto & Perkins,[b] (1971) carried out electrometric and spectrophotometric titrations which showed vancomycin to contain groups with pK_a values of approximately 2.9, 7.2, 8.6, 9.6, 10.5 and 11.7. Other researchers have similarly assigned pK_a values of 8.7 and 9.6 to groups involving phenolic dissociation (Popieniek & Pratt, 1991). To determine which groups were phenolic, titrations of vancomycin were carried out in the basic region and it was found that above pH 7.8, phenolic groups were ionised and these were attributed to the pK_a values 8.6, 9.6, 10.5 and the group titrated with a pK_a of 11.7 was assigned to the vancosamine $-NH_2^+$ The titrated group with a pK_a of between 7.1 and 7.2 was assumed to be due to the terminal α-NH_3^+. Nieto & Perkins,[b] (1971) also showed that the UV spectrum of vancomycin was altered by the addition of acid. When vancomycin was titrated in the acidic region, a carboxyl group was titrated, accompanied by a change in absorbance. Since absorbance is influenced by the presence of phenolic groups, this titration of a carboxyl group may have induced a change in the aromatic chromophores if the carboxyl group was attached to or was located close to the aromatic groups or if variation of charge in the carboxyl group at low pH induced a change in the conformation of vancomycin that modified the interactions involving the aromatic chromophores, therefore changing the UV spectrum. The pK_a value of 2.9 is assumed to be due to this titrated carboxyl group. When the acid-base titration of vancomycin complexed to the tripeptide diacetyl-L-Lysyl-D-Alanyl-D-Alanine was carried out, it was noticed that titration of the first three phenolic groups was hindered, suggesting these groups may play a role in the binding process. It is thought that the phenolic hydroxyl groups may lie inside a cleft at the binding site and ionisation of these groups at high pH

may therefore reduce the affinity for peptide by electrostatic repulsion between the antibiotic and the negatively charged peptide (Rajagopalan *et al.*, 1995). Complex formation has been shown to occur over a wide pH range, but as soon as phenolic ionisation occurs i.e. after pH 7.8, the complex has been shown from spectrophotometric titrations to become less stable and also at acidic pH where ionisation of carboxyl groups may be prevented. Therefore, it is indicated that carboxyl groups must be ionised and phenolic groups unionised or at least the carboxyl group in the peptide substrate must be ionised (Nieto & Perkins,[a] 1971) for complex formation to occur. These prerequisites are met at neutral pH, explaining the optimum vancomycin binding affinity for peptide around this pH observed from our microcalorimetric studies. Binding affinity was significantly reduced at the extremes of pH, where the stability of the antibiotic/peptide complex was reduced.

All entropy-enthalpy compensation plots for ligand binding in aqueous solution under various temperature and pH conditions exhibit slopes near unity ($R \geq 0.91$), signifying that changes in the free energy of the process are much smaller in magnitude than the corresponding changes in enthalpy and entropy. This phenomenon has been related to the role of solvent water molecules in the association process. The release of structured water molecules from the interacting surfaces of both antibiotic and peptide out to join bulk solvent results in an increase in entropy which is compensated by a decrease in the enthalpy due to enthalpically weaker hydrogen bonds in bulk water than at the interacting surfaces (Bundle & Sigurskjold, 1994). Such plots contain experimental errors on both axes, but these errors are statistically correlated since entropy values have been calculated directly from enthalpy values obtained from microcalorimetry, therefore it is important that proper regression analysis is carried out on the data to take this into account (Johnson, 1985). The role of heat capacity is also implicated in entropy-enthalpy compensation since it contains contributions from both these parameters.

In an attempt to determine the contribution of the peptide carboxyl group to the overall interaction at the antibiotic binding site, microcalorimetry has been used to study the

binding of an acetate anion to vancomycin (Cooper & McAuley-Hecht, 1993), although indirectly by competition experiments with $N_{\alpha},N_{\varepsilon}$-diacetyl-Lys-D-Ala-D-Ala, since binding of the acetate anion itself is too weak to measure directly. From these studies it was shown that increasing concentrations of acetate in the reaction mixture progressively inhibited binding to vancomycin of the much stronger ligand $N_{\alpha},N_{\varepsilon}$-diacetyl-Lys-D-Ala-D-Ala, consistent with simple competitive binding of acetate and $N_{\alpha},N_{\varepsilon}$-diacetyl-Lys-D-Ala-D-Ala for the same antibiotic binding site. Before binding of $N_{\alpha},N_{\varepsilon}$-diacetyl-Lys-D-Ala-D-Ala to antibiotic can occur, there must be displacement of the acetate, which reduces the association constant and apparent enthalpy of $N_{\alpha},N_{\varepsilon}$-diacetyl-Lys-D-Ala-D-Ala binding. Our results for vancomycin binding to $N_{\alpha},N_{\varepsilon}$-diacetyl-Lys-D-Ala-D-Ala in the presence of acetate are consistent with those found by Cooper & McAuley-Hecht, (1993). A contribution to this effect has been shown to be made by electrostatic interactions, with the same experiment repeated in the presence of salt showing the same trends. Electrostatic interactions between molecules in the presence of salt are known to be modified, since these small ions will collect around a macromolecule of opposite charge forming a counter-ion atmosphere which screens it from another molecule. The larger the concentration or ionic strength of these small ions present, the more effective this screening should be, although our results show little difference in thermodynamic parameters between monovalent KCl and divalent $CaCl_2$.

The binding of vancomycin to $N_{\alpha},N_{\varepsilon}$-diacetyl-Lys-D-Ala-D-Ala has also been investigated in the presence of deuterium oxide. Solvent isotopic substitution affects many of the interactions that occur between biomolecules, such as hydrogen bonding and the hydrophobic effect and even electrostatic interactions which are influenced through the dielectric constant of the solvent. Although comparisons are made between the binding of vancomycin to ligand in both water and deuterium oxide, where pH = pD, this is not really ideal since ionisation constants are known to differ between heavy and light water. The pK of proteins in deuterium oxide have been shown to be approximately 0.4-0.5 pH units higher than in water (Kalinichenko & Lobyshev, 1976) therefore there is no electrostatic equivalence between these solvents under conditions of pH = pD. When

thought of in terms of proteins, this means that the net charge on a protein at a particular pH in water will not be the same in deuterium oxide at the same pD. The point at which there is equivalence and where comparisons should be made is when the apparent pH of the deuterium oxide is equal to the actual pH of the water. However, in our series of experiments where pH = pD, any differences are interpreted in terms of deuterium oxide alone since our results in deuterium oxide do not follow the trends found in going to a lower pH, therefore any differences in ionisation states between the solvents are thought to be negligible. Solvent isotopic substitution results in differences in the interaction between the hydrogen bond acceptor on the molecule and the deuterium or hydrogen nucleus in the solvent, with such differences ultimately affecting the overall enthalpy of association (Chervenak & Toone, 1994). It has long been known that deuterium bonds are stronger than hydrogen bonds. The cause of this difference can be resolved by considering the basis of the hydrogen bond. H-O (and therefore D-O) bonds are very polar with the donor H (or D) carrying a partial positive charge and it is the interaction of this partial positive charge with a pair of non-bonding electrons on the O atom which gives rise to the hydrogen bond. Due to the small volume of the hydrogen atom it has a high charge density. The strength of the donor depends upon its electronegativity, therefore it is possible that the D carries a greater partial positive charge (less electronegative than H) and therefore greater charge density, due to D atoms having a greater nuclear mass than H atoms, producing the stronger D-O covalent bond relative to that of H-O and therefore stronger deuterium bonds. It has been shown that the enthalpy of an intermolecular hydrogen bond in deuterium oxide is close to 10% greater than in water (Nemethy & Scheraga, 1964 : Marcus & Ben-Naim, 1985) and that solute-solvent deuterium bonds are stronger and more localised relative to protium, this effect could contain contributions from deuterium oxide molecules being more ordered around the solute than water, therefore reducing entropy, but increasing enthalpy of association. These differences in the rotational motions of solvent were revealed by differences in libration frequencies in both deuterium oxide and water (Chervenak and Toone, 1994). The molarity of both water and deuterium oxide is almost identical (~55M) so that there is virtually no chance of any exposed exchangeable hydrogens being left on the molecule

in deuterium oxide, so that solute-solvent bonds will be almost exclusively deuterium. However, in bulk solvent, the exchange may include some D-O...H or H-O...D, but again with virtually no H-O...H bonds. If hydrogen bonds are buried within the hydrophobic core of a protein for example, these will remain simply because they are unexposed and therefore cannot exchange with solvent. Similarly for intermolecular hydrogen bonds across a tight dimer interface for example, although given time they will exchange with deuterated solvent depending on the dissociation constant. Therefore isotopic substitution will affect solute-solvent interactions with these being hydrogen bonds in water but deuterium bonds in deuterated solvent and also hydrogen bonds between antibiotic and peptide will be affected since exchangeable hydrogens within the binding site will be exposed prior to peptide binding. It follows then that an increase in the enthalpy of these interactions will lead to a differential enthalpy of binding in deuterium oxide compared with water (Chervenak & Toone, 1994). Enthalpy and entropy work in such a way as to cancel each other out to some degree, so that the associated free energy exhibits little or no change in either solvent.

The magnitude of the thermodynamic parameters calculated in the study by Chervenak & Toone, (1994) for the binding of vancomycin to N_{α},N_{ε}-diacetyl-Lys-D-Ala-D-Ala in deuterium oxide and water are comparable to our results, although in our study enthalpy changes are more exothermic in deuterium oxide than in water, contrasting with the trend found in the Chervenak & Toone, (1994) study. The errors associated with our enthalpy changes are large and therefore the estimated values will be less accurate.

In the Chervenak & Toone, (1994) study comparison of changes in specific heat capacity plots in both deuterium oxide and water show significant differences. Factors affecting heat capacity changes have been thought to include changes in solvent structure, hydrogen bonding (Chervenak & Toone, 1994), low frequency protein vibrations and solvent reorganisation, the latter two thought to be the major contributors (Sturtevant, 1977). Solvent isotopic substitution will affect each of these to some extent and contribute to the differences in heat capacity found in deuterium oxide compared with water.

5.1.2 Dimerisation studies using isothermal titration microcalorimetry

The dissociation of vancomycin and ristocetin dimers in the presence and absence of peptidoglycan precursors and their analogues has also been studied using the Microcal Omega Ultrasensitive Isothermal Titration Microcalorimeter. Dilution of vancomycin solutions into the microcalorimetric cell were studied in the absence of ligand and in the presence of N-acetyl-D-Ala, N-acetyl-D-Ala-D-Ala and $N_{\alpha},N_{\varepsilon}$-diacetyl-Lys-D-Ala-D-Ala over a range of temperature (15-45°C) and pH (3-11) conditions. As a comparison, dilution of ristocetin solutions into the cell were carried out in the absence of ligand and in the presence of N-acetyl-D-Ala and $N_{\alpha},N_{\varepsilon}$-diacetyl-Lys-D-Ala-D-Ala. Selected vancomycin dilution experiments were also carried out in the presence of acetate, salts of different ionic strengths, deuterium oxide and buffers with different heats of ionisation. Dimerisation constants (K_{dim}) and enthalpy changes (ΔH_{dim}) were determined from non-linear regression techniques, which led directly to the determination of standard entropy changes ($\Delta S°_{dim}$) and standard Gibbs free energy ($\Delta G°_{dim}$) with standard deviations shown in brackets. van't Hoff enthalpies were calculated from the gradient of the line from plots of lnK against 1/T. Molar heat capacity changes (ΔC_p) were determined from the gradient of the line obtained from plots of ΔH_{dim} against T.

Dilution of antibiotic solutions by injection of small aliquots into the microcalorimeter cell containing a larger volume of buffer is an endothermic process consistent with the dissociation of antibiotic dimers or higher oligomers. A sequence of dilution injections gives a series of endothermic heat pulses which after integration and correction for control mixing experiments, gives the absolute heat uptake per injection. In such a dilution series, successive injections become progressively less endothermic as the antibiotic concentration builds up in the cell. For simplicity, results are expressed in terms of antibiotic dimerisation.

All experiments were carried out in phosphate buffer (pH 7, 0.1M) unless stated otherwise.

All deuterium oxide, acetate and heat of ionisation experiments and those involving changes in pH and ionic strength were carried out at 25°C.

Typical thermal profiles given in the following section show: *Upper panel*; endothermic responses for injection of vancomycin into buffer alone or ligand solution, under the same conditions. *Lower panel*; integrated dilution heat effects with theoretical fits to a dimer dissociation model.

Figures in parentheses are standard deviations of multiple experiments. (-) single determination only.

Data in tables are quoted in the SI unit of Joules, whereas figures generated by Origin are in calories (1 cal = 4.184J).

Microcalorimetric measurements were made for dissociation of vancomycin dimers (as shown by thermal profiles), but are tabulated in terms of the dimerisation process.

5.1.2.1 Vancomycin dimerisation studies

5.1.2.1.1 No ligand

In the absence of ligand, the aggregation of vancomycin molecules in solution is fairly weak, shown by the relatively small dimerisation constants and enthalpy changes. In addition to a decrease in the dimerisation constants with increasing temperature, consistent with a reduction in the stability of the complex at higher temperatures, the enthalpies become more exothermic, corresponding to a negative change in molar heat capacity. Results are shown in Table 5.9(a), with a typical isotherm in Figure 5.22.

Vancomycin dimerisation occurs over a wide pH range. The stability of the vancomycin dimer shows relatively little variation with pH in the acid to neutral region, but falls significantly above pH 8. Results are shown in Table 5.9(b).

Temperature (°C)	**K_{dim} (M^{-1})**	**ΔH_{dim} ($kJmol^{-1}$)**	**$\Delta G°_{dim}$ ($kJmol^{-1}$)**	**$\Delta S°_{dim}$ ($JK^{-1}mol^{-1}$)**	**ΔC_p ($JK^{-1}mol^{-1}$)**
15	480 (70)	-27.5 (0.5)	-14.8	-44	
25	475 (80)	-29.2 (1.7)	-15.3	-47	-550 (90)
35	265 (25)	-36.9 (0.4)	-14.3	-73	
45	225 (65)	-43.3 (0.1)	-14.3	-91	

Table 5.9(a) Vancomycin dimerisation in the absence of ligand at various temperatures.

pH	K_{dim} (M^{-1})	ΔH_{dim} ($kJmol^{-1}$)	$\Delta G°_{dim}$ ($kJmol^{-1}$)	$\Delta S°_{dim}$ ($JK^{-1}mol^{-1}$)
3	470 (200)	-28.6 (5.8)	-15.2	-45
5	380 (40)	-24.0 (4.5)	-14.7	-31
7	475 (80)	-29.2 (1.7)	-15.3	-47
8	610 (70)	-27.1 (4.2)	-15.9	-38
11	170 (5)	-49.5 (7.6)	-12.7	-123

Table 5.9(b) Vancomycin dimerisation in the absence of ligand at various pH.

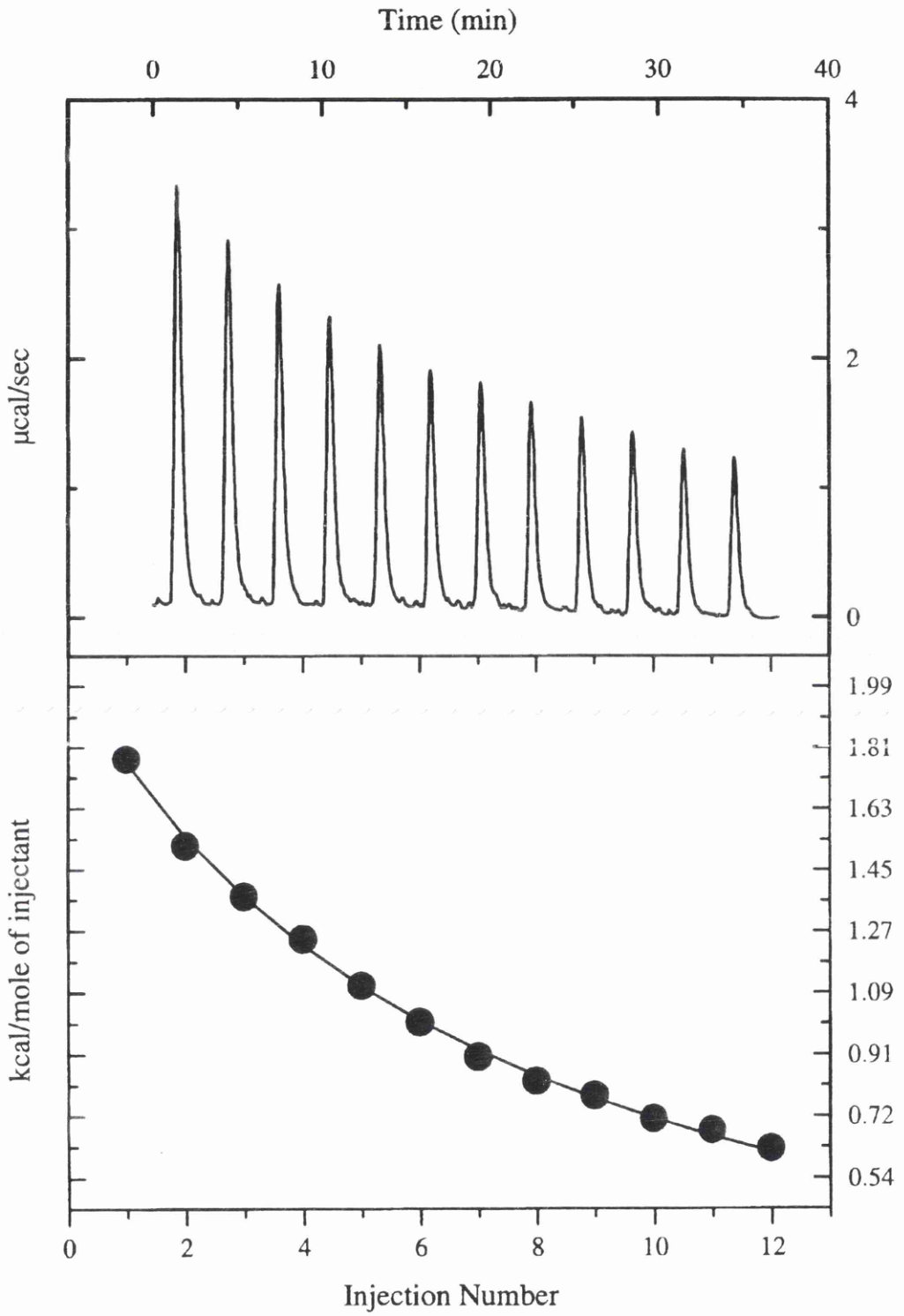

Figure 5.22 Vancomycin (2.83mM) dissociation in the absence of ligand at pH 7.0, 25°C.

5.1.2.1.2 N-acetyl-D-Ala

This weakly binding ligand encourages dimerisation, shown by an increase in dimerisation constants. The weak binding of this peptide gives rise to a weakly bound dimer, although more strongly bound than in the absence of cell wall analogues. Again, dimer stability is reduced with increasing temperature. The small change in free energy of dimerisation upon ligand binding is accompanied by an increase in exothermicity of dimerisation but with a decrease in entropy, consistent with an increase in the order of the complex. Dimerisation in the presence of N-acetyl-D-Ala also exhibits a corresponding negative change in molar heat capacity. Results are shown in Table 5.10(a) and a typical isotherm in Figure 5.23.

Dimerisation in the presence of this peptide is greatly reduced above pH 8, shown by the decrease in dimerisation constant within this range. Results are shown in Table 5.10(b).

Temperature (°C)	K_{dim} (M^{-1})	ΔH_{dim} ($kJmol^{-1}$)	$\Delta G°_{dim}$ ($kJmol^{-1}$)	$\Delta S°_{dim}$ ($JK^{-1}mol^{-1}$)	ΔC_p ($JK^{-1}mol^{-1}$)
15	5100 (-)	-35.0 (-)	-20.4	-51	
25	2300 (230)	-36.5 (1.8)	-19.2	-58	-445 (90)
35	980 (135)	-41.2 (0.1)	-17.6	-76	
45	570 (40)	-48.3 (0.1)	-16.8	-99	

Table 5.10(a) Vancomycin dimerisation in the presence of N-acetyl-D-Ala at various temperatures.

pH	K_{dim} (M^{-1})	ΔH_{dim} ($kJmol^{-1}$)	$\Delta G°_{dim}$ ($kJmol^{-1}$)	$\Delta S°_{dim}$ ($JK^{-1}mol^{-1}$)
3	1085 (185)	-35.7 (0.2)	-17.3	-61
5	1250 (75)	-36.2 (1.2)	-17.7	-62
7	2300 (230)	-36.5 (1.8)	-19.2	-58
8	900 (20)	-33.5 (1.7)	-16.8	-56
11	395 (10)	-27.6 (2.0)	-14.8	-43

Table 5.10(b) Vancomycin dimerisation in the presence of N-acetyl-D-Ala at various pH.

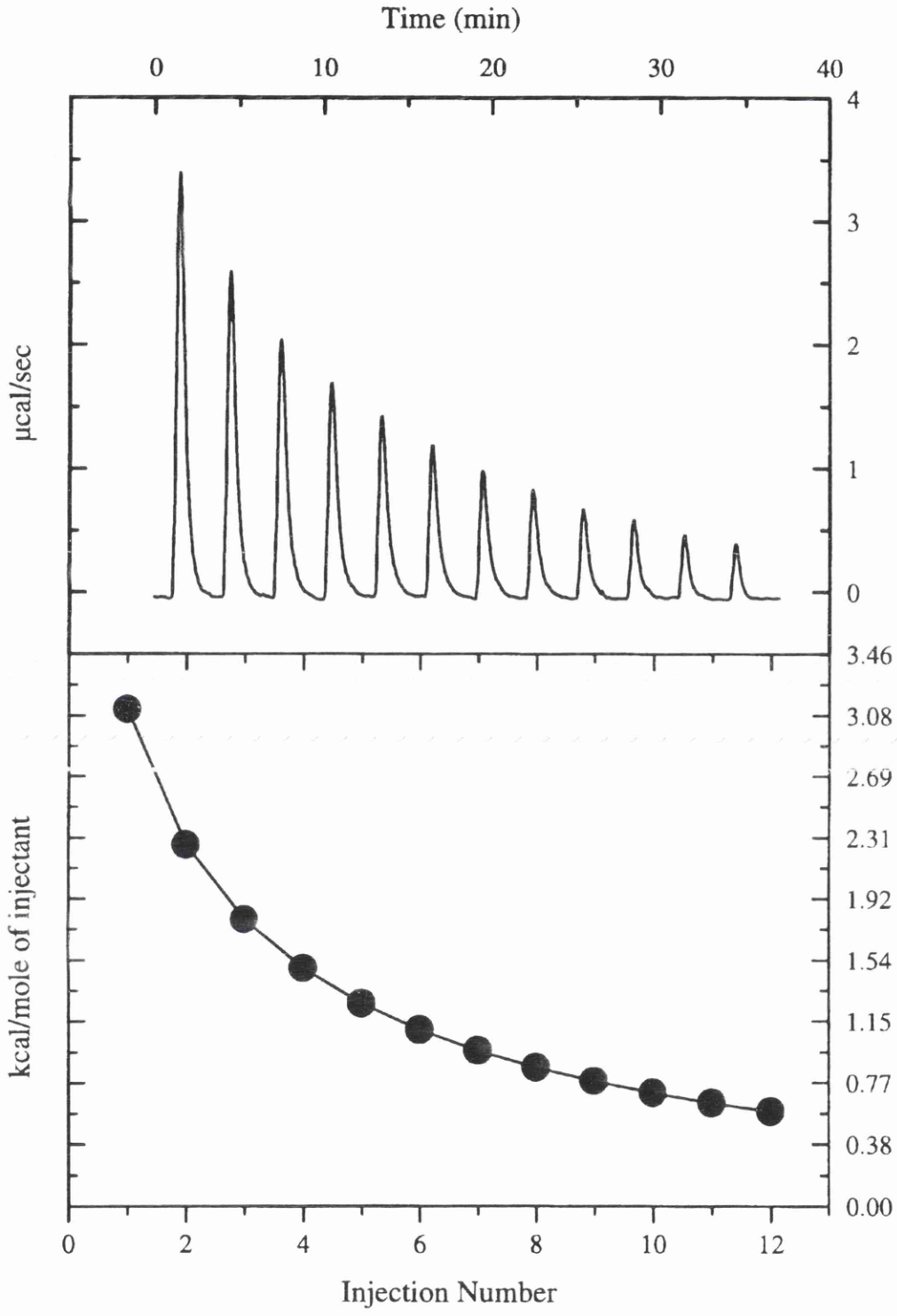

Figure 5.23 Vancomycin (3.20mM) dissociation in the presence of N-acetyl-D-Ala (98.60mM) at pH 7.0, 25°C.

5.1.2.1.3 N-acetyl-D-Ala-D-Ala

Trial experiments using this dipeptide with vancomycin at the concentrations required for calorimetric dilution measurements led to precipitation of the antibiotic-dipeptide complex. Since homogenous sample is essential in such experiments, this prevented any further use of the dipeptide in this context. However, this did provide us with conditions suitable for the growth of single crystals of the complex, from which the structure may be derived (see chapter 6).

5.1.2.1.4 N_α,N_ε-diacetyl-Lys-D-Ala-D-Ala

The presence of this strongly binding tripeptide increases vancomycin dimerisation constants by a factor of 10, illustrating that dimerisation is becoming stronger. The endothermic heat pulses, shown in the upper panel of the thermal profile in Figure 5.24, are also broader and take longer to return to baseline than for dimerisation in the presence and absence of other ligand, therefore titrations were carried out over a longer time period i.e. 60mins. This is further evidence for the increased strength of the vancomycin dimer in the presence of this ligand. The strength of the dimer is also shown by the more exothermic enthalpies, where significantly more heat is required to dissociate the complex. Dimerisation constants are reduced by increasing the temperature showing that the dimer is less stable at elevated temperatures, therefore leading to an increase in dissociation from the dimer form. As in the previous cases, a negative change in molar heat capacity is obtained. Dimerisation in the presence of N_α,N_ε-diacetyl-Lys-D-Ala-D-Ala is a good example of ligand induced dimerisation, where ligand binding appears to significantly encourage antibiotic dimerisation. Results are shown in Table 5.11(a), with a typical isotherm in Figure 5.24.

No accurate data could be obtained for dimerisation in the presence of this peptide at pH 11. Above pH 8, a series of erratic heat pulses were produced due to the reduction in

stability of the dimer and antibiotic/peptide complex, which were difficult to fit to the dilution model. Results are shown in Table 5.11(b).

Temperature (°C)	K_{dim} (M^{-1})	ΔH_{dim} ($kJmol^{-1}$)	$\Delta G°_{dim}$ ($kJmol^{-1}$)	$\Delta S°_{dim}$ ($JK^{-1}mol^{-1}$)	ΔC_p ($JK^{-1}mol^{-1}$)
15	9600 (4000)	-21.1 (0.9)	-21.9	3	
25	5050 (1080)	-39.3 (2.8)	-21.1	-61	-1745 (155)
35	3150 (985)	-61.1 (6.1)	-20.6	-131	
45	1800 (50)	-72.0 (15.0)	-19.8	-164	

Table 5.11(a) Vancomycin dimerisation in the presence of N_α,N_ε-diacetyl-Lys-D-Ala-D-Ala at various temperatures.

pH	K_{dim} (M^{-1})	ΔH_{dim} ($kJmol^{-1}$)	$\Delta G°_{dim}$ ($kJmol^{-1}$)	$\Delta S°_{dim}$ ($JK^{-1}mol^{-1}$)
3	2655 (540)	-30.1 (2.0)	-19.5	-36
5	3775 (-)	-30.9 (-)	-20.4	-35
7	5050 (1080)	-39.3 (2.8)	-21.1	-61
8	2285 (-)	-25.3 (-)	-19.2	-21

Table 5.11(b) Vancomycin dimerisation in the presence of $N_{\alpha},N_{\varepsilon}$-diacetyl-Lys-D-Ala-D-Ala at various pH.

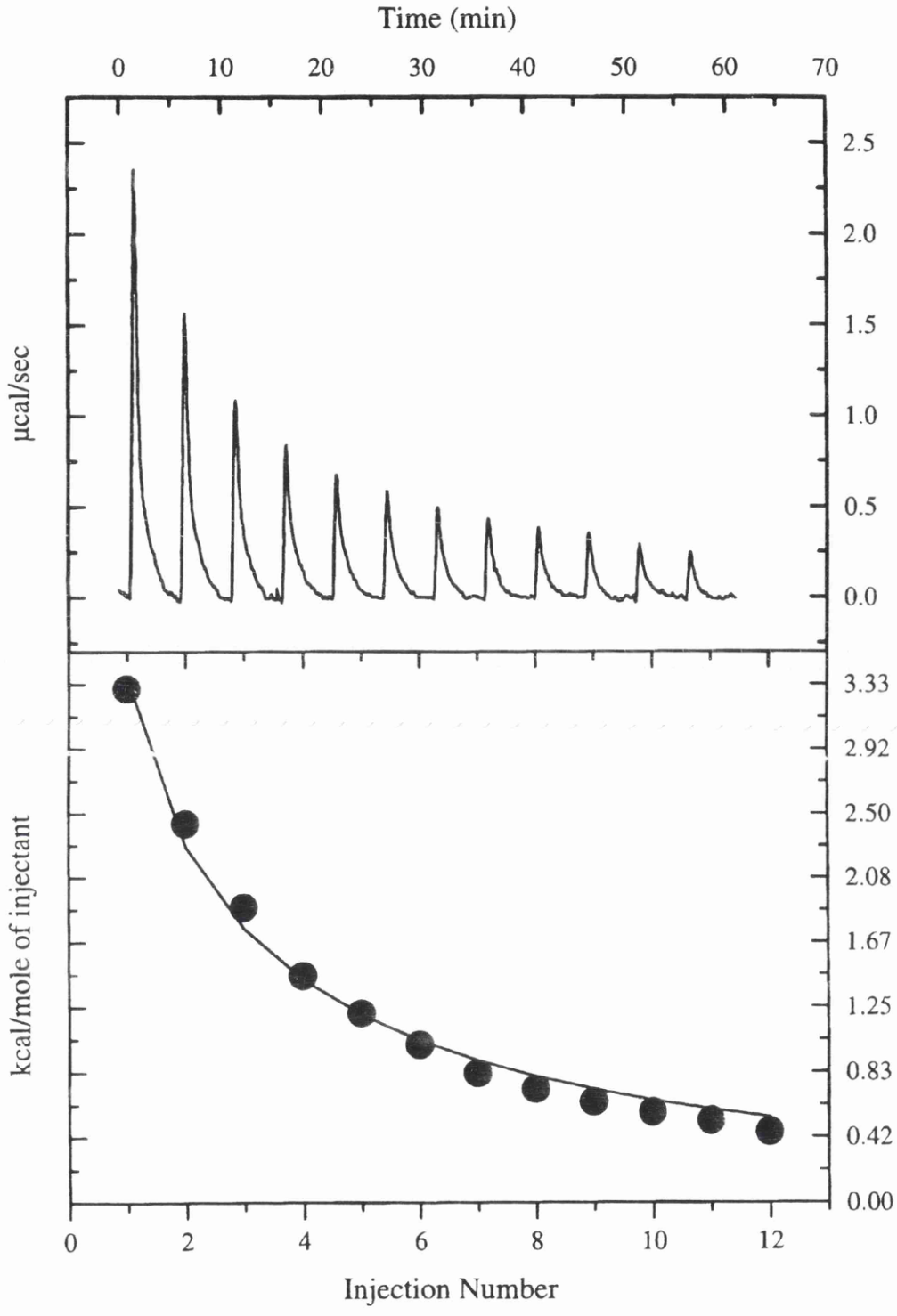

Figure 5.24 Vancomycin (2.70mM) dissociation in the presence of $N_{\alpha},N_{\varepsilon}$-diacetyl-Lys-D-Ala-D-Ala (1.50mM) at pH 7.0, 25°C.

van't Hoff and ΔC_p plots are shown in Figures 5.25-5.28 and 5.29-5.32, respectively. Comparisons of microcalorimetric and theoretical van't Hoff plots are shown in Figures 5.33-5.35. van't Hoff enthalpies were calculated using a simple 2-state model and are shown in Table 5.12 with entropy-enthalpy compensation plots in Figures 5.36 and 5.37.

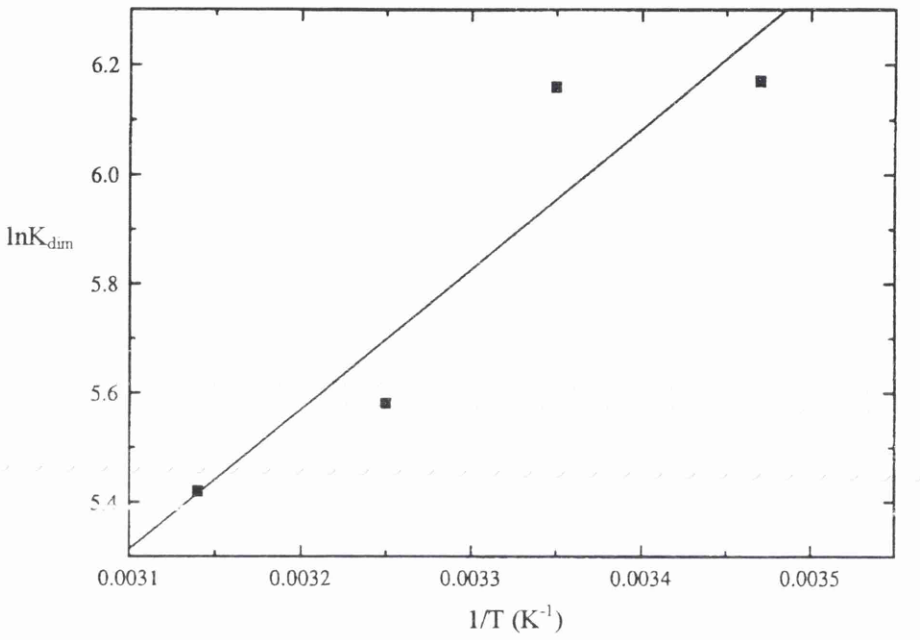

Figure 5.25 van't Hoff plot of vancomycin dimerisation in the absence of ligand.

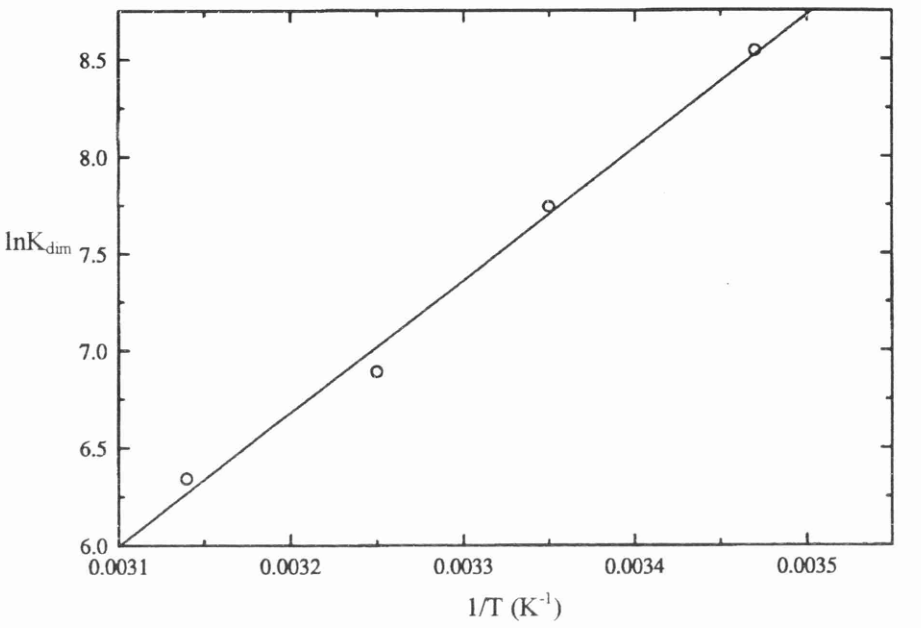

Figure 5.26 van't Hoff plot of vancomycin dimerisation in the presence of N-acetyl-D-Ala.

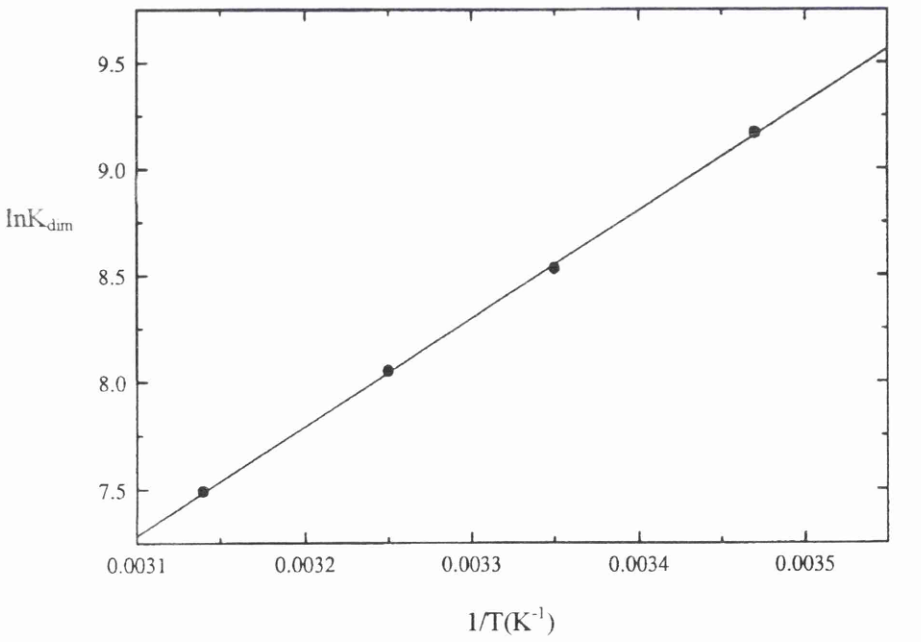

Figure 5.27 van't Hoff plot of vancomycin dimerisation in the presence of N_{α},N_{ε}-diacetyl-Lys-D-Ala-D-Ala.

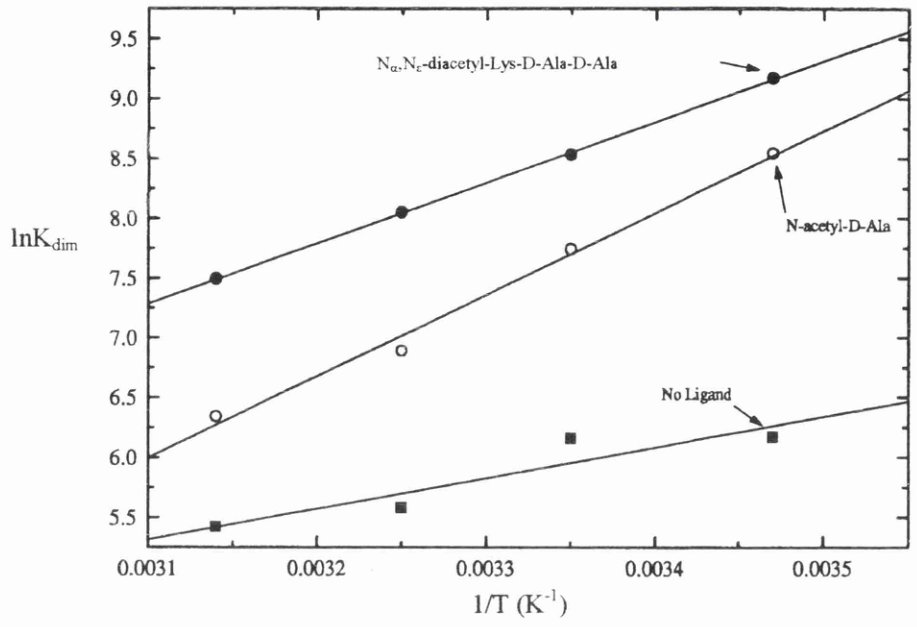

Figure 5.28 Summary of all van't Hoff plots of vancomycin dimerisation.

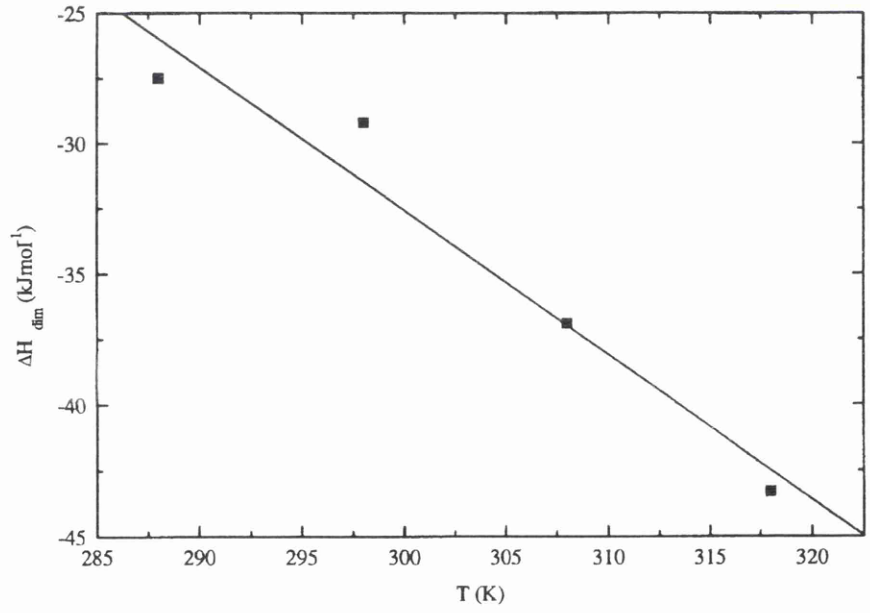

Figure 5.29 ΔC_p plot of vancomycin dimerisation in the absence of ligand.

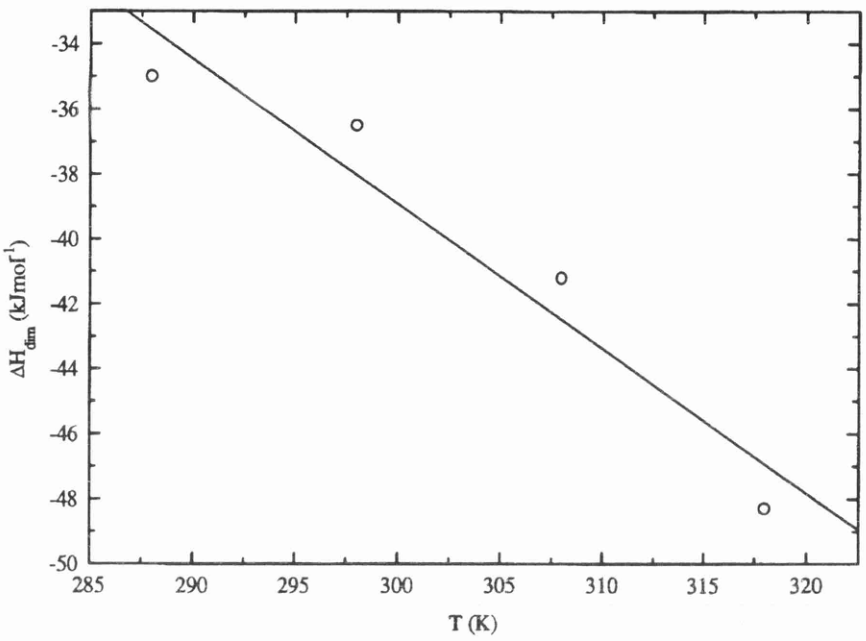

Figure 5.30 ΔC_p plot of vancomycin dimerisation in the presence of N-acetyl-D-Ala.

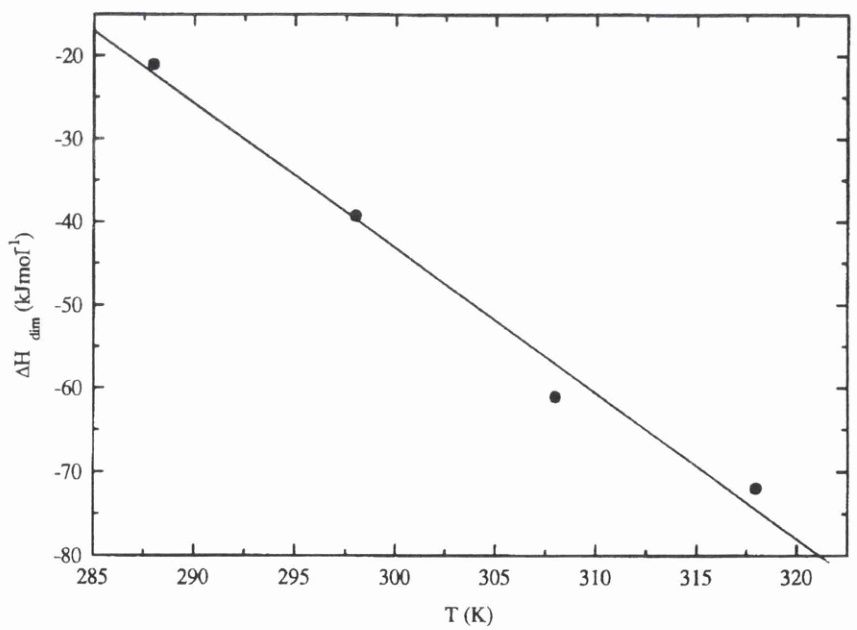

Figure 5.31 ΔC_p plot of vancomycin dimerisation in the presence of N_α,N_ε-diacetyl-Lys-D-Ala-D-Ala.

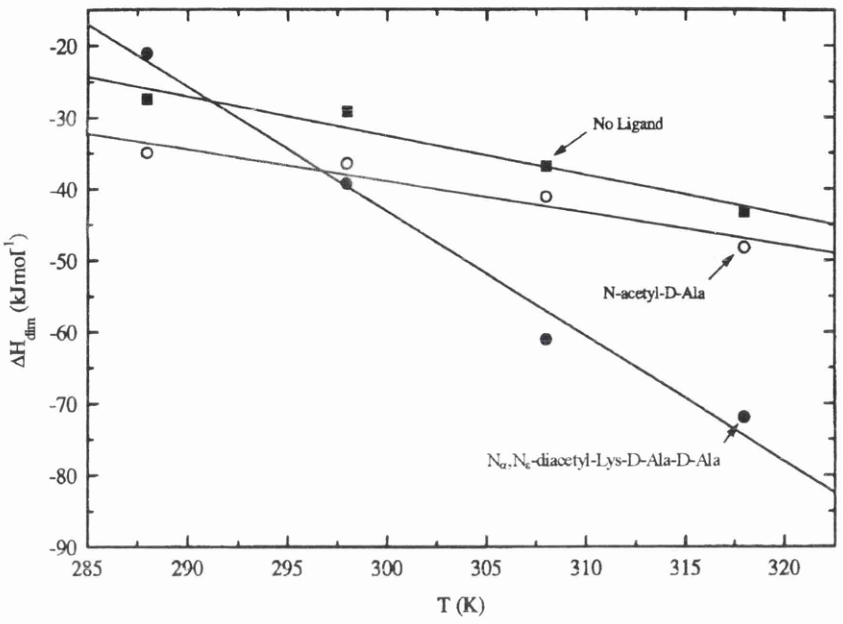

Figure 5.32 Summary of all ΔC_p plots of vancomycin dimerisation.

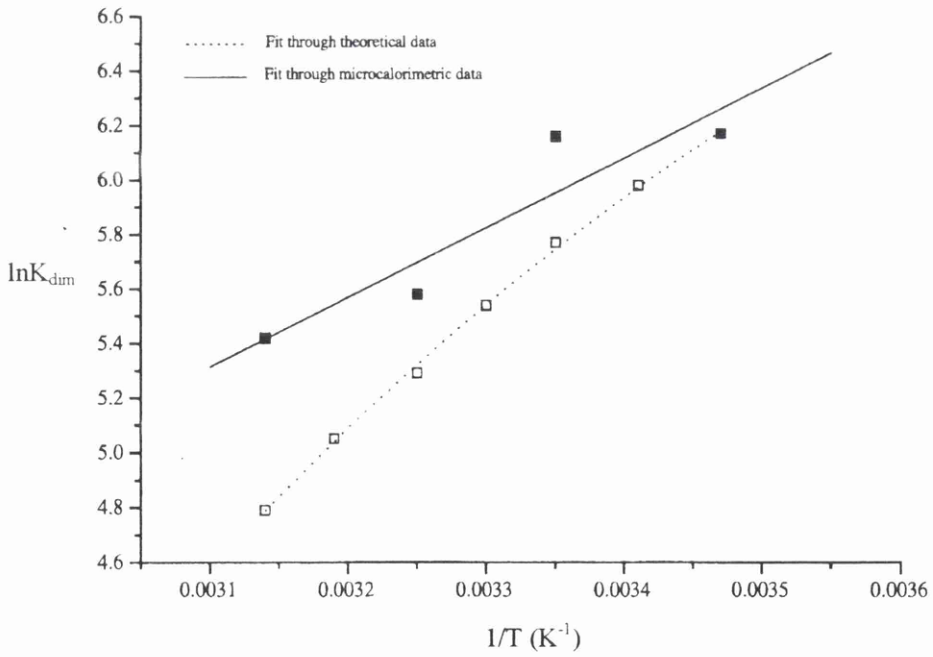

Figure 5.33 Comparison of microcalorimetric and theoretical van't Hoff plots of vancomycin dimerisation in the absence of ligand.

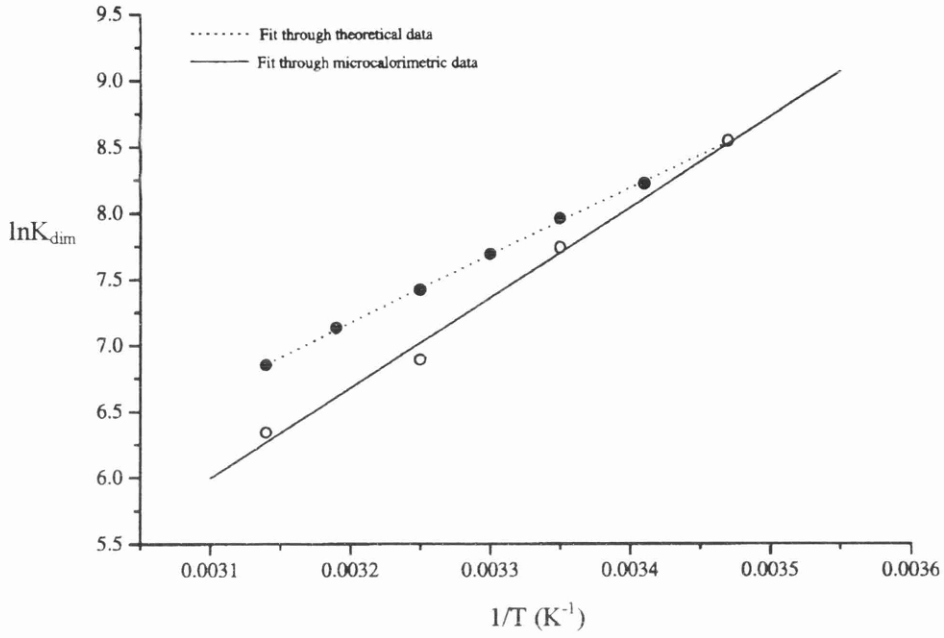

Figure 5.34 Comparison of microcalorimetric and theoretical van't Hoff plots of vancomycin dimerisation in the presence of N-acetyl-D-Ala.

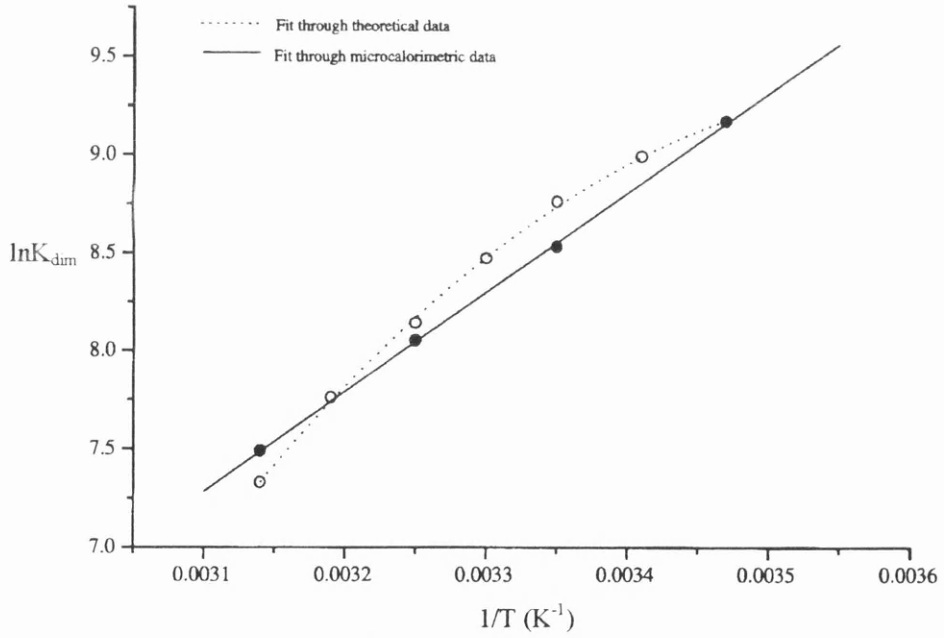

Figure 5.35 Comparison of microcalorimetric and theoretical van't Hoff plots of vancomycin dimerisation in the presence of N_{α},N_{ε}-diacetyl-Lys-D-Ala-D-Ala.

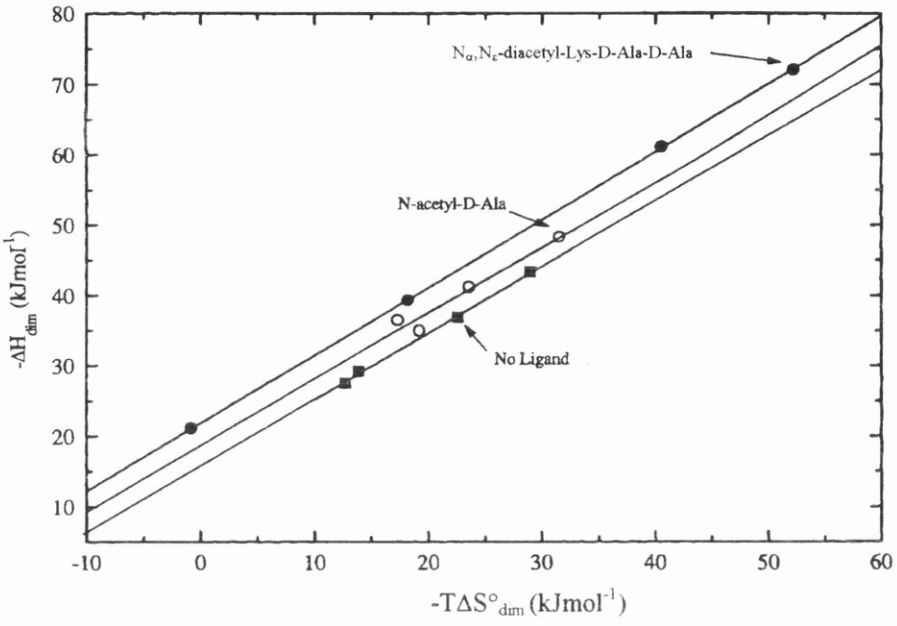

Figure 5.36 Entropy-enthalpy compensation plot of vancomycin dimerisation at various temperatures.

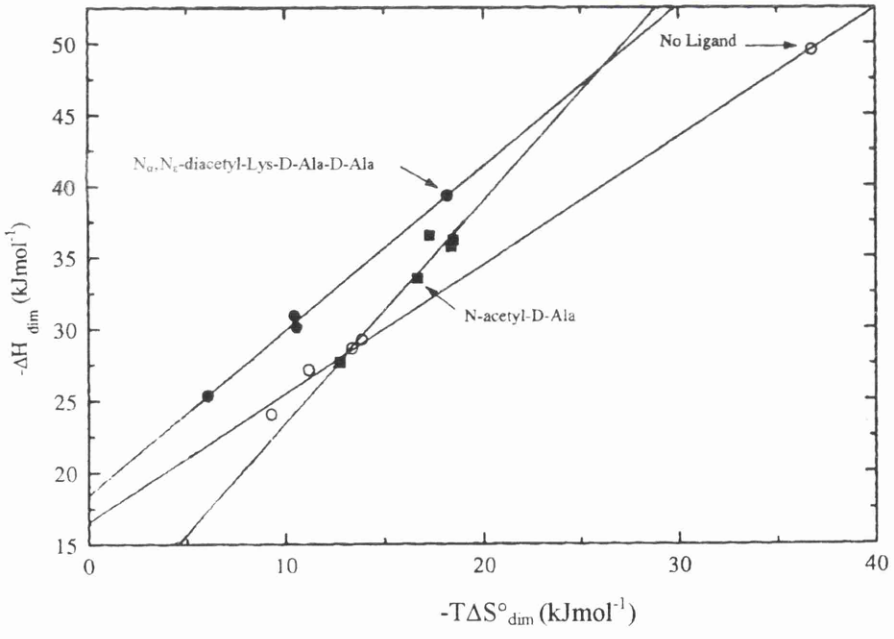

Figure 5.37 Entropy-enthalpy compensation plot of vancomycin dimerisation at various pH.

	van't Hoff enthalpy ($kJmol^{-1}$)
No Ligand	-21.3 (6.1)
N-acetyl-D-Ala	-56.8 (3.7)
N_α,N_ε-diacetyl-Lys-D-Ala-D-Ala	-42.1 (0.6)

Table 5.12 van't Hoff enthalpies of vancomycin dimerisation in the presence and absence of cell wall analogues.

5.1.2.1.5 Acetate

Vancomycin dimerisation in the absence of cell wall analogues appears to be encouraged in the presence of acetate, particularly at higher concentrations, shown by a small, but significant enhancement in dimerisation constant, consistent with its action as a very weak ligand (Cooper & McAuley-Hecht, 1993). Results are shown in Table 5.13, with typical isotherms in Figure 5.38. As with vancomycin binding to N_α,N_ε-diacetyl-Lys-D-Ala-D-Ala in the presence of acetate, this may also be a consequence of salt effects, therefore the experiment must be repeated in the presence of salt to elucidate the possible electrostatic contribution made to the dimerisation process.

	K_{dim} (M^{-1})	ΔH_{dim} ($kJmol^{-1}$)	$\Delta G°_{dim}$ ($kJmol^{-1}$)	$\Delta S°_{dim}$ ($JK^{-1}mol^{-1}$)
No acetate	475 (80)	-29.2 (1.7)	-15.3	-47
0.1M acetate	470 (70)	-30.8 (3.8)	-15.2	-52
0.5M acetate	860 (80)	-36.2 (1.5)	-16.7	-65

Table 5.13 Vancomycin dimerisation in the absence of ligand in the absence and presence of various concentrations of acetate.

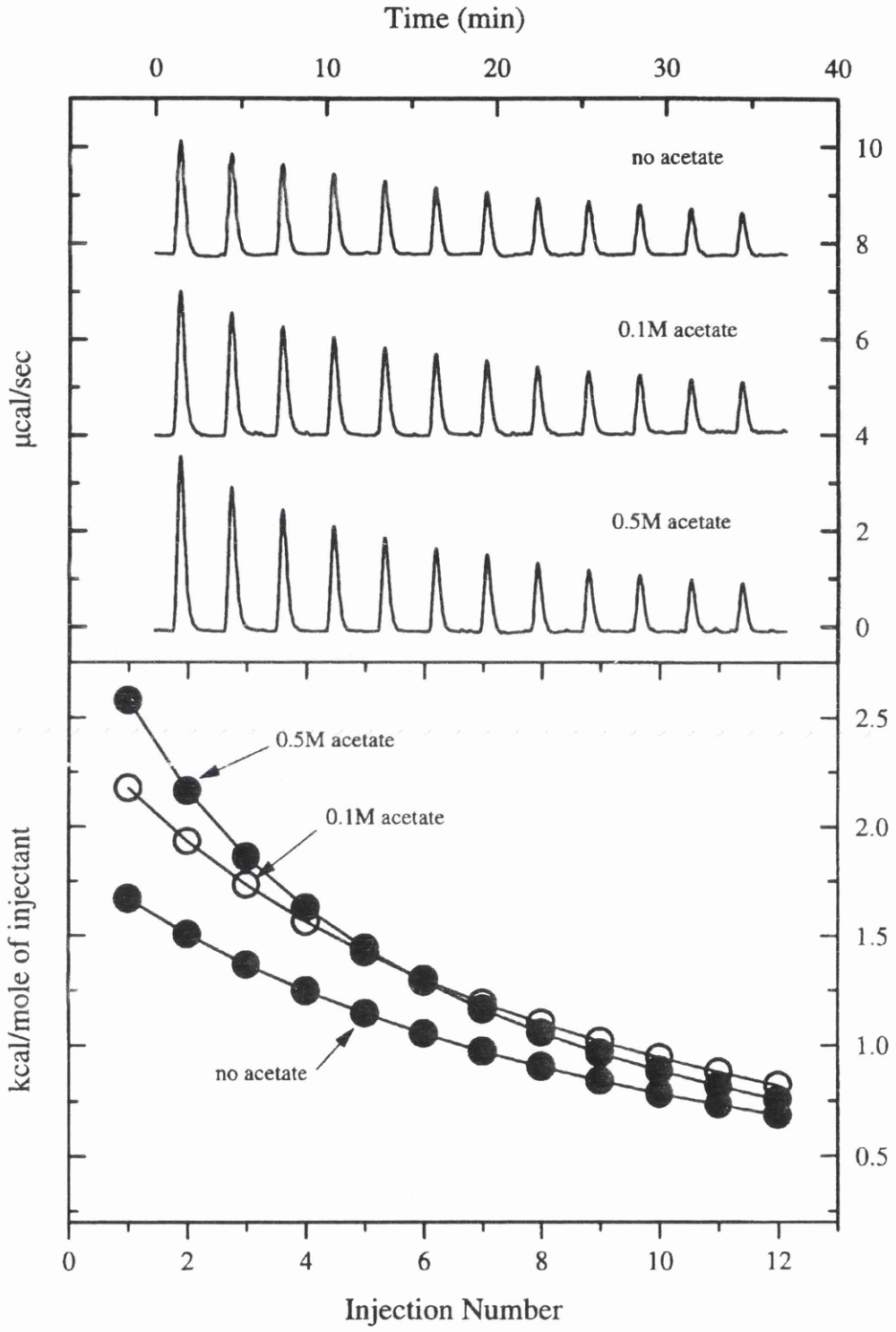

Figure 5.38 Vancomycin (2.50mM, 2.47mM, 2.40mM) dissociation in the absence and presence of 0.1M and 0.5M acetate, respectively at pH 7.0, 25°C.

5.1.2.1.6 Salt

To investigate the contribution of electrostatic interactions at the dimer interface, vancomycin dimerisation in the absence of ligand was carried out in the presence of salts with different ionic strengths in MOPS buffer (pH 7, 0.1M). From these results it is shown that the addition of salts to the buffer mixture has no significant effect on vancomycin dimerisation in the absence of ligand, suggesting that the energetics of association of the unliganded monomers have little non-specific electrostatic contribution. However, there is a significant reduction in dimerisation enthalpy without a change in dimerisation constant in the absence of salt using this buffer compared with that associated with phosphate, suggesting that buffer ionisation heats may be involved. It is possible that carrying out the same process at the same pH, but in different buffers may give rise to different apparent enthalpies due to the different proton ionisation enthalpies of the different buffers (Sturtevant, 1962). Results are shown in Table 5.14, with typical isotherms in Figure 5.39.

	K_{dim} (M^{-1})	ΔH_{dim} ($kJmol^{-1}$)	$\Delta G°_{dim}$ ($kJmol^{-1}$)	$\Delta S°_{dim}$ ($JK^{-1}mol^{-1}$)
no salt	470 (180)	-19.6 (1.9)	-15.2	-15
0.1M KCl	475 (5)	-16.1 (0.4)	-15.3	-3
0.1M $CaCl_2$	420 (60)	-23.9 (0.3)	-14.9	-30

Table 5.14 Vancomycin dimerisation in the absence of ligand in the absence and presence of salts of various ionic strengths.

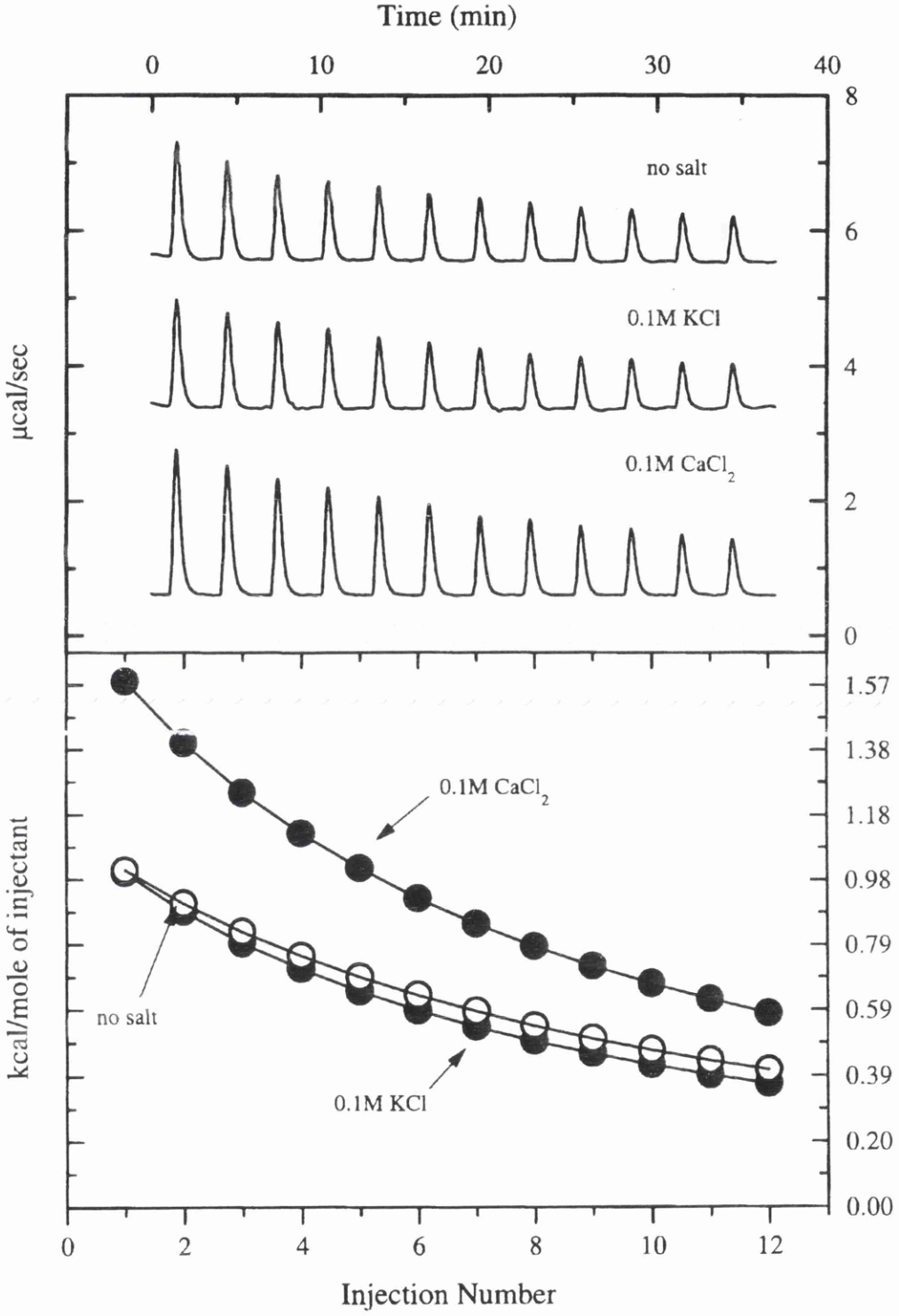

Figure 5.39 Vancomycin (2.54mM, 2.70mM, 2.64mM) dissociation in the absence of ligand in the absence and presence of 0.1M KCl and 0.1M $CaCl_2$, respectively in 0.1M MOPS buffer at pH 7.0, 25°C.

5.1.2.1.7 Heats of ionisation of buffers

To investigate the contribution buffer ionisation may make to the total heat effects associated with dimerisation, vancomycin dimerisation in the absence of ligand was carried out under identical conditions, but in buffers with different heats of ionisation. The enthalpy of ionisation of phosphate is zero at pH 7, PIPES is 11.3kJmol^{-1}, MOPS is 20.5kJmol^{-1} and Imidazole is 36.6kJmol^{-1} (Christensen *et al.*, 1976 : Cooper & Johnson,[c] 1994). There are different contributions to these enthalpies, not just those associated with pulling the ions apart, but also from solvation/hydrogen bond changes in the water around the ions. Results are shown in Table 5.15, with isotherms in Figure 5.41. The relationship between the observed dimerisation enthalpy (ΔH_{dim}) and the enthalpy of ionisation (ΔH_i) of the individual buffers is shown in Figure 5.40. Buffers with increasing endothermic heats of ionisation appear to lead to a greater reduction in the apparent exothermic enthalpy of dimerisation, as would be expected.

	K_{dim} (M^{-1})	ΔH_{dim} ($kJmol^{-1}$)	$\Delta G°_{dim}$ ($kJmol^{-1}$)	$\Delta S°_{dim}$ ($JK^{-1}mol^{-1}$)
Phosphate	475 (80)	-29.2 (1.7)	-15.3	-47
PIPES	360 (250)	-24.4 (5.4)	-14.6	-33
MOPS	470 (180)	-19.6 (1.9)	-15.2	-15
Imidazole	410 (240)	-18.2 (1.2)	-14.9	-11

Table 5.15 Vancomycin dimerisation in the absence of ligand in buffers with different heats of ionisation.

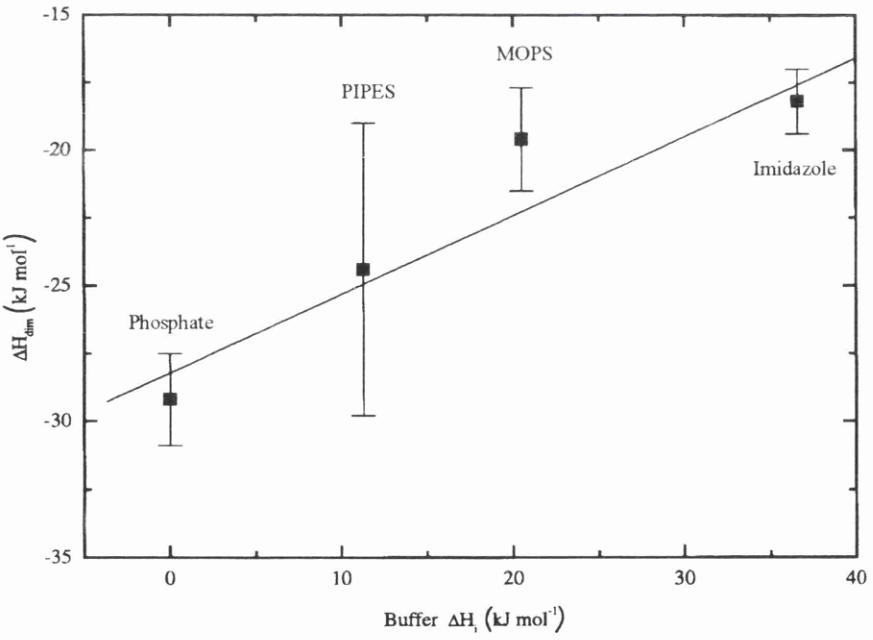

Figure 5.40 Effect of different buffers on vancomycin heat of dimerisation, with error bars shown.

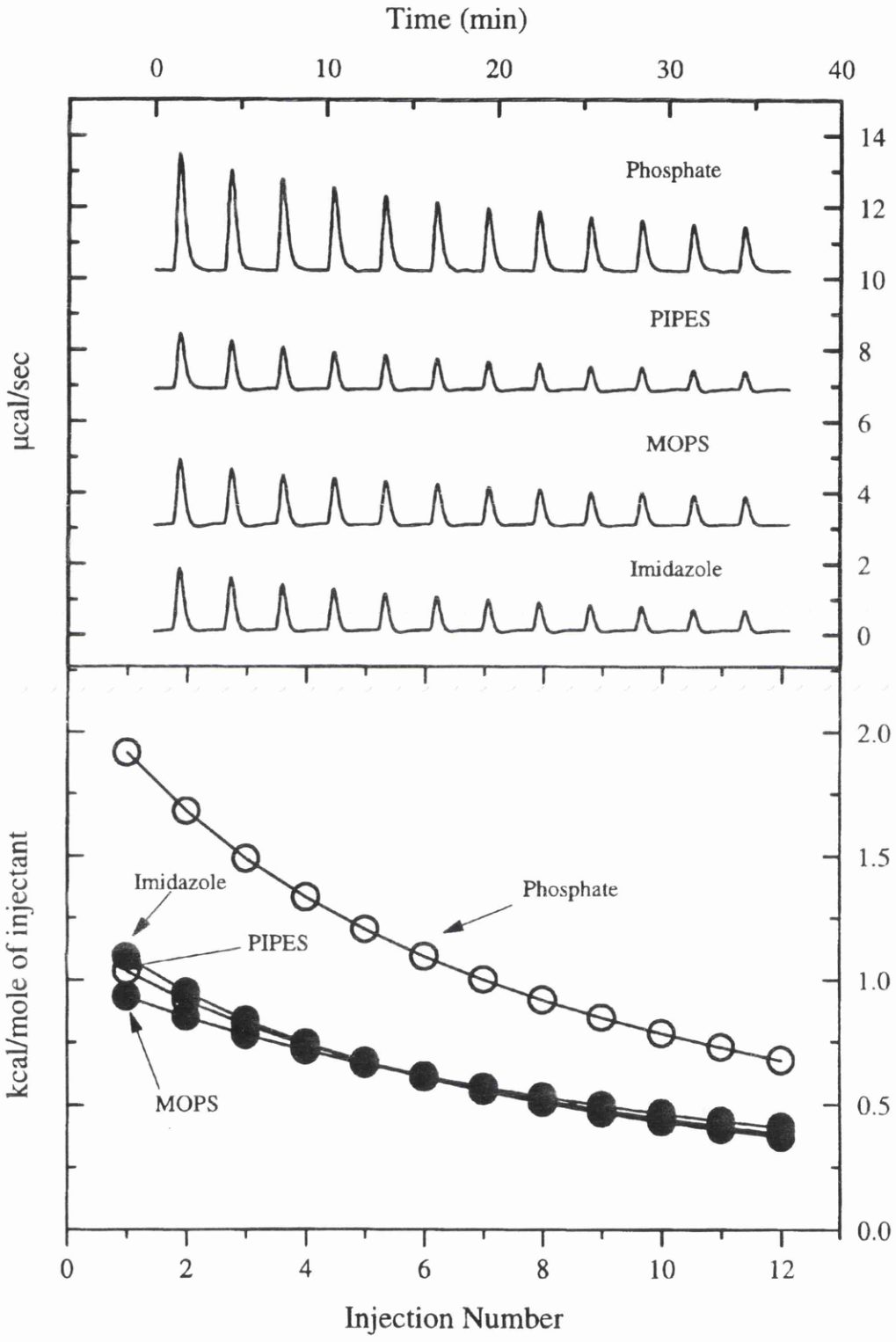

Figure 5.41 Vancomycin (2.83mM, 2.35mM, 2.62mM, 2.76mM) dissociation in the absence of ligand in phosphate, PIPES, MOPS and Imidazole buffers, respectively at pH 7.0, 25°C.

5.1.2.1.8 Deuterium oxide

There appears to be little difference in dimerisation in deuterium oxide, with trends similar to those obtained in water. Vancomycin dimerisation appears to be slightly more favourable in deuterium oxide, with a small increase in dimerisation constants. In both examples, enthalpy changes are less exothermic in deuterium oxide, suggesting that dimerisation is enthalpically less favourable than in water, but with a corresponding increase in entropy. Comparing dimerisation in the absence and presence of $N_{\alpha},N_{\varepsilon}$-diacetyl-Lys-D-Ala-D-Ala in deuterium oxide, both enthalpies of dimerisation are the same, suggesting that the effect is entirely entropic. This is consistent with a significant thermodynamic contribution from solvent reorganisation during the dimerisation process. Although dimerisation in both water and deuterium oxide have different enthalpic and entropic contributions, the free energies are similar. Results are shown in Tables 5.16(a) and 5.16(b), with isotherms in Figures 5.42.

Temperature (°C)	K_{dim} (M^{-1})	ΔH_{dim} ($kJmol^{-1}$)	$\Delta G°_{dim}$ ($kJmol^{-1}$)	$\Delta S°_{dim}$ ($JK^{-1}mol^{-1}$)
25	745 (15)	-26.2 (0.5)	-16.3	-33

Table 5.16(a) Vancomycin dimerisation in the absence of ligand in deuterium oxide.

Temperature (°C)	K_{dim} (M^{-1})	ΔH_{dim} ($kJmol^{-1}$)	$\Delta G°_{dim}$ ($kJmol^{-1}$)	$\Delta S°_{dim}$ ($JK^{-1}mol^{-1}$)
25	6700 (1300)	-26.2 (1.5)	-21.8	-15

Table 5.16(b) Vancomycin dimerisation in the presence of $N_{\alpha},N_{\varepsilon}$-diacetyl-Lys-D-Ala-D-Ala in deuterium oxide.

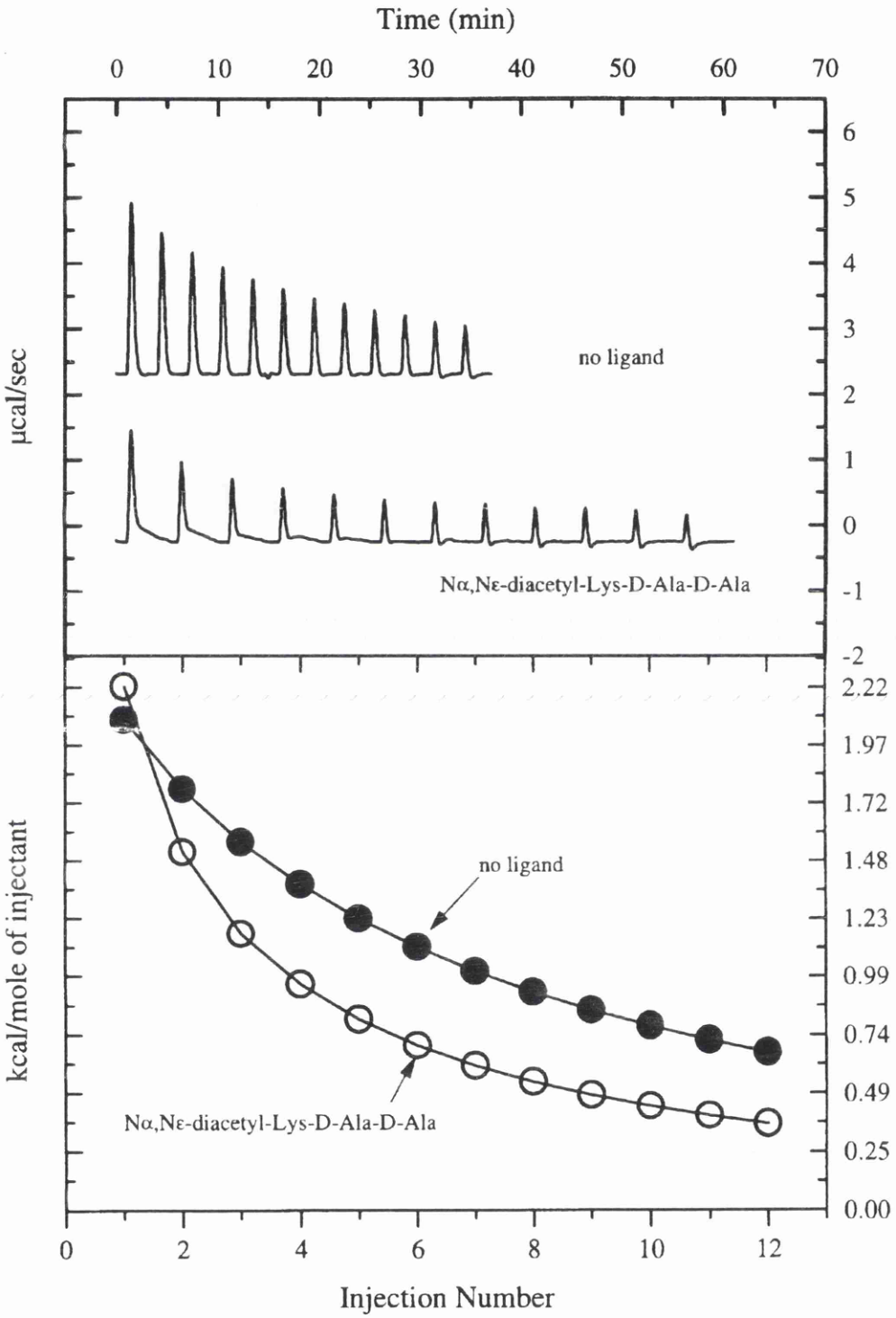

Figure 5.42 Vancomycin (2.50mM, 2.10mM) dissociation in the absence and presence of N_{α},N_{ε}-diacetyl-Lys-D-Ala-D-Ala (2.62mM), respectively in deuterium oxide at pD 7.0, 25°C.

5.1.2.2 Ristocetin dimerisation studies

5.1.2.2.1 No ligand

In the absence of ligand, the dimerisation parameters of ristocetin are similar to vancomycin in that both exhibit low dimerisation constants. Results are shown in Table 5.17.

Temperature (°C)	K_{dim} (M^{-1})	ΔH_{dim} ($kJmol^{-1}$)	$\Delta G°_{dim}$ ($kJmol^{-1}$)	$\Delta S°_{dim}$ ($JK^{-1}mol^{-1}$)
25	280 (95)	-21.5 (2.0)	-14.0	-25

Table 5.17 Ristocetin dimerisation in the absence of ligand.

5.1.2.2.2 N-acetyl-D-Ala

Addition of N-acetyl-D-Ala shows little significant effect on the ristocetin dimerisation constant, although it possibly reduces the dimerisation enthalpy slightly. Results are shown below in Table 5.18.

Temperature (°C)	K_{dim} (M^{-1})	ΔH_{dim} ($kJmol^{-1}$)	$\Delta G°_{dim}$ ($kJmol^{-1}$)	$\Delta S°_{dim}$ ($JK^{-1}mol^{-1}$)
25	390 (85)	-15.6 (2.7)	-14.8	-3

Table 5.18 Ristocetin dimerisation in the presence of N-acetyl-D-Ala.

5.1.2.2.3 $N_{\alpha},N_{\varepsilon}$-diacetyl-Lys-D-Ala-D-Ala

Introduction of $N_{\alpha},N_{\varepsilon}$-diacetyl-Lys-D-Ala-D-Ala in this case gives rise to a slight reduction in dimerisation constant, although with an exothermicity comparable to vancomycin under similar conditions. Dimerisation of ristocetin appears to be relatively insignificant, even in the presence of this strongly binding ligand. This phenomenon is in direct contrast to vancomycin's ligand induced dimerisation, whereas ristocetin exhibits ligand induced dissociation, with the binding of ligand discouraging antibiotic dimerisation. Not only is there a slight reduction in dimerisation constant, but when we compare the shape of the endothermic responses in the upper panel of the thermal profile in Figure 5.43 with those associated with vancomycin under the same conditions, it is obvious that those for ristocetin do not take as long to return to baseline, therefore suggesting that dissociation of the ristocetin dimers is 'easier', indicating that they are not as tightly bound as those of vancomycin in the presence of $N_{\alpha},N_{\varepsilon}$-diacetyl-Lys-D-Ala-D-Ala. Results are shown in Table 5.19.

Temperature (°C)	K_{dim} (M^{-1})	ΔH_{dim} ($kJmol^{-1}$)	$\Delta G°_{dim}$ ($kJmol^{-1}$)	$\Delta S°_{dim}$ ($JK^{-1}mol^{-1}$)
25	185 (25)	-32.1 (0.3)	-12.9	-64

Table 5.19 Ristocetin dimerisation in the presence of $N_{\alpha},N_{\varepsilon}$-diacetyl-Lys-D-Ala-D-Ala.

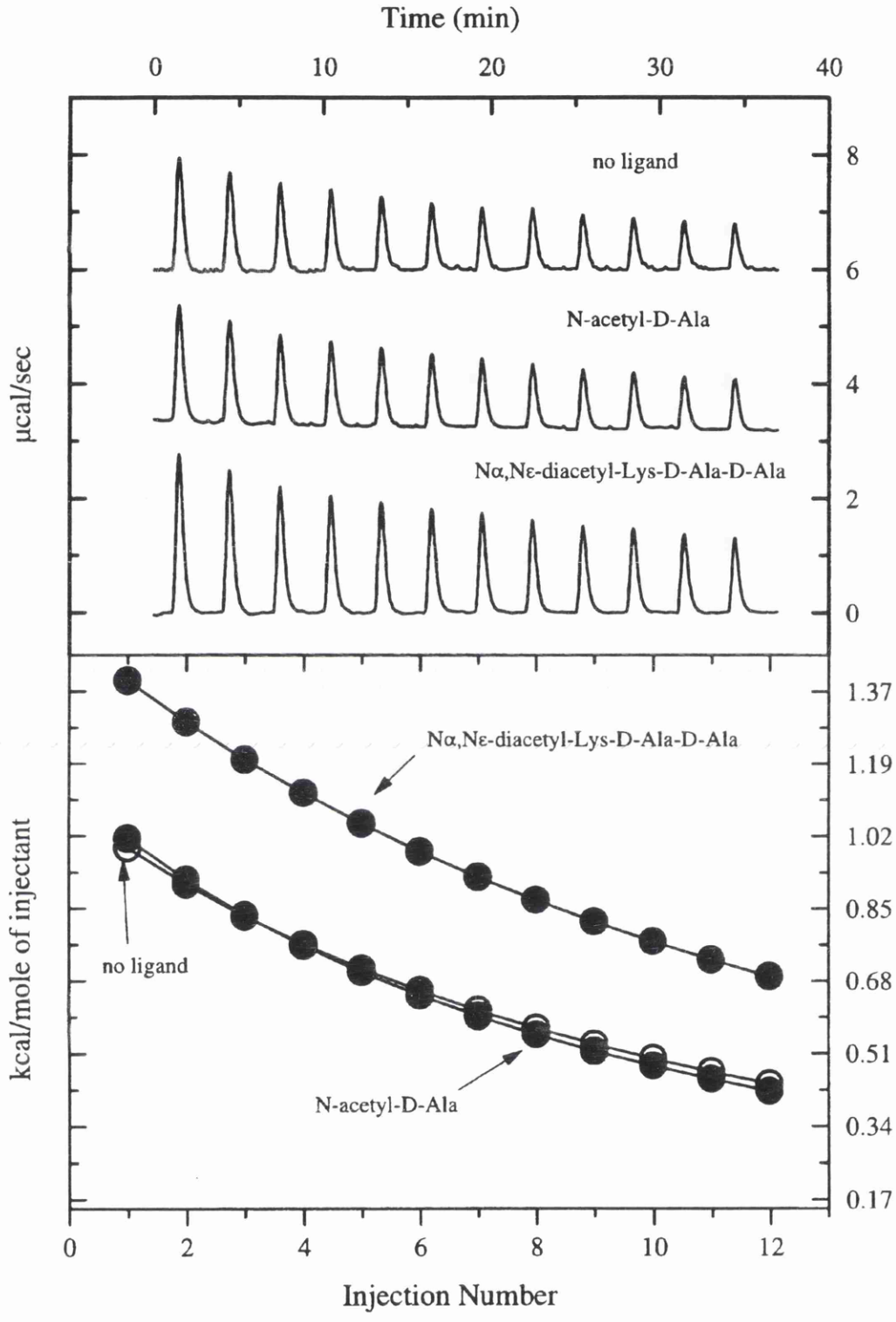

Figure 5.43 Ristocetin (2.74mM, 2.95mM, 2.93mM) dissociation in the absence and presence of N-acetyl-D-Ala (98.76mM) and $N_{\alpha},N_{\varepsilon}$-diacetyl-Lys-D-Ala-D-Ala (3.03mM) respectively, at pH 7.0, 25°C.

5.1.2.2.4 Acetate

To compare with vancomycin dimerisation in the presence of acetate, ristocetin dimerisation was carried out under identical conditions in the absence of other ligand. Similarly, ristocetin dimerisation appears to be encouraged in the presence of acetate, shown by a small, but significant enhancement in dimerisation constants. Acetate is known to act as a very weak ligand and it has been shown previously i.e. with N-acetyl-D-Ala, that such a ligand has little significant effect on ristocetin dimerisation other than possibly reducing the dimerisation enthalpy slightly. Therefore, the effects shown here may be a consequence of ionic strength, rather than specific binding. Results are shown in Table 5.20, with typical thermal profiles in Figure 5.44.

	K_{dim} (M^{-1})	ΔH_{dim} ($kJmol^{-1}$)	$\Delta G°_{dim}$ ($kJmol^{-1}$)	$\Delta S°_{dim}$ ($JK^{-1}mol^{-1}$)
no acetate	280 (95)	-21.5 (2.0)	-14.0	-25
0.1M acetate	465 (5)	-18.5 (1.5)	-15.2	-11
0.5M acetate	450 (85)	-16.7 (0.5)	-15.1	-5

Table 5.20 Ristocetin dimerisation in the absence of ligand in the presence of various concentrations of acetate.

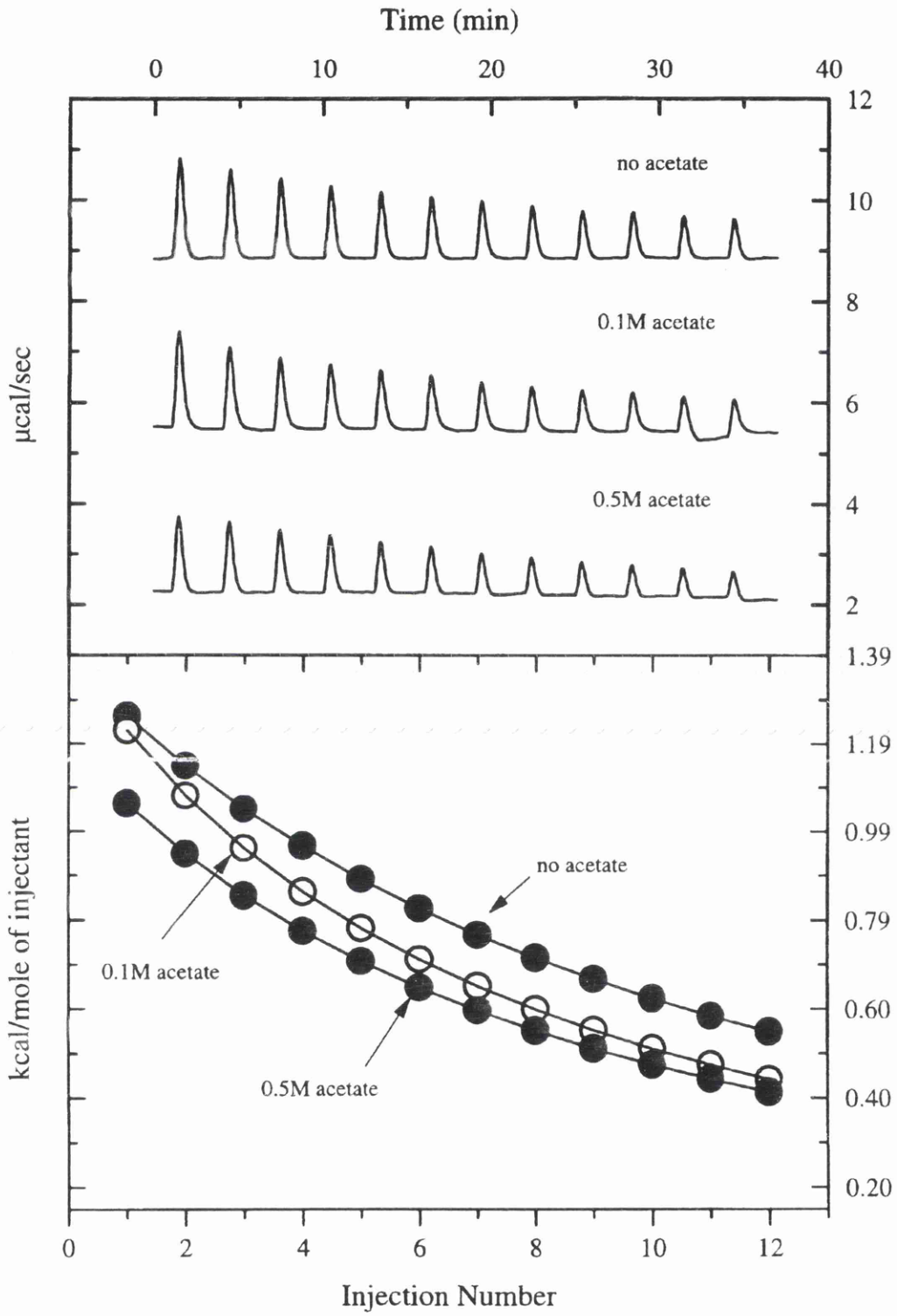

Figure 5.44 Ristocetin (3.00mM, 2.92mM, 2.85mM) dissociation in the absence of ligand in the absence and presence of 0.1M and 0.5M acetate, respectively at pH 7.0, 25°C.

5.1.2.2.5 Salt

Ristocetin dimerisation in the absence of ligand but presence of salts with different ionic strengths was carried out in MOPS buffer (pH 7, 0.1M). The addition of salts to the buffer mixture shows a small increase in dimerisation constant, increasing with the ionic strength of the salt. High ionic strengths give rise to effective electrostatic screening between charged molecules and it is therefore possible that the association of ristocetin monomers may involve an electrostatic contribution between like charges, since screening between such charges would enhance dimerisation. In this case, the heats of protonation of buffers do not appear to make a significant contribution to the overall observed enthalpy of dimerisation when comparing enthalpies of ristocetin dimerisation in the absence of ligand in the presence of phosphate or MOPS buffer. Results are shown in Table 5.21 with thermal profiles in Figure 5.45.

	K_{dim} (M^{-1})	ΔH_{dim} ($kJmol^{-1}$)	$\Delta G°_{dim}$ ($kJmol^{-1}$)	$\Delta S°_{dim}$ ($JK^{-1}mol^{-1}$)
no salt	210 (15)	-18.5 (1.3)	-13.2	-18
0.1M KCl	255 (20)	-19.7 (1.4)	-13.7	-20
0.1M $CaCl_2$	335 (55)	-18.8 (1.2)	-14.4	-15

Table 5.21 Ristocetin dimerisation in the absence of ligand in the presence of salts of different ionic strengths.

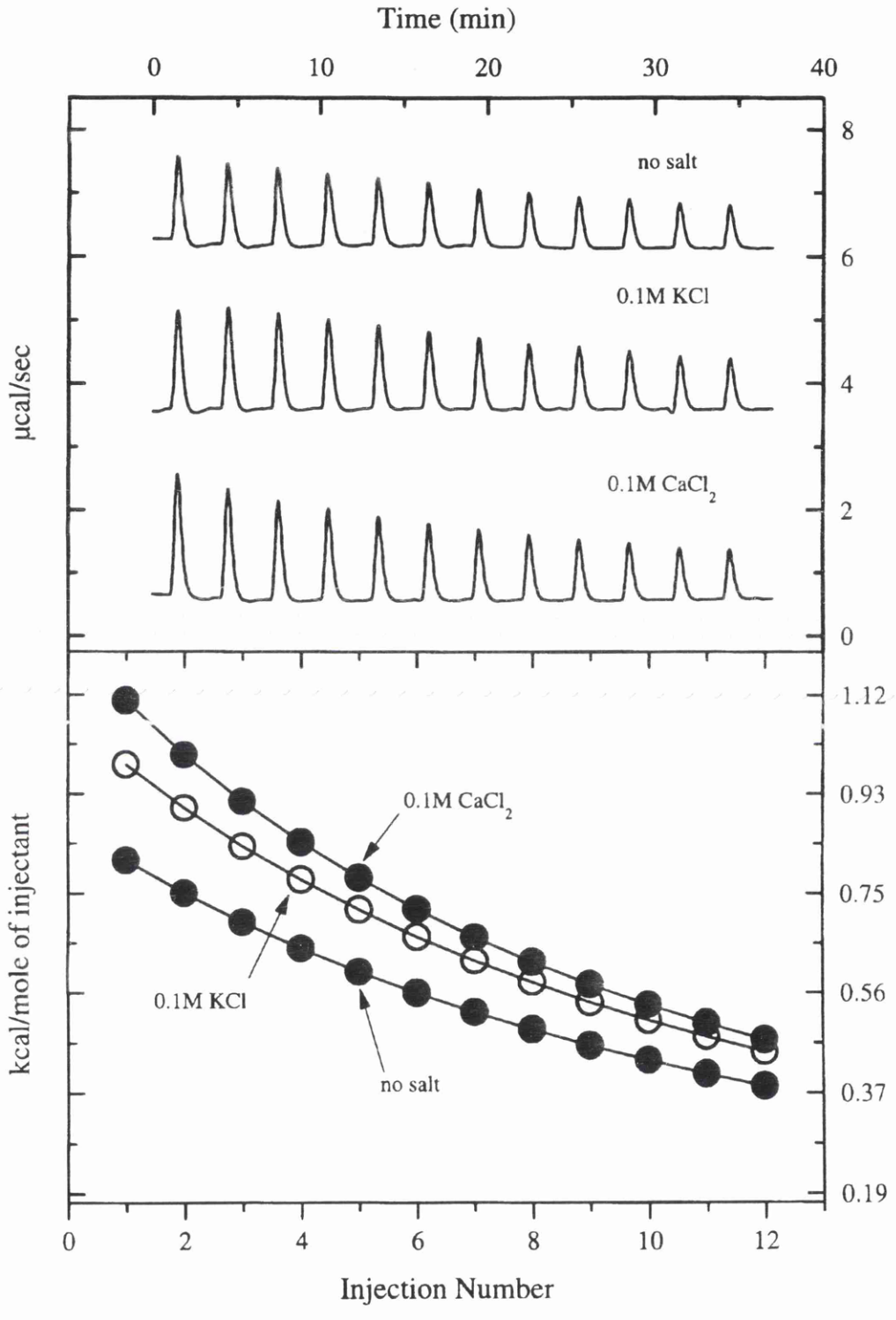

Figure 5.45 Ristocetin (2.79mM, 2.88mM, 2.87mM) dissociation in the absence of ligand in the absence and presence of salts of 0.1M KCl and 0.1M $CaCl_2$, respectively in MOPS buffer at pH 7.0, 25°C.

5.1.2.2.6 Deuterium oxide

Ristocetin dimerisation constants are increased and enthalpy changes are less exothermic in deuterium oxide compared with water. These changes are consistent with those found for vancomycin dimerisation in deuterium oxide. Ristocetin dimerisation is still insignificant in the presence of ligand with little difference in the free energy of dimerisation in both water and deuterium oxide. Results are shown in Tables 5.22(a) and 5.22(b), with isotherms in Figure 5.46.

Temperature (°C)	K_{dim} (M^{-1})	ΔH_{dim} ($kJmol^{-1}$)	$\Delta G°_{dim}$ ($kJmol^{-1}$)	$\Delta S°_{dim}$ ($JK^{-1}mol^{-1}$)
25	595 (65)	-20.7 (1.4)	-15.8	-16

Table 5.22(a) Ristocetin dimerisation in the absence of ligand in deuterium oxide.

Temperature (°C)	K_{dim} (M^{-1})	ΔH_{dim} ($kJmol^{-1}$)	$\Delta G°_{dim}$ ($kJmol^{-1}$)	$\Delta S°_{dim}$ ($JK^{-1}mol^{-1}$)
25	335 (-)	-30.6 (-)	-14.4	-54

Table 5.22(b) Ristocetin dimerisation in the presence of N_{α},N_{ε}-diacetyl-Lys-D-Ala-D-Ala in deuterium oxide.

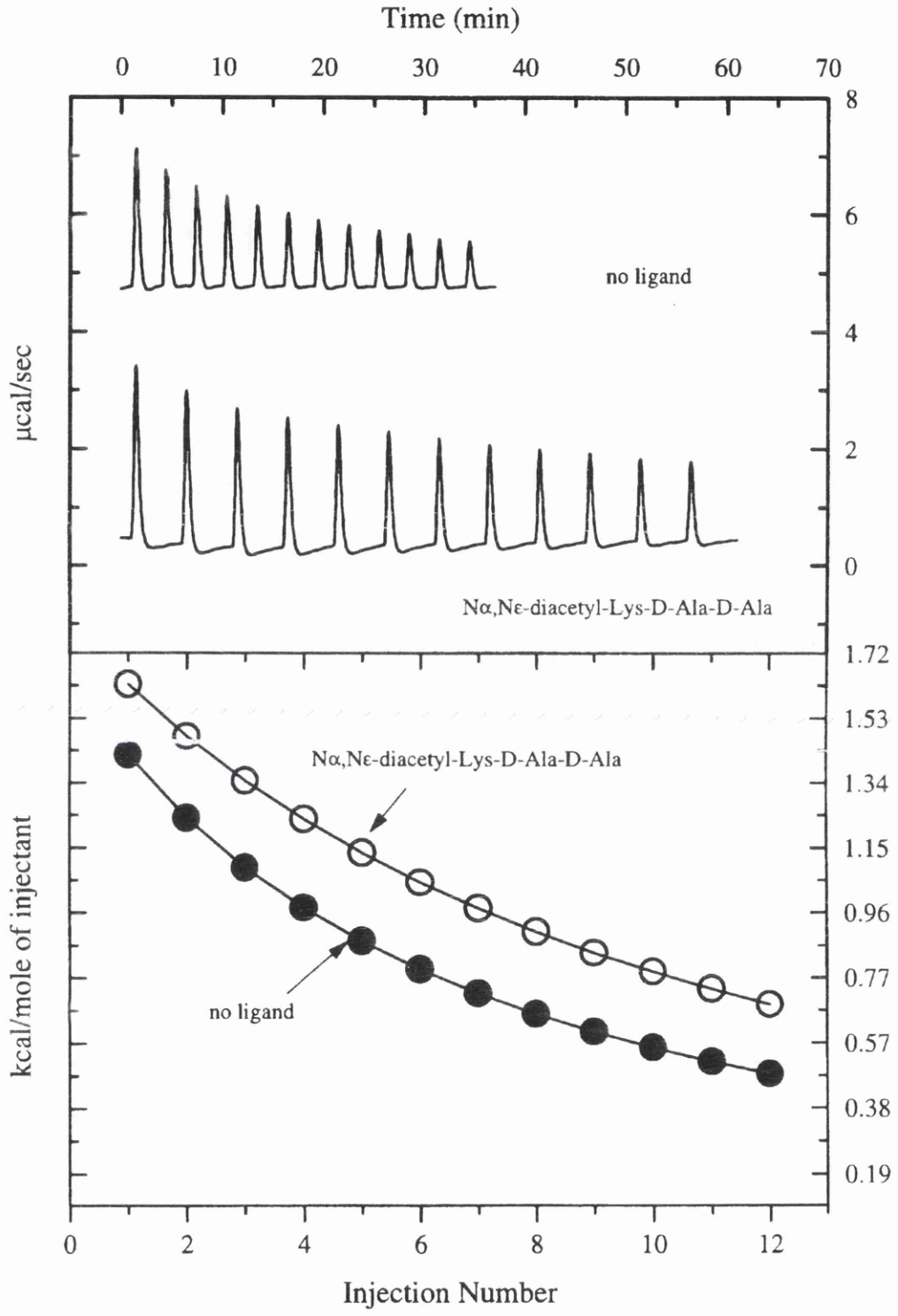

Figure 5.46 Ristocetin (2.92mM, 2.61mM) dissociation in the absence and presence of $N_{\alpha},N_{\varepsilon}$-diacetyl-Lys-D-Ala-D-Ala (2.50mM) respectively, in deuterium oxide at pD 7.0, 25°C.

5.1.2.2.7 Discussion

Binding affinity of the vancomycin group of antibiotics for cell wall analogue peptides has been shown to be influenced by aggregation (Cooper & McAuley-Hecht, 1993 : McAuley-Hecht, 1993) and our studies show that ligand binding can in turn affect dimerisation. In the case of vancomycin, dimerisation is enhanced in the presence of ligand, with the strongest dimerisation occurring upon introduction of the ligand $N_{\alpha},N_{\varepsilon}$-diacetyl-Lys-D-Ala-D-Ala, weaker dimerisation in the presence of N-acetyl-D-Ala and weaker still in the absence of ligand. This enhancement of dimerisation on ligand binding is in contrast to that found with ristocetin, where dimerisation is discouraged in the presence of ligand, with dimerisation shown to be weaker in the presence of $N_{\alpha},N_{\varepsilon}$-diacetyl-Lys-D-Ala-D-Ala than in the absence of ligand. Both examples show that dimerisation is not simply a consequence of interactions made at the dimer interface, but is also influenced by interactions at the antibiotic binding site. The following discussion is an attempt to explain such contrasting features of otherwise similar members of the same group of antibiotics.

NMR studies have resolved the structure of the ristocetin dimer (Williams *et al.*, 1979 : Williamson & Williams, 1985 : Waltho & Williams, 1989) and since ristocetin and vancomycin are structurally similar, both are assumed to form dimers in the same way. The dimer is thought to be formed by the combination of the two back faces of each monomer through intermolecular hydrogen bonds, leaving both binding sites accessible to peptide. Electrostatic interactions are also thought to make a contribution to dimerisation (Groves *et al.*, 1994) as are hydrophobic interactions.

Dimerisation of each antibiotic will be dealt with in turn. Firstly, our discussion will concentrate on the cooperativity that exists between ligand binding and vancomycin dimerisation. At the antibiotic/ligand concentrations used in our series of microcalorimetric experiments, the vancomycin (either monomer or dimer) will be present predominately as the ligand complex, so any complications brought about by a

change in the liganded state during the dilution/dissociation process may be ignored. Since it has been shown that vancomycin dimerisation and ligand binding are clearly linked, with vancomycin dimerisation affecting ligand binding (Cooper & McAuley-Hecht, 1993) and ligand binding affecting dimerisation, the overall ligand binding/dimerisation equilibrium scheme can be summarised as follows, beginning with binding of ligand to monomeric antibiotic:

$$A + L \rightleftharpoons AL \quad ; \quad K_L = [AL]/[A][L] \quad ; \quad \Delta H_L$$

together with dimerisation of un-liganded or liganded species:

$$A + A \rightleftharpoons A_2 \quad ; \quad K_{dim,0} = [A_2]/[A]^2 \quad ; \quad \Delta H_{dim,0}$$

$$AL + AL \rightleftharpoons A_2L_2 \quad ; \quad K_{dim,L} = [A_2L_2]/[AL]^2 \quad ; \quad \Delta H_{dim,L}$$

where A = antibiotic, L = ligand, and the square brackets indicate molar concentrations (strictly activities). For an ideal gas we could use concentrations or partial pressures because the molecules/atoms do not interact with each other and do not take up any volume etc. However, this is not true of any real molecule/atom and therefore the activity coefficient is used to take into account any interactions etc.

Binding of ligand to dimeric species is described by:

$$A_2 + L \rightleftharpoons A_2L \quad ; \quad K_{L1} = [A_2L]/[A_2][L] \quad ; \quad \Delta H_{L1}$$

and

$$A_2L + L \rightleftharpoons A_2L_2 \quad ; \quad K_{L2} = [A_2L_2]/[A_2L][L] \quad ; \quad \Delta H_{L2}$$

So, for sequential binding of ligand to dimer:

$$K_{L1} K_{L2} = K_L^2(K_{dim,L}/K_{dim,0})$$

showing that, though we cannot necessarily resolve the individual constants K_{L1} and K_{L2}, the overall binding affinity to the dimer is enhanced in cases where $K_{dim,L} > K_{dim,0}$. With the ligand N_α,N_ε-diacetyl-Lys-D-Ala-D-Ala and assuming binding affinity is unaffected by ligand binding to un-liganded dimer or to a dimer of which one binding site is already occupied by ligand i.e. $K_{L1} = K_{L2}$, the ligand binding affinity would therefore be enhanced roughly 3-fold in the dimer compared to the monomer, corresponding to a change in standard Gibbs free energy of ligand binding of approximately -3kJmol^{-1}. The enthalpies and entropies of ligand binding are similarly affected by dimerisation. The change in overall ligand binding enthalpy is given by the difference in dimerisation enthalpies thus:

$$\Delta H_{dim,L} - \Delta H_{dim,0} = \Delta H_{L1} + \Delta H_{L2} - 2.\Delta H_L$$

with a similar expression for entropies. The data for the binding of vancomycin to N_α,N_ε-diacetyl-Lys-D-Ala-D-Ala suggests that binding to the dimer is more exothermic than to the monomer by about -5kJmol^{-1}, with this offset by a positive change in ligand binding entropy of +7JK^{-1}mol^{-1}. None of these changes are particularly large compared to the overall ligand binding parameters and for the weaker binding ligand the changes will be much less (McPhail & Cooper, 1997).

Two hypotheses have been proposed for the possible mechanism of cooperativity between antibiotic dimerisation and ligand binding. One being, when amide functional groups of the antibiotic are hydrogen bonded to solvent in the monomer, they possess an amount of motional freedom. But, when dimerisation takes place these groups become hydrogen bonded to each other, imparting a certain degree of motional restriction which should promote ligand binding due to a decrease in entropy and a corresponding increase in enthalpy of hydrogen bonding at the antibiotic binding site (Mackay *et al.*, 1994). Another reason put forward for this phenomenon is that in the ligand bound dimer, the alkylammonium ion of the amino sugar on residue 6, where present (although not in vancomycin), forms an indirect salt bridge to the carboxylate anion of the cell wall peptide, mediated through the amide bond which connects residues 2 and 3 of the

antibiotic. This sugar may be located in this position to co-operatively promote both dimerisation and ligand binding. Therefore, dimer formation strengthens the hydrogen bonds at the antibiotic binding site (Mackay *et al.*, 1994).

All cases of vancomycin dimerisation, whether in the presence or absence of ligand, showed large temperature dependence (ΔC_p) effects consistent with solvation changes associated with the burial of non-polar surfaces during macromolecular association (Weber, 1993 : Weber, 1995 : Spolar and Record, 1994), although contributions from other interactions such as the hydrophobic effect, intramolecular vibrations and hydrogen bonds cannot be ruled out (Sturtevant, 1977). The heat capacity of any hydrophobic molecule or part of a molecule arises from the fact that a hydrophobic component exposed to water causes an increase in the structure of the water molecules surrounding the hydrophobic parts, this occurs because the water cannot hydrogen bond to the hydrophobic portion and so to compensate forms a very ordered structure in which as many water-water hydrogen bonds are made as possible. This arrangement has a structure similar to ice and it gradually 'melts' as heat is added, therefore taking up heat and consequently increasing the overall heat capacity. Any movement including vibrations within the molecule requires energy and if the energy goes into causing that movement it cannot raise the temperature, therefore increasing the heat capacity. If there are more internal modes of vibration due to more degrees of freedom in the free state than in the bound state, then the heat capacity will be positive since the heat energy put into a system can do several things, such as heating up the system or exciting internal modes of vibration, but not both. The energy used up in these ways cannot also contribute to the heating up of the system, so the heat capacity will be higher in the free state, since more energy must be put in to raise the temperature. Hydrogen bonds contribute to the overall heat capacity because in the free state molecules of water will be immobile at the surface of the molecule and adding heat will gradually pull them away from the surface, therefore increasing the heat capacity. Changes in heat capacity can be correlated with changes in exposed non-polar surface area during complexation using the empirical procedure of Spolar & Record, 1994, allowing the following estimations to be

made. The burial of non-polar surface areas range from about 400Å^2 for vancomycin alone, up to 1300Å^2 for vancomycin complexed with the ligand N_α,N_ε-diacetyl-Lys-D-Ala-D-Ala. This compares to an estimate from model building of about 300Å^2 (Williams *et al.*, 1993), assuming no conformational change in the monomers during dimerisation. These estimations imply that vancomycin dimerisation in the presence of ligand covers more non-polar surface area than in the absence of ligand, suggesting flexibility in the carboxylate binding pocket in which some ligand-induced conformational change may be involved in affecting dimerisation. Solvation effects, such as the hydrophobic effect, alongwith the large non-polar surface area buried upon dimerisation in the presence of N_α,N_ε-diacetyl-Lys-D-Ala-D-Ala contribute to the large molar heat capacity associated with this process, which also brings about a large temperature variation in both enthalpy and entropy compared with dimerisation in the absence of ligand. Vancomycin dimerisation in the presence of N_α,N_ε-diacetyl-Lys-D-Ala-D-Ala exhibits the largest free energies, giving an indication of the strength of the dimer involved compared with the relatively low free energies associated with dimerisation in the absence of ligand.

The van't Hoff enthalpies of vancomycin dimerisation in the presence and absence of cell wall analogues were calculated from the slope of lnK against 1/T plots. Comparing with the enthalpies directly determined from microcalorimetry, the trend is the same with vancomycin dimerisation in the presence of N_α,N_ε-diacetyl-Lys-D-Ala-D-Ala having a more exothermic enthalpy associated with it than dimerisation in the absence of ligand. Although the trend is the same, the magnitudes show some degree of variation (Naghibi *et al.*, 1995), in one case possibly due to regression analysis carried out on slopes assumed to be linear. Vancomycin dimerisation in the absence of ligand shows a significant difference between microcalorimetric and calculated van't Hoff enthalpies, with the van't Hoff plot showing a great scatter of points along the calculated gradient (R=0.93), therefore reducing the accuracy of the overall enthalpy determination. It is possible that the temperature dependence of the enthalpy due to the molar heat capacity gives rise to a scatter of points to which a curve should be fitted rather than a straight line. This procedure did not seem feasible in this case since the scatter was too great to

accurately assign either a curve or a straight line to the data. Other discrepancies may be because over the temperature range studied, the curvature of the van't Hoff plot is too small to see with any certainty, given the relatively large experimental errors. This problem may be resolved by carrying out further titration experiments over a wider range of temperatures. This seems feasible since theoretical values for the dimerisation constant over a wider range of temperatures can be fitted to a curve due to ΔC_p not being equal to zero, illustrating the difference between theoretical and microcalorimetric data within experimental error.

Vancomycin dimers are shown to vary little in stability with pH in the acid to neutral region, but dimerisation is reduced significantly above pH 8. As discussed previously in section 5.1.1.1.8, various ionisable groups have been identified in vancomycin, including groups having pK_a values of about 2.9 (-COOH), 7.2 (terminal α-NH_3^+), with a further four at pK_a 8.6, 9.6, 10.5 and 11.7 assigned to three phenolic groups and a vancosamine -NH_3^+ (Nieto & Perkins,[b] 1971). It seems possible that ionisation of these phenolic groups may be responsible for the reduction in dimerisation at high pH. The model of antibiotic dimerisation proposed by Williams *et al.*, 1979 : Williamson & Williams, 1985 : Waltho & Williams, 1989, involves interaction between the sugar components and the convex face of the monomers. Such an arrangement suggests that the phenolic hydroxyl groups cannot participate in stabilisation of the dimer structure due to their far removed position from the dimer interface (Rajagopalan *et al.*, 1995). Therefore, since we already know that high pH also reduces the stability of the vancomycin-peptide complex due to electrostatic repulsion, this will also contribute to a reduction in dimer stability at higher pH in the ligand-bound situation. In the case of dimerisation in the absence of ligand, ionisation of the phenolic groups at high pH will give rise to a change in the overall charge of each monomer, therefore it is possible that dimerisation is reduced under these conditions due to a certain degree of electrostatic repulsion between the monomers.

All entropy-enthalpy compensation plots for vancomycin dimerisation in the presence and absence of cell wall analogues in aqueous solution under various temperature and pH

conditions exhibit slopes near unity ($R \geq 0.96$), with this thought to be related to the role of solvent molecules in the dimerisation process. Solvent reorganisation is not the only cause of entropy-enthalpy compensation. Other factors include shifts in equilibria among solvent species when the pure solvent consists of two or more molecular species (Grunwald, 1986 : Grunwald & Comeford, 1988). Examples include shifts in the equilibrium between environmental isomers of water when non-polar solutes are present and shifts in hydrogen-bonded linkage equilibria in alcohol solvents when hydrogen-bonded solutes are present. Such shifts have been shown to contribute compensating additive terms to the standard enthalpy and entropy of the solute and therefore add to the overall compensation phenomenon (Grunwald & Steel, 1995).

Vancomycin dimerisation in the absence of cell wall analogues appears to be encouraged in the presence of acetate, particularly at higher concentrations, shown by a small, but significant enhancement in dimerisation constant, consistent with its action as a very weak ligand (Cooper & McAuley-Hecht, 1993), mimicking the binding of the terminal carboxylate of larger peptide ligands in the flexible binding pocket of vancomycin (Williams *et al.*, 1990). However, it was thought that this and other forms of ligand induced dimerisation may simply be an electrostatic effect, since the ligands used in our series of experiments will carry a negative charge at neutral pH and it is possible that their effect on vancomycin dimerisation may represent a change in electrostatic interactions between the monomers. If the charge on the vancomycin monomers is modified by ligand binding in such a way as to moderate the overall charge by making it less repulsive than before, dimerisation would be encouraged to some extent. For example using the group pK values, the net charge on vancomycin at pH 7 is +0.59 and on binding the ligand $N_{\alpha},N_{\varepsilon}$-diacetyl-Lys-D-Ala-D-Ala which carries a net charge of -0.99, the overall charge would be reduced to -0.4. However, addition of salts of different ionic strengths i.e. KCl and $CaCl_2$ to the buffer mixture showed no significant effect on vancomycin dimerisation in the absence of ligand, suggesting that the energetics of dimerisation of the unliganded monomers at neutral pH has little non-specific

electrostatic contribution, since such salts would screen electrostatic interactions to varying degrees, producing differences in dimerisation constants.

The N-terminal amine on vancomycin is clearly also important in stabilisation of interactions at the antibiotic binding site, since deprotonation contributes to instability of the antibiotic peptide complex (Rajagopalan *et al.*, 1995 : Convert *et al.*, 1980), suggesting a contribution from electrostatic interactions. It is also possible that protonation of this group is also required for association between vancomycin molecules. The reduction in dimerisation above pH 7-8 is consistent with this. The $-^{+}NH_2CH_3$ of residue 1 is orientated such that the hydrophobic methyl group is adjacent to the peptide carboxylate anion and should thereby enhance the hydrophobic surroundings of the binding pocket (Cristofaro *et al.*, 1995). If protonation is required for dimer formation, this will involve the uptake of protons from solution under pH conditions where the relevant groups are only partly protonated. Such an effect is observed in the reduction in dimerisation enthalpy for vancomycin dimerisation in the absence of ligand at pH 7 using MOPS buffer rather than phosphate without a change in dimerisation constant, consistent with the uptake of a proton which causes the overall dimerisation enthalpy to be less exothermic. Since calorimetry measures the total of heat effects associated with a process, if proton ionisation effects are involved, the overall heat will include a component from buffer ionisation (Cooper & Converse, 1976). The same process observed at the same pH but in a range of different buffers gives rise to different apparent enthalpies, although with similar dimerisation constants and free energies, due to the different proton ionisation enthalpies of the different buffers (Sturtevant, 1962). Buffers with increasing endothermic heats of ionisation appear to lead to a greater reduction in the apparent exothermic enthalpy of dimerisation. This relationship is illustrated in Figure 5.43. Such enthalpy changes can be correlated with the number of protons uptaken from the buffer. The difference of almost $10kJmol^{-1}$ between vancomycin dimerisation in phosphate and MOPS buffer is consistent with an uptake of approximately 0.5 H^{+} ions per dimer, since 20.5kJ of heat must be supplied to ionise 1 H^{+} ion, the difference of almost $5kJmol^{-1}$ between phosphate and PIPES buffer is consistent

with an uptake of approximately 0.4 H^+ ions per dimer and the difference of 11kJmol^{-1} between phosphate and Imidazole buffer with an uptake of about 0.3 H^+ ions per dimer.

Vancomycin dimerisation in deuterium oxide show the same overall trends as those found in water, with slight changes in thermodynamic parameters. Dimerisation is slightly more favoured in deuterium oxide and significantly enhanced by N_α,N_ε-diacetyl-Lys-D-Ala-D-Ala binding, though in this case the effect appears to be entirely entropic, since dimerisation enthalpies are the same. This is consistent with a significant thermodynamic contribution from solvation effects to the dimerisation process. Dimerisation enthalpies are more exothermic in water than in deuterium oxide due to differences in the O...H versus O...D interaction, with this trend consistent with that found in the Chervenak & Toone, (1994) study. The differences in enthalpies of dimerisation in water and deuterium oxide are compensated by a change in entropy which leaves the free energies of dimerisation virtually unchanged, this effect being a characteristic of processes in aqueous solution.

Discussion so far has concentrated on data for vancomycin, where it is shown that ligand induced dimerisation is observed over a wide range of temperature and pH conditions and it is clearly an important feature of vancomycin and peptide molecular recognition at high antibiotic concentrations. In contrast, dilution experiments with the related antibiotic ristocetin, show only slight or even opposite effects with added ligands. In the absence of ligand the dimerisation parameters of ristocetin are similar to vancomycin, (although ristocetin dimers are clearly weaker), but addition of N_α,N_ε-diacetyl-Lys-D-Ala-D-Ala gives rise to a slight reduction in dimerisation constant, albeit with an increase in exothermicity comparable to vancomycin under similar conditions. Addition of N-acetyl-D-Ala has little significant effect on ristocetin dimerisation constant, though it possibly reduces the dimerisation enthalpy slightly. At this stage, it is unclear why this obvious anti-cooperativity between ligand binding and dimerisation exists in ristocetin, whereas dimerisation of another member of the same group of antibiotics is clearly enhanced in the presence of ligand, although possible mechanisms have been proposed.

One such mechanism centres around the idea that the sugar ristosamine on ristocetin is directly involved in hydrogen bonding at the dimer interface, therefore perturbation of this interaction by the binding of ligand may contribute to the anti-cooperative phenomenon which is characteristic of ristocetin. Significant perturbation does not occur with the natural substrate, or even that of closely related substrates, therefore the dimerisation constant is only slightly affected. However, upon the introduction of tightly binding 'unnatural' structural motifs which are unable to simultaneously satisfy a second set of weak interactions necessary for dimerisation, the dimerisation constant is significantly reduced e.g. indole-2-carboxylate reduces K_{dim} from $500M^{-1}$ in the absence of ligand to $20M^{-1}$ and in the case of the fluorenone ligand the K_{dim} is reduced so much that it is too small to determine (Searle *et al.*, 1994). The carboxylate groups of these ligands are tightly bound in a similar way to the carboxylate of the natural substrate. The large anti-cooperative effects are thought to be due to 'unnatural' interactions between the aromatic components of these ligands and the antibiotic tetrasaccharide and ristosamine sugars. NOE data show that in ristocetin binding of the fluorenone complex, the methyl groups of rhamnose, ristosamine and residue 7 appear to form part of a hydrophobic wall that accommodates the ligand, with short range interactions between the aromatic portion of the ligand and the methyl group of ristosamine and intramolecular interactions between this group on ristosamine and the methyl group on residue 7. Such interactions are not found between ristocetin and the natural substrate, since an aromatic ring is lacking. Although the model proposed for ristocetin binding to the fluorenone complex is thought to perturb the interaction of ristosamine at the dimer interface, it seems unlikely that ristocetin binding to indole-2-carboxylate will also disrupt this interaction since this ligand will not extend as far along the binding site as the fluorenone, therefore should be able to participate in hydrogen bonding at the dimer interface. The anti-cooperative effect of this ligand on ristocetin dimerisation must therefore arise from different means. The reduction in dimerisation observed from binding of this ligand is thought to be linked with the role of the residue 4 tetrasaccharide in dimerisation. Removal of the tetrasaccharide reduces the dimerisation constant in the absence of ligand by a factor of 10, but in the presence of ligand dimerisation is co-

operatively enhanced by a factor of 10 (Williams *et al.*, 1993), but with ristocetin A ligand binding, dimerisation is reduced anti-cooperatively. Although the precise role of the tetrasaccharide is unclear, it appears to be able to promote dimerisation of ristocetin A, but interferes anti-cooperatively with dimerisation in the presence of ligand (Searle *et al.*, 1994). In the asymmetric dimer, tetrasaccharides are related by 180° and it is also thought that the anti-cooperativity observed with ristocetin may be the result of this parallel alignment of tetrasaccharides leading to different sugars 'capping' the two ligand binding sites. NOE data has suggested that in one conformation, the rhamnose sugar lies over the ligand binding site and the hydrophilic edge of the sugar (namely the hydroxyl groups on C3, C4 and C5) is in a position to form hydrogen bonds with the amino and carboxyl groups of the cell wall peptide, while the glucose sugar forms a hydrophobic cap that blocks the alanine methyl side chain of the cell wall analogue from solvent. In contrast, at the other binding site the arabinose sugar is located above the ligand binding site and has only one hydroxyl group to hydrogen bond to the peptide. In this binding site, the different orientation of the tetrasaccharides with respect to bound peptide may result in less effective 'capping' (Groves *et al.*, 1995). It is possible that such differences in tetrasaccharide positions may produce differences in binding affinity at each site, therefore contributing to the anti-cooperativity phenomenon.

Ristocetin dimerisation appears to be slightly encouraged in the presence of acetate, albeit with a reduction in enthalpy. The acetate anion is thought to act as a weak ligand and its effect on ristocetin dimerisation is consistent with this, since the introduction of another weak ligand, N-acetyl-D-Ala to ristocetin was shown to have a similar influence on dimerisation. As with vancomycin, it was possible that such effects were a consequence of salt. Addition of salts to the buffer showed a small increase in dimerisation constant, increasing with the ionic strength of the salt. This suggests that there may be a degree of electrostatic repulsion between like charges at the dimer interface, which are screened from each other in the presence of salt, therefore enhancing dimerisation, although it is not possible to assign the origin of such interactions. This is in contrast to vancomycin, where there was no evidence for electrostatic contributions to

dimerisation. It is therefore possible that the phenomenon of ligand induced dissociation of ristocetin, may be influenced by a change in repulsion between the monomers on ligand binding. In simple terms, if the binding of ligand to the ristocetin dimer alters the charge on each monomer in such a way as to enhance the repulsion between them, then dimerisation would be reduced.

Unlike with vancomycin, the heats of ionisation of buffers do not appear to make a significant contribution to the overall observed enthalpy of ristocetin dimerisation, with enthalpies similar in both phosphate and MOPS buffers. This is not really surprising since ristocetin dimerisation shows contrasting behaviour to that of vancomycin. It is possible that whatever group encourages vancomycin dimerisation is not involved in that of ristocetin.

A limited number of calorimetric dilution experiments with ristocetin were carried out in deuterium oxide. The same trends were found in deuterium oxide as in water, with dimerisation reduced in the presence of $N_{\alpha},N_{\varepsilon}$-diacetyl-Lys-D-Ala-D-Ala. Ristocetin dimerisation appears to be favoured more in deuterium oxide, as is that of vancomycin. Our experiments show that ristocetin dimerisation is more exothermic in water than in deuterium oxide, consistent with results from the Chervenak & Toone, (1994) study. As mentioned previously in 5.1.1.1.8, isotopic substitution affects both solute-solvent interactions and also hydrogen bonds between biological molecules (antibiotic monomers in this case), since exchangeable hydrogens at the dimer interface will be exposed to deuterated solvent prior to dimerisation. An increase in the enthalpy of these interactions in deuterium oxide, due to stronger deuterium bonds, will lead to a differential enthalpy of association in deuterium oxide compared with water.

5.2 Studies using UV difference spectroscopy

5.2.1 Binding studies

Rather than relying entirely on microcalorimetry for the determination of association constants, selected experiments were carried out with vancomycin and ligand using UV difference spectroscopy as a complementary technique. The association between vancomycin and N-acetyl-D-Ala-D-Ala was investigated using the method published by Billot-Klein,[a] (1994). Unfortunately, no accurate data were obtained for vancomycin associations with other ligands, due to smaller changes in observed absorbance. The association constant between vancomycin and N-acetyl-D-Ala-D-Ala obtained from this method was $4.50\times10^{4}M^{-1}$, which is comparable to that obtained from microcalorimetric experiments, the binding curve of which is shown in Figure 5.47.

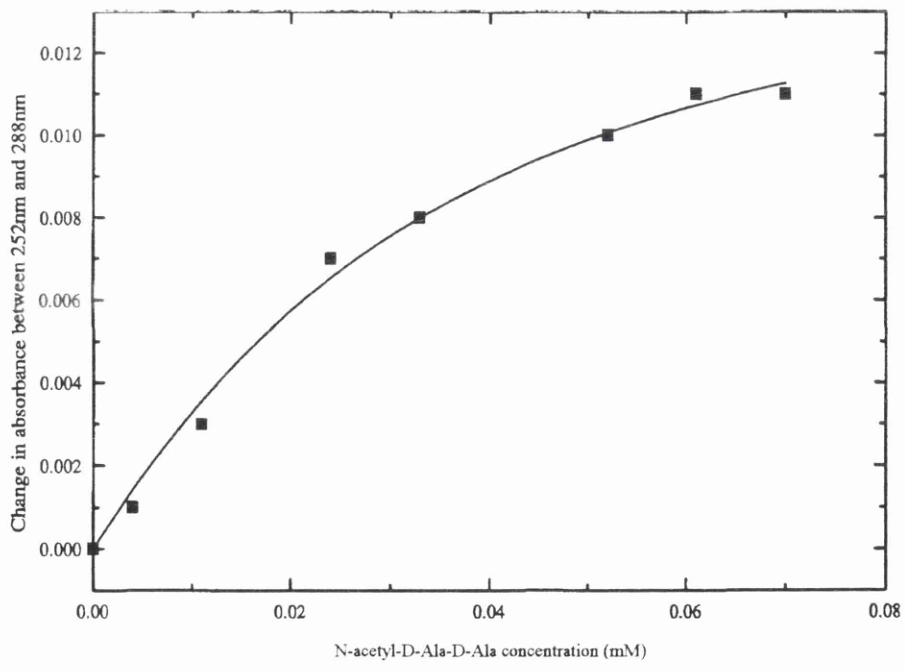

Figure 5.47 Binding curve for the association between vancomycin and N-acetyl-D-Ala-D-Ala.

5.2.2 Kinetic studies

As shown previously, dissociation of the vancomycin dimer in the presence of $N_{\alpha},N_{\varepsilon}$-diacetyl-Lys-D-Ala-D-Ala gave a series of endothermic heat pulses which were significantly broader and took longer to return to baseline than normal for fast reactions, suggesting that dissociation is slow under such conditions. This led to the possibility of using UV difference spectroscopy to study the kinetics of this process in more detail and this was confirmed by observing the relatively slow decrease in UV absorbance upon dilution of vancomycin and $N_{\alpha},N_{\varepsilon}$-diacetyl-Lys-D-Ala-D-Ala solutions into buffer, of which typical data is shown in Figure 5.48. Dissociation in the absence of ligand and with the weakly binding ligand, N-acetyl-D-Ala was too fast to measure using this technique.

The process involved was a simple first-order reaction, where the rate of reaction was proportional to the concentration (rate = k[A]). The term concentration is used interchangeably with absorbance in this case. In general, if the initial absorbance of A is A_0, then at a later time t, it will have fallen to $[A]_t$, where $[A]_t = [A]_o e^{-kt}$, which shows that the absorbance follows an exponential decrease. Taking natural logarithms gives, $\ln[A]_t/[A]_0 = -kt$. Any reaction which produces a straight line from a graph of ln[A] against time is first-order, with a slope equal to -k which gives the rate constant. Such characteristics are unique to first-order reactions. This was the basis from which apparent rate constants were determined over a range of temperature and pH conditions. A more precise description can be found in chapter 4.

Arrhenius activation energy was determined from the slope of the line from a plot of lnK against 1/T.

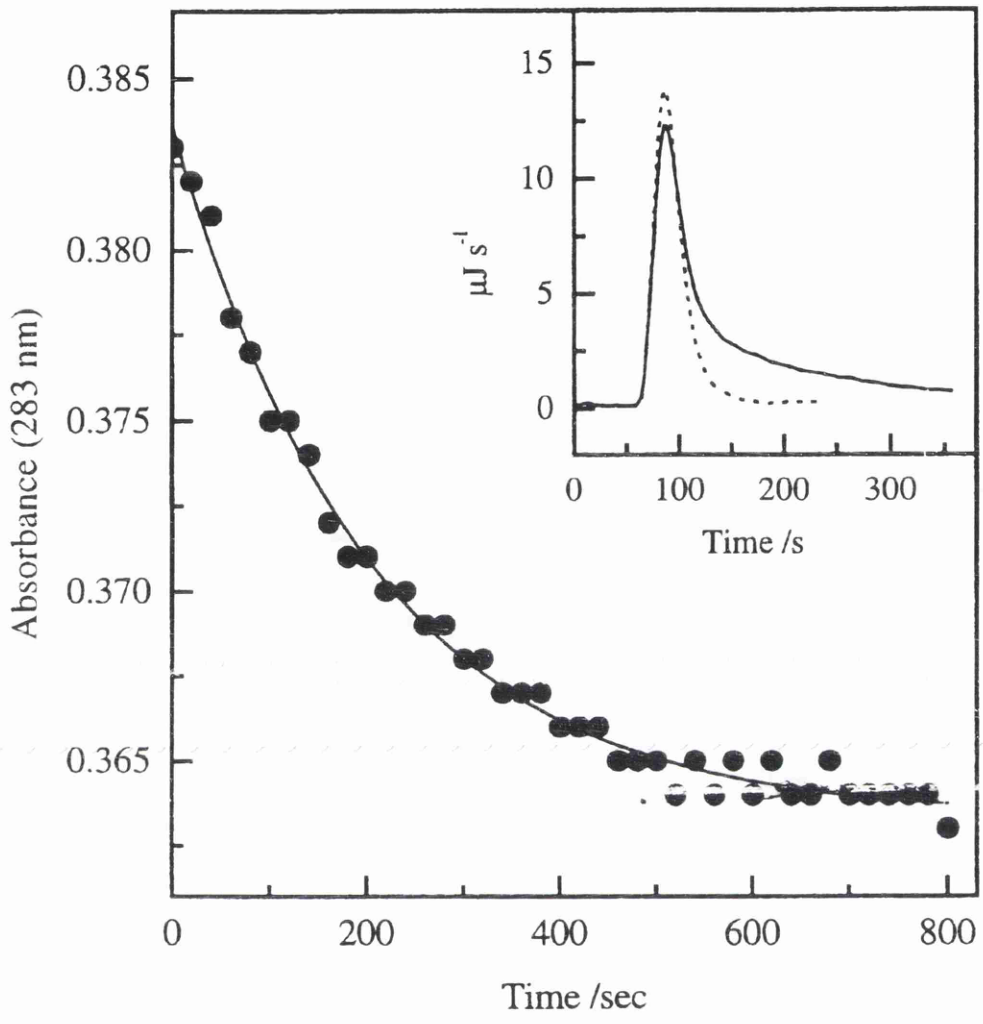

Figure 5.48 First-order kinetic data for the dissociation of vancomycin dimers in the presence of excess $N_{\alpha},N_{\varepsilon}$-diacetyl-Lys-D-Ala-D-Ala. *Inset:* Comparison of ITC dilution heat pulses for vancomycin alone (dotted line) or in the presence of $N_{\alpha},N_{\varepsilon}$-diacetyl-Lys-D-Ala-D-Ala (solid line).

5.2.2.1 $N_{\alpha},N_{\varepsilon}$-diacetyl-Lys-D-Ala-D-Ala

Apparent rate constants of vancomycin dissociation from the dimer form in the presence of the cell wall analogue, $N_{\alpha},N_{\varepsilon}$-diacetyl-Lys-D-Ala-D-Ala showed no significant

variation with ligand concentration over a three-fold concentration range, provided that ligand was in excess, but increased with temperature and also with pH, becoming too fast to measure above pH 8. This is due to a reduction in stability of the complex consistent with the ionisation of phenolic groups which results in electrostatic repulsion between antibiotic and ligand at the binding site, which in turn reduces dimerisation. Similar observations were made from microcalorimetric studies. Results are shown in Tables 5.23(a) and 5.23(b). Studying the temperature dependence of the reaction rate allowed the determination of the Arrhenius activation energy. The plot from which this was determined is shown in Figure 5.49, the points of which are the mean of the three rate determinations. The slope of the graph is equal to $-E_a/R$, where E_a is the activation energy. For this process at pH 7, it was estimated at 73 ($\pm$6) kJmol^{-1}.

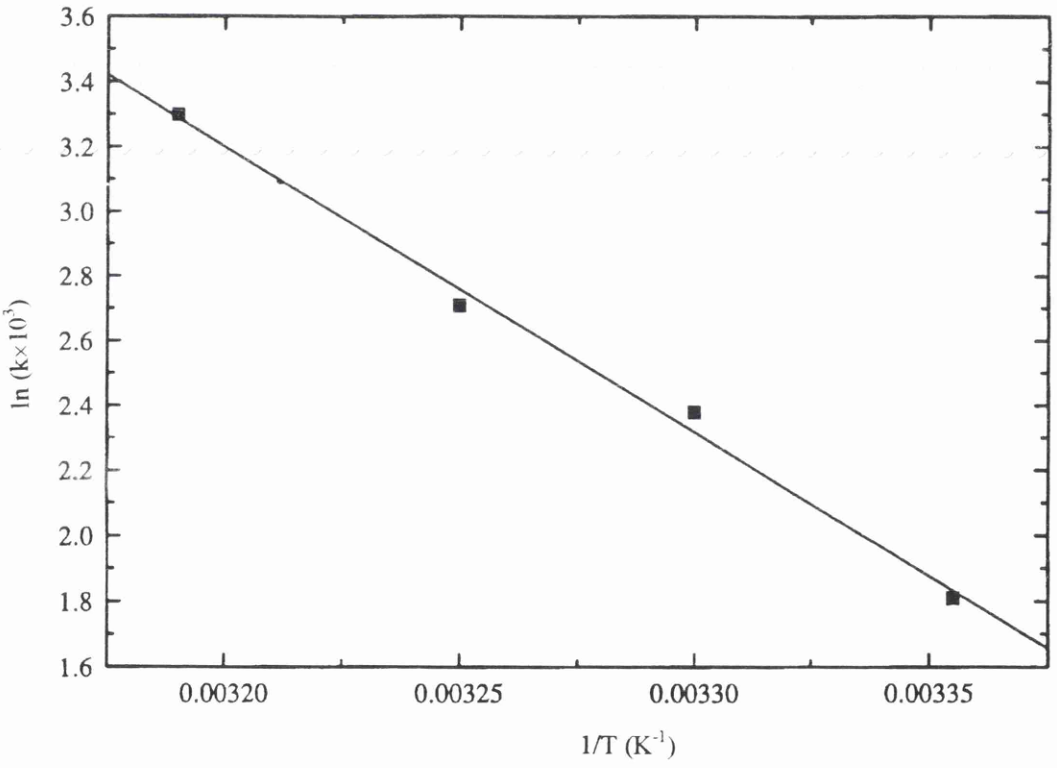

Figure 5.49 Arrhenius activation energy graph for the dissociation of vancomycin in the presence of N_α,N_ε-diacetyl-Lys-D-Ala-D-Ala.

Temperature (°C)	Volume of injectant (µl)	Rate constant ($\times 10^{-3} sec^{-1}$)
25	10	4.8(0.6)
	20	6.0(0.5)
	30	7.4(1.2)
30	10	7.9(2.5)
	20	13.6(6.4)
	30	10.9(3.2)
35	10	11.6(6.5)
	20	12.9(2.1)
	30	20.3(2.2)
40	10	24.3(1.5)
	20	25.6(2.9)
	30	30.0(0.4)

Table 5.23(a) Vancomycin dissociation in the presence of N_{α},N_{ε}-diacetyl-Lys-D-Ala-D-Ala at various temperatures.

pH	Volume of injectant (µl)	Rate constant ($\times 10^{-3} sec^{-1}$)
3	10	10.4(0)
	20	12.0(2.7)
	30	9.7(1.6)
5	10	3.7(0.2)
	20	4.0(0.9)
	30	4.7(1.4)
7	10	4.8(0.6)
	20	6.0(0.5)
	30	7.4(1.2)
8	10	5.9(0.6)
	20	8.9(3.2)
	30	9.8(0.1)

Table 5.23(b) Vancomycin dissociation in the presence of $N_{\alpha},N_{\varepsilon}$-diacetyl-Lys-D-Ala-D-Ala at various pH at 25°C.

5.2.2.2 Discussion

The rate of vancomycin dissociation from the dimer form in the presence of $N_{\alpha},N_{\varepsilon}$-diacetyl-Lys-D-Ala-D-Ala is clearly dependant on temperature and pH, consistent with microcalorimetric observations. The rate constant of dissociation in the presence of this ligand is considerably slower than the rate reported for dissociation of the ligand itself from vancomycin under similar conditions (Popieniek & Pratt, 1991), although these latter measurements were carried out at lower vancomycin concentrations where dimerisation is not significant. This led to questions regarding the mechanism of dimer dissociation in the presence of ligand such as, does dissociation of the ligand bound dimer occur directly or does it require prior release of the ligand? Under the conditions used in our series of dilution experiments to follow dimer dissociation, the $N_{\alpha},N_{\varepsilon}$-

diacetyl-Lys-D-Ala-D-Ala concentration remained significantly high to guarantee that the vancomycin is predominately in the ligand bound form either as monomer or dimer. Consider the following scheme of dimer dissociation:

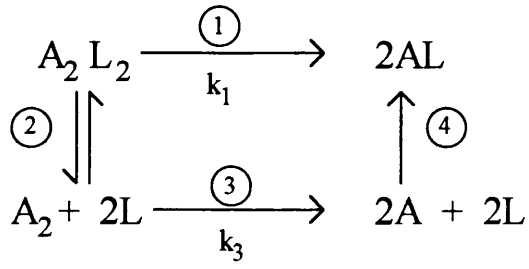

We have already established that vancomycin dissociation from the dimer form is a first-order reaction, therefore for direct dissociation (step 1) we would expect a rate law of the form: rate = $k_1[A_2L_2]$, with no dependence on free ligand concentration, since all ligand is assumed to be bound. However, an indirect dissociation mechanism involving ligand dissociation might involve ligand concentration dependent steps. For example, for the indirect steps 2→3→4 with step 3 rate determining we might expect: rate = $k_3[A_2] = k_3^* [A_2L_2]$ where $k_3^* = k_3.K_{dim,0} / K_{dim,L} K_L^2 [L]^2$ is the apparent first order rate constant for dissociation of the liganded dimer. In this case, the rate of dimer dissociation under the conditions used here where the free ligand [L] is in excess, we would anticipate a strong inverse-square dependence on ligand concentration for the apparent first order rate constant. However, our dilution kinetic studies over a three-fold range of ligand concentration, showed no significant variation in apparent rate constant, so this pathway may be discounted. Direct dissociation (without prior release of ligand) appears to be the most likely scenario since the free energy for vancomycin/N_α,N_ε-diacetyl-Lys-D-Ala-D-Ala complex formation is much greater than that for dimerisation, suggesting that interactions between monomers in the dimer are weaker than those between monomer and ligand.

Chapter 6:
X-ray Crystallography
Results and Discussion

6.1 X-ray crystallography

The aim of carrying out crystallographic studies was to further develop previous work on the crystal structure of vancomycin (Sheldrick *et al.*, 1978 : Sheldrick *et al.*, 1995 : Schafer *et al.*, 1996) with a view to obtaining a greater understanding of the way in which the vancomycin dimer complexes with cell wall peptides. A brief account of the previous crystallographic work carried out on this family of antibiotics follows.

Early attempts to solve the crystal structure of vancomycin were based not on vancomycin itself, but on a degradation product, CDP-I, which crystallised as a monomer. The high resolution X-ray data obtained, and the fact that CDP-I crystallised with only one molecule in the asymmetric unit, allowed the structure to be solved by small molecule techniques (Sheldrick *et al.*, 1978). Vancomycin has been built from the crystal structure of this degradation product and its binding to cell wall substrate compared with a DD-peptidase (Knox & Pratt, 1990). However, it wasn't until 1995 that X-ray data, collected from weakly diffracting crystals, allowed the first crystal structure of a naturally occurring member of the vancomycin family of antibiotics in the dimer form, which was not the subject of degradation and ring rearrangement, to be determined (Sheldrick *et al.*, 1995). This took the form of ureido-balhimycin, an antibiotic structurally similar to vancomycin. It was only recently, however, that the crystal structure of the vancomycin dimer itself was determined using advanced direct method protocols (Schafer *et al.*, 1996).

All previous attempts at solving the crystal structure involved vancomycin alone. It was only when we discovered that the introduction of N-acetyl-D-Ala-D-Ala to vancomycin at the concentrations required for calorimetric dilution measurements led to precipitation of the antibiotic-dipeptide complex, that the possibility arose that crystals could be grown, providing a route to the structure of the vancomycin dimer complexed with peptide.

It was from this initial observation that we began an extensive array of crystallisation trials to find the optimum conditions for the growth of suitable crystals which would produce high resolution diffraction data.

Initial trials employing techniques for small molecule crystallisation were unsuccessful, so we decided to apply macromolecular crystallisation methods. Crystallisation of biological molecules is essentially a trial-and-error process, whereby even small changes in pH or concentration can affect crystal growth. It is therefore important to try a wide variety of conditions to improve the quality and size of the crystals. Successful crystallisation of vancomycin/N-acetyl-D-Ala-D-Ala complex was achieved using the sitting drop method, in which the introduction of measured aliquots of both antibiotic and ligand to the sample well and buffer to the surrounding reservoir allowed equilibrium to be reached through vapour diffusion between the two volumes. This produced slow supersaturation of the sample and therefore crystal growth.

All crystallisations were carried out in a temperature controlled room at 20°C.

6.1.1 Initial crystallisation attempts of the vancomycin/N-acetyl-D-Ala-D-Ala complex

The first trial was to prepare vancomycin and N-acetyl-D-Ala-D-Ala solutions at concentrations at which precipitation was known to occur. Since our calorimetric

dilution measurements showed precipitation in pH 7, 0.1M phosphate buffer, crystallisations were initially carried out under these conditions. A stock vancomycin solution at 0.87mM and a stock N-acetyl-D-Ala-D-Ala solution at 1.97mM was prepared in pH 7, 0.1M phosphate buffer and used as in Figure 6.1, which represents the twenty four well crystallisation tray, in an attempt to determine the antibiotic to ligand ratios which would give rise to crystal growth. This and subsequent trials in this section were carried out using the evaporation method of crystallisation.

	1	2	3	4	5	6
A	2 V 18 L	4 V 16 L	6 V 14 L	8 V 12 L	10 V 10 L	12 V 8 L
B	3 V 17 L	5 V 15 L	7 V 13 L	9 V 11 L	11 V 9 L	13 V* 7 L
C	1 V 19 L	2 V 23 L	4 V 21 L	6 V 19 L	8 V 17 L	14 V* 6 L
D	20 buffer	23 V 2 L	21 V 4 L	19 V 6 L	17 V 8 L	18 V* 7 L

Figure 6.1 Drop volumes (μl) of stock vancomycin (V) and stock N-acetyl-D-Ala-D-Ala (L) added to sample well. Well D1 was used as a control. Stock concentrations of vancomycin and N-acetyl-D-Ala-D-Ala were 0.87mM and 1.97mM, respectively in each well in pH 7, 0.1M phosphate buffer.

After a few days, no precipitation was found in any of the twenty four wells, indicating that supersaturation of the sample drop may not occur, since usually after this period of time there is a slight precipitation from which crystals can develop. Therefore, conditions needed to be changed, to those that would encourage slow supersaturation of the sample.

Another crystallisation tray was prepared using the same setup as above, but with much higher concentrations of vancomycin and N-acetyl-D-Ala-D-Ala e.g. stock

concentrations of 4.12mM and 7.90mM, respectively in pH 7, 0.1M phosphate buffer. After ten days, small, torpedo shaped crystals were found in wells B6, C6 and D6 (marked with a * in Figure 6.1). Since the crystals were so small, the relative concentrations of vancomycin and N-acetyl-D-Ala-D-Ala may have been too high and therefore needed to be reduced.

The next crystallisation trial involved using the same ratios as previously, but with stock solutions of vancomycin and N-acetyl-D-Ala-D-Ala over a range of concentrations from 2.00mM to 4.10mM and 2.00mM to 7.00mM, respectively, as in Figure 6.2.

	1	2	3	4	5	6
A	2V(2.00) 18L(2.00)	4V(2.50) 16L(2.00)	6V(2.75) 14L(2.00)	8V(3.00) 12L(2.00)	10V(3.50) 10L(2.00)	12V(4.10) 8L(2.00)
B	3V(2.00) 17L(4.00)	5V(2.50) 15L(4.00)	7V(2.75) 13L(4.00)	9V(3.00) 11L(4.00)	11V(3.50) 9L(4.00)	13V(4.10) 7L(4.00)
C	1V(2.00) 19L(5.50)	2V(2.50) 23L(5.50)	4V(2.75) 21L(5.50)	6V(3.00) 19L(5.50)	8V(3.50) 17L(5.50)	14V(4.10) 6L(5.50)
D	100 buffer	23V(2.50) 2L(7.00)	21V(2.75) 4L(7.00)	19V(3.00) 6L(7.00)	17V(3.50) 8L(7.00)	18V(4.10) 7L(7.00)

Figure 6.2 Drop volumes (μl) of stock vancomycin (V) and stock N-acetyl-D-Ala-D-Ala (L) added to sample well. Relative concentrations (mM) are given in brackets. Well D1 was used as a control. Stock solutions were prepared in pH 7, 0.1M phosphate buffer.

Since even small changes in concentration can affect crystallisation, another tray was prepared using the same conditions but over a slightly different range of stock concentrations e.g. from 2.00 to 3.64mM vancomycin and 2.00 to 7.10mM N-acetyl-D-Ala-D-Ala, as in Figure 6.3.

	1	2	3	4	5	6
A	2V(2.00) 18L(2.00)	4V(2.50) 16L(2.00)	6V(2.75) 14L(2.00)	8V(3.00) 12L(2.00)	10V(3.50) 10L(2.00)	12V(3.64) 8L(2.00)
B	3V(2.00) 17L(4.00)	5V(2.50) 15L(4.00)	7V(2.75) 13L(4.00)	9V(3.00) 11L(4.00)	11V(3.50) 9L(4.00)	13V(3.64) 7L(4.00)
C	1V(2.00) 19L(5.50)	2V(2.50) 23L(5.50)	4V(2.75) 21L(5.50)	6V(3.00) 19L(5.50)	8V(3.50) 17L(5.50)	14V(3.64) 6L(5.50)
D	100 buffer	23V(2.50) 2L(7.10)	21V(2.75) 4L(7.10)	19V(3.00) 6L(7.10)*	17V(3.50) 8L(7.10)	18V(3.64) 7L(7.10)

Figure 6.3 Drop volumes (μl) of stock vancomycin (V) and stock N-acetyl-D-Ala-D-Ala (L) added to sample well. Relative concentrations (mM) are given in brackets. Well D1 was used as a control. Stock solutions were prepared in pH 7, 0.1M phosphate buffer.

After a period of two weeks, small crystals were found in well D4 (marked with a * in Figure 6.3). Therefore, a tray using this setup in all twenty four wells was prepared.

Since it is difficult to make up solutions of exactly the same concentrations as used in previous trials, the wells were filled with slightly different stock concentrations of vancomycin and N-acetyl-D-Ala-D-Ala e.g. 2.63mM and 8.86mM, respectively. Instead of forming crystals as we expected, introduction of these solutions into the sample well caused instant precipitation, consistent with supersaturation being reached too quickly. Crystals will not develop under such conditions. The rapid approach to crystallisation must be discouraged to allow time for crystals to develop. Therefore, other crystallisation techniques must be tried.

6.1.2 Application of protein crystallisation techniques

6.1.2.1 Phosphate buffer

After these initial trials, crystallisation was investigated using the alternative sitting drop method, which is ideal for gradually approaching the conditions for crystallisation. This method also allows much easier retrieval of crystals from the sample well. A crystal tray was set up with smaller volumes but the same ratios i.e. 6μl of 2.73mM vancomycin and 2μl of 7.27mM N-acetyl-D-Ala-D-Ala in all twenty four wells, with the same concentration of phosphate buffer (pH 7, 0.1M) in the surrounding reservoir and sample drop. After a period of about three weeks, small crystals (shown in Figure 6.4) formed in two of the wells, but were still too small and fragile to use for diffraction studies. However, the possibility arose for using them to seed other solutions to encourage growth of much larger crystals by providing a nucleation site.

Figure 6.4 Photograph showing small 'torpedo' shaped crystals.

Seeding was carried out by taking the microcrystals and crushing them in a little of the same buffer used in the mother liquor i.e. pH 7, 0.1M phosphate buffer and adding various concentrations of this solution to antibiotic and ligand samples prepared in the original way. Seeding was also performed by using crushed crystals as the complex in solution and adding various concentrations to buffer within each well. The seeding tray

was set up as in Figure 6.5. Columns 1 and 2 contained 6µl 3.68mM vancomycin and 2µl 9.02mM N-acetyl-D-Ala-D-Ala in the sample well to which buffer and crushed crystals were added, the volumes of which are given below. Columns 3 and 4 contained 15µl of buffer in the well to which was added <1µl of crystals. Columns 5 and 6 were used as a control and contained no crystals, just the vancomycin and N-acetyl-D-Ala-D-Ala solutions.

	1	2	3	4	5	6
A	1 b 1 c	1 b 1 c	15 b	15 b		
B	2 b 1 c	2 b 1 c	15 b	15 b		
C	3 b 1 c	3 b 1 c	15 b	15 b		
D	4 b 1 c	4 b 1 c	15 b	15 b		

Figure 6.5 Volumes (µl) of phosphate buffer (b) and crushed microcrystals (c) added to sample well.

After approximately four weeks, only precipitation had developed in the wells.

In addition, another trial was set up under similar conditions as before which gave rise to crystals (2.43mM vancomycin and 7.18mM N-acetyl-D-Ala-D-Ala), but this time using a higher concentration of phosphate buffer in the solvent reservoir (0.5M) than in the sample drop. This was to encourage the diffusion of water from the sample drop to the reservoir, until the vapour pressures are equal, which gradually leads to supersaturation. However, no crystals were formed in this trial either.

A crystallisation trial was also carried out using a constant concentration of vancomycin, 3.14mM and a range of N-acetyl-D-Ala-D-Ala concentrations, from 3.24mM to 5.40mM in pH 7, 0.1M phosphate buffer, in a 2:1 ratio as illustrated in Figure 6.6.

	1	2	3	4	5	6
A	4V(3.14) 2L(3.24)	6V(3.14) 3L(3.24)	8V(3.14) 4L(3.24)	10V(3.14) 5L(3.24)	12V(3.14) 6L(3.24)	14V(3.14) 7L(3.24)
B	4V(3.14) 2L(4.13)	6V(3.14) 3L(4.13)	8V(3.14) 4L(4.13)	10V(3.14) 5L(4.13)	12V(3.14) 6L(4.13)	14V(3.14) 7L(4.13)
C	4V(3.14)* 2L(5.31)	6V(3.14) 3L(5.31)	8V(3.14) 4L(5.31)	10V(3.14) 5L(5.31)	12V(3.14) 6L(5.31)	14V(3.14) 7L(5.31)
D	4V(3.14) 2L(5.40)	6V(3.14) 3L(5.40)	8V(3.14) 4L(5.40)	10V(3.14) 5L(5.40)	12V(3.14) 6L(5.40)	14V(3.14) 7L(5.40)

Figure 6.6 Drop volumes (μl) of stock vancomycin (V) and stock N-acetyl-D-Ala-D-Ala (L) added to sample well. Relative concentrations (mM) are shown in brackets. Stock solutions were prepared in pH 7, 0.1M phosphate buffer.

After about four weeks, small crystals showing two morphologies were found in well C1 (marked with a * in Figure 6.6) i.e. hexagonal and torpedo, with slight precipitation in the other wells.

Another tray was set up using the same volumes as shown in Figure 6.6, but this time using a constant stock concentration of N-acetyl-D-Ala-D-Ala i.e. 5.40mM and a range of vancomycin concentrations, from 3.14mM to 4.51mM, all in pH 7, 0.1M phosphate buffer as shown in Figure 6.7. After three weeks, precipitation in the wells had developed with no crystal growth.

	1	2	3	4	5	6
A	4V(3.14) 2L(5.40)	6V(3.14) 3L(5.40)	8V(3.14) 4L(5.40)	10V(3.14) 5L(5.40)	12V(3.14) 6L(5.40)	14V(3.14) 7L(5.40)
B	4V(3.60) 2L(5.40)	6V(3.60) 3L(5.40)	8V(3.60) 4L(5.40)	10V(3.60) 5L(5.40)	12V(3.60) 6L(5.40)	14V(3.60) 7L(5.40)
C	4V(3.80) 2L(5.40)	6V(3.80) 3L(5.40)	8V(3.80) 4L(5.40)	10V(3.80) 5L(5.40)	12V(3.80) 6L(5.40)	14V(3.80) 7L(5.40)
D	4V(4.51) 2L(5.40)	6V(4.51) 3L(5.40)	8V(4.51) 4L(5.40)	10V(4.51) 5L(5.40)	12V(4.51) 6L(5.40)	14V(4.51) 7L(5.40)

Figure 6.7 Drop volumes (μl) of stock vancomycin (V) and stock N-acetyl-D-Ala-D-Ala (L) added to sample well. Relative concentrations (mM) are given in brackets. Stock solutions were prepared in pH 7, 0.1M phosphate buffer.

6.1.2.2 Imidazole maleic buffer

As we know, crystallisation can be affected by altering the pH, therefore our next step was to carry out trials over a range of physiological pH values, rather than relying entirely on crystal growth to occur at pH 7, as with previous attempts. A tray was set up using 0.1M Imidazole maleic buffers, rather than phosphate, at pH values between 5.4 and 8.0, using between 4.10mM and 4.90mM stock vancomycin and between 5.35mM and 12.50mM stock N-acetyl-D-Ala-D-Ala, as shown in Figure 6.8. However, after a few weeks, only precipitation with microcrystals in wells A3 and A4 (marked with a * in Figure 6.8) were evident. These microcrystals were used for electrospray mass spectrometry, as discussed in section 6.2.

	1	2	3	4	5	6
A	2V(4.86) 1L(9.60)	4V(4.10) 2L(11.1)	6V(4.50)* 3L(8.82)	8V(4.90)* 4L(10.7)	10V(4.50) 5L(12.50)	12V(4.80) 6L(5.35)
B	13V(4.86) 7L(9.60)	14V(4.10) 8L(11.1)	15V(4.50) 9L(8.82)	16V(4.90) 10L(10.7)	17V(4.5)* 11L(12.5)	18V(4.80) 12L(5.35)
C	19V(4.86) 13L(9.60)	12V(4.10) 14L(11.1)	2V(4.50) 15L(8.82)	4V(4.90) 16L(10.7)	6V(4.50) 17L(12.5)	8V(4.80) 18L(5.35)
D	10V(4.86) 19L(9.60)	12V(4.10) 20L(11.1)	13V(4.50) 21L(8.82)	14V(4.90) 22L(10.7)	15V(4.50) 23L(12.5)	16V(4.80) 24L(5.35)
	pH 5.4	6.2	6.4	7.2	7.6	8.0

Figure 6.8 Drop volumes (μl) of vancomycin (V) and N-acetyl-D-Ala-D-Ala (L) added to sample well. Relative concentrations (mM) are given in brackets. Stock concentrations were prepared in 0.1M Imidazole maleic buffer.

Different percentages of isoproponyl added to phosphate buffer solutions (pH 7, 0.1M) solutions were also used in an attempt to promote crystal growth. Isoproponyl is an organic solvent, commonly used as a precipitant. The trial set up involved adding previously determined concentrations and volumes of antibiotic and ligand i.e. 18μl vancomycin and 6μl N-acetyl-D-Ala-D-Ala in each well, using the concentrations shown in Figure 6.9.

	1	2	3	4	5	6
A	18V(1.92) 6L(8.46)	18V(1.92) 6L(8.46)	18V(1.92) 6L(8.46)	18V(1.92) 6L(8.46)	18V(1.92) 6L(8.46)	18V(1.92) 6L(8.46)
B	18V(1.92) 6L(8.46)	18V(1.92) 6L(8.46)	18V(1.92) 6L(8.46)	18V(1.92) 6L(8.46)	18V(1.92) 6L(8.46)	18V(1.92) 6L(8.46)
C	18V(2.78) 6L(8.28)	18V(2.78) 6L(8.28)	18V(2.78) 6L(8.28)	18V(2.78) 6L(8.28)	18V(2.78) 6L(8.28)	18V(2.78) 6L(8.28)
D	18V(2.99) 6L(8.53)	18V(2.99) 6L(8.53)	18V(2.99) 6L(8.53)	18V(2.99) 6L(8.53)	18V(2.99) 6L(8.53)	18V(2.99) 6L(8.53)

Figure 6.9 Drop volumes (μl) of stock vancomycin (V) and stock N-acetyl-D-Ala-D-Ala (L) added to sample well. Relative concentrations (mM) are given in brackets. No isoproponyl, 5% isoproponyl and 10% isoproponyl. Stock solutions were initially made up in pH 7, 0.1M phosphate buffer.

Crystallisation proved unsuccessful with this arrangement. Therefore, another crystal tray was prepared using the same setup as that in Figure 6.8. over a pH range between 5.4 and 8.0 in 0.1M Imidazole maleic buffer, but this time varying the vancomycin and N-acetyl-D-Ala-D-Ala concentrations. The vancomycin concentrations varied from 4.38mM to 5.04mM and N-acetyl-D-Ala-D-Ala concentrations from 4.72mM to 7.59mM. After several months, well formed and sturdy, rounded crystals developed in well B5, which contained 17μl of 4.63mM stock vancomycin and 11μl of 5.41mM stock N-acetyl-D-Ala-D-Ala at pH 7.6, which were ultimately used for diffraction studies. Photographs of which are shown in Figure 6.10. Another tray was set up using the conditions of optimal growth and further crystals developed which gave rise to the same diffraction as previously. These crystals were subsequently used for crystal density measurements. In addition to this, another tray was set up under the same conditions, but over a slightly different range of concentrations of vancomycin and N-acetyl-D-Ala-D-Ala i.e. between 4.60mM and 5.56mM and between 6.18mM and 8.87mM, respectively, since even slight differences in conditions can affect crystallisation. However, only small crystals were found in well A3, even after a few months. This well

contained 4.65mM vancomycin and 8.87mM N-acetyl-D-Ala-D-Ala at pH 6.4. The other wells showed precipitation.

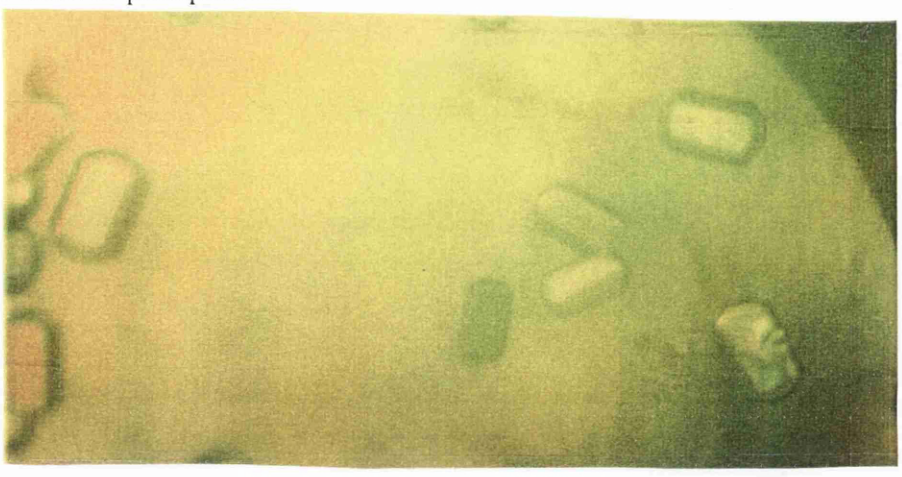

Figure 6.10 Photograph of crystals with 'rounded' morphology.

Other attempts involved setting up crystal trays over a narrower pH range and with varying ratios of antibiotic to ligand in 0.1M Imidazole maleic buffer. Vancomycin and N-acetyl-D-Ala-D-Ala concentrations at pH 7.6 were 3.60mM and 11.26mM, respectively and at pH 8.0 were 3.48mM and 5.89mM , respectively. Each tray was set up as in Figures 6.11 and 6.12.

	1	2	3	4	5	6
A	17V(3.60) 11L(11.26)	17V(3.60) 11L(11.26)	17V(3.60) 11L(11.26)	16V(3.60) 10L(11.26)	16V(3.60) 10L(11.26)	16V(3.60) 10L(11.26)
B	17V(3.60) 11L(11.26)	17V(3.60) 11L(11.26)	17V(3.60) 11L(11.26)	16V(3.60) 10L(11.26)	16V(3.60) 10L(11.26)	16V(3.60) 10L(11.26)
C	17V(3.60) 11L(11.26)	17V(3.60) 11L(11.26)	17V(3.60) 11L(11.26)	16V(3.60) 10L(11.26)	16V(3.60) 10L(11.26)	16V(3.60) 10L(11.26)
D	17V(3.60) 11L(11.26)	17V(3.60) 11L(11.26)	17V(3.60) 11L(11.26)	16V(3.60) 10L(11.26)	16V(3.60) 10L(11.26)	16V(3.60) 10L(11.26)

Figure 6.11 Drop volumes (μl) of stock vancomycin (V) and stock N-acetyl-D-Ala-D-Ala (L) added to sample well. Relative concentrations are given in brackets. Stock solutions were prepared in pH 7.6, 0.1M Imidazole maleic buffer.

No crystals were found in any of the wells of this crystallisation tray.

	1	2	3	4	5	6
A	18V(3.48) 12L(5.89) *	18V(3.48) 12L(5.89)	18V(3.48) 12L(5.89)	12V(3.48) 6L(5.89) *	12V(3.48) 6L(5.89)	12V(3.48) 6L(5.89)
B	18V(3.48) 12L(5.89)	18V(3.48) 12L(5.89)	18V(3.48) 12L(5.89)	12V(3.48) 6L(5.89)	12V(3.48) 6L(5.89)	12V(3.48) 6L(5.89)
C	18V(3.48) 12L(5.89)	18V(3.48) 12L(5.89)	18V(3.48) 12L(5.89)	12V(3.48) 6L(5.89)	12V(3.48) 6L(5.89)	12V(3.48) 6L(5.89)
D	18V(3.48) 12L(5.89)	18V(3.48) 12L(5.89) *	18V(3.48) 12L(5.89)	12V(3.48) 6L(5.89)	12V(3.48) 6L(5.89)	12V(3.48) 6L(5.89)

Figure 6.12 Drop volumes (μl) of vancomycin (V) and N-acetyl-D-Ala-D-Ala (L) added to sample well. Relative concentrations (mM) are given in brackets. Stock solutions were prepared in pH 8.0, 0.1M Imidazole maleic buffer.

After approximately two months, showers of microcrystals were found in wells A1, A4 and D2 (marked with a * in Figure 6.12), the others contained precipitate.

Another trial was set up using various ratios of vancomycin and N-acetyl-D-Ala-D-Ala in pH 7.2, 0.1M Imidazole maleic buffer, as shown in Figure 6.13.

	1	2	3	4	5	6
A	12V(2.87) 6L(6.06) *	12V(3.42) 6L(6.47) *	12V(3.85) 6L(7.18)	6V(2.87) 12L(6.06)	6V(3.42) 12L(6.47)	6V(3.85) 12L(7.18)
B	12V(2.87) 6L(6.06) *	12V(3.42) 6L(6.47) *	12V(3.85) 6L(7.18)	6V(2.87) 12L(6.06)	6V(3.42) 12L(6.47)	6V(3.85) 12L(7.18)
C	12V(2.87) 6L(6.06)	12V(3.42) 6L(6.47) *	12V(3.85) 6L(7.18) *	6V(2.87) 12L(6.06)	6V(3.42) 12L(6.47)	6V(3.85) 12L(7.18)
D	12V(2.87) 6L(6.06)	12V(3.42) 6L(6.47)	12V(3.85) 6L(7.18)*	6V(2.87) 12L(6.06)	6V(3.42) 12L(6.47)	6V(3.85) 12L(7.18)

Figure 6.13 Drop volumes (µl) of vancomycin (V) and N-acetyl-D-Ala-D-Ala (L) added to sample well. Relative concentrations (mM) are given in brackets. Stock solutions were prepared in pH 7.2, 0.1M Imidazole maleic buffer.

After several months, short, rounded, fragile crystals developed in wells A1, A2, B1, B2, C2, C3 and D3 (marked with a * in Figure 6.13), too fragile, however, to use for diffraction studies.

6.2 Electrospray mass spectrometry

The initial results of the unit cell dimensions (a=73.5, b=73.5, c=277.0, γ=120°) surprised us, since they were of similar dimensions to proteins. The diffraction pattern and limited resolution of 2.8Å (although more complete at 3.0Å) was also similar to protein diffraction. In order to eliminate the possibility of having crystallised an impurity,

either from the vancomycin sample or the N-acetyl-D-Ala-D-Ala, we took some crystals and carried out electrospray mass spectrometry on them.

This technique was used to provide an estimate of the purity of the vancomycin/N-acetyl-D-Ala-D-Ala microcrystals. As a comparison, separate solutions of the vancomycin and N-acetyl-D-Ala-D-Ala were prepared and analysed under the same conditions. The results are shown in Figure 6.14.

The peak at 725Da/e of the vancomycin sample is clearly shown in the signal of the complex as is the peak around 200Da/e associated with the N-acetyl-D-Ala-D-Ala solution. There do not appear to be any erroneous peaks within the signal of the complex which could have been due to the presence of impurities, therefore the microcrystals can be assumed to be free from contaminants.

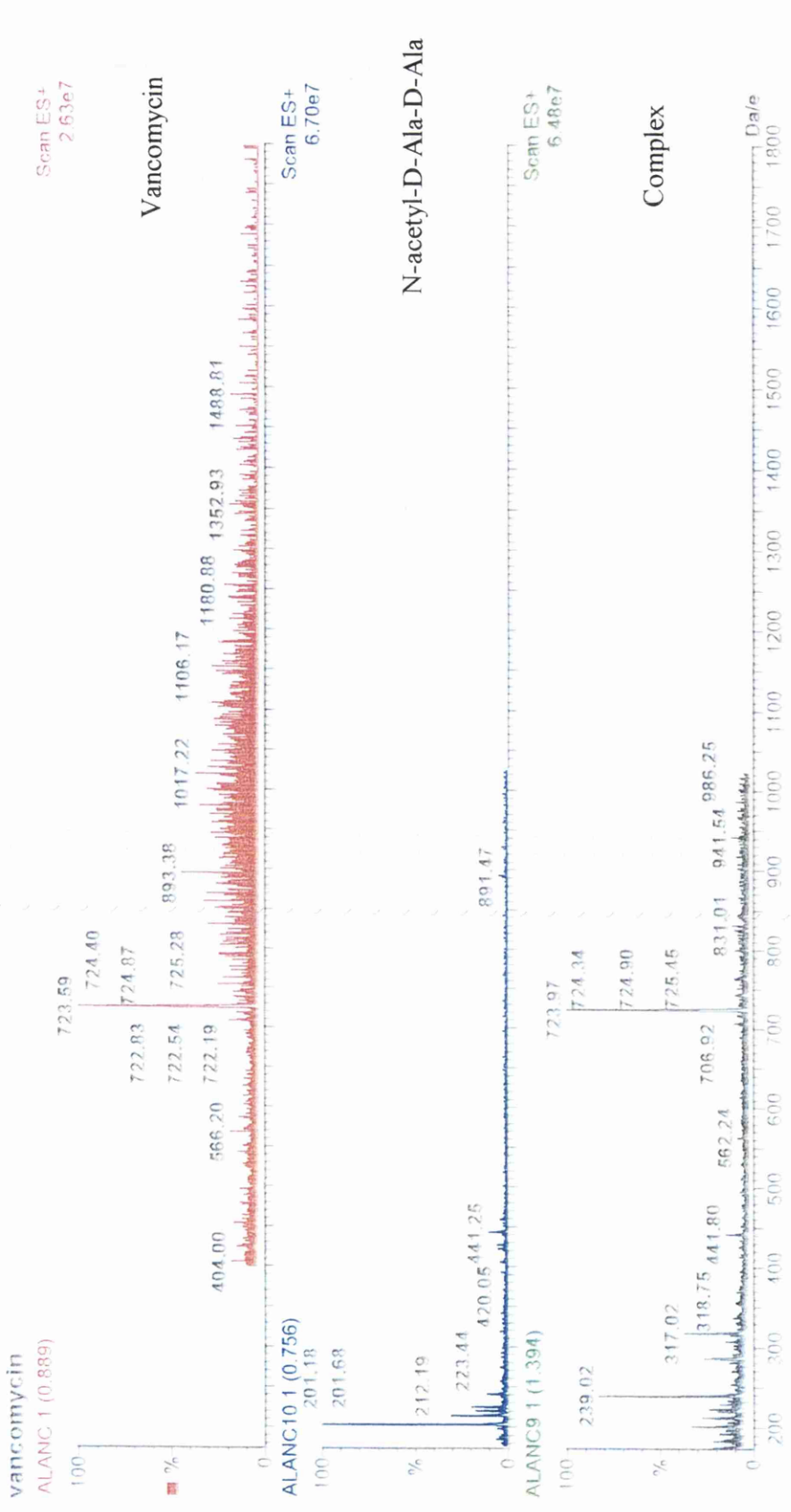

Figure 6.14 Electrospray mass spectrometry results of vancomycin and N-acetyl-D-Ala-D-Ala alone and vancomycin/N-acetyl-D-Ala-D-Ala complex.

6.3 Crystal density measurements

With such a large unit cell calculated from the diffraction pattern, it was important to establish the number of vancomycin molecules and solvent content present in the unit cell. Therefore, density measurements were made, as described in section 4.11. In the case of the vancomycin/peptide complex, the crystal density was estimated to be 1.106(0.01)g/cm^3. An example of one of the graphs from which the densities were determined is shown in Figure 6.15.

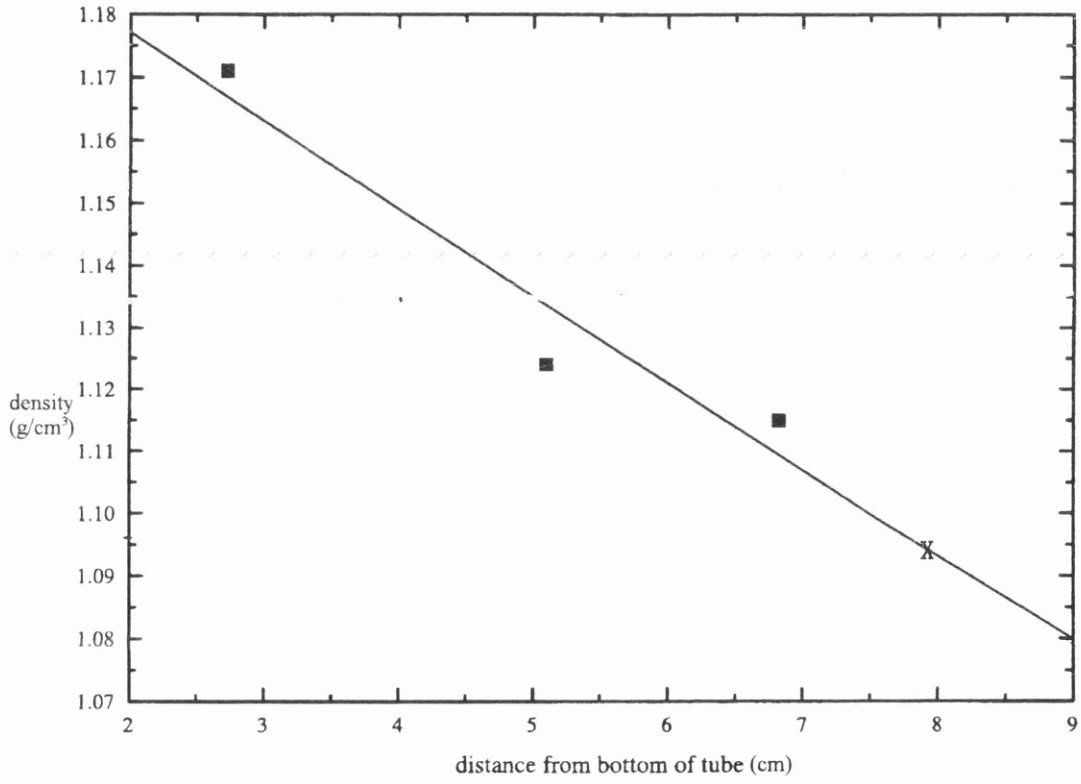

Figure 6.15 Graph from which crystal density was measured. Black squares represent marker positions and X represents crystal position.

This allowed the following calculations to be made:

$$V_m = \frac{V}{M \times Z} \qquad (6.1)$$

where V_m = Matthew's number

V = volume of the unit cell ($Å^3$)

Z = number of symmetry operators × no. of molecules in asymmetric unit

M = molecular mass (Da)

Therefore, for the results given in section 6.4:

where V = 73.5×73.5×277.0×sin120° (hexagonal unit cell)

Z = 12n (12 symmetry operators determined from space group, see section 6.4)

M = 1687.9 (monomer of vancomycin/peptide complex)

$$V_m = \frac{1.29\times10^6}{1687.9 \times 12}$$

$$= 63.69/n \text{ Å}^3/\text{Da}$$

Therefore, if there were 35 molecules in the asymmetric unit, V_m = 1.82

If there were 30 molecules in the asymmetric unit, V_m = 2.12

If there were 25 molecules in the asymmetric unit, V_m = 2.55

If there were 20 molecules in the asymmetric unit, V_m = 3.18

At the acceptable limits of the Matthew's number (V_m) (Matthews, 1968) i.e. between 1.6 and 4.0, the number of molecules within the asymmetric unit varies between 20 and 35. Within this range, 24 molecules (or 12 dimers) in the asymmetric unit is likely, which corresponds to a V_m of 2.6.

Using this calculated V_m, it is possible to provide an estimate of the solvent content. For example:

$$V_{solv} = 1 - V_{prot} \qquad (6.2)$$

$$V_{prot} = \frac{1}{(N \times D_p \times V_m)} \qquad (6.3)$$

where N = Avogadro's constant

D_p = density (g/Å^3)

V_m = Matthew's number

assuming $N = 6.02 \times 10^{23}$

$D_p = 1.106 \times 10^{-24}$

$V_m = 2.6$

$$V_{prot} = \frac{1}{(6.02 \times 10^{23} \times 1.106 \times 10^{-24} \times 2.6)}$$

$V_{prot} = 0.58 = 58\%$, therefore $V_{solv} = 1\text{-}0.58 = 42\%$

The ratio of protein:solvent for the vancomycin dimer/peptide complex is comparable to that found for the vancomycin dimer alone (Schafer *et al.*, 1996). Although in the absence of peptide, vancomycin crystallises with just 2 molecules in the asymmetric unit i.e. 1 dimer, but our study suggests that the vancomycin dimer in the presence of peptide may crystallise with 24 molecules in the asymmetric unit i.e. 12 dimers, corresponding to 144 dimers in the large unit cell. Estimates of the solvent content depend on the Matthew's number chosen which in our case represents the mean of the reasonably expected values.

6.4 X-ray diffraction results

As mentioned in section 6.1.2.2, diffraction data was collected from two different crystals at different periods of time. An example of a diffraction pattern obtained is given in Figure 6.16. For the two crystals, seven separate data sets were collected and concatenated into one unique data set. The reason for collecting so many separate data sets was that the long c-axis of the crystal required the detector swing angle to be moved to three different θ values to collect all the reflections in the reciprocal lattice. Therefore, wedges of data were collected at swing angles 5°, 10° and 20° for each crystal. This strategy collected 93% of the available data and the seven data sets took more than 4 weeks of continuous data collection on the Siemans-Xentronics area detector. The protocol for analysing each data set was the same, using the XDS data processing package. An example of the method used is shown for the first data set collected on frames 1-628. Initially strong reflections are collected and these are then automatically indexed by the program IDXREF. This, when run successfully, indicates the unit cell dimensions and Bravais lattice type and possible space group assignment. As indicated by the IDXREF output shown in Appendix I, the best fit number twelve (marked *****) was chosen as the correct unit cell dimensions i.e. 73.7, 73.9 and 278.2. The solution with the highest degree of symmetry is chosen. This corresponds to the hexagonal primitive Bravais lattice type. At this stage there are a number of space groups which are possible from this Bravais lattice. The correct space group is chosen by using the assigned transformation matrix corresponding to that space group (from IDXREF). The space group choice is input into the program CORRECT which analyses the data and fits the recorded reflections to calculated reflections using that space group symmetry. The agreement between the space group assignment and reflections recorded is shown on the final five lines of the CORRECT output in Appendix II, which indicates (for this batch) that no reflections have been rejected from 15381 recorded intensities. This shows that the space group assignment $P6_322$ (which contains 12 symmetry operators) was the correct space group. Once the unit cell dimensions and space group have been correctly assigned, all the data and goniometer constants are refined in the

program GLOREF (Global Refinement Program), the output of which is shown in Appendix III. This shows that the final refined unit cell dimensions are a=b=73.43(1), c=277.17(4), α=90°, β=90°, γ=120°. This process was adopted for each of the data sets in turn and similar results were obtained.

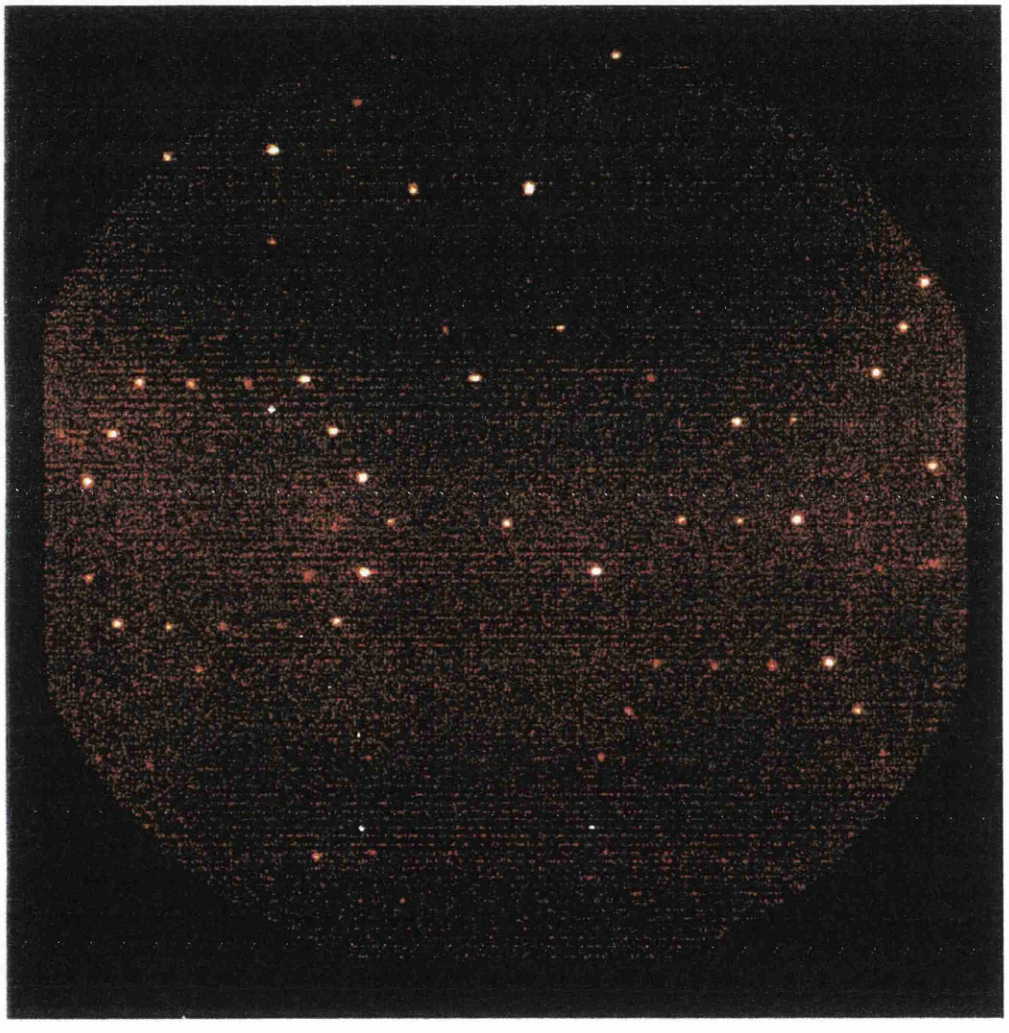

Figure 6.16 Vancomycin/N-acetyl-D-Ala-D-Ala complex diffraction pattern obtained from frame 101 of the fifth data set, showing reflections of different intensities.

All seven data sets were merged in the program XSCALE, the output of which is shown in Appendix IV. Scaling into one unique data set gave good merging statistics and we

were happy with these results. A total R-factor for 47584 reflections of 7.2% is well within the accepted range for a data set of this type. For good data, the value of R approaches a small value (1% at best), therefore our results show similar diffraction from different crystals. In order that the data collected can be used in the universally accepted CCP4 (Crystallographic Computing Project 4) suite of programs, the data is further processed by the CCP4 programs, TRUNCATE, ROTAPREP, SORT, MERGE and AGROVATA. The output from AGROVATA, shown in Appendix V, shows that 93% of data has been collected. The object of processing data in CCP4 is to create an *mtz* file, which is required for molecular replacement packages, such as AMORE. Some graphical representations of the AGROVATA output are shown below.

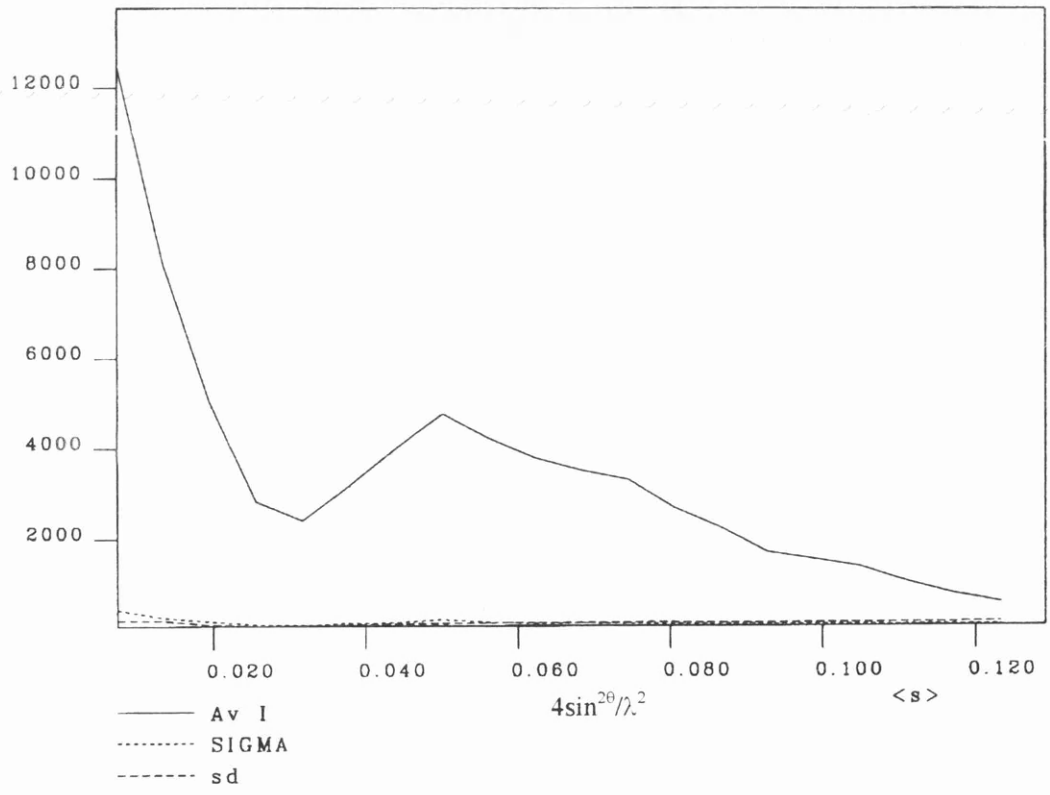

Figure 6.17 Graph to show how average intensity, SIGMA and standard deviation vary with resolution.

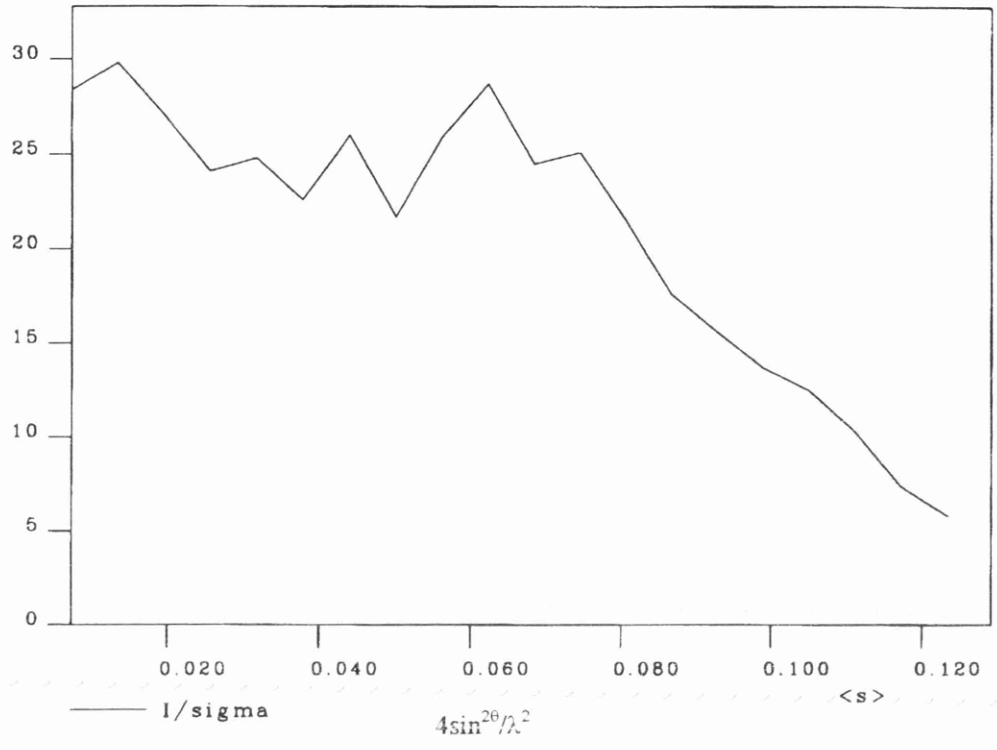

Figure 6.18 Graph to show how I/SIGMA varies with resolution.

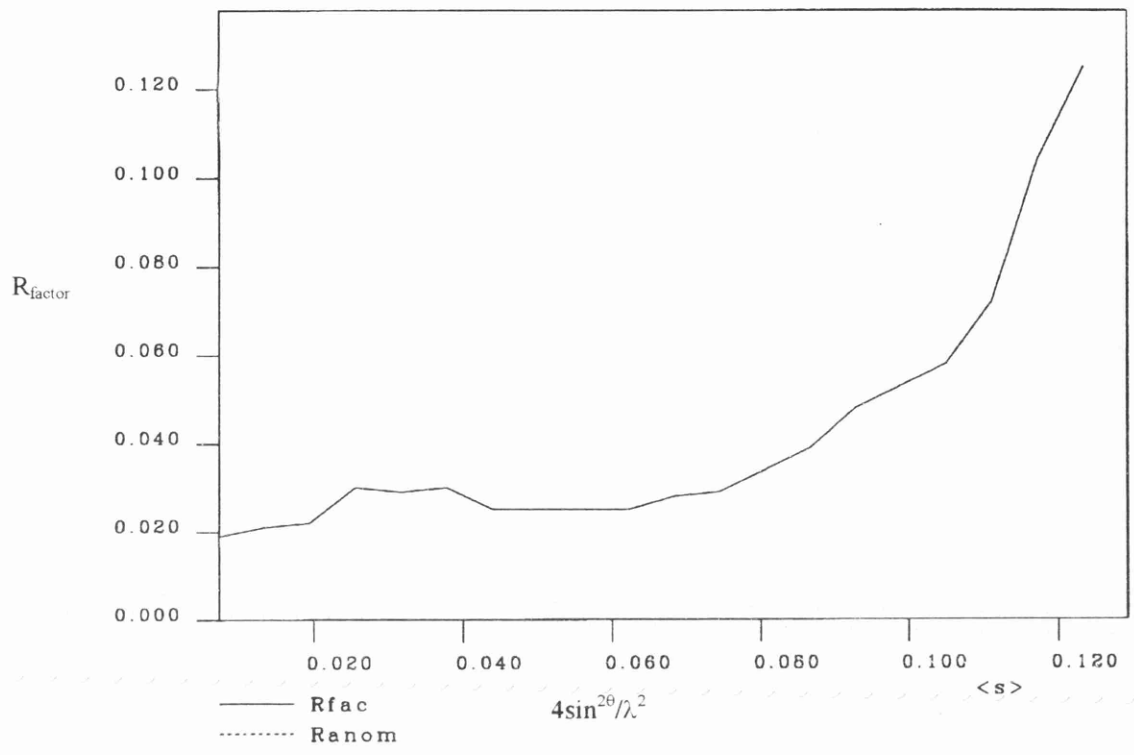

Figure 6.19 Plot of R-factor against resolution.

Figure 6.17 shows graphically that as the resolution increases, the average intensity is reduced. Figure 6.18 shows that 1/SIGMA is also reduced with increasing resolution, since 'noise' becomes more apparent at high resolutions which reduces the reliability of reflection. Figure 6.19 shows that as resolution increases, so does the R-factor, illustrating that data becomes less reliable at high resolutions.

Molecular replacement was carried out using the program AMORE. The principal behind using this technique was that it may provide a way of solving the crystal structure of our vancomycin complex, by comparing our data with a model of an homologous molecule, the crystal structure of which has already been determined. The model coordinates used were not from vancomycin itself, but from the derivative ureido-balhimycin. The atomic coordinates of ureido-balhimycin are given in Appendix VI, with the AMORE self-rotation results given below in Table 6.1.

SELF:Self RF - vancomycin

	ALPHA	BETA	GAMMA	CHIang	DC_X	DC_Y	DC_Z	CORR
SOLUTIONRS	0.00	0.00	0.00	0.00	0.00000	0.00000	1.00000	100.0
SOLUTIONRS	60.00	0.00	0.00	60.00	0.00000	0.00000	1.00000	100.0
SOLUTIONRS	28.70	68.37	28.70	86.97	0.00000	0.81647	0.57739	34.6
SOLUTIONRS	31.29	68.37	31.29	90.04	0.00000	0.79432	0.60751	34.6
SOLUTIONRS	0.00	66.48	0.00	66.48	0.00000	1.00000	0.00000	10.9
SOLUTIONRS	0.00	45.66	0.00	45.66	0.00000	1.00000	0.00000	8.0

Table 6.1 AMORE program output.

To determine the angular relationship between the subunits in the crystal, self-rotation functions were carried out. The basis behind the self-rotation function is that the Patterson function contains two basic types of vectors: the intramolecular vectors due to atoms within each particular subunit within the asymmetric unit and the intermolecular vectors due to atoms in different subunits. The angular relationship between any two subunits can then be determined by rotating the Patterson function relative to itself until a point of maximum coincidence is reached. The polar rotation angles are shown below in Figure 6.20.

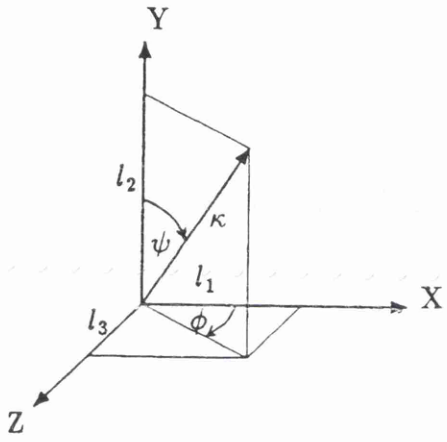

Figure 6.20 Polar rotation angles.

The self-rotation function was used to look for any non-crystallographic symmetry within our crystal. Non-crystallographic symmetry is derived from the arrangement of the molecules within the unit cell and can give an indication of the form of the subunit e.g. dimer or tetramer, whereas crystallographic symmetry is derived from the space group.

From the results in Table 6.1, rotation function correlation values were plotted onto a stereonet in order to view the results geometrically, using the program POLARRFM. This program looks at both the crystallographic and non-crystallographic symmetry of

the crystal. The ψ, ϕ and κ angles are clearly shown. Examples of these stereographic projections are given in Figures 6.21 and 6.22.

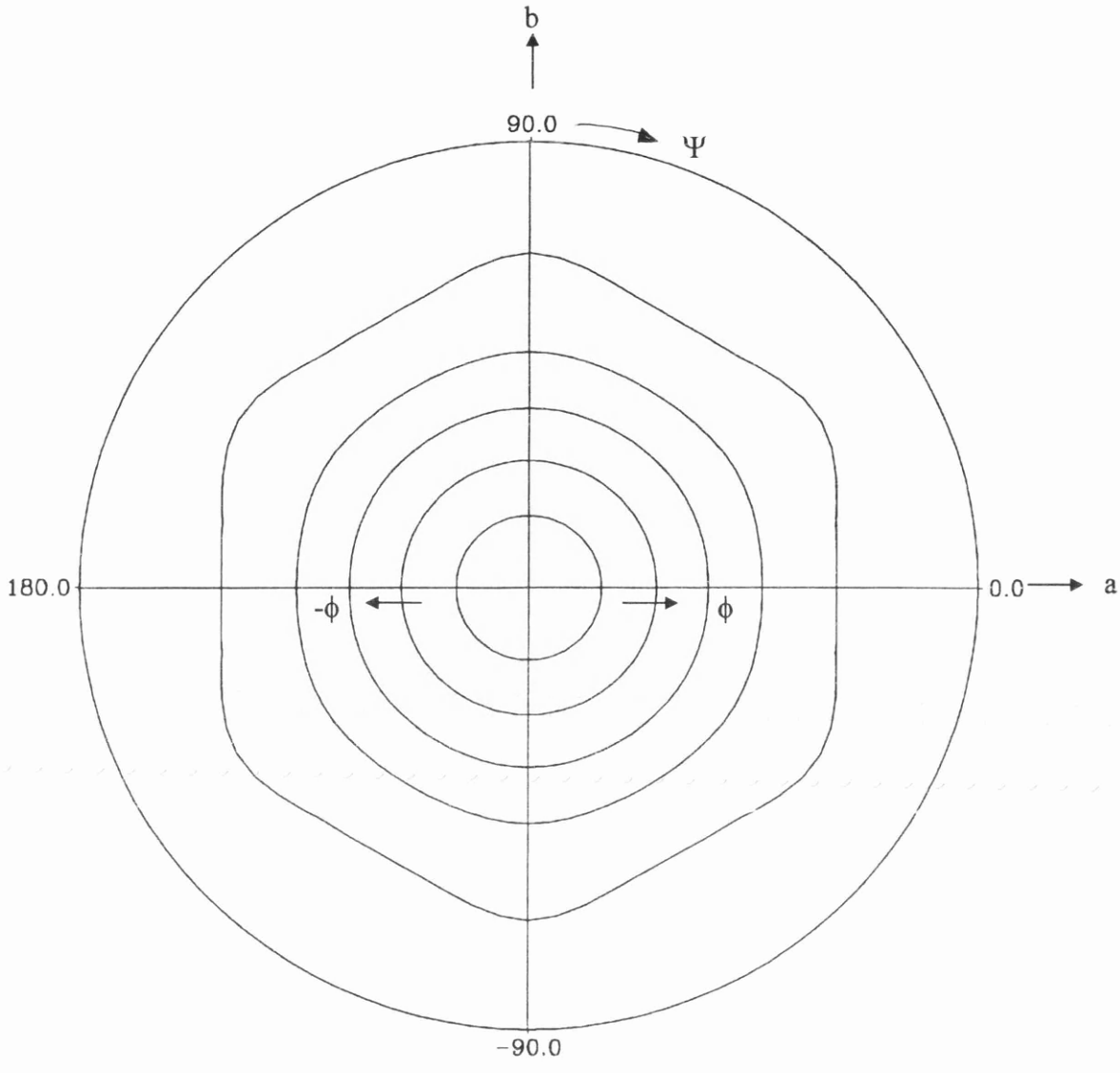

Figure 6.21 Stereographic projection down the c-axis of the $\kappa = 30°$ section of the real space rotation function.

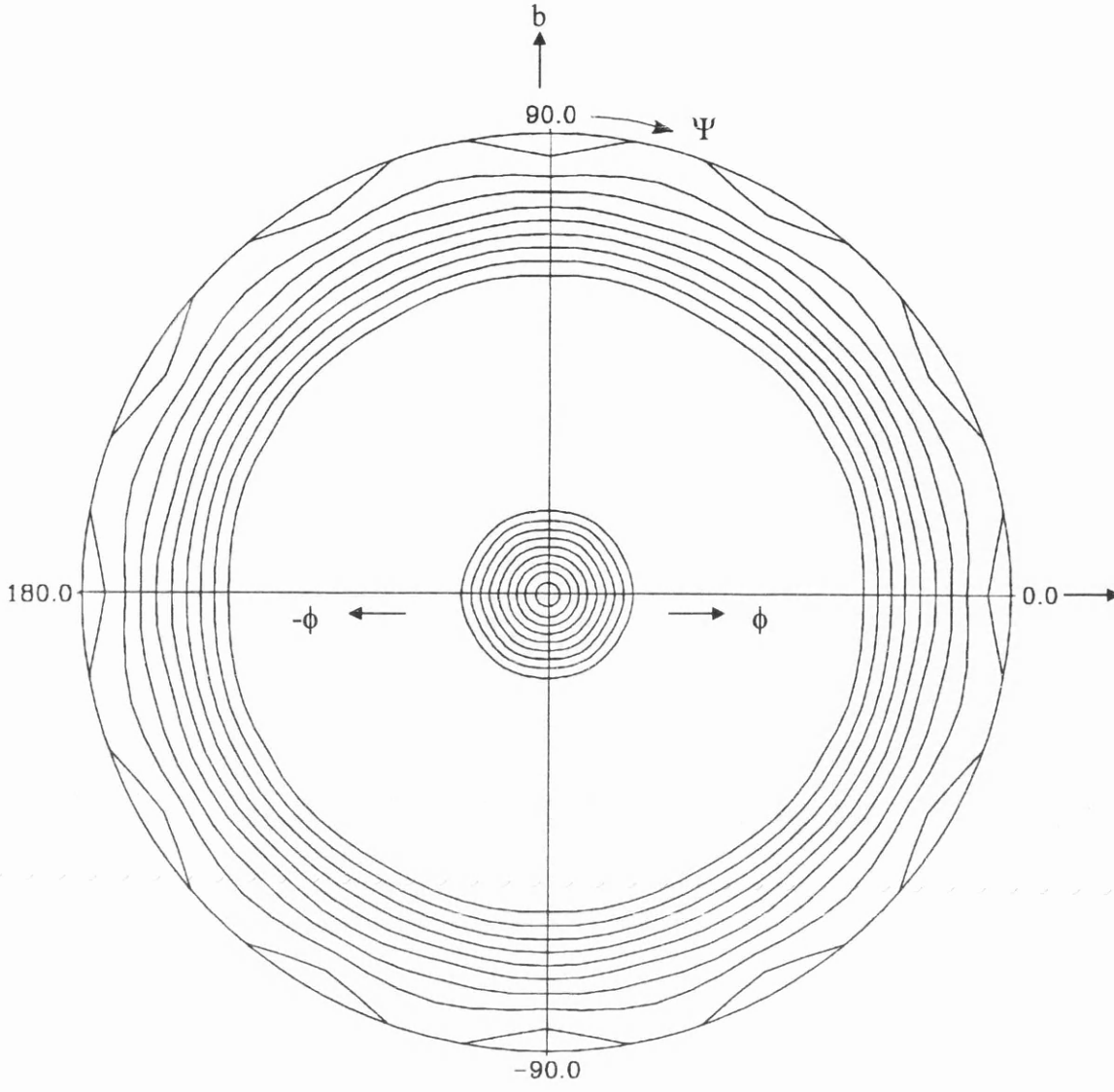

Figure 6.22 Stereographic projection down the c-axis of the $\kappa = 180°$ section of the real space rotation function.

The chi angle results in Table 6.1 indicate a four-fold axis of non-crystallographic symmetry due to the arrangement of the molecules within the asymmetric unit. In addition, the stereogram projection in Figure 6.21 suggests a six-fold axis of crystallographic symmetry, which is consistent with a correlation of 100 associated with this symmetry given in Table 6.1. Figure 6.22 suggests a possible additional twelve-fold axis of symmetry. The crystal symmetry changes with changes in these angles, therefore different stereogram projections can be produced for the same complex. In such diagrams, only the κ angle is quoted, the other two angles are represented in the two-dimensional plot. It would be convenient to suggest exactly where the non-crystallographic symmetry lay in relation to these stereonets, but when the non-crystallographic symmetry is coupled with high symmetry of the space groups, deconvoluting the information is almost impossible.

In our case, molecular replacement wasn't successful. There are thought to be two main reasons for this. One being that the model we used was only a small subunit of a much larger oligomer i.e. it was a monomer model with no complexed peptides, whereas our structure was of a dimer complexed with the cell wall analogue peptide, N-acetyl-D-Ala-D-Ala. Therefore, as mentioned in section 3.4, the more different the model is to the unknown structure, the more difficult the process of molecular replacement can be. However, since our work was carried out, the structure of the vancomycin dimer itself has been solved crystallographically (Schafer *et al.*, 1996) and even in this case, structure determination was not reached through molecular replacement, but rather from high powered direct method techniques. It may be worthwhile in the future to try molecular replacement with this model and our data, although our cell dimensions are far greater than those quoted for this work, so it is unclear how helpful this will actually be. In addition, the high symmetry space group for our vancomycin complex makes the structure difficult to solve with molecular replacement techniques, since there are so many ways the structure could be orientated within the unit cell, it is difficult to provide a 'match'. Further work would require considerable crystallographic effort, simply due to the size of the structure, however this was outwith the scope of this thesis. The

structure of the vancomycin complex is simply too large for conventional 'direct methods' and crystallises with too many molecules in the asymmetric unit for conventional protein techniques to be of any use. An alternative method could be to use heavy atom derivatives, but this in itself is fraught with difficulties, as discussed in section 3.3.2. If there are a large number of molecules within the asymmetric unit, as in our case, the heavy atoms may become liganded to each molecule, giving an extremely difficult Patterson to interpret.

Although at this stage, it is impossible to accurately model the way in which the vancomycin and peptide molecules are arranging themselves within the unit cell, it is possible that they are 'stacking' themselves in long chains, facilitated by the peptide, along the c-axis of the crystal. It appears that the presence of peptide is responsible for the significant enlargement of the unit cell dimensions, compared with the dimensions obtained in the absence of cell wall analogue peptides (Schafer *et al.*, 1996).

Appendix I

Automatic Indexing Program (IDXREF) Output

```
***** IDXREF *****          13-Jul-95

vancol. DIRECT HARVARD
 SPACE GROUP AND CELL PARAMETERS ARE UNKNOWN


 AUTOINDEXING IS BASED ON   2753 OBSERVED SPOT POSITIONS

 ***** DETERMINATION OF THE REDUCED CELL *****
 NUMBER OF DIFFERENCE VECTOR CLUSTERS USED                  57
 MINIMUM ALLOWED VALUE OF RECIPROCAL CELL VOLUME   0.1294E-07
 DIMENSION OF SPACE SPANNED BY DIFFERENCE VECTOR CLUSTERS   3

 PARAMETERS OF THE REDUCED CELL (ANGSTROEM & DEGREES)
     73.66     73.86    278.21     89.98     89.99     60.33

 INDICES OF DIFFERENCE VECTOR CLUSTERS WITH RESPECT TO REDUCED CELL
   #       DIFFERENCE VECTOR CLUSTER    FREQUENCY     REDUCED CELL INDICES
    1 -0.0001541-0.0000265 0.0035839      1541.      0.00      0.00      1.00
    2 -0.0003074-0.0000404 0.0071689      1518.      0.00      0.00      2.00
    3 -0.0004595-0.0000582 0.0107615      1435.      0.00      0.00      3.00
    4 -0.0006116-0.0000848 0.0143643      1412.      0.00      0.00      4.00
    5  0.0035315-0.0152602 0.0000663      1408.     -1.00     -1.00      0.00
    6 -0.0007609-0.0001059 0.0179557      1379.      0.00      0.00      5.00
    7  0.0032289-0.0153018 0.0072380      1370.     -1.00     -1.00      2.00
    8 -0.0038373 0.0152248 0.0071074      1369.      1.00      1.00      2.00
    9  0.0113506 0.0107118 0.0005424      1351.      1.00      0.00      0.00
   10  0.0033804-0.0152814 0.0036546      1348.     -1.00     -1.00      1.00

 ***** DETERMINATION OF LATTICE CHARACTER AND BRAVAIS LATTICE *****
 REFERENCE: INTERNATIONAL TABLES FOR CRYSTALLOGRAPHY Volume A,
            KLUWER ACADEMIC PUBLISHERS, DORDRECHT/BOSTON/LONDON
            Second, revised edition 1989, p. 746.
 COMMENTS:  LOW VALUES FOR THE "QUALITY OF FIT". TYPICALLY  BELOW 20,
 INDICATE THAT THE CORRESPONDING LATTICES WITH THE LISTED CELL CONSTANTS
 ARE COMPATIBLE WITH THE OBSERVED  DIFFRACTION SPOTS. THE RESULTS FOR
 THE 44 POSSIBLE CASES PRINTED BELOW ARE FOR YOUR INFORMATION AND NOT
 USED BY XDS AT THIS EARLY STAGE OF DATA PROCESSING.

 LATTICE-  BRAVAIS-   QUALITY  UNIT CELL CONSTANTS (ANGSTROEM & DEGREES)  REINDEXING CARD (CORRECT & GLOREP)
 CHARACTER LATTICE     OF FIT      a      b      c   alpha  beta gamma

     1        cF        999.0   287.9  306.0  287.9 151.4  29.8 151.5    1 -1  1  0  1  1 -1  0 -1  1  1  0
     2        hR        999.0    74.1  287.8  306.1 141.9  89.9  97.4    1 -1  0  0 -1  0  1  0 -1 -1 -1  0
     3        cP        999.0    73.7   73.9  278.2  90.0  90.0 119.7    1  0  0  0  0 -1  0  0  0  0 -1  0
     5        cI        999.0   287.8   74.1  287.8  82.6  25.6  82.7   -1  0 -1  0 -1  1  0  0  0  1 -1  0
     4        hR        999.0   127.5  287.8  287.9 154.3  89.9 102.8    1  1  0  0 -1  0 -1  0 -1  1  1  0
     6        tI        999.0   287.9  287.8   73.7  82.7  82.6  25.8    1 -1 -1  0  0  1 -1  0  1  0  0  0
     7        tI        999.0   287.8   73.7  287.9  82.6  25.8  82.7    0  1 -1  0  1  0  0  0  1 -1 -1  0
     8        oI        999.0    73.7  287.8  287.9  25.8  82.6  82.7   -1  0  0  0  0 -1  1  0 -1  1  1  0
     9        hR        750.4    73.7   74.1  844.3  90.0  97.5 120.0    1  0  0  0 -1  1  0  0 -1 -1  3  0
    10        mC          3.1   127.5   74.1  278.2  90.0  90.0  90.2    1  1  0  0  1 -1  0  0  0  0 -1  0
    11        tP        252.0    73.7   73.9  278.2  90.0  90.0 119.7   -1  0  0  0  0  1  0  0  0  0 -1  0
    12        hP *****    5.6    73.7   73.9  278.2  90.0  90.0 119.7   -1  0  0  0  0  1  0  0  0  0 -1  0
    13        oC          3.8    74.1  127.5  278.2  90.0  90.0  89.8   -1  1  0  0  1  1  0  0  0  0 -1  0
    15        tI        750.7    73.7   73.9  561.3  86.2  86.2 119.7   -1  0  0  0  0  1  0  0 -1  1 -2  0
    16        oP        757.7    73.7  128.3  561.3  90.0  97.5  89.8   -1  0  0  0 -1  2  0  0  1  0 -2  0
    14        mC          3.8    74.1  127.5  278.2  90.0  90.0  89.8   -1  1  0  0  1  1  0  0  0  0 -1  0
    17        mC        756.6   128.3   73.7  287.8  82.7 102.8  89.8   -1  2  0  0 -1  0  0  0  0 -1  1  0
    18        tI        999.0   287.8  287.9   73.7  82.6  97.3 154.2    0 -1  1  0  1 -1 -1  0  1  0  0  0
    19        oI        999.0    73.7  287.8  287.9  25.8  82.6  82.7   -1  0  0  0  0 -1  1  0 -1  1  1  0
    20        mC        999.0   287.9  287.8   73.7  97.3  97.3 150.3    0  1  1  0  0  1 -1  0 -1  0  0  0
    21        tP        999.0    73.9  278.2   73.7  90.0 119.7  90.0    0  1  0  0  0  0 -1  0 -1  0  0  0
    22        hP        999.0    73.9  278.2   73.7  90.0 119.7  90.0    0  1  0  0  0  0 -1  0 -1  0  0  0
    23        oC        999.0   287.8  287.9   73.7  82.7  97.3  29.7    0  1 -1  0  0 -1 -1  0 -1  0  0  0
    24        hR        999.0   306.3  287.9   73.7  82.6  90.1  38.4    1 -2  1  0 -1  1  1  0 -1  0  0  0
    25        mC        999.0   287.9  287.8   73.7  82.7  97.3  29.7    0 -1 -1  0  0  1 -1  0  1  0  0  0
    26        oP        622.8    73.7  128.3  561.3  90.0  97.5  90.2    1  0  0  0 -1  2  0  0 -1  0  2  0
    27        mC        498.4   128.3   73.7  287.8  82.7 102.8  89.8   -1  2  0  0 -1  0  0  0  0 -1  1  0
    28        mC        373.2    73.7  561.3   73.9  93.7 119.7  82.5   -1  0  0  0 -1  0  2  0  0  1  0  0
    29        mC          2.3    73.7  128.3  278.2  90.0  90.0  89.8    1  0  0  0  1 -2  0  0  0  0 -1  0
    30        mC        374.5    73.9  561.3   73.7  93.7 119.7  82.5    0  1  0  0  0  1 -2  0 -1  0  0  0
    31        aP          0.0    73.7   73.9  278.2  90.0  90.0  60.3    1  0  0  0  0  1  0  0  0  0  1  0
    32        oP        249.4    73.7   73.9  278.2  90.0  90.0 119.7   -1  0  0  0  0  1  0  0  0  0 -1  0
    40        oC        499.4    73.9  561.3   73.7  86.3 119.7  97.5    0 -1  0  0  0  1 -2  0  1  0  0  0
    35        mP        248.7    73.9   73.7  278.2  90.0  90.0 119.7    0 -1  0  0  1  0  0  0  0  0  1  0
    36        oC        499.3    73.7  561.3   73.9  86.3 119.7  97.5    1  0  0  0 -1  0  2  0  0 -1  0  0
    33        mP        249.1    73.7   73.9  278.2  90.0  90.0 119.7   -1  0  0  0  0  1  0  0  0  0 -1  0
    38        oC          3.0    73.7  128.3  278.2  90.0  90.0  90.2    1  0  0  0 -1  2  0  0  0  0  1  0
    34        mP          1.2    73.7  278.2   73.9  90.0 119.7  90.0    1  0  0  0  0  0  1  0  0 -1  0  0
```

```
   42        oI        749.4      73.7   73.9  561.3  93.8  93.8 119.7    1  0  0  0  0 -1  0  0 -1  1 -2  0
   41        mC        499.1      561.3  73.9   73.7 119.7  93.7  82.5    0 -1  2  0  0 -1  0  0  1  0  0  0
   37        mC        498.6      561.3  73.7   73.9 119.7  93.7  82.5    1  0 -2  0  1  0  0  0  0 -1  0  0
   39        mC          2.3      128.3  73.7  278.2  90.0  90.0  89.8    1 -2  0  0  1  0  0  0  0  0  1  0
   43        mI        999.0      73.7  561.3   73.9  93.7 119.7  82.5   -1  0  0  0 -1  0  2  0  0  1  0  0
   44        aP          0.3      73.7   73.9  278.2  90.0  90.0 119.7   -1  0  0  0  0  1  0  0  0  0 -1  0
```

AFTER ALL THE INDIVIDUAL PROGRAM STEPS HAVE BEEN CARRIED OUT SUCCESSFULLY
BY "XDS" (COLPROF,PROFIT,CORRECT,GLOREP) YOU SHOULD COME BACK AND READ THIS
FILE AGAIN IN CASE YOU DO NOT KNOW THE SPACE GROUP AND THE CELL CONSTANTS
OF YOUR CRYSTAL (AS SPECIFIED BY A ZERO FOR IGROUP IN "XDS.DATA").
INSPECT THE ABOVE TABLE OF FIT-VALUES FOR EACH POSSIBLE LATTICE AND PICK
THE ONE WITH HIGHEST LATTICE SYMMETRY WHICH HAS AN ACCEPTABLE QUALITY-OF-FIT VALUE.
USE YOUR EDITOR TO PICK THE APPROPRIATE LINE IN THIS TABLE AND TO
MOVE THE CELL CONSTANTS AND REINDEXING TRANSFORMATION TO THE PROPER LOCATION
IN "XDS.DATA". DO NOT FORGET TO CLEAN THE CELL CONSTANTS IF THE LATTICE
SYMMETRY REQUIRES EXACT 90 OR 120 DEGREES OR A=B, ETC.!!! THE POSSIBLE SPACE
GROUP NUMBERS CORRESPONDING TO EACH BRAVAIS-TYPE ARE GIVEN BELOW FOR YOUR
CONVENIENCE. FOR EXAMPLE THE BRAVAIS-TYPE hP INCLUDES ALL PRIMITIVE TRIGONAL
AND HEXAGONAL SPACE GROUPS. YOU HAVE TO TRY SEVERAL DIFFERENT SPACE GROUPS
BY RUNNING "CORRECT" AND "GLOREF" AND TO COMPARE THE OUTPUT TO FIND OUT
WHICH SYMMETRY ELEMENTS ARE PRESENT AND WHICH ARE NOT. (DO NOT FORGET TO
RENAME "CORRECT.LP". OTHERWISE IT WILL BE OVERWRITTEN BY THE NEXT RUN OF
"CORRECT"!) FOR EXAMPLE, A COMPARISON OF THE RESULTS FOR IGROUP=143 (P3)
AND IGROUP=168 (P6) SHOULD CLEARLY SHOW WHETHER YOU HAVE A TRIGONAL OR
HEXAGONAL SPACE GROUP. EXCEPT FOR THE PRESENCE OF SCREW-AXES, AT MOST 4
TRIALS ARE SUFFICIENT TO ESTABLISH THE CORRECT SYMMETRY GROUP. THE
PRESENCE OR ABSENCE OF SCREW-AXES CAN BE DEDUCED FROM THE INTENSITIES
OF THE REFLECTIONS OF TYPE h00,0k0,001 LISTED IN "CORRECT.LP".

BRAVAIS-TYPE	POSSIBLE SPACE-GROUPS FOR PROTEIN CRYSTALS (SPACE GROUP NUMBER.SYMBOL)
aP	[1,P1]
mP	[3,P2] [4,P2(1)]
mC,mI	[5,C2]
oP	[16,P222] [17,P222(1)] [18,P2(1)2(1)2] [19,P2(1)2(1)2(1)]
oC	[21,C222] [20,C222(1)]
oF	[22,F222]
oI	[23,I222] [24,I2(1)2(1)2(1)]
tP	[75,P4] [76,P4(1)] [77,P4(2)] [78,P4(3)] [89,P422] [90,P42(1)2] [91,P4(1)22] [92,P4(1)2(1)2] [93,P4(2)22] [94,P4(2)2(1)2] [95,P4(3)22] [96,P4(3)2(1)2]
tI	[79,I4] [80,I4(1)] [97,I422] [98,I4(1)22]
hP	[143,P3] [144,P3(1)] [145,P3(2)] [149,P312] [150,P321] [151,P3(1)12] [152,P3(1)21] [153,P3(2)12] [154,P3(2)21] [168,P6] [169,P6(1)] [170,P6(5)] [171,P6(2)] [172,P6(4)] [173,P6(3)] [177,P622] [178,P6(1)22] [179,P6(5)22] [180,P6(2)22] [181,P6(4)22] [182,P6(3)22]
hR	[146,R3] [155,R32]
cP	[195,P23] [198,P2(1)3] [207,P432] [208,P4(2)32] [212,P4(3)32] [213,P4(1)32]
cF	[196,F23] [209,F432] [210,F4(1)32]
cI	[197,I23] [199,I2(1)3] [211,I432] [214,I4(1)32]

***** REFINED SOLUTION IN SPACE GROUP P1 (#1) BASED ON THE REDUCED CELL *****

```
REFINED VALUES OF DIFFRACTION PARAMETERS DERIVED FROM   2411 INDEXED SPOTS
STANDARD DEVIATION OF SPOT    POSITION (PIXELS)      0.85
STANDARD DEVIATION OF SPINDLE POSITION (DEGREES)     0.02
DETECTOR ORIGIN (PIXELS) AT    266.91    243.10
CRYSTAL TO DETECTOR DISTANCE (mm)    250.00
LAB COORDINATES OF DETECTOR X-AXIS -0.342020 -0.939693  0.000000
LAB COORDINATES OF DETECTOR Y-AXIS  0.000000  0.000000  1.000000
DIRECT BEAM COORDINATES (REC. ANGSTROEM)  -0.648593  0.000000  0.000000
COORDINATES OF UNIT CELL A-AXIS    21.379    70.269     1.227
COORDINATES OF UNIT CELL B-AXIS   -50.078    53.710    -1.922
COORDINATES OF UNIT CELL C-AXIS   -12.299    -1.453   276.958
REC. CELL PARAMETERS   0.015725  0.015725  0.003607  90.059  89.909 120.037
UNIT CELL PARAMETERS     73.459    73.459   277.235  89.984  90.071  59.963
STANDARD DEVIATIONS       0.054     0.056     0.059   0.056   0.056   0.055
SPACE GROUP NUMBER      1
```

***** DIFFRACTION PARAMETERS USED AT START OF INTEGRATION *****

```
REFINED VALUES OF DIFFRACTION PARAMETERS DERIVED FROM   2719 INDEXED SPOTS
STANDARD DEVIATION OF SPOT    POSITION (PIXELS)      0.90
STANDARD DEVIATION OF SPINDLE POSITION (DEGREES)     0.02
DETECTOR ORIGIN (PIXELS) AT    266.97    243.13
```

```
CRYSTAL TO DETECTOR DISTANCE (mm)    250.00
LAB COORDINATES OF DETECTOR X-AXIS -0.342020 -0.939693  0.000000
LAB COORDINATES OF DETECTOR Y-AXIS  0.000000  0.000000  1.000000
DIRECT BEAM COORDINATES (REC. ANGSTROEM)  -0.648593  0.000000  0.000000
COORDINATES OF UNIT CELL A-AXIS    21.364    70.260     1.239
COORDINATES OF UNIT CELL B-AXIS   -50.077    53.703    -1.918
COORDINATES OF UNIT CELL C-AXIS   -12.448    -1.433   277.139
REC. CELL PARAMETERS   0.015728  0.015727  0.003605  90.086  89.900 120.044
UNIT CELL PARAMETERS     73.447    73.453   277.422  89.959  90.065  59.956
STANDARD DEVIATIONS       0.055     0.056     0.059   0.056   0.055   0.054
SPACE GROUP NUMBER        1

  NO ERROR. SOLUTION IS UNIQUE.

***** DETERMINATION OF LATTICE CHARACTER AND BRAVAIS LATTICE *****
THIS IS A REPEAT OF THE PREVIOUS LIST NOW BASED ON THE REFINED CELL CONSTANTS.
```

LATTICE-CHARACTER	BRAVAIS-LATTICE	QUALITY OF FIT	UNIT CELL CONSTANTS (ANGSTROEM & DEGREES) a	b	c	alpha	beta	gamma	REINDEXING CARD (CORRECT & GLOREF)											
1	cF	999.0	287.0	305.0	286.9	151.5	29.7	151.5	0	1	1	0	-2	1	-1	0	0	-1	1	0
2	hR	999.0	73.5	286.8	305.4	141.9	90.0	97.3	0	1	0	0	1	-1	1	0	2	-1	-1	0
3	cP	999.0	73.4	73.5	277.4	90.0	90.1	120.0	-1	0	0	0	0	1	0	0	0	0	-1	0
5	cI	999.0	286.9	73.4	286.9	82.8	25.6	82.8	-1	0	-1	0	-1	1	0	0	0	1	-1	0
4	hR	999.0	127.2	287.1	286.8	154.4	90.0	102.8	-1	-1	0	0	1	0	-1	0	1	-1	1	0
6	tI	999.0	286.9	286.9	73.4	82.8	82.8	25.6	0	1	-1	0	-1	0	-1	0	-1	1	0	0
7	tI	999.0	286.9	73.4	286.9	82.8	25.6	82.8	-1	0	-1	0	-1	1	0	0	0	1	-1	0
8	oI	999.0	73.4	286.9	286.9	25.6	82.8	82.8	1	-1	0	0	1	0	1	0	0	-1	1	0
9	hR	738.5	73.4	73.5	841.7	90.0	97.5	120.0	1	0	0	0	0	-1	0	0	-2	1	-3	0
10	mC	2.0	127.2	73.5	277.4	90.0	90.1	90.0	-2	1	0	0	0	1	0	0	0	0	-1	0
11	tP	254.7	73.5	73.4	277.4	90.1	90.0	120.0	0	-1	0	0	1	0	0	0	0	0	1	0
12	hP *****	4.6	73.5	73.4	277.4	90.1	90.0	120.0	0	-1	0	0	1	0	0	0	0	0	1	0
13	oC	4.3	73.4	127.2	277.4	90.0	90.1	90.0	1	-1	0	0	1	1	0	0	0	0	1	0
15	tI	747.6	73.4	73.5	559.5	86.3	86.3	120.0	-1	0	0	0	0	1	0	0	-1	1	-2	0
16	oF	739.2	73.4	127.2	559.5	90.0	97.4	90.0	1	-1	0	0	-1	-1	0	0	-1	1	-2	0
14	mC	1.6	73.4	127.2	277.4	90.0	90.1	90.0	1	-1	0	0	1	1	0	0	0	0	1	0
17	mC	738.5	127.2	73.4	286.9	82.8	102.8	90.0	-1	-1	0	0	1	-1	0	0	1	0	1	0
18	tI	999.0	286.8	287.0	73.4	82.7	97.3	154.4	-1	1	-1	0	0	1	1	0	1	0	0	0
19	oI	999.0	73.4	286.9	286.9	25.6	82.8	82.8	1	-1	0	0	1	0	1	0	0	-1	1	0
20	mC	999.0	287.1	286.9	73.4	97.2	97.4	150.3	-1	0	1	0	-1	0	-1	0	1	-1	0	0
21	tP	999.0	73.5	277.4	73.4	90.1	120.0	90.0	0	1	0	0	0	0	-1	0	-1	0	0	0
22	hP	999.0	73.4	277.4	73.5	90.0	120.0	90.1	-1	1	0	0	0	0	-1	0	0	-1	0	0
23	oC	999.0	286.9	287.1	73.5	82.7	97.4	29.7	1	0	1	0	-1	0	1	0	0	-1	0	0
24	hR	999.0	305.0	287.0	73.4	82.7	90.1	38.2	-1	2	-1	0	0	-1	-1	0	-1	0	0	0
25	mC	999.0	287.0	286.9	73.4	82.8	97.5	29.7	0	1	1	0	0	-1	1	0	1	-1	0	0
26	oF	612.9	73.4	127.2	559.6	89.9	97.5	90.0	1	0	0	0	1	-2	0	0	-1	0	-2	0
27	mC	491.4	127.2	73.4	286.8	82.7	102.7	90.0	1	-2	0	0	-1	0	0	0	-1	1	-1	0
28	mC	368.8	73.4	559.5	73.4	93.7	120.0	82.6	1	-1	0	0	1	-1	2	0	-1	0	0	0
29	mC	0.4	73.4	127.2	277.4	90.0	90.1	90.0	-1	1	0	0	1	1	0	0	0	0	-1	0
30	mC	369.1	73.4	559.6	73.4	93.7	120.0	82.5	-1	0	0	0	-1	0	-2	0	1	-1	0	0
31	aP	0.0	73.4	73.4	277.4	89.9	89.9	60.0	-1	1	0	0	-1	0	0	0	0	0	1	0
32	oP	254.6	73.5	73.4	277.4	90.1	90.0	120.0	0	-1	0	0	1	0	0	0	0	0	1	0
40	oC	499.3	73.4	559.5	73.5	86.3	120.0	97.4	1	-1	0	0	-1	1	-2	0	0	1	0	0
35	mP	252.4	73.4	73.5	277.4	90.0	90.1	120.0	-1	0	0	0	0	1	0	0	0	0	-1	0
36	oC	498.7	73.4	559.5	73.5	86.3	120.0	97.4	1	-1	0	0	-1	1	-2	0	0	1	0	0
33	mP	252.4	73.4	73.5	277.4	90.0	90.1	120.0	-1	0	0	0	0	1	0	0	0	0	-1	0
38	oC	4.5	73.5	127.2	277.4	89.9	90.0	90.0	0	1	0	0	2	-1	0	0	0	0	-1	0
34	mP	4.2	73.5	277.4	73.4	90.1	120.0	90.0	0	1	0	0	0	0	-1	0	-1	0	0	0
42	oI	747.6	73.5	73.4	559.5	93.7	93.7	120.0	0	1	0	0	-1	0	0	0	1	-1	2	0
41	mC	498.0	559.5	73.4	73.5	120.0	93.7	82.6	1	-1	2	0	1	-1	0	0	0	1	0	0
37	mC	497.4	559.5	73.4	73.5	120.0	93.7	82.6	1	-1	2	0	1	-1	0	0	0	1	0	0
39	mC	2.4	127.2	73.5	277.4	90.0	90.1	90.0	-2	1	0	0	0	1	0	0	0	0	-1	0
43	mI	985.4	73.4	559.5	73.4	93.7	120.0	82.6	1	-1	0	0	1	-1	2	0	-1	0	0	0
44	aP	0.7	73.5	73.4	277.4	90.1	90.0	120.0	0	-1	0	0	1	0	0	0	0	0	1	0

Appendix II

CORRECT Program Output

```
***** CORRECT *****          13-Jul-95
FIRST FRAME NUMBER    1
LAST  FRAME NUMBER  628
NAME ROOT OF FRAME FILES vancol. DIRECT HARVARD
SPINDLE POSITION AT START    0.000 DEGREES
OSCILLATION RANGE PER FRAME   0.10000
FILE NAME OF REFERENCE DATA SET:NONE
RADIUS (pixel) OF TRUSTED REGION ON DETECTOR FACE    265.0
LOW RESOLUTION LIMIT (ANGSTROEM) FOR ACCEPTING DATA  50.0
SPACE GROUP NUMBER OF CRYSTAL     182
MAXIMUM NUMBER OF FRAMES BETWEEN FRIEDEL RELATED REFLECTIONS
USED FOR COMPUTING ANOMALOUS DIFFERENCES       50


  15880 REFLECTIONS ON INPUT FILE
  15880 REFLECTIONS OCCURING ON DATA FRAMES     1 ...   628
      0 REFLECTIONS OUTSIDE TRUSTED REGION ON DETECTOR
    499 REFLECTIONS WITH A BAD PROFILE
  15381 REFLECTIONS ACCEPTED


*** REC. SCALING FACTORS AS FUNCTION OF DETECTOR POSITION AND FRAME NUMBER ***
REC. SCALING FACTORS ARE DETERMINED AT 9 POSITIONS ON THE DETECTOR SURFACE.
POSITION NUMBER         1      2      3      4      5      6      7      8      9
X-COORDINATE (pixel)  256.0  453.5  395.7  256.0  116.3   58.5  116.3  256.0  395.7
Y-COORDINATE (pixel)  256.0  256.0  395.7  453.5  395.7  256.0  116.3   58.5  116.3
NUMBER OF ACCEPTED OBSERVATIONS       10125
NUMBER OF REJECTED OBSERVATIONS           0
NUMBER OF REFERENCE REFLECTIONS USED      0
The reciprocal scaling factors printed below were determined from
intensities already corrected by the scaling factors printed above.
Accuracy of scaling factors is  0.000001
Rank of normal matrix    281
      SCALING FACTORS
FRAME-                              POSITION NUMBER
NUMBER      1      2      3      4      5      6      7      8      9
 13.6   0.9934 0.9896 0.9906 0.9938 0.9946 0.9939 0.9962 0.9964 0.9940
 38.7   0.9974 0.9921 0.9941 0.9988 0.9988 0.9942 1.0041 1.0088 1.0041
 63.8   1.0004 0.9970 0.9950 0.9994 0.9985 0.9928 1.0047 1.0139 1.0149
 88.9   1.0035 1.0029 0.9953 0.9970 0.9937 0.9964 1.0066 1.0133 1.0191
114.0   1.0068 1.0008 0.9931 0.9929 0.9948 1.0081 1.0073 1.0105 1.0096
139.2   1.0058 0.9974 0.9920 0.9905 1.0004 1.0098 1.0000 1.0056 0.9992
164.3   1.0025 0.9955 0.9934 0.9911 1.0063 1.0044 0.9935 1.0019 0.9934
189.4   0.9993 0.9982 0.9945 0.9905 1.0079 0.9936 0.9961 1.0067 0.9997
214.5   0.9998 1.0048 0.9925 0.9905 1.0015 0.9923 1.0055 1.0131 1.0119
239.6   0.9981 1.0083 0.9946 0.9911 0.9968 0.9941 1.0101 1.0175 1.0198
264.8   0.9993 1.0060 0.9966 0.9937 0.9961 1.0082 1.0086 1.0148 1.0170
289.9   0.9994 0.9975 0.9946 0.9922 0.9952 1.0078 1.0042 1.0075 1.0065
315.0   1.0017 0.9972 0.9931 0.9918 0.9977 1.0100 1.0005 1.0026 1.0002
340.1   0.9998 1.0031 0.9947 0.9912 0.9963 1.0025 0.9963 1.0005 1.0020
365.2   0.9959 1.0067 0.9978 0.9932 0.9895 0.9892 0.9950 1.0065 1.0058
390.4   0.9968 1.0064 0.9939 0.9899 0.9910 0.9914 1.0058 1.0138 1.0096
415.5   0.9983 1.0048 0.9904 0.9825 0.9934 1.0059 1.0084 1.0127 1.0109
440.6   0.9975 1.0011 0.9944 0.9847 0.9954 1.0084 1.0005 1.0046 1.0072
465.7   0.9961 0.9983 0.9975 0.9891 0.9979 1.0034 1.0009 1.0047 1.0033
490.8   0.9952 1.0028 0.9993 0.9917 0.9955 1.0030 1.0079 1.0088 1.0023
516.0   0.9963 1.0075 1.0007 0.9906 0.9936 1.0050 1.0142 1.0119 1.0069
541.1   1.0045 1.0078 0.9983 0.9939 1.0046 1.0138 1.0133 1.0163 1.0133
566.2   1.0060 1.0014 0.9899 0.9897 1.0014 1.0089 1.0064 1.0155 1.0122
591.3   1.0026 0.9918 0.9807 0.9861 0.9954 0.9963 0.9941 1.0030 1.0028
616.4   1.0003 0.9868 0.9720 0.9857 0.9982 0.9958 0.9805 0.9906 0.9950

 FINAL    SCALING FACTOR APPLIED TO REFERENCE DATA SET   1.000000


***** STATISTICAL INFORMATION ABOUT DATA OCCURING ON FRAMES    1 ...  628 *****

THE FOLLOWING OUTPUT IS REPEATED SEVERAL TIMES WITH DIFFERENT UPPER LIMIT
ON THE NUMBER OF FRAMES INCLUDED. IT PROVIDES THE USER WITH THE INFORMATION
NECESSARY TO MAKE HIS CHOICE OF THE BEST LAST FRAME NUMBER. IF THIS NUMBER
DIFFERS FROM THAT ON THE DATA CARDS THE 'CORRECT'-STEP MUST BE RERUN.


    ------- REFLECTIONS OF TYPE H,0,0  0,K,0  0,0,L -------
  H    K    L  RESOLUTION  INTENSITY     SIGMA    INTENSITY/SIGMA  #OBSERVED
```

8	0	0	7.978	0.5220E+03	0.9339E+02	5.59	1
9	0	0	7.092	0.1810E+05	0.5861E+03	30.89	1
10	0	0	6.383	0.1495E+04	0.1460E+03	10.24	1
11	0	0	5.802	0.2189E+03	0.1231E+03	1.78	1
12	0	0	5.319	0.7690E+04	0.3586E+03	21.44	1
13	0	0	4.910	0.7755E+04	0.3871E+03	20.03	1
14	0	0	4.559	0.2926E+05	0.9725E+03	30.09	1
16	0	0	3.989	0.3039E+03	0.2127E+03	1.43	1
17	0	0	3.754	0.8265E+04	0.4539E+03	18.21	1
18	0	0	3.546	0.7435E+04	0.4748E+03	15.66	1
19	0	0	3.359	0.0000E+00	0.2723E+03	0.00	1
20	0	0	3.191	0.0000E+00	0.2653E+03	0.00	1
21	0	0	3.039	0.1862E+04	0.3512E+03	5.30	1
22	0	0	2.901	0.3834E+03	0.3211E+03	1.19	1

======= REFLEX DISTRIBUTIONS =======

NUMBER OF ACCEPTED REFLECTIONS AS FUNCTION OF INTENSITY
SIGNAL/NOISE-RATIO (horizontally) AND (2*SIN(THETA)/LAMBDA)**2 (downwards)

	0 ... 3	3 ... 6	6 ... 9	9 ... 12	12 ... 15
0.000 ... 0.025	96	123	131	105	518
0.025 ... 0.050	570	659	581	532	1373
0.050 ... 0.075	805	835	714	538	1257
0.075 ... 0.100	1630	1060	722	415	270
0.100 ... 0.125	1727	524	164	21	11

NUMBER OF UNIQUE REFLECTIONS AS FUNCTION OF INTENSITY
SIGNAL/NOISE-RATIO (horizontally) AND (2*SIN(THETA)/LAMBDA)**2 (downwards)

	0 ... 3	3 ... 6	6 ... 9	9 ... 12	12 ... 15
0.000 ... 0.025	17	28	20	31	220
0.025 ... 0.050	92	120	103	113	677
0.050 ... 0.075	139	149	122	120	678
0.075 ... 0.100	257	250	191	136	352
0.100 ... 0.125	337	238	106	47	42

======= SYMMETRY R-FACTORS OF THIS DATA SET =======

DEFINITION OF SYMMETRY R-FACTOR USED :
(SUM(ABS(I(h,i)-I(h))))/(SUM(I(h,i)))

R-FACTORS FOR REFLECTION INTENSITIES LARGER THAN A GIVEN SIGNAL/NOISE-RATIO

SIGNAL/NOISE	R-FACTOR	NUMBER OF REFLECTIONS
0	6.4%	15041
3	5.3%	10340
6	4.6%	7195
9	4.1%	4925
12	3.8%	3348

R-FACTORS FOR REFLECTION INTENSITIES AS FUNCTION OF RESOLUTION

(2*SIN(THETA)/LAMBDA)**2	R-FACTOR	NUMBER OF REFLECTIONS
0.000 ... 0.025	3.7%	945
0.025 ... 0.050	5.0%	3640
0.050 ... 0.075	5.5%	4083
0.075 ... 0.100	9.1%	4018
0.100 ... 0.125	18.1%	2355

======= COMPLETENESS OF DATA SET =======

COMPLETENESS OF DATA SET AS FUNCTION OF RESOLUTION

(2*SIN(THETA)/LAMBDA)**2	NUMBER OF UNIQUE OBSERVED REFLECTIONS	NUMBER OF UNIQUE POSSIBLE REFLECTIONS	COMPLETENESS OF DATA
0.000 ... 0.025	316	1191	26.5%
0.025 ... 0.050	1105	1950	56.7%
0.050 ... 0.075	1208	2424	49.8%
0.075 ... 0.100	1186	2823	42.0%
0.100 ... 0.125	770	3141	24.5%

TOTAL NUMBER OF REFLECTIONS OCCURING ON FRAMES 1 ... 628 IS 15381
NUMBER OF REJECTED MISFITS 0
NUMBER OF SYSTEMATIC ABSENT REFLECTIONS 0
NUMBER OF REFLECTIONS ON LONG OUTPUT FILE 15381
NUMBER OF UNIQUE REFLECTIONS ON SHORT OUTPUT FILE 4585

Appendix III

Global Refinement Program (GLOREF) Output

```
***** GLOREF *****        13-Jul-95
NAME ROOT OF FRAME FILES vancol. DIRECT HARVARD
WAVELENGTH (ANGSTROEM)  1.54180
DIRECT BEAM DIRECTION (SOURCE TOWARDS CRYSTAL)  -1.000000  0.000000  0.000000
FIRST FRAME NUMBER    1
LAST  FRAME NUMBER  628
SPINDLE POSITION AT START    0.000 DEGREES
OSCILLATION RANGE PER FRAME   0.10000
COORDINATES OF ROTATION AXIS   0.000000  0.000000 -1.000000
CRYSTAL TO DETECTOR DISTANCE (mm)    250.00
DETECTOR ORIGIN (PIXELS) AT    262.00    243.00
LAB COORDINATES OF DETECTOR X-AXIS -0.342020 -0.939693  0.000000
LAB COORDINATES OF DETECTOR Y-AXIS  0.000000  0.000000  1.000000
SPACE GROUP NUMBER OF CRYSTAL     182
UNIT CELL PARAMETERS     73.700    73.700   278.200  90.000  90.000 120.000
RADIUS (pixel) OF TRUSTED REGION ON DETECTOR FACE    265.0
LOW RESOLUTION LIMIT (ANGSTROEM) FOR ACCEPTING DATA   50.0
MINIMUM SIGNAL/NOISE-RATIO FOR ACCEPTING REFLECTIONS   3.0


  15880 REFLECTIONS ON INPUT FILE
  15880 REFLECTIONS OCCURING ON DATA FRAMES     1 ...   628
      0 REFLECTIONS OUTSIDE TRUSTED REGION ON DETECTOR
    499 REFLECTIONS WITH A BAD PROFILE
   6550 WEAK REFLECTIONS
   8831 REFLECTIONS ACCEPTED


========== REFINE DIRECT BEAM, ORIENTATION, AND  CELL PARAMETERS ==========


REFINED VALUES OF DIFFRACTION PARAMETERS DERIVED FROM   8831 INDEXED SPOTS
STANDARD DEVIATION OF SPOT    POSITION (PIXELS)     1.25
STANDARD DEVIATION OF SPINDLE POSITION (DEGREES)    0.02
DETECTOR ORIGIN (PIXELS) AT    276.14    245.90
CRYSTAL TO DETECTOR DISTANCE (mm)    250.00
LAB COORDINATES OF DETECTOR X-AXIS -0.335443 -0.942058  0.002342
LAB COORDINATES OF DETECTOR Y-AXIS  0.006982  0.000000  0.999976
DIRECT BEAM COORDINATES (REC. ANGSTROEM)  -0.648578  0.000000  0.004340
COORDINATES OF UNIT CELL A-AXIS   -21.415   -70.297    -0.833
COORDINATES OF UNIT CELL B-AXIS   -50.130    53.709    -1.840
COORDINATES OF UNIT CELL C-AXIS    10.310     0.140  -276.764
REC. CELL PARAMETERS   0.015712  0.015712  0.003611  90.000  90.000  60.000
UNIT CELL PARAMETERS     73.492    73.492   276.956  90.000  90.000 120.000
STANDARD DEVIATIONS       0.003     0.003     0.016   0.000   0.000   0.000
SPACE GROUP NUMBER    182


========== REFINE ORIGIN, DISTANCE AND ORIENTATION OF THE DETECTOR ==========


REFINED VALUES OF DIFFRACTION PARAMETERS DERIVED FROM   8831 INDEXED SPOTS
STANDARD DEVIATION OF SPOT    POSITION (PIXELS)     1.10
STANDARD DEVIATION OF SPINDLE POSITION (DEGREES)    0.04
DETECTOR ORIGIN (PIXELS) AT    270.81    240.95
CRYSTAL TO DETECTOR DISTANCE (mm)    249.95
LAB COORDINATES OF DETECTOR X-AXIS -0.339182 -0.940716  0.002970
LAB COORDINATES OF DETECTOR Y-AXIS  0.001369  0.002663  0.999996
DIRECT BEAM COORDINATES (REC. ANGSTROEM)  -0.648590  0.000000  0.001778
COORDINATES OF UNIT CELL A-AXIS   -21.412   -70.297    -0.918
COORDINATES OF UNIT CELL B-AXIS   -50.122    53.709    -2.038
COORDINATES OF UNIT CELL C-AXIS    11.403     0.140  -276.721
REC. CELL PARAMETERS   0.015712  0.015712  0.003611  90.000  90.000  60.000
UNIT CELL PARAMETERS     73.492    73.492   276.956  90.000  90.000 120.000
STANDARD DEVIATIONS       0.000     0.000     0.000   0.000   0.000   0.000
SPACE GROUP NUMBER    182


========== REFINE DIRECT BEAM, ORIENTATION, AND  CELL PARAMETERS ==========


REFINED VALUES OF DIFFRACTION PARAMETERS DERIVED FROM   8831 INDEXED SPOTS
STANDARD DEVIATION OF SPOT    POSITION (PIXELS)     0.83
STANDARD DEVIATION OF SPINDLE POSITION (DEGREES)    0.02
DETECTOR ORIGIN (PIXELS) AT    273.67    244.66
CRYSTAL TO DETECTOR DISTANCE (mm)    249.95
LAB COORDINATES OF DETECTOR X-AXIS -0.337462 -0.941332  0.003585
```

```
LAB COORDINATES OF DETECTOR Y-AXIS  0.003186  0.002666  0.999991
DIRECT BEAM COORDINATES (REC. ANGSTROEM)  -0.648591  0.000000  0.001574
COORDINATES OF UNIT CELL A-AXIS   -21.402   -70.230    -0.967
COORDINATES OF UNIT CELL B-AXIS   -50.070    53.668    -1.980
COORDINATES OF UNIT CELL C-AXIS    11.336     0.360  -276.916
REC. CELL PARAMETERS   0.015726  0.015726  0.003608  90.000  90.000  60.000
UNIT CELL PARAMETERS     73.425    73.425   277.148  90.000  90.000 120.000
STANDARD DEVIATIONS       0.001     0.001     0.005   0.000   0.000   0.000
SPACE GROUP NUMBER    182

========== REFINE ORIGIN, DISTANCE AND ORIENTATION OF THE DETECTOR ==========

REFINED VALUES OF DIFFRACTION PARAMETERS DERIVED FROM   8831 INDEXED SPOTS
STANDARD DEVIATION OF SPOT    POSITION (PIXELS)      0.80
STANDARD DEVIATION OF SPINDLE POSITION (DEGREES)     0.03
DETECTOR ORIGIN (PIXELS) AT    271.86    239.34
CRYSTAL TO DETECTOR DISTANCE (mm)    249.96
LAB COORDINATES OF DETECTOR X-AXIS -0.338737 -0.940874  0.003641
LAB COORDINATES OF DETECTOR Y-AXIS -0.001435  0.004387  0.999989
DIRECT BEAM COORDINATES (REC. ANGSTROEM)  -0.648592  0.000000  0.000707
COORDINATES OF UNIT CELL A-AXIS   -21.400   -70.230    -0.996
COORDINATES OF UNIT CELL B-AXIS   -50.067    53.668    -2.047
COORDINATES OF UNIT CELL C-AXIS    11.706     0.360  -276.900
REC. CELL PARAMETERS   0.015726  0.015726  0.003608  90.000  90.000  60.000
UNIT CELL PARAMETERS     73.425    73.425   277.148  90.000  90.000 120.000
STANDARD DEVIATIONS       0.000     0.000     0.000   0.000   0.000   0.000
SPACE GROUP NUMBER    182

========== REFINE DIRECT BEAM, ORIENTATION, AND  CELL PARAMETERS ==========

REFINED VALUES OF DIFFRACTION PARAMETERS DERIVED FROM   8831 INDEXED SPOTS
STANDARD DEVIATION OF SPOT    POSITION (PIXELS)      0.81
STANDARD DEVIATION OF SPINDLE POSITION (DEGREES)     0.02
DETECTOR ORIGIN (PIXELS) AT    272.89    240.34
CRYSTAL TO DETECTOR DISTANCE (mm)    249.96
LAB COORDINATES OF DETECTOR X-AXIS -0.337996 -0.941140  0.003907
LAB COORDINATES OF DETECTOR Y-AXIS -0.000654  0.004386  0.999990
DIRECT BEAM COORDINATES (REC. ANGSTROEM)  -0.648592  0.000000  0.001002
COORDINATES OF UNIT CELL A-AXIS   -21.401   -70.236    -0.963
COORDINATES OF UNIT CELL B-AXIS   -50.072    53.670    -2.056
COORDINATES OF UNIT CELL C-AXIS    11.638     0.250  -276.931
REC. CELL PARAMETERS   0.015725  0.015725  0.003608  90.000  90.000  60.000
UNIT CELL PARAMETERS     73.430    73.430   277.175  90.000  90.000 120.000
STANDARD DEVIATIONS       0.001     0.001     0.004   0.000   0.000   0.000
SPACE GROUP NUMBER    182
```

Appendix IV

XSCALE Program Output

```
     182     73.50     73.50    277.00   90.000   90.000  120.000
 XDS.HKL_1    DIRECT  30.0 2.0 50 8
 XDS.HKL_2    DIRECT  30.0 2.0 50 8
 XDS.HKL_3    DIRECT  30.0 2.0 50 8
 XDS.HKL_4    DIRECT  30.0 2.0 50 8
 XDS.HKL_5    DIRECT  30.0 2.0 50 8
 XDS.HKL_6    DIRECT  30.0 2.0 50 8
 XDS.HKL_7    DIRECT  30.0 2.0 50 8

ALL DATA SETS WILL BE SCALED TO XDS.HKL_1


       ======= B-FACTOR DETERMINATION =======
CORRELATION      = Initial correlation factor between common intensities
                   from two data sets at B-FACTOR=0.
B-FACTOR         = A B-FACTOR B between data sets i,j is determined to maximize
                   the correlation between I(i)*exp(B*SS) and I(j), where
                   I(i),I(j) are intensities of a common reflection in data sets
                   i,j and SS is (2*sin(theta)/lambda)**2.
B-FACTOR WEIGHT  = Standard deviation of the distribution of SS-values
                   of the common reflections from two data sets.

DATA SETS   NUMBER OF COMMON   CORRELATION      B-FACTOR        B-FACTOR
 #i   #j      REFLECTIONS     BETWEEN i,j     BETWEEN i,j       WEIGHT
  2    1            429          0.997       -0.20611E+01    0.5508E-02
  3    1            876          0.995        0.26631E+01    0.1123E-01
  4    1           3650          0.982        0.32213E+00    0.2634E-01
  5    1            213          0.995       -0.32208E+01    0.8511E-02
  6    1            264          0.992       -0.19895E+01    0.1098E-01
  7    1            606          0.995       -0.29401E+01    0.5446E-02
  1    2            429          0.997        0.13253E+01    0.5508E-02
  3    2            213          0.999        0.48298E+00    0.6818E-02
  4    2            507          0.991       -0.29034E-02    0.5693E-02
  5    2            177          0.994        0.87999E+00    0.4766E-02
  6    2            138          0.994       -0.21829E+01    0.5025E-02
  7    2            613          0.998       -0.31627E+01    0.8540E-02
  1    3            876          0.995       -0.27826E+01    0.1123E-01
  2    3            213          0.999       -0.19521E+01    0.6818E-02
  4    3            978          0.986        0.19565E+00    0.1137E-01
  5    3            244          0.989       -0.64999E+01    0.8411E-02
  6    3            301          0.990       -0.50108E+01    0.8810E-02
  7    3            497          0.998       -0.34304E+01    0.8273E-02
  1    4           3650          0.982       -0.71546E+00    0.2634E-01
  2    4            507          0.991       -0.23237E+01    0.5693E-02
  3    4            978          0.986       -0.53919E+00    0.1137E-01
  5    4           1108          0.966       -0.25083E+01    0.2077E-01
  6    4           1015          0.961       -0.25797E+01    0.2306E-01
  7    4            613          0.983       -0.42968E+01    0.5552E-02
  1    5            213          0.995        0.31513E+01    0.8331E-02
  2    5            177          0.994       -0.12143E+01    0.4766E-02
  3    5            244          0.989        0.72807E+01    0.8411E-02
  4    5           1108          0.966        0.13529E+01    0.2077E-01
  6    5           2514          0.997        0.24843E+00    0.2782E-01
  7    5            102          0.994       -0.77884E+01    0.4584E-02
  1    6            264          0.992        0.19276E+01    0.1098E-01
  2    6            138          0.994        0.11736E+01    0.5025E-02
  3    6            301          0.990        0.54512E+01    0.8810E-02
  4    6           1015          0.961        0.12970E+01    0.2306E-01
  5    6           2514          0.997       -0.35552E+00    0.2782E-01
  7    6            130          0.994       -0.26173E+01    0.4981E-02
```

1	7	606	0.995	0.21078E+01	0.5446E-02
2	7	613	0.998	0.24986E+01	0.8540E-02
3	7	497	0.998	0.32685E+01	0.8273E-02
4	7	613	0.983	0.12740E+01	0.5552E-02
5	7	102	0.994	0.68910E+01	0.4584E-02
6	7	130	0.994	0.71600E+00	0.4981E-02

======= SCALE-FACTOR DETERMINATION =======
CORRELATION = Final correlation factor between common intensities from two data sets after B-FACTOR correction
E.S.D. OF RATIO = Estimated standard deviation of the ratio between common intensities from two data sets

DATA SETS #i	#j	NUMBER OF COMMON REFLECTIONS	CORRELATION BETWEEN i,j	RATIO OF COMMON INTENSITIES (i/j)	E.S.D. OF RATIO
1	2	429	0.997	0.15873E+01	0.6472E-02
1	3	876	0.996	0.14098E+01	0.4222E-02
1	4	3650	0.982	0.22688E+00	0.3070E-03
1	5	213	0.996	0.65694E+00	0.3798E-02
1	6	264	0.993	0.72471E+00	0.4394E-02
1	7	606	0.996	0.25619E+01	0.1092E-01
2	3	213	0.999	0.89214E+00	0.5978E-02
2	4	507	0.991	0.14220E+00	0.4821E-03
2	5	177	0.994	0.42181E+00	0.2401E-02
2	6	138	0.994	0.45983E+00	0.3567E-02
2	7	613	0.998	0.16416E+01	0.5224E-02
3	4	978	0.985	0.16068E+00	0.4206E-03
3	5	244	0.992	0.46467E+00	0.2434E-02
3	6	301	0.992	0.50730E+00	0.2653E-02
3	7	497	0.999	0.18205E+01	0.7733E-02
4	5	1108	0.968	0.28936E+01	0.6879E-02
4	6	1015	0.962	0.31817E+01	0.9644E-02
4	7	613	0.984	0.11527E+02	0.4758E-01
5	6	2514	0.997	0.11137E+01	0.2243E-02
5	7	102	0.994	0.39244E+01	0.5070E-01
6	7	130	0.994	0.36246E+01	0.4178E-01

CORRECTION-FACTOR APPLIED TO EACH DATA SET IS K*EXP(B*SS)

K	B	DATA SET NAME
1.000000	0.000	XDS.HKL_1
1.581638	-0.295	XDS.HKL_2
1.413497	1.672	XDS.HKL_3
0.226646	0.542	XDS.HKL_4
0.654597	-1.661	XDS.HKL_5
0.725500	-1.395	XDS.HKL_6
2.588691	-2.594	XDS.HKL_7

*** REC. SCALING FACTORS AS FUNCTION OF DETECTOR POSITION AND FRAME NUMBER ***
REC. SCALING FACTORS ARE DETERMINED AT 9 POSITIONS ON THE DETECTOR SURFACE.

POSITION NUMBER	1	2	3	4	5	6	7	8	9
X-COORDINATE (pixel)	256.0	453.5	395.7	256.0	116.3	58.5	116.3	256.0	395.7
Y-COORDINATE (pixel)	256.0	256.0	395.7	453.5	395.7	256.0	116.3	58.5	116.3

NUMBER OF ACCEPTED OBSERVATIONS 44606
NUMBER OF REJECTED OBSERVATIONS 7
The reciprocal scaling factors printed below were determined from intensities already corrected by the scaling factors printed above.

Accuracy of scaling factors is 0.000030
Number of cycles carried out 3
Rank of normal matrix 503

SCALING FACTORS FOR DATA SET XDS.HKL_1

FRAME-NUMBER	POSITION NUMBER 1	2	3	4	5	6	7	8	9
42.0	1.0043	1.0045	0.9997	0.9925	0.9869	1.0001	0.9940	1.0027	1.0110
120.0	1.0093	1.0036	1.0006	0.9981	0.9979	1.0095	0.9991	1.0041	1.0074
198.0	1.0135	1.0026	0.9970	1.0012	1.0086	1.0153	1.0064	1.0065	1.0047
276.0	1.0117	1.0028	0.9959	1.0017	1.0115	1.0175	1.0107	1.0097	1.0055
354.0	1.0088	1.0074	1.0011	1.0005	1.0071	1.0139	1.0080	1.0086	1.0118
432.0	1.0040	1.0137	1.0055	0.9952	0.9954	1.0071	0.9986	1.0006	1.0124
510.0	0.9976	1.0130	1.0016	0.9880	0.9834	1.0034	0.9880	0.9918	1.0089
588.0	0.9977	1.0119	0.9983	0.9847	0.9753	0.9973	0.9809	0.9860	1.0095

SCALING FACTORS FOR DATA SET XDS.HKL_2

FRAME-NUMBER	POSITION NUMBER 1	2	3	4	5	6	7	8	9
20.7	0.9977	0.9768	0.9961	0.9886	0.9741	0.9513	0.9712	0.9962	0.9939
56.1	1.0070	1.0017	1.0103	1.0009	0.9931	0.9802	0.9908	1.0065	1.0071
91.4	1.0072	0.9999	1.0084	0.9992	1.0106	1.0187	1.0039	1.0044	0.9950
126.8	0.9971	0.9998	1.0032	0.9981	1.0132	1.0261	1.0102	1.0018	0.9945
162.2	0.9929	1.0088	0.9989	0.9934	1.0105	1.0164	1.0080	0.9990	1.0034
197.6	0.9947	1.0151	0.9952	0.9948	1.0101	1.0173	1.0090	0.9999	1.0130
232.9	0.9983	1.0184	0.9956	1.0029	1.0114	1.0142	1.0098	1.0029	1.0188
268.3	0.9986	1.0205	0.9962	1.0082	1.0099	1.0100	1.0056	1.0069	1.0220

SCALING FACTORS FOR DATA SET XDS.HKL_3

FRAME-NUMBER	POSITION NUMBER 1	2	3	4	5	6	7	8	9
18.3	0.9704	0.9402	0.9606	0.9666	0.9740	0.9741	0.9861	0.9868	0.9645
46.8	0.9905	0.9629	0.9841	0.9884	0.9967	0.9938	0.9978	1.0058	0.9908
75.3	1.0083	1.0106	1.0057	1.0049	1.0087	1.0092	1.0098	1.0169	1.0144
103.8	1.0035	1.0044	1.0032	1.0072	1.0144	1.0179	1.0149	1.0150	1.0092
132.3	1.0027	1.0003	0.9959	1.0040	1.0176	1.0229	1.0159	1.0120	1.0043
160.8	0.9990	0.9917	0.9976	1.0074	1.0142	1.0242	1.0168	1.0113	1.0041
189.3	0.9943	0.9812	1.0028	1.0125	1.0043	1.0248	1.0192	1.0053	0.9984
217.8	0.9919	0.9854	1.0006	1.0122	0.9959	1.0179	1.0161	1.0009	0.9981

SCALING FACTORS FOR DATA SET XDS.HKL_4

FRAME-NUMBER	POSITION NUMBER 1	2	3	4	5	6	7	8	9
32.7	1.0018	0.9983	0.9955	0.9944	0.9989	0.9950	0.9961	0.9980	0.9998
92.1	1.0088	1.0035	0.9991	0.9985	1.0035	1.0138	1.0097	1.0084	1.0079
151.4	1.0178	1.0140	1.0085	1.0075	1.0170	1.0354	1.0264	1.0163	1.0135
210.8	1.0194	1.0181	1.0141	1.0133	1.0213	1.0366	1.0283	1.0152	1.0120
270.2	1.0179	1.0169	1.0148	1.0138	1.0163	1.0276	1.0241	1.0138	1.0114
329.6	1.0150	1.0136	1.0123	1.0129	1.0161	1.0189	1.0174	1.0115	1.0097
388.9	1.0145	1.0091	1.0079	1.0125	1.0179	1.0157	1.0117	1.0084	1.0055
448.3	1.0140	1.0045	1.0031	1.0106	1.0158	1.0149	1.0068	1.0059	1.0023

SCALING FACTORS FOR DATA SET XDS.HKL_5

FRAME-NUMBER	POSITION NUMBER 1	2	3	4	5	6	7	8	9
27.8	0.9986	0.9965	0.9980	0.9963	1.0016	0.9976	0.9931	0.9884	0.9899
77.3	0.9968	0.9962	0.9950	0.9932	1.0022	0.9970	0.9947	0.9906	0.9929
126.8	0.9946	0.9936	0.9913	0.9892	0.9977	0.9946	0.9934	0.9918	0.9952
176.3	0.9943	0.9916	0.9904	0.9918	0.9964	0.9955	0.9935	0.9947	0.9981
225.8	0.9933	0.9921	0.9895	0.9905	0.9948	0.9970	0.9946	0.9972	0.9970

275.3	0.9941	0.9925	0.9866	0.9893	0.9916	0.9923	0.9946	0.9959	0.9939
324.8	0.9945	0.9905	0.9863	0.9901	0.9908	0.9917	0.9935	0.9943	0.9908
374.3	0.9939	0.9903	0.9877	0.9889	0.9867	0.9916	0.9933	0.9924	0.9900

SCALING FACTORS FOR DATA SET XDS.HKL_6

FRAME-	POSITION NUMBER								
NUMBER	1	2	3	4	5	6	7	8	9
13.6	0.9903	0.9959	1.0010	0.9868	0.9924	0.9893	0.9919	0.9865	0.9801
34.7	0.9869	0.9876	0.9901	0.9784	0.9807	0.9899	0.9938	0.9810	0.9782
55.8	0.9840	0.9897	0.9822	0.9771	0.9828	0.9918	0.9913	0.9774	0.9773
76.9	0.9834	0.9981	0.9923	0.9931	0.9908	0.9888	0.9821	0.9738	0.9774
98.1	0.9884	1.0054	1.0126	1.0047	1.0033	0.9851	0.9777	0.9733	0.9781
119.2	0.9896	1.0038	1.0155	0.9990	1.0002	0.9895	0.9816	0.9774	0.9813
140.3	0.9935	1.0022	1.0100	0.9881	0.9980	0.9896	0.9817	0.9801	0.9828
161.4	0.9958	1.0037	1.0096	0.9894	1.0028	0.9886	0.9791	0.9787	0.9800

SCALING FACTORS FOR DATA SET XDS.HKL_7

FRAME-	POSITION NUMBER								
NUMBER	1	2	3	4	5	6	7	8	9
232.7	1.0289	1.0084	1.0152	1.0345	1.0172	1.0129	0.9926	0.9889	0.9996
292.1	1.0178	0.9991	1.0093	1.0249	1.0155	1.0088	0.9890	0.9790	0.9868
351.4	1.0056	1.0000	1.0045	1.0109	1.0079	1.0079	0.9899	0.9778	0.9889
410.8	0.9976	1.0078	1.0062	0.9992	0.9985	1.0003	0.9918	0.9879	1.0009
470.2	0.9979	1.0102	1.0121	0.9915	0.9888	0.9889	0.9889	1.0012	1.0066
529.6	1.0003	1.0141	1.0106	0.9850	0.9856	0.9882	0.9919	1.0053	1.0074
588.9	1.0035	1.0150	1.0103	0.9851	0.9842	0.9921	0.9953	1.0002	1.0068
648.3	1.0038	1.0162	1.0120	0.9876	0.9837	0.9921	0.9919	0.9939	1.0075

R-FACTORS FOR INTENSITIES OF DATA SET XDS.HKL_1

HIGH RESOLUTION LIMIT	R-FACTOR	NUMBER OF REFLECTIONS	ESTIMATED R-FACTOR
8.00	3.2%	79	2.7%
6.00	6.3%	1223	4.9%
5.00	8.9%	1714	6.4%
4.50	9.0%	1511	5.9%
4.00	9.6%	2170	6.2%
0.00	13.0%	8611	12.1%

R-FACTORS FOR INTENSITIES OF DATA SET XDS.HKL_2

HIGH RESOLUTION LIMIT	R-FACTOR	NUMBER OF REFLECTIONS	ESTIMATED R-FACTOR
20.00	3.5%	61	1.9%
15.00	3.3%	113	2.2%
12.00	2.9%	151	2.4%
10.00	4.5%	176	3.2%
8.00	3.9%	374	3.0%
6.00	7.4%	913	6.0%
5.00	10.6%	337	10.8%

R-FACTORS FOR INTENSITIES OF DATA SET XDS.HKL_3

HIGH RESOLUTION LIMIT	R-FACTOR	NUMBER OF REFLECTIONS	ESTIMATED R-FACTOR
20.00	2.1%	17	1.9%
15.00	2.2%	31	1.7%
12.00	4.4%	85	2.9%
10.00	3.7%	137	2.7%
8.00	3.7%	276	2.8%
6.00	7.0%	724	5.3%
5.00	8.6%	710	7.7%
4.50	8.8%	509	7.9%
4.00	9.0%	310	8.0%

R-FACTORS FOR INTENSITIES OF DATA SET XDS.HKL_4

HIGH RESOLUTION LIMIT	R-FACTOR	NUMBER OF REFLECTIONS	ESTIMATED R-FACTOR
8.00	5.9%	66	2.1%
6.00	6.9%	867	2.5%
5.00	6.6%	1248	3.0%
4.50	6.7%	1089	2.9%
4.00	6.4%	1537	3.0%
0.00	7.0%	5686	5.3%

R-FACTORS FOR INTENSITIES OF DATA SET XDS.HKL_5

HIGH RESOLUTION LIMIT	R-FACTOR	NUMBER OF REFLECTIONS	ESTIMATED R-FACTOR
8.00	5.3%	50	3.2%
6.00	5.0%	756	3.4%
5.00	5.4%	1067	3.5%
4.50	4.2%	933	2.7%
4.00	5.9%	1337	4.3%
0.00	6.7%	5264	6.6%

R-FACTORS FOR INTENSITIES OF DATA SET XDS.HKL_6

HIGH RESOLUTION LIMIT	R-FACTOR	NUMBER OF REFLECTIONS	ESTIMATED R-FACTOR
8.00	6.2%	22	3.9%
6.00	7.2%	332	4.1%
5.00	7.0%	453	4.7%
4.50	6.5%	398	4.0%
4.00	8.5%	565	5.6%
0.00	9.2%	2235	9.0%

R-FACTORS FOR INTENSITIES OF DATA SET XDS.HKL_7

HIGH RESOLUTION LIMIT	R-FACTOR	NUMBER OF REFLECTIONS	ESTIMATED R-FACTOR
20.00	3.2%	99	2.2%
15.00	4.1%	169	3.2%
12.00	4.8%	227	3.6%
10.00	4.5%	322	4.1%
8.00	5.1%	621	4.1%
6.00	11.2%	1510	10.4%
5.00	19.3%	500	20.5%

======= COMPLETENESS OF DATA SET =======

COMPLETENESS OF DATA WITH SIGNAL/NOISE >= 0.0 AS FUNCTION OF RESOLUTION

HIGH RESOLUTION LIMIT	NUMBER OF UNIQUE OBSERVED REFLECTIONS	NUMBER OF UNIQUE POSSIBLE REFLECTIONS
20.00	28	3
15.00	56	8
12.00	89	10
10.00	128	7
8.00	260	27
6.00	752	75
5.00	894	108
4.50	784	66
4.00	1200	114

======= COMPLETENESS OF DATA SET =======

COMPLETENESS OF DATA WITH SIGNAL/NOISE >= 1.0 AS FUNCTION OF RESOLUTION

HIGH RESOLUTION LIMIT	NUMBER OF UNIQUE OBSERVED REFLECTIONS	NUMBER OF UNIQUE POSSIBLE REFLECTIONS
20.00	28	3
15.00	56	8
12.00	89	10

10.00	123	7
8.00	256	27
6.00	743	75
5.00	882	108
4.50	769	66
4.00	1172	114

======= COMPLETENESS OF DATA SET =======
COMPLETENESS OF DATA WITH SIGNAL/NOISE >= 2.0 AS FUNCTION OF RESOLUTION

HIGH RESOLUTION LIMIT	NUMBER OF UNIQUE OBSERVED REFLECTIONS	NUMBER OF UNIQUE POSSIBLE REFLECTIONS
20.00	27	3
15.00	53	8
12.00	87	10
10.00	119	7
8.00	253	27
6.00	726	75
5.00	866	108
4.50	757	66
4.00	1144	114

======= COMPLETENESS OF DATA SET =======
COMPLETENESS OF DATA WITH SIGNAL/NOISE >= 3.0 AS FUNCTION OF RESOLUTION

HIGH RESOLUTION LIMIT	NUMBER OF UNIQUE OBSERVED REFLECTIONS	NUMBER OF UNIQUE POSSIBLE REFLECTIONS
20.00	27	3
15.00	51	8
12.00	87	10
10.00	114	7
8.00	251	27
6.00	699	75
5.00	844	108
4.50	742	66
4.00	1102	114

======= COMPLETENESS OF DATA SET =======
COMPLETENESS OF DATA WITH SIGNAL/NOISE >= 4.0 AS FUNCTION OF RESOLUTION

HIGH RESOLUTION LIMIT	NUMBER OF UNIQUE OBSERVED REFLECTIONS	NUMBER OF UNIQUE POSSIBLE REFLECTIONS
20.00	27	3
15.00	50	8
12.00	86	10
10.00	111	7
8.00	246	27
6.00	687	75
5.00	823	108
4.50	722	66
4.00	1068	114

======= COMPLETENESS OF DATA SET =======
COMPLETENESS OF DATA WITH SIGNAL/NOISE >= 5.0 AS FUNCTION OF RESOLUTION

HIGH RESOLUTION LIMIT	NUMBER OF UNIQUE OBSERVED REFLECTIONS	NUMBER OF UNIQUE POSSIBLE REFLECTIONS
20.00	27	3
15.00	49	8
12.00	85	10

10.00	107	7
8.00	239	27
6.00	673	75
5.00	807	108
4.50	710	66
4.00	1037	114

======= COMPLETENESS OF DATA SET =======
COMPLETENESS OF DATA WITH SIGNAL/NOISE >= 6.0 AS FUNCTION OF RESOLUTION

HIGH RESOLUTION LIMIT	NUMBER OF UNIQUE OBSERVED REFLECTIONS	NUMBER OF UNIQUE POSSIBLE REFLECTIONS
20.00	27	3
15.00	49	8
12.00	84	10
10.00	106	7
8.00	236	27
6.00	657	75
5.00	790	108
4.50	694	66
4.00	1008	114

9 OUT OF 48375 REFLECTIONS REJECTED
NUMBER OF UNIQUE REFLECTIONS ON OUTPUT FILE 10380

R-FACTORS FOR INTENSITIES OF SCALED DATA SET

HIGH RESOLUTION LIMIT	NUMBER OF OBSERVED REFLECTIONS	NUMBER OF UNIQUE REFLECTIONS	R-FACTOR	NUMBER OF COMPARED REFLECTIONS	ESTIMATED R-FACTOR
20.00	182	28	3.3%	177	2.0%
15.00	317	56	3.4%	312	2.5%
12.00	472	89	3.9%	463	3.0%
10.00	647	128	4.3%	635	3.6%
8.00	1503	260	4.4%	1488	3.4%
6.00	6332	752	7.6%	6325	5.8%
5.00	6036	894	7.8%	6029	5.7%
4.50	4449	784	6.2%	4440	3.9%
4.00	5933	1200	7.7%	5919	5.0%
0.00	22495	6189	9.2%	21796	8.4%
total	48366	10380	7.2%	47584	5.6%

Appendix V

AGROVATA Program Output

Number of independent reflexions = 10378
(including 206 .LE. ZERO):
comprising 2490 CENTRIC and 7888 ACENTRIC

Overall mean Standard deviation (SIGMA) is: 146.78
or 0.044 of mean INTENSITY for 12012. measurements

SIGM0 & R FACTOR relative to overall MEAN 146.78 0.032
for 12012. measurements from 6006 independent HKLs.

Rcum :- R-factor up to this range,
Ranom :- Sum |<I+> - <I->| / Sum (<I+> + <I->)
Nref :- number of independent hkl's
SIGMA :- rms scatter of observations
sd :- average standard deviation derived from experimental SDs, after
:- application of SDFAC SDADD
FRCBIAS :- Mean(<If> - Ip)/Mean(<If>)
for Nbias mixed sets only

By 4SINTH/LASQ bins (all statistics use <I+>,<I->etc)

$TABLE: Analysis against resolution:
$GRAPHS:Rfactor v Resolution:N:2,4,6:
: Average I,sd and Sigma :A:2,8,9,11::I/sigma:N:2,10: $$

N	<s>	Dmin(A)	Rfac	Rcum	Ranom	Nanom	Av_I	SIGMA	I/sigma	sd	Nmeas	Nref	Ncent	FRCBIAS	Nbias $$
$$															
1	[illegible]	[illegible]	[illegible]	0.019	0.000	0	12495.	446.7	28.4	211.85	136	68	0	0.0000	0
2	0.0134	8.63	0.021	0.020	0.000	0	8083.	271.4	29.8	203 30	290	145	0	0.0000	0
3	0.0195	7.16	0.022	0.021	0.000	0	5026.	185.3	27.1	112.93	384	192	0	0.0000	0
4	0 0256	6.25	0.030	0.022	0.000	0	2824.	117.4	24.1	81.46	438	219	0	0.0000	0
5	0.0317	5.61	0.029	0.023	0.000	0	2404.	96.9	24.8	80.12	472	236	0	0.0000	0
6	0.0378	5.14	0.030	0.024	0.000	0	3161.	140.1	22.6	102.37	560	280	0	0.0000	0
7	0.0440	4.77	0.025	0.024	0.000	0	4001.	154.1	26.0	122.31	600	300	0	0.0000	0
8	0.0501	4.47	0.025	0.025	0.000	0	4760.	219.6	21.7	138.68	640	320	0	0.0000	0
9	0.0562	4.22	0.025	0.025	0.000	0	4211.	162.5	25.9	145.06	658	329	0	0.0000	0
10	0.0623	4.01	0.025	0.025	0.000	0	3780	131.5	28.7	152.01	736	368	0	0.0000	0
11	0.0684	3.82	0.028	0.025	0.000	0	3507.	142.9	24.5	153.93	768	384	0	0.0000	0
12	0.0745	3.66	0.029	0.026	0.000	0	3308.	131.9	25.1	158.31	806	403	0	0.0000	0
13	0.0806	3.52	0.034	0.026	0.000	0	2677.	124.5	21.5	154.75	800	400	0	0.0000	0
14	0.0867	3.40	0.039	0.027	0.000	0	2243.	127.8	17.6	151.97	854	427	0	0.0000	0
15	0 0928	3.28	0.048	0.028	0.000	0	1698.	108.9	15.6	148.32	814	407	0	0.0000	0
16	0.0989	3.18	0.053	0.029	0.000	0	1545.	113.0	13.7	153.69	778	389	0	0.0000	0
17	0.1050	3.09	0.058	0.030	0.000	0	1383.	111.0	12.5	159.21	754	377	0	0.0000	0
18	0.1111	3.00	0.072	0.031	0.000	0	1046.	101.6	10.3	161.89	694	347	0	0.0000	0
19	0.1172	2.92	0.104	0.031	0.000	0	783.	106.1	7.4	165.00	538	269	0	0.0000	0
20	0.1234	2.85	0.125	0.032	0.000	0	591.	101.8	5.8	172.18	292	146	0	0.0000	0
$$															

BY INTENSITY ranges (all statistics use <I+>,<I->etc)

$TABLE: Analysis against intensity:
$GRAPHS.Rfactor v Intensity :N:1,2,3:

Imax	Rfac	Ranom	Nanom	Av_I	SIGMA	I/Sigma	sd	Nmeas	Nref	Ncent	FRCBIAS	Nbias	NIndep	Abs.BIAS $$
$$														
500.	0.189	0.000	0	278.	70.4	3.9	114.1	2536.	1268	0	0.0000	0	0	0.0
1000.	0.080	0.000	0	739.	77.0	9.6	121.2	2044.	1022	0	0.0000	0	0	0.0
1500.	0 055	0.000	0	1234.	86.8	14.2	123.8	1344.	672	0	0.0000	0	0	0.0
2000.	0.049	0.000	0	1741.	111.9	15.6	128.9	1026.	513	0	0.0000	0	0	0.0
2500.	0.040	0.000	0	2249.	114.2	19.7	135.2	872.	436	0	0.0000	0	0	0.0
3000.	0 035	0.000	0	2756.	121.1	22.8	137.0	604.	302	0	0.0000	0	0	0.0
3500.	0.033	0.000	0	3243.	130.9	24.8	143.3	524.	262	0	0.0000	0	0	0.0
4000.	0.028	0.000	0	3735.	136.5	27.4	155.0	426.	213	0	0.0000	0	0	0.0
4500.	0.025	0.000	0	4247.	134.7	31.5	151.1	370.	185	0	0.0000	0	0	0.0
5000.	0.025	0.000	0	4737.	153.2	30.9	155.7	306.	153	0	0.0000	0	0	0.0
5500.	0.024	0.000	0	5246.	156.1	33.6	166.6	248.	124	0	0.0000	0	0	0.0
6000.	0.024	0.000	0	5749.	176.2	32.6	173.4	196.	98	0	0.0000	0	0	0.0
442600.	0.019	0.000	0	11512.	312.4	36.8	254.7	1516.	758	0	0.0000	0	0	0.0

TOTALS	0.032	0.000	0	2954.	146.8	20.1	145.1	12012.	6006	0	0.0000	0	0	0.0

Completeness and multiplicity, including reflections measured only once

$TABLE: Completeness & multiplicity v. resolution:
$GRAPHS:Completeness v Resolution :N:2,6:
:Multiplicity v Resolution :N:2,7: $$

N	<s>	Dmin	Nmeas	Nref	%poss	Multiplicity $$
$$						
1	0.007	11.70	255	187	95.8	1.4
2	0.013	8.63	412	267	97.8	1.5
3	0.020	7.16	517	325	98.3	1.6
4	0.026	6.25	602	383	100.6	1.6
5	0.032	5.61	654	418	99.1	1.6
6	0.038	5.14	737	457	100.3	1.6
7	0.044	4.77	789	489	100.3	1.6
8	0.050	4.47	852	532	101.9	1.6
9	0.056	4.22	860	531	97.7	1.6
10	0.062	4.01	940	572	99.9	1.6
11	0.068	3.82	984	600	99.7	1.6
12	0.074	3.66	1024	621	99.7	1.6
13	0.081	3.52	1044	644	99.7	1.6
14	0.087	3.40	1102	675	101.8	1.6
15	0.093	3.28	1084	677	98.3	1.6
16	0.099	3.18	1063	674	96.6	1.6
17	0.105	3.09	1062	685	95.6	1.6
18	0.111	3.00	1018	671	90.2	1.5
19	0.117	2.92	850	581	76.9	1.5
20	0.123	2.85	535	389	50.3	1.4
$$						
		Total	16384	10378	93.2	1.6

Number of accepted HKLs by THETA and Multiples of SD

Dmin(A)	INTENSITIES								ANOMALOUS DIFFS(<I+> - <I->)							
	Number in bin			TOTAL	Cumulative Percentages				Number in bin			TOTAL	Cumulative Percentages			
	.LE.1*SD	2*SD	3*SD		.LE.1*SD	2*SD	3*SD	.GT.3*	.LE.1*SD	2*SD	3*SD		.LE.1*SD	2*SD	3*SD	.GT.3*
11.70	1	6	2	187	0.5	3.7	4.8	95.2	0	0	0	0	0.0	0.0	0.0	100.0
8.63	5	6	7	267	1.9	4.1	6.7	93.3	0	0	0	0	0.0	0.0	0.0	100.0
7.16	6	6	4	325	1.8	3.7	4.9	95.1	0	0	0	0	0.0	0.0	0.0	100.0
6.25	4	7	16	383	1.0	2.9	7.0	93.0	0	0	0	0	0.0	0.0	0.0	100.0
5.61	4	12	17	418	1.0	3.8	7.9	92.1	0	0	0	0	0.0	0.0	0.0	100.0
5.14	8	6	8	457	1.8	3.1	4.8	95.2	0	0	0	0	0.0	0.0	0.0	100.0
4.77	8	9	13	489	1.6	3.5	6.1	93.9	0	0	0	0	0.0	0.0	0.0	100.0
4.47	11	9	6	532	2.1	3.8	4.9	95.1	0	0	0	0	0.0	0.0	0.0	100.0
4.22	8	10	22	531	1.5	3.4	7.5	92.5	0	0	0	0	0.0	0.0	0.0	100.0
4.01	17	12	19	572	3.0	5.1	8.4	91.6	0	0	0	0	0.0	0.0	0.0	100.0
3.82	15	32	20	600	2.5	7.8	11.2	88.8	0	0	0	0	0.0	0.0	0.0	100.0
3.66	23	20	27	621	3.7	6.9	11.3	88.7	0	0	0	0	0.0	0.0	0.0	100.0
3.52	23	23	32	644	3.6	7.1	12.1	87.9	0	0	0	0	0.0	0.0	0.0	100.0
3.40	25	37	30	675	3.7	9.2	13.6	86.4	0	0	0	0	0.0	0.0	0.0	100.0
3.28	26	50	41	677	3.8	11.2	17.3	82.7	0	0	0	0	0.0	0.0	0.0	100.0
3.18	30	51	49	674	4.5	12.0	19.3	80.7	0	0	0	0	0.0	0.0	0.0	100.0
3.09	43	52	66	685	6.3	13.9	23.5	76.5	0	0	0	0	0.0	0.0	0.0	100.0
3.00	55	65	77	671	8.2	17.9	29.4	70.6	0	0	0	0	0.0	0.0	0.0	100.0
2.92	60	90	68	581	10.3	25.8	37.5	62.5	0	0	0	0	0.0	0.0	0.0	100.0
2.85	51	65	77	389	13.1	29.8	49.6	50.4	0	0	0	0	0.0	0.0	0.0	100.0
Overall	423	568	601	10378.	4.1	9.5	15.3	84.7	0	0	0	0.	0.0	0.0	0.0	100.0

ANALYSIS OF STANDARD DEVIATIONS

This plots the distribution of the number of REFLECTIONS
with (I(J) - I<+/->MEAN)/SD(J) in ranges from -5 to +5 .
If the SD is a true estimate of the error, this distribution
should have Mean=0.0 and Sigma=1.0 for all ranges of INTENSITY.
The analysis is repeated for ranges of increasing Imean .
The Mean is expected to increase with Imean since the

latter is a weighted mean and SD(J) & I(J) are correlated
If the Sigma increases with Imean, increase the value of SDADD.

$TABLE : Analysis of standard deviation v. Intensity:
$GRAPHS: Sigma(scatter/SD):N:4,7: $$

Range	Imin	Imax	Irms	Number Fully_recordeds	Mean	Sigma	$$
$$							
1	0.	500.	311.	2536.	0.00	0.60	
2	500.	1000.	757.	2044.	0.00	0.70	
3	1000.	1500.	1245.	1344.	0.00	0.75	
4	1500.	2000.	1751.	1026.	0.00	0.94	
5	2000.	2500.	2256.	872.	0.00	0.94	
6	2500.	3000.	2762.	604.	0.00	0.93	
7	3000.	3500.	3249.	524.	0.00	0.96	
8	3500.	4000.	3740.	426.	0.00	0.90	
9	4000.	4500.	4252.	370.	0.00	0.91	
10	4500.	5000.	4742.	306.	0.00	1.04	
11	5000.	5500.	5251.	248.	0.00	1.00	
12	5500.	6000.	5754.	196.	0.00	1.03	
13	6000.	442600.	14959.	1516.	0.00	1.10	
$$							
TOTALS:							
0	0.	442600.	5722.	12012.	0.00	0.85	

For all REFLECTIONS, histogram of mean fractional
deviations: FULLYS first and then PARTIALS

DEL(I)/SD NUMBER in bin with upper limit DEL(I)/SD as shown

```
-5.0   0
-4.5   0       2
-4.0   0       2
-3.5   0       5
-3.0   0       8
-2.5   0      34 *
-2.0   1     133 ****
-1.5   2     288 *********
-1.0   6     767 ************************
-0.5  15    1782 ************************************************************
 0.0  25    2970 ****************************************************************************************************
 0.5  25    3000 ****************************************************************************************************
 1.0  15    1782 ************************************************************
 1.5   6     767 ************************
 2.0   2     288 *********
 2.5   1     133 ****
 3.0   0      34 *
 3.5   0       8
 4.0   0       5
 4.5   0       2
 5.0   0       1
 5.5   0       1
```

Appendix VI

Fractional atomic coordinates and equivalent isotropic displacement parameters (Å^2)

$$U_{eq} = (1/3)\Sigma_i\Sigma_j U_{ij} a_i^* a_j^* a_i . a_j .$$

	x	*y*	*z*	U_{eq}
C101	0.5285 (4)	0.7818 (4)	0.9148 (4)	0.0406 (15)
C102	0.4883 (5)	0.7876 (4)	0.8358 (4)	0.0386 (14)
C103	0.4137 (5)	0.8010 (4)	0.8095 (4)	0.0421 (15)
C104	0.3728 (5)	0.8036 (4)	0.8572 (4)	0.0406 (15)
C105	0.4089 (4)	0.7940 (4)	0.9350 (3)	0.0380 (14)
C106	0.4885 (4)	0.7858 (4)	0.9635 (4)	0.0426 (15)
C107	0.5782 (4)	0.7069 (4)	0.7273 (3)	0.0374 (14)
C108	0.5718 (4)	0.6295 (4)	0.6983 (4)	0.0389 (14)
C109	0.5077 (4)	0.5547 (4)	0.6989 (4)	0.0411 (14)
C110	0.4459 (4)	0.5540 (4)	0.7251 (3)	0.0352 (13)
C111	0.4501 (4)	0.6304 (4)	0.7526 (4)	0.0381 (14)
C112	0.5165 (4)	0.7049 (4)	0.7543 (4)	0.0380 (14)
C113	0.5834 (5)	0.4966 (4)	0.5848 (4)	0.049 (2)
C114	0.5852 (5)	0.4220 (5)	0.5763 (4)	0.053 (2)
C115	0.6519 (5)	0.4157 (5)	0.6447 (4)	0.051 (2)
C116	0.7173 (5)	0.4857 (5)	0.7171 (5)	0.056 (2)
C117	0.7130 (5)	0.5592 (4)	0.7243 (4)	0.053 (2)
C118	0.6440 (5)	0.5643 (4)	0.6600 (4)	0.0423 (15)
C119	0.6431 (6)	0.3295 (5)	0.6400 (5)	0.065 (2)
C120	0.5908 (5)	0.2851 (5)	0.6845 (4)	0.057 (2)
C121	0.4884 (5)	0.2661 (5)	0.6421 (4)	0.061 (2)
C122	0.3555 (6)	0.2579 (5)	0.6576 (7)	0.096 (3)
C123	0.3332 (5)	0.3306 (4)	0.6529 (4)	0.053 (2)
C124	0.3702 (4)	0.4714 (4)	0.7216 (3)	0.0333 (13)
C125	0.3622 (4)	0.4905 (4)	0.7998 (4)	0.0389 (14)
C126	0.2796 (5)	0.5368 (4)	0.8543 (3)	0.0386 (14)
C127	0.2232 (5)	0.5795 (4)	0.8189 (3)	0.0390 (14)
C128	0.2922 (4)	0.6824 (4)	0.9576 (3)	0.0384 (14)
C129	0.3564 (5)	0.7805 (4)	0.9827 (3)	0.0385 (14)
C130	0.2317 (5)	0.4788 (4)	0.8921 (3)	0.0416 (15)
C131	0.1397 (5)	0.4070 (5)	0.8425 (4)	0.060 (2)

	x	*y*	*z*	U_{eq}
C132	0.0928 (6)	0.3600 (5)	0.8769 (4)	0.074 (3)
C133	0.1315 (5)	0.3838 (5)	0.9620 (4)	0.058 (2)
C134	0.2228 (5)	0.4557 (4)	1.0151 (4)	0.047 (2)
C135	0.2713 (4)	0.4998 (4)	0.9774 (3)	0.0389 (15)
C136	0.2664 (5)	0.4830 (5)	1.1076 (4)	0.052 (2)
C137	0.3051 (6)	0.4395 (5)	1.1508 (4)	0.056 (2)
C138	0.3442 (6)	0.4611 (5)	1.2356 (4)	0.063 (2)
C139	0.3485 (5)	0.5281 (5)	1.2797 (4)	0.057 (2)
C140	0.3087 (5)	0.5731 (5)	1.2396 (4)	0.053 (2)
C141	0.2683 (5)	0.5512 (4)	1.1532 (4)	0.049 (2)
C142	0.2239 (5)	0.5988 (5)	1.1095 (4)	0.052 (2)
C143	0.2338 (5)	0.6559 (4)	1.0009 (4)	0.046 (2)
C144	0.7398 (4)	0.8171 (4)	0.7929 (4)	0.0423 (15)
C145	0.8434 (5)	0.9080 (5)	0.9316 (4)	0.065 (2)
C146	0.9175 (5)	0.9638 (5)	0.9122 (5)	0.069 (2)
C147	0.9098 (5)	0.9108 (6)	0.8384 (5)	0.074 (2)
C148	0.8091 (5)	0.8650 (5)	0.7661 (4)	0.054 (2)
C149	0.8441 (6)	0.9540 (6)	1.0041 (5)	0.076 (2)
C150	0.7033 (6)	0.3126 (5)	0.8266 (5)	0.070 (2)
C151	0.7655 (6)	0.3739 (5)	0.9159 (5)	0.071 (2)
C152	0.7168 (7)	0.3449 (6)	0.9663 (5)	0.094 (3)
C153	0.7647 (8)	0.3984 (9)	1.0522 (6)	0.119 (4)
C154	0.7149 (10)	0.3605 (12)	1.0977 (8)	0.172 (7)
C155	0.7823 (17)	0.4885 (11)	1.0614 (9)	0.196 (9)
C156	0.9154 (8)	0.4184 (9)	0.9096 (8)	0.113 (4)
C157	0.3139 (8)	0.2069 (7)	0.7073 (10)	0.129 (4)
C158	0.3554 (16)	0.2590 (15)	0.7926 (14)	0.129 (6)
C159	0.3484 (6)	0.9060 (4)	0.9980 (4)	0.054 (2)
C160	0.3425 (5)	0.9130 (5)	1.1228 (4)	0.057 (2)
C161	0.2677 (5)	0.9396 (5)	1.0947 (4)	0.056 (2)
C162	0.2126 (6)	0.9216 (5)	0.9993 (4)	0.062 (2)
C163	0.2811 (6)	0.9388 (5)	0.9650 (5)	0.058 (2)
C164	0.4113 (7)	0.9547 (7)	1.2172 (5)	0.090 (3)
C165	0.1232 (6)	0.8334 (6)	0.9493 (5)	0.084 (3)
C166	0.2498 (7)	1.0536 (6)	1.0727 (5)	0.077 (2)
C167	0.2086 (6)	0.6550 (5)	1.1639 (4)	0.060 (2)
C111	0.62332 (14)	0.76521 (15)	0.94981 (12)	0.0710 (6)
C112	0.50144 (15)	0.50607 (13)	0.50199 (12)	0.0707 (6)
N101	0.6448 (4)	0.3329 (4)	0.7727 (4)	0.058 (2)
N102	0.4568 (4)	0.2868 (4)	0.6897 (4)	0.064 (2)

	x	*y*	*z*	U_{eq}
N103	0.3918 (4)	0.4034 (3)	0.7158 (3)	0.0400 (12)
N104	0.2858 (4)	0.4966 (3)	0.7866 (3)	0.0385 (12)
N105	0.2290 (4)	0.6425 (3)	0.8690 (3)	0.0400 (12)
N106	0.2787 (4)	0.6483 (4)	1.0736 (3)	0.0482 (14)
N107	0.8592 (5)	0.3780 (5)	0.9489 (4)	0.084 (2)
N108	0.3033 (15)	0.2717 (14)	0.8132 (15)	0.143 (6)
N109	0.1899 (6)	0.9896 (5)	0.9996 (4)	0.078 (2)
N110	0.3042 (5)	1.0300 (4)	1.1249 (4)	0.070 (2)
O101	0.5262 (3)	0.7836 (3)	0.7844 (3)	0.0444 (10)
O102	0.6450 (3)	0.7813 (3)	0.7273 (2)	0.0398 (10)
O103	0.6350 (3)	0.6347 (3)	0.6710 (3)	0.0500 (11)
O104	0.7357 (4)	0.3398 (4)	0.6804 (4)	0.083 (2)
O105	0.4382 (4)	0.2332 (5)	0.5662 (3)	0.104 (2)
O106	0.2598 (5)	0.3164 (4)	0.5944 (4)	0.109 (3)
O107	0.4247 (4)	0.5045 (3)	0.8690 (3)	0.0619 (13)
O108	0.1669 (4)	0.5521 (3)	0.7425 (2)	0.0635 (14)
O109	0.2969 (3)	0.8157 (3)	0.9645 (3)	0.0460 (11)
O110	0.0829 (5)	0.3385 (4)	0.9970 (4)	0.088 (2)
O111	0.3027 (5)	0.3739 (4)	1.1048 (3)	0.078 (2)
O112	0.3898 (5)	0.5482 (4)	1.3639 (3)	0.081 (2)
O113	0.1509 (4)	0.6362 (4)	0.9685 (3)	0.0653 (14)
O114	0.7514 (3)	0.3724 (3)	0.8603 (3)	0.0576 (13)
O115	1.0108 (4)	1.0023 (5)	0.9818 (4)	0.116 (3)
O116	0.9766 (5)	0.9677 (4)	0.8183 (5)	0.117 (3)
O117	0.8032 (4)	0.8101 (4)	0.7014 (3)	0.070 (2)
O118	0.8297 (5)	1.0194 (4)	0.9900 (4)	0.090 (2)
O119	0.7079 (5)	0.2490 (4)	0.8080 (4)	0.098 (2)
O120	0.4430 (14)	0.2805 (17)	0.8473 (15)	0.176 (9)
O121	0.3996 (3)	0.9366 (3)	1.0856 (3)	0.0549 (12)
O122	0.2052 (5)	0.8966 (4)	1.1235 (4)	0.079 (2)
O123	0.2534 (7)	1.1233 (5)	1.0894 (4)	0.116 (3)
O124	0.1288 (5)	0.6220 (4)	1.1594 (4)	0.086 (2)
O125	0.2737 (5)	0.7288 (4)	1.2050 (3)	0.082 (2)
C358	0.3822 (24)	0.2381 (20)	0.7964 (16)	0.209 (13)
O320	0.4595 (17)	0.3143 (14)	0.8455 (12)	0.156 (7)
N308	0.4149 (26)	0.1854 (21)	0.8022 (24)	0.275 (19)
C201	0.2365 (5)	0.5985 (4)	0.4178 (4)	0.048 (2)
C202	0.3101 (4)	0.6285 (4)	0.4986 (4)	0.0423 (15)
C203	0.3346 (5)	0.5746 (4)	0.5313 (4)	0.046 (2)

	x	*y*	*z*	U_{eq}
C204	0.2832 (4)	0.4891 (4)	0.4865 (4)	0.044 (2)
C205	0.2036 (4)	0.4542 (4)	0.4065 (3)	0.0429 (15)
C206	0.1825 (5)	0.5112 (4)	0.3719 (4)	0.050 (2)
C207	0.3423 (4)	0.8266 (4)	0.5983 (4)	0.0390 (14)
C208	0.2904 (4)	0.8531 (4)	0.6213 (4)	0.0411 (14)
C209	0.2120 (5)	0.7970 (4)	0.6255 (4)	0.0439 (15)
C210	0.1865 (4)	0.7115 (4)	0.6081 (4)	0.0389 (14)
C211	0.2363 (4)	0.6841 (4)	0.5834 (4)	0.0382 (14)
C212	0.3108 (5)	0.7400 (4)	0.5752 (4)	0.0404 (14)
C213	0.2560 (5)	0.9801 (4)	0.7138 (4)	0.052 (2)
C214	0.1847 (5)	0.9910 (5)	0.7156 (5)	0.057 (2)
C215	0.1121 (5)	0.9842 (5)	0.6432 (5)	0.057 (2)
C216	0.1156 (6)	0.9714 (5)	0.5705 (5)	0.064 (2)
C217	0.1870 (5)	0.9598 (5)	0.5693 (4)	0.055 (2)
C218	0.2545 (5)	0.9606 (4)	0.6409 (4)	0.048 (2)
C219	0.0263 (6)	0.9836 (5)	0.6426 (5)	0.067 (2)
C220	-0.0591 (5)	0.8921 (5)	0.6117 (4)	0.056 (2)
C221	-0.0299 (5)	0.8412 (5)	0.6645 (4)	0.053 (2)
C222	-0.0599 (6)	0.6987 (5)	0.6669 (5)	0.067 (2)
C223	0.0245 (6)	0.6866 (5)	0.6812 (4)	0.056 (2)
C224	0.1041 (4)	0.6491 (4)	0.6177 (4)	0.0378 (14)
C225	0.0442 (4)	0.5656 (4)	0.5437 (3)	0.0398 (15)
C226	0.0225 (4)	0.4258 (4)	0.4942 (4)	0.0417 (15)
C227	0.0949 (4)	0.3983 (4)	0.5284 (3)	0.043 (2)
C228	0.0588 (5)	0.3309 (4)	0.3865 (3)	0.047 (2)
C229	0.1360 (5)	0.3598 (4)	0.3618 (4)	0.047 (2)
C230	-0.0749 (5)	0.3489 (4)	0.4608 (4)	0.049 (2)
C231	-0.0956 (6)	0.3016 (6)	0.5113 (5)	0.080 (3)
C233	-0.2407 (6)	0.1891 (5)	0.3926 (5)	0.080 (3)
C232	-0.1782 (7)	0.2238 (7)	0.4769 (5)	0.101 (4)
C234	-0.2240 (5)	0.2318 (5)	0.3402 (4)	0.056 (2)
C235	-0.1415 (4)	0.3135 (4)	0.3767 (4)	0.048 (2)
C236	-0.2897 (5)	0.1960 (5)	0.2481 (4)	0.057 (2)
C237	-0.3735 (5)	0.1990 (6)	0.2135 (5)	0.070 (2)
C238	-0.4338 (6)	0.1669 (6)	0.1300 (5)	0.073 (2)
C239	-0.4118 (5)	0.1345 (5)	0.0772 (4)	0.068 (2)
C240	-0.3304 (5)	0.1259 (5)	0.1085 (4)	0.070 (2)
C241	-0.2710 (5)	0.1557 (5)	0.1952 (4)	0.062 (2)
C242	-0.1874 (5)	0.1403 (5)	0.2315 (5)	0.068 (2)
C243	-0.0211 (5)	0.2368 (5)	0.3407 (4)	0.057 (2)

	x	*y*	*z*	U_{eq}
C244	0.5089 (4)	0.9090 (4)	0.6608 (4)	0.049 (2)
C245	0.6083 (5)	0.9845 (5)	0.8060 (4)	0.059 (2)
C246	0.6880 (5)	1.0457 (5)	0.7943 (5)	0.065 (2)
C247	0.6808 (5)	1.0025 (5)	0.7167 (5)	0.068 (2)
C248	0.5827 (5)	0.9653 (5)	0.6417 (5)	0.058 (2)
C249	0.6044 (6)	1.0192 (5)	0.8820 (5)	0.066 (2)
C250	-0.1785 (6)	0.8490 (6)	0.4672 (5)	0.069 (2)
C251	-0.2074 (7)	0.8129 (7)	0.3773 (6)	0.096 (3)
C252	-0.2990 (14)	0.7246 (10)	0.3349 (9)	0.216 (9)
C253	-0.3288 (19)	0.6563 (14)	0.3558 (16)	0.140 (8)
C254	-0.3483 (18)	0.6583 (16)	0.4235 (16)	0.127 (7)
C255	-0.4105 (25)	0.5733 (18)	0.2836 (20)	0.199 (16)
C353	-0.3263 (22)	0.6631 (18)	0.2660 (20)	0.206 (12)
C354	-0.2610 (29)	0.6354 (28)	0.2618 (30)	0.253 (18)
C355	-0.4222 (24)	0.5820 (19)	0.2383 (23)	0.222 (18)
C256	-0.1470 (13)	0.9585 (10)	0.3707 (10)	0.178 (7)
C257	-0.1550 (7)	0.6081 (7)	0.6174 (8)	0.105 (3)
C258	-0.1778 (9)	0.5699 (9)	0.5323 (10)	0.138 (5)
C259	0.2472 (5)	0.3214 (5)	0.3578 (4)	0.051 (2)
C260	0.1369 (6)	0.1971 (5)	0.2352 (4)	0.060 (2)
C261	0.1842 (5)	0.1481 (5)	0.2713 (4)	0.059 (2)
C262	0.2444 (6)	0.1824 (5)	0.3671 (4)	0.061 (2)
C263	0.3019 (5)	0.2810 (5)	0.3981 (4)	0.060 (2)
C264	0.0963 (7)	0.1732 (6)	0.1419 (4)	0.084 (3)
C265	0.1872 (7)	0.1482 (6)	0.4092 (5)	0.076 (2)
C266	0.3201 (7)	0.1415 (6)	0.3101 (5)	0.079 (2)
C267	-0.1951 (7)	0.0734 (6)	0.1685 (5)	0.086 (3)
C121	0.2104 (2)	0.6680 (2)	0.37392 (13)	0.0857 (7)
C122	0.34348 (15)	0.9851 (2)	0.80352 (13)	0.0767 (6)
N201	-0.1016 (4)	0.8499 (4)	0.5237 (4)	0.063 (2)
N202	-0.0663 (5)	0.7585 (4)	0.6237 (4)	0.063 (2)
N203	0.0435 (4)	0.6819 (3)	0.6200 (3)	0.0405 (12)
N204	0.0522 (4)	0.4999 (3)	0.5599 (3)	0.0396 (12)
N205	0.1028 (4)	0.3498 (4)	0.4767 (3)	0.0455 (13)
N206	-0.0964 (4)	0.2225 (4)	0.2713 (3)	0.059 (2)
N207	-0.2281 (7)	0.8712 (6)	0.3344 (5)	0.107 (3)
N208	-0.1901 (15)	0.4932 (8)	0.5184 (15)	0.273 (11)
N209	0.3098 (5)	0.1513 (5)	0.3777 (4)	0.074 (2)
N210	0.2528 (5)	0.1503 (4)	0.2503 (4)	0.068 (2)
O201	0.3601 (3)	0.7152 (3)	0.5477 (3)	0.0470 (11)

	x	*y*	*z*	U_{eq}
O202	0.4181 (3)	0.8848 (3)	0.5929 (3)	0.0454 (11)
O203	0.3195 (3)	0.9396 (3)	0.6366 (3)	0.0522 (11)
O204	-0.0084 (5)	1.0254 (4)	0.5919 (5)	0.093 (2)
O205	0.0203 (4)	0.8732 (4)	0.7399 (3)	0.0689 (15)
O206	0.0669 (5)	0.6746 (5)	0.7455 (3)	0.088 (2)
O207	-0.0048 (4)	0.5623 (3)	0.4735 (3)	0.0613 (13)
O208	0.1445 (4)	0.4182 (3)	0.6047 (3)	0.0604 (13)
O209	0.1810 (3)	0.3113 (3)	0.3840 (2)	0.0476 (11)
O210	-0.3212 (5)	0.1091 (5)	0.3560 (4)	0.135 (3)
O211	-0.3949 (5)	0.2365 (6)	0.2633 (4)	0.104 (2)
O212	-0.4710 (4)	0.1046 (5)	-0.0085 (3)	0.093 (2)
O213	-0.0176 (4)	0.1815 (4)	0.3693 (3)	0.076 (2)
O214	0.5181 (3)	0.9562 (3)	0.7315 (3)	0.0533 (12)
O215	0.7811 (4)	1.0790 (4)	0.8640 (4)	0.086 (2)
O216	0.7534 (5)	1.0617 (5)	0.7040 (5)	0.099 (2)
O217	0.5765 (4)	0.9171 (4)	0.5725 (4)	0.087 (2)
O218	0.6067 (5)	1.0956 (4)	0.8879 (4)	0.091 (2)
O219	-0.2226 (4)	0.8764 (4)	0.4849 (4)	0.088 (2)
O220	-0.1830 (7)	0.6062 (7)	0.4817 (6)	0.159 (4)
O221	0.2003 (3)	0.2872 (3)	0.2698 (3)	0.0545 (12)
O222	0.1110 (5)	0.0608 (3)	0.2406 (4)	0.080 (2)
O223	0.3797 (5)	0.1271 (5)	0.3043 (4)	0.185 (2)
O224	-0.2528 (6)	-0.0048 (4)	0.1530(5)	0.120(3)
O225	-0.1483 (5)	0.0980 (5)	0.1339 (5)	0.129 (3)
O1	0.6003 (7)	0.4555 (6)	0.8440(5)	0.144 (4)
O2	-0.0339 (6)	0.7440 (5)	0.4676 (4)	0.107 (2)
O3	0.4770 (5)	0.7015 (6)	1.1218 (6)	0.141 (3)
O4	-0.0606 (5)	0.3868 (5)	0.2403 (4)	0.105 (2)
O5	1.0079 (5)	0.4566 (5)	1.1177 (4)	0.113 (2)
O6	-0.2740 (14)	0.8390 (10)	0.1690 (7)	0.245 (8)
O7	0.3241 (27)	0.3441 (23)	0.9563 (21)	0.221 (12)
O8	-0.4013 (11)	0.8609 (13)	0.2805 (12)	0.259 (9)
O9	0.1215 (21)	0.1912 (19)	0.7556 (25)	0.247 (14)
O10	-0.1904 (14)	1.0335 (10)	0.5858 (12)	0.235 (7)
O11	0.1020 (5)	0.3643 (5)	1.1541 (4)	0.093 (2)
O12	-0.3468 (14)	0.0149 (14)	0.4513 (12)	0.304 (11)
O13	0.3932 (9)	0.2992 (7)	1.1885 (7)	0.165 (4)
O14	-0.3388(31)	0.2976 (26)	0.4300 (17)	0.248 (141)
O15	0.4650 (5)	0.7200 (5)	1.4395 (4)	0.110 (2)
O16	-0.0485 (11)	0.0110 (14)	0.2461 (12)	0.266 (9)

	x	*y*	*z*	U_{eq}
O17	1.0714 (6)	0.9409 (6)	1.1051 (5)	0.131 (3)
O18	0.4624 (17)	0.9277 (15)	0.4304 (9)	0.302 (10)
O19	0.6584 (7)	0.8195 (7)	0.5581 (5)	0.111 (3)
O20	-0.0437 (21)	0.1830 (20)	0.8867 (20)	0.250 (15)
O21	-0.1069 (9)	0.2408 (8)	0.9516 (8)	0.091 (4)
O22	-0.5773 (9)	0.1896 (8)	-0.0474 (7)	0.177 (4)
O23	0.8110 (12)	0.2170 (9)	0.9747 (11)	0.116 (5)
O24	-0.2043 (23)	0.3801 (21)	0.5724 (20)	0.211 (11)
O25	0.4887 (7)	0.1136 (6)	0.7212 (8)	0.163 (4)
O26	-0.0182 (6)	0.5909 (6)	0.8337 (5)	0.137 (3)
O27	0.9222 (7)	0.2491 (7)	0.1169 (6)	0.156 (4)
O28	0.6472 (28)	0.5964 (24)	0.9313 (25)	0.302 (21)
O29	0.7480 (24)	0.6538 (17)	0.9121 (11)	0.191 (10)
O30	0.4597 (7)	0.8007 (7)	0.3162 (7)	0.167 (4)
O31	0.3982 (15)	0.0461 (11)	0.5349 (12)	0.245 (7)
O32	0.9004 (17)	0.4478 (13)	0.6769 (13)	0.140 (7)
O33	0.7358 (19)	0.1913 (13)	0.6608 (16)	0.170 (9)
O34	0.6962 (19)	0.1716 (13)	0.6119 (14)	0.160 (9)
O35	0.2330 (15)	0.8351 (10)	0.2696 (11)	0.244 (7)
O36	0.2162 (14)	0.1089 (10)	0.8925 (11)	0.232 (6)
O37	0.0624 (10)	1.1598 (10)	0.5245 (8)	0.242 (8)
O38	0.5239 (110)	0.5984 (11)	0.0442 (8)	0.224 (6)
O39	0.1254 (14)	0.1769 (9)	0.9680 (8)	0.236 (7)
O40	0.0564 (15)	0.7202 (14)	0.0833 (14)	0.299 (10)
O41	0.9172 (13)	0.5207 (9)	0.3008 (6)	0.236 (7)
O42	0.5898 (7)	0.9496 (8)	0.1776 (7)	0.169 (4)
O43	-0.4232 (23)	0.2289 (27)	0.4074 (16)	0.228 (13)
O44	0.1239 (15)	0.2620 (15)	0.6664 (13)	0.167 (8)
O45	1.1389 (29)	0.9338 (20)	0.3152 (28)	0.462 (19)
O46	0.9474 (13)	1.1144 (13)	0.7922 (13)	0.137 (6)
O47	1.0342 (36)	1.1249 (31)	0.8171 (28)	0.320 (18)
O48	1.0165 (18)	0.6522 (17)	0.2403 (13)	0.162 (8)
O49	-0.2937 (28)	0.4179 (16)	0.3008 (23)	0.227 (12)
O50	-0.4100 (43)	0.3809 (34)	0.2134 (42)	0.335 (23)
O51	0.5372 (25)	0.4301 (29)	0.9483 (20)	0.262 (15)
O52	0.5978 (29)	1.1090 (28)	0.4980 (24)	0.306 (21)
O53	-0.2384 (36)	0.4969 (38)	0.3176 (33)	0.304 (17)
O54	0.4138 (25)	0.4094 (20)	1.0175 (18)	0.193 (10)
O55	0.9037 (12)	0.2947 (11)	0.6920 (10)	0.238 (7)
O56	0.0856 (11)	0.7658 (11)	0.4042 (9)	0.234 (7)

	x	*y*	*z*	U_{eq}
O57	0.9652 (13)	0.1925 (12)	0.6768 (12)	0.267 (9)
O58	0.8991 (11)	0.6147 (13)	0.9270 (9)	0.245 (7)
O59	0.2485 (20)	0.8878 (15)	0.4192 (13)	0.320 (11)
O60	-0.4924 (20)	0.3431 (18)	0.1026 (23)	0.205 (11)
O61	0.5240 (15)	0.3549 (18)	0.3624 (11)	0.311 (11)
O62	0.7340 (23)	0.6900 (20)	0.0884 (18)	0.381 (14)
O63	0.9481 (27)	0.6496 (22)	0.2575 (21)	0.253 (14)
O64	-0.0147(23)	0.8777 (20)	0.3310 (19)	0.367 (13)
O65	0.4818 (32)	1.0848 (31)	0.4393 (23)	0.291 (19)
O66	0.8295 (39)	0.6664 (41)	1.2418 (36)	0.360 (25)
O67	-0.1672 (45)	0.5849 (43)	0.3455 (42)	0.378 (24)
O68	0.9375 (50)	0.7346 (39)	0.1679 (41)	0.402 (31)
O69	0.9485 (30)	0.7802 (33)	0.0964 (31)	0.304 (19)
O70	0.6607 (41)	0.7251 (42)	0.5373 (35)	0.181 (22)
O71	0.8686 (38)	0.8183 (36)	0.1094 (38)	0.383 (28)
O72	1.0487 (30)	0.7051 (26)	0.2038 (27)	0.288 (17)
O73	0.9659 (19)	0.4629 (18)	0.7227 (19)	0.196 (10)

REFERENCES

Allen, N.E., Hobbs Jnr, J.N., Richardson, J.M., Riggin, R.M. (1992) *FEMS Microbiol. Lett.* **98,** 109

Antipas, A.S., Velde, D.V., Stella, V.J. (1994) *Int. J. Pharm.* **109,** 261

Anton, A. H. (1973) *Ann. N. Y. Acad. Sci.* **226,** 273

Arnoux, B., Ducruix, A., Reiss-Husson, F., Lutz, M., Norris, J., Schiffer, M., Chang, C. H. (1989) *FEBS Lett.* **258,** 47

Aronow, R. H., Witten, L. (1960) *J. Phys. Chem.* **64,** 1643

Atha, D. H., Ackers, G. K. (1971) *J. Biol. Chem.* **246,** 5845

Atkins, P.W., Clugston, M.J., Frazer, M.J., Jones, R.A.Y. (1988) In *Chemistry Principles and Applications,* Longman Group U.K. Ltd., England, 81

Atkins, P.W.[a] (1996) In *The Elements of Physical Chemistry,* Second Edition, Oxford University Press, 35

Atkins, P.W.[b] (1996) In *The Elements of Physical Chemistry,* Second Edition, Oxford University Press, 75

Atkins, P.W.[c] (1996) In *The Elements of Physical Chemistry,* Second Edition, Oxford University Press, 390

Austin, B. (1989) *J. App. Bact.* **67,** 461

Barna, J.C.J., Williams, D.H. (1984) *Ann. Rev. Microbiol.* **38,** 339

Beauregard, D.A., Williams, D.H., Gwynn, M.N., Knowles, D.J.C. (1995) *Antimicrob. Agents Chemother.* **39:3,** 781

Billot-Klein, D., Blanot, D., Gutman, L., van Heijenoort, J.[a] (1994) *J. Biochem.* **304,** 1021

Billot-Klein, D., Gutmann, L., Sable, S, Guittet, E., van Heijenoort, J.[b] (1994) *J. Bact.* **176:8,** 2398

Biltonen, R. L., Langerman, N. (1979) *Methods Enzymol.* **61,** 287

Blow, D. M. (1985) *Proceedings of the Daresbury Study Weekend 15-16 February,* 2

Branden, C., Tooze, J. (1991) In *Introduction to Protein Structure,* Garland Publishing Inc, 269

Bugg, T.D.H., Dutken-Malen, S., Arthur, M., Courvalin, P., Walsh, C.T.[a] (1991) *Biochemistry* **30,** 2017

Bugg, T.D.H., Wright, G.D., Dutka-Malen, S., Arthur, M., Courvalin, P., Walsh, C.T.[b] (1991) *Biochemistry* **30,** 10408

Bundle, D.R., Sigurskjold, B.W. (1994) *Methods Enzymol.* **247,** 288

Burova, T. V., Bernhardt, R., Pfeil, W. (1995) *Protein Science* **4,** 909

Chervenak, M.C., Toone, E.J. (1994) *J. Am. Chem. Soc.* **116,** 10533

Christensen, J.J., Hansen, L.D., Izatt, R.M. (1976) In *Handbook of Proton Ionization Heats,* Wiley, New York

Convert, O., Bongini, A., Feeney, J. (1980) *J. Chem. Soc., Perkin Trans II,* 1262

Cooper, A. (1974) *Biochemistry* **13,** 2853

Cooper, A., Converse, C. A. (1976) *Biochemistry* **15:14,** 2970

Cooper, A., Johnson, C. M.[a] (1994) In *Methods in Molecular Biology, Microscopy, Optical Spectroscopy and Macroscopic Techniques.* Eds. C. Jones, B. Mulloy & A. H. Thomas **22,** 137

Cooper, A., Johnson, C. M.[b] (1994) In *Methods in Molecular Biology, Microscopy, Optical Spectroscopy and Macroscopic Techniques.* Eds. C. Jones, B. Mulloy & A. H. Thomas **22,** 125

Cooper, A., Johnson, C.M.[c] (1994) In *Methods in Molecular Biology, Microscopy, Optical Spectroscopy and Macroscopic Techniques.* Eds. C. Jones, B. Mulloy & A. H. Thomas **22,** 109

Cooper, A., McAuley-Hecht, K.E. (1993) *Phil. Trans. R. Soc. Lond. A,* **345,** 23

Cooper, A. (1996) In *Protein:A Comprehensive Treatise.* Ed. G. Allen, Published by J.A.I. Press Inc. (in press)

Covington, A. K., Paabo, M., Robinson, R. A., Bates, R. G. (1968) *Analyt. Chem.* **40:4,** 700

Cristofaro, M.F., Beauregard, D.A., Yan, H., Osborn, N.J., Williams, D.H. (1995) *J. Antibiot.* **48:8,** 805

Davies, D. R., Segal, D. M. (1971) *Methods Enzymol.* **22,** 266

Decker, R. V., Foster, J. F. (1966) *Biochemistry* **5,** 1252

Dock, A. C., Lorber, B., Moras, D., Pixa, G., Thierry, J. C., Giege, R. (1984) *Biochemie* **66,** 179

Donner, J., Caruthers, M. H., Gill, S. J. (1982) *J. Biol. Chem.* **257,** 14826

Ducruix, A., Giege, R. (1992) In *Crystallization of Nucleic Acids and Proteins:A Practical Approach* Eds. A. Ducruix & R. Giege, Oxford University Press, 73

Eftink, M., Biltonin, R. (1980) In *Biological Microcalorimetry.* Ed. A.E. Beezer, Academic Press, N.Y, 343

Estabrook, R.W., Suzuki, K., Mason, J. I., Baron, J., Taylor, W.E., Simpson, E. R., Purvis, J., McCarthy, J. (1973) In *Iron-Sulphur Proteins, Volume 2,* New York, Academic Press, 193

Evans, L. J. A., Cooper, A., Lakey, J. H. (1996) *J. Mol. Biol.* **255,** 559

Feher, G., Kam, Z. (1985) *Methods Enzymol.* **114,** 77

Fekety, R. (1995) In *Principles and Practice of Infectious Diseases.* Fourth edition, Eds. G.L. Mandell, J. E. Bennett, R. Dolin, New York, 346

Freire, E., Mayorga, O.L., Straume, M. (1990) *Analyt. Chem.* **62:18,** 950A

Frigero, A. (1974) In *Spectrum Publications Inc*, 1

Gerhard, U., Mackay, J.P., Maplestone, R.A., Williams, D.H. (1993) *J. Am. Chem. Soc.* **115,** 232

Giege, R., Dock, A.C., Kern, D., Lorber, B., Thierry, J. C., Moras, D. (1986) *J. Cryst. Growth* **76,** 554

Giege, R., Ducruix, A. (1992) In *Crystallization of Nucleic Acids and Proteins: A Practical Approach.* Eds. A. Ducruix & R. Geige Oxford University Press, 1

Gilliland, G. L. (1988) *J. Cryst. Growth* **90,** 51

Green, A. A. (1931) *J. Biol. Chem.* **93,** 495

Green, A. A. (1932) *J. Biol. Chem.* **95,** 47

Greenwood, D. (1989) In *Antimicrobial Chemotherapy.* Second Edition, Oxford Medical Publications, 14

Grenthe, I., Ots, H., Ginstrup, O. (1970) *Acta Chem. Scand.* **24:3,** 1067

Groves, P., Searle, M.S., Mackay, J.P., Williams, D.H. (1994) *Structure* **2,** 747

Groves, P., Searle, M.S., Waltho, J.P., Williams, D.H. (1995) *J. Am. Chem. Soc.* **117,** 7958

Grunwald, E. (1986) *J. Am. Chem. Soc.* **108,** 5726

Grunwald, E., Comeford, L. (1988) In *Environmental Influences and Recognition in Enzyme Chemistry.* Eds. J. F. Liebman, A. Greenberg, V.C.H. Publishers, New York

Grunwald, E., Steel, C. (1995) *J. Am. Chem. Soc.* **117,** 5687

Harding, M.M. (1985) *Proceedings of the Daresbury Study Weekend 15-16 February,* 50

Hemminger, W., Hohne, G. (1984) In *Calorimetry;Fundamentals and Practice.* Verlag Chemie GmbH D-6940 Weinheim, 1

Higgins, H. M., Harrison, W.H., Wild, G.M., Bungay, H. R., McCormick, M. H. (1958) *Antibiot. Annu.* 1957-1958, 906

Howarth, O. W. (1975) *J. Chem. Soc. Faraday Trans. I* **71,** 2303

ITC Data Analysis in Origin :Tutorial Guide. Version 2.8. Microcal Inc. (1993)

Jackson, W., Brandts, J.F. (1970) *Biochemistry* **9,** 2294

Jakoby, W. B. (1971) *Methods Enzymol.* **22,** 248

Jakoby, M. G., Covey, D. F., Cistola, D. P. (1995) *Biochemistry* **34,** 8780

Johnson, M. L. (1985) *Analyt. Biochem.* **148,** 471

Jordan, D.C., Inniss, W.E. (1959) *Nature* **184,** 1894

Kabsch, W. (1988) *J. Appl. Cryst.* **21,** 916

Kalinichenko, L. P., Lobyshev, V. P. (1976) *Stud. Biophys.* **58,** 235

Kauzmann, W. (1959) *Adv. Protein. Chem.* **14,** 1

Kim, S. H., Rich, A. (1968) *Science* **162,** 1381

Knox, J.R., Pratt, R.F. (1990) *Antimicrob. Agents. Chemother.* **34:7,** 1342

Koenigbauer, M. J. (1994) *Pharm. Res.* **11:6,** 777

Krishnan, K. S., Brandts, J. F. (1978) *Methods Enzymol.* **49,** 3

Ladd, M. F. C., Palmer, R. A. (1994) In *Structure Determination by X-ray Crystallography.* Third Edition, Plenum Press, New York and London, 1

Lambeth, J. D. (1990) In *Fronteirs in Biotransformation.* Volume Three. Eds. K. Ruckpaul, H. Rein, Berlin: Akademie-Verlag, 58

Lamprecht, I. (1980) In *Biological Microcalorimetry.* Eds. A.E. Beezer, Academic Press, N.Y, 43

Langerman, N., Biltonen, R. L. (1979) *Methods Enzymol.* **61,** 261

Leder, L., Berger, C., Bornhauser, S., Wendt, H., Ackermann, F., Jelesarov, I., Bosshard, H.R. (1995) *Biochemistry* **34,** 16509

Lee, J. C., Lee, L. L. Y. (1981) *J. Biol. Chem.* **256,** 625

Leslie, A. G. W. (1985) *Proceedings of the Daresbury Study Weekend 15-16 February,* 78

Lorber, B., Giege, R. (1992) In *Crystallization of Nucleic Acids and Proteins:A Practical Approach.* Eds. A. Ducruix & R. Giege, Oxford University Press, 19

Mackay, J.P., Gerhard, U., Beauregard, D.A., Westwell, M.S., Searle, M.S., Williams, D.H. (1994) *J. Am. Chem. Soc.* **116:11,** 4581

Mann, M., Wilm, M. (1995) *TIBS.* **20,** 219

Maplestone, R.A., Stone, M.J., Williams, D.H. (1992) *Gene* **115,** 151

Marcus, Y., Ben-Naim, A. (1985) *J. Chem. Phys.* **83,** 4744

Marky, L. A., Snyder, J. G., Remeta, D. P., Breslauer, K. J. (1983) *J. Biomol. Struct. Dyn.* **1,** 487

Mathews, C.K., van Holde K.E.[a] (1990) In *Biochemistry,* Benjamin/Cummings Inc, 30

Mathews, C.K., van Holde K.E.[b] (1990) In *Biochemistry,* Benjamin/Cummings Inc, 171

Mathews, C.K., van Holde K.E.[c] (1990) In *Biochemistry,* Benjamin/Cummings Inc, 260

Mathews, C.K., van Holde K.E.[d] (1990) In *Biochemistry,* Benjamin/Cummings Inc, 538

Mathews, C.K., van Holde K.E.[c] (1990) In *Biochemistry,* Benjamin/Cummings Inc, 742

Matthews, B. V. (1968) *J. Mol. Biol.* **33,** 491

McAuley-Hecht, K.E. (1993) In *Thermodynamics of Biomolecular Recognition. PhD Thesis*

McCormick, M.H., Stark, W.M., Pittenger, G.E., Pittenger, R.C., McGuire, J.M. (1956) In *Antibiot. Annu.* 1955-56, New York, 606

McKinnon, I. R., Fall, L., Parody, A., Gill, S. J. (1984) *Anal. Biochem.* **139,** 134

McPhail, D., Cooper, A. (1997) *J. Chem. Soc. Faraday Trans.* **93:13**, 2283

McPherson, A. (1982) In *Preparation and Analysis of Protein Crystals.* John Wiley & Sons, New York

McPherson, A.[a] (1985) *Methods Enzymol.* **114,** 112

McPherson, A.[b] (1985) *Methods Enzymol.* **114,** 120

Michel, H. (1982) *J. Mol. Biol.* **158,** 567

Mikol, V., Giege, R. (1992) In *Crystallization of Nucleic Acids and Proteins:A Practical Approach.* Eds. A. Ducruix & R. Giege, Oxford University Press, 219

Mikol, V., Rodeau, J.-L., Giege, R. (1989) *J. Appl. Cryst.* **22,** 155

Monk, P., Wadso, I. (1969) *Acta Chem. Scand.* **23,** 29

Monks, A., Boobis, S., Wadsworth, J., Richens, A. (1978) *Br. J. Clin. Pharmacol.* **6,** 487

Myers, M., Mayorga, O. L., Emtage, J., Freire, E. (1987) *Biochemistry* **26,** 4309

Naghibi, H., Tamura, A., Sturtevant, J. M. (1995) *Proc. Natl. Acad. Sci. U.S.A.* **92,** 5597

Nairn, J., Krell, T., Coggins, J.R., Pitt, A.R., Fothergill-Gilmore, L.A., Walter, R., Price, N.C. (1995) *FEBS Lett.* **359,** 192

Nemethy, G., Scheraga, H. A. (1964) *J. Chem. Phys.* **41,** 680

Neu, H.C. (1992) *Science* **257,** 1064

Nieto, M., Perkins, H.R.[a] (1971) *J. Biochem.* **123,** 789

Nieto, M., Perkins, H.R.[b] (1971) *J. Biochem.* **123,** 773

Perkins, H. R. (1969) *Biochem. J.* **111,** 195

Perutz, M.F. (1992) *Discuss. Faraday Soc.* **93,** 1

Popieniek. P. H., Pratt, R. F. (1991) *J. Am. Chem. Soc.* **113,** 2264

Privalov, P. L., Filimonov, V. V., Venkstern, T. V., Bayev, A. A. (1975) *J. Mol. Biol.* **97,** 279

Privalov, P. L. (1980) *Pure & Appl. Chem* **52,** 479

Privalov, P. L., Potekhin, S. A. (1986) *Methods Enzymol.* **131,** 4

Rajagopalan, J. S., Harris, C. M., Harris, T. M. (1995) *Bioorg. Chem.* **23,** 54

Ramsay, G., Prabhu, R., Freire, E. (1986) *Biochemistry* **25,** 2265

Rasmussen, J.R., Strominger, J.L. (1978) *Proc. Natl. Acad. Sci. U.S.A.* **75,** 84

Ries-Kautt, M., Ducruix, A. (1992) In *Crystallization of Nucleic Acids and Proteins:A Practical Approach.* Eds. A. Ducruix & R. Giege, Oxford University Press, 195

Rodriguez-Tebar. A., Vazquez, D., Perez, Velazquez, J. L., Laynez, J., Wadso, I. (1986) *J. Antibiotics* **39,** 1578

Saunders, J. (1993) In *Principles of Molecular Recognition.* Blackie Academic & Professional, 137

Sawyer, L., Turner, M. A. (1992) In *Crystallization of Nucleic Acids and Proteins:A Practical Approach.* Eds. A. Ducruix & R. Giege, Oxford University Press, 255

Schafer, M., Schneider, T. R., Sheldrick, G. M. (1996) *Structure* **4:12,** 1509

Schon, A., Freire, E. (1989) *Biochemistry* **28,** 5019

Searle, M.S., Groves, P., Williams, D.H. (1994) *Proc. Ind. Acad. Sci. (Chem. Sci.)* **106:5,** 937

Sellers, E. M., Koch-Weser, J. (1971) *Ann. N. Y. Acad. Sci.* **179,** 213

Sheldrick, G.M., Jones, P.G., Kennard, O., Williams, D.H., Smith, G.A. (1978) *Nature* **271,** 223

Sheldrick, G.M., Paulus, E., Vertesy, L., Hahn, F. (1995) *Acta Cryst.* **B51,** 89

Shiao, D. D. F., Sturtevant, J. M. (1970) *Fed. Proc. Fed. Am. Soc. Exp. Biol.* **29,** 335

Skinner, H. A. (1969) In *Biochemical Microcalorimetry.* Academic Press, 1

Smith, E.B. (1990) In *Basic Chemical Thermodynamics,* Oxford Chemistry Series 35, Fourth Edition, 36

Spokane, R. B., Gill, S. J. (1981) *Rev. Sci. Instrum.* **52,** 1728

Spolar, R. S., Record Jnr, M. T. (1994) *Science* **263,** 777

Sturtevant, J.M. (1962) In *Experimental Thermochemistry,* Volume II, Ed. H. A. Skinner, New York, N. Y., Interscience, 427

Sturtevant, J.M. (1977) *Proc. Natl. Acad. Sci. U. S. A.* **74,** 2236

Sturtevant, J.M. (1987) *Ann. Rev. Phys. Chem.* **38,** 463

Timasheff, S. N., Arakawa, T. (1985) *Methods Enzymol.* **114,** 49

Usanov, S. A., Chashchin, V. L., Akhrem, A. A. (1990) In *Frontiers in Biotransformation,* Volume Three, Eds. K. Ruckpaul, H. Rein, Berlin: Academie-Verlag, 1

Vining, L.C. (1992) *Ciba Foundation. Symp.* **171,** 184

Voet, D., Voet, J.G.[a] (1990) In *Biochemistry,* John Wiley & Sons, 30

Voet, D., Voet, J.G.[b] (1990) In *Biochemistry,* John Wiley & Sons, 144

Von Hippel, P. H., Schleich, T. (1969) In *Biological Macromolecules,* Volume II, Eds. S. Timasheff & G. Fasman, New York: Dekker, 417

Wadso, I. (1983) *Pure & Appl. Chem.* **55:3,** 515

Wadso, I. (1992) *Ind. J. Tech.* **30,** 537

Waltho, J.P., Williams, D.H. (1991) *Ciba Foundation. Symp.* **158,** 73

Waltho, J.P., Williams, D.H. (1989) *J. Am. Chem. Soc.* **111,** 2475

Watson, J. D., Hopkins, N. H., Roberts, J. W., Steitz, J. A., Weiner, A. M. (1987) In *Molecular Biology of the Gene,* Fourth Edition, Volume I : General Principles, Benjamin/Cummings Inc, 126

Weber, G. (1993) *J. Phys. Chem.* **97,** 7108

Weber, G. (1995) *J. Phys. Chem.* **99,** 1052

Wesseling, H., Mols-Thurkow, I. (1975) *Eur. J. Clin. Pharmacol.* **8,** 75

Westwell, M.S., Gerhard, U., Williams, D.H. (1995) *J. Antibiotics* **48:11,** 1292

Williams, D. H., Stone, M. J., Mortishire-Smith, R. J., Hauck, P. R. (1990) *Biochem. Pharmacol.* **40,** 27-34

Williams, D. H., Searle, M. S., Mackay, J. P., Gerhard U., Maplestone R. A. (1993) *Proc. Natl. Acad. Sci.* **99,** 1172

Williams, D.H., Searle, M.S, Groves, P., Mackay, J.P., Westwell, M.S., Beauregard, D.A., Cristofaro, M.F. (1994) *Pure & Appl. Chem.* **66:10/11,** 1975

Williams, D. H., Rajananda, V., Kalman, J. R. (1979) *J. Chem. Soc. Perkin Trans.* **1,** 787

Williams, D. H., Maplestone, R. A. (1992) *Ciba Foundation. Symp.* **171,** 45

Williamson, M.P., Williams, D.H., Hammond, S.J. (1984) *Tetrahedron* **40:3,** 569

Williamson, M.P., Williams, D. H. (1985) *J. Chem. Soc. Perkin Trans.* **1,** 949

Wiseman, T., Williston, S., Brandts, J.F., Lin, L-N. (1989) *Anal. Biochem.* **179,** 131

Woodford, N., Johnson, A.P. (1994) *J. Med. Micro.* **40,** 375

Wright, G.D., Walsh, C.T. (1992) *Acc. Chem. Res.* **25,** 468

Yonath, A., Mussig, J., Wittmann, H. G. (1982) *J. Cell. Biochem.* **19,** 145

Zeppezauer, M. (1971) *Methods Enzymol.* **22,** 253

Zurawski, V. R., Kohr, W. J., Foster, J. F. (1975) *Biochemistry* **14,** 5579